THERAPEUTIC & DIAGNOSIS TARGET DISCOVERY BASED ON METABOLOMICS

EDITED BY: Linsheng Liu, Bei Cao, Hiu Yee Kwan, Jiye Aa, Ying Zhou and Giuseppe Lucarelli

PUBLISHED IN: Frontiers in Pharmacology

frontiers Research Topics

frontiers

ISSN 1664-8714
ISBN 978-2-88976-011-4
DOI 10.3389/978-2-88976-011-4

About Frontiers

Frontiers is more than just an open-access publisher of scholarly articles: it is a pioneering approach to the world of academia, radically improving the way scholarly research is managed. The grand vision of Frontiers is a world where all people have an equal opportunity to seek, share and generate knowledge. Frontiers provides immediate and permanent online open access to all its publications, but this alone is not enough to realize our grand goals.

Frontiers Journal Series

The Frontiers Journal Series is a multi-tier and interdisciplinary set of open-access, online journals, promising a paradigm shift from the current review, selection and dissemination processes in academic publishing. All Frontiers journals are driven by researchers for researchers; therefore, they constitute a service to the scholarly community. At the same time, the Frontiers Journal Series operates on a revolutionary invention, the tiered publishing system, initially addressing specific communities of scholars, and gradually climbing up to broader public understanding, thus serving the interests of the lay society, too.

Dedication to Quality

Each Frontiers article is a landmark of the highest quality, thanks to genuinely collaborative interactions between authors and review editors, who include some of the world's best academicians. Research must be certified by peers before entering a stream of knowledge that may eventually reach the public - and shape society; therefore, Frontiers only applies the most rigorous and unbiased reviews.
Frontiers revolutionizes research publishing by freely delivering the most outstanding research, evaluated with no bias from both the academic and social point of view. By applying the most advanced information technologies, Frontiers is catapulting scholarly publishing into a new generation.

What are Frontiers Research Topics?

Frontiers Research Topics are very popular trademarks of the Frontiers Journals Series: they are collections of at least ten articles, all centered on a particular subject. With their unique mix of varied contributions from Original Research to Review Articles, Frontiers Research Topics unify the most influential researchers, the latest key findings and historical advances in a hot research area! Find out more on how to host your own Frontiers Research Topic or contribute to one as an author by contacting the Frontiers Editorial Office: frontiersin.org/about/contact

THERAPEUTIC & DIAGNOSIS TARGET DISCOVERY BASED ON METABOLOMICS

Topic Editors:
Linsheng Liu, The First Affiliated Hospital of Soochow University, China
Bei Cao, Nanjing Drum Tower Hospital, China
Hiu Yee Kwan, Hong Kong Baptist University, Hong Kong, SAR China
Jiye Aa, China Pharmaceutical University, China
Ying Zhou, The First Affiliated Hospital of Nanchang University, China
Giuseppe Lucarelli, University of Bari Aldo Moro, Italy

Citation: Liu, L., Cao, B., Kwan, H. Y., Aa, J., Zhou, Y., Lucarelli, G., eds. (2022). Therapeutic & Diagnosis Target Discovery Based on Metabolomics. Lausanne: Frontiers Media SA. doi: 10.3389/978-2-88976-011-4

Table of Contents

frontiers | Frontiers in Pharmacology

EDITORIAL
published: 04 April 2022
doi: 10.3389/fphar.2022.893905

Editorial: Therapeutic and Diagnosis Target Discovery Based on Metabolomics

*Linsheng Liu**

Department of Pharmacy, The First Affiliated Hospital of Soochow University, Suzhou, China

Keywords: metabolomics, diagnostic target discovery, therapeutic target discovery, biomarkers, precision medicine

Editorial on the Research Topic

Therapeutic and Diagnosis Target Discovery Based on Metabolomics

With the completion of the human genome sequencing project, the functions of gene fragments have gradually been deciphered, ushering in the postgenome era, and many "omics" technologies have been developed. Transcriptomics, proteomics, and metabolomics have all become research hotspots in the medical and biological fields at this stage and have gradually been applied to every aspect of clinical research. Metabolomics was first formally proposed at the end of the last century, and is described as a quantitative analysis of all metabolites in an organism and a research method to determine the relative relationship between metabolites and physiological and pathological changes. It is an integral part of systems biology. Metabolomics facilitates the identification of biologically meaningful markers compared with other omics sciences, such as genomics, transcriptomics or proteomics, because far fewer metabolites are present in an organism than genes, mRNAs and proteins. Metabolomics has been the backbone of system-wide analyses of disease and medicine owing to the critical roles of metabolites in biological processes and the growing understanding of how the metabolome dynamically affects biological systems. Therefore, metabolomics has been gradually applied to all aspects of clinical research in the past decade, promoting the development of precision medicine, such as determining the prognosis of diseases, monitoring adverse drug reactions, and discovering diagnostic biomarkers.

Over the past 10 years, researchers have gradually conducted an increasing number of metabolomic studies on the pathogenesis of various diseases to identify the differentially abundant metabolites between diseased and normal individuals and thus identify biologically valuable diagnostic or therapeutic metabolites. These studies involve analyzing cells, animal models of diseases, and clinical patients with the NMR and MS analytical platforms. This research topic "*Therapeutic and Diagnostic Target Discovery Based on Metabolomics*" consists of 9 articles contributed by more than 71 authors in the fields of metabolic pathways of small-molecule endogenous substances in the treatment or diagnosis of some diseases. The topic revealed the mechanisms underlying the pharmacological interactions between metabolic targets and available intervention strategies that provide further insights into the treatment of these diseases.

Osteoporosis is a highly occult disease with no obvious symptoms or sensitive biomarkers, and many patients are only diagnosed after a fracture occurs. Deng et al. integrated untargeted metabolomics, lipidomics and targeted metabolomics to screen biomarkers for osteoporosis. Changes in metabolites in patients with osteoporosis suggested a disturbance in the bile acid metabolism pathway and the potential of using HCA as a biomarker for the early diagnosis of osteoporosis. As important active small-molecule compounds involved in the interaction between the body and the gut microbiota, bile acids are also a hot spot of current research. Hu et al. documented the effect of metformin on the gut microbiota and host metabolic profiles in STZ- and high-fat diet-

OPEN ACCESS

Edited and reviewed by:
Alastair George Stewart,
The University of Melbourne, Australia

***Correspondence:**
Linsheng Liu
linsheng_liu@126.com

Specialty section:
This article was submitted to Translational Pharmacology, a section of the journal Frontiers in Pharmacology

Received: *11 March 2022*
Accepted: *16 March 2022*
Published: *04 April 2022*

Citation:
Liu L (2022) Editorial: Therapeutic and Diagnosis Target Discovery Based on Metabolomics. Front. Pharmacol. 13:893905. doi: 10.3389/fphar.2022.893905

induced type 2 diabetic rats using 16S rRNA sequencing and untargeted and targeted metabolomics assays. More genera in DM rats were regulated by metformin than by insulin. Several genera, metabolites and bile acids were found to be related to metformin and insulin treatments. Qu et al. clarified that aberrant activation of the secondary bile acid biosynthesis pathway increased the hydrophobicity of the bile acid pool that might subsequently promote metabolic disturbances and disease progression in mice subjected to chronic unpredictable mild stress using an untargeted metabolomics method. Due to many adverse effects of gestational diabetes mellitus, Raczkowska et al. conducted an exhaustive assessment of multiple biomarkers for the prediction and diagnosis of gestational glucose intolerance in two OGTT categories (high FPG levels with normal postglucose PG levels and normal FPG levels with high postglucose PG levels).

Lipids are also an important component of the metabolome. Zhi et al. used UHPLC-HRMS to acquire lipid profiles from patients with Wilson's disease (WD) and their relatives (and a control group) to determine characteristic lipid profiles of patients with WD and identify potential diagnostic or therapeutic biomarkers for WD. The findings may provide valuable insights into identifying diagnostic and therapeutic biomarkers for Wilson disease. Changes in amino acids are the most common features detected in metabolomics studies. Sun et al. presented a GC/MS-based metabolomics method to profile the dynamic endogenous metabolic changes in the serum of mice at different time points after partial hepatectomy. Several amino acid and glucose metabolism pathways were dynamically altered during liver regeneration. They also used machine learning algorithms to identify potential metabolites that predict liver regeneration performance. Metabolomics is often also studied in conjunction with other omics techniques. Li et al. evaluated the effect of mesoporous silica nanoparticles (MSNs) on the liver using histopathology, metabolomics, proteomics and transcriptomics. MSNs administered i.v. substantially altered the levels of several metabolites involved in hepatic metabolism, oxidative stress and inflammation pathways, and the changes were more significant than those observed after oral administration.

Arjmand et al. conducted a review focusing on a clinically interesting issue regarding the treatment resistance of patients with cancer and proposed the molecular docking modeling method as a novel approach to target the metabolic pathways in cancer stem cells. Finally, as one of the most relevant approaches to investigate metabolic phenotypes, Emwas et al. presented a brief review of fluxomics research conducted in recent decades by discussing recent studies and common analytical tools.

In conclusion, the "*Therapeutic and Diagnostic Target Discovery Based on Metabolomics*" research topic highlights the importance of developing novel targets and biomarkers for the discovery of targets for the diagnosis and treatment of complex diseases.

AUTHOR CONTRIBUTIONS

The author confirms being the sole contributor of this work and has approved it for publication.

FUNDING

This work was supported by the Suzhou Science and Technology Development Plan-Suzhou Integrated Traditional Chinese and Western Medicine Research Fund (SKJYD2021219).

ACKNOWLEDGMENTS

Thanks to Bei Cao, Hiu Yee Kwan, Jiye Aa, Ying Zhou and Giuseppe Lucarelli for their contributions to this Research Topic.

Conflict of Interest: The author declares that the research was conducted in the absence of any commercial or financial relationships that could be construed as a potential conflict of interest.

Publisher's Note: All claims expressed in this article are solely those of the authors and do not necessarily represent those of their affiliated organizations, or those of the publisher, the editors and the reviewers. Any product that may be evaluated in this article, or claim that may be made by its manufacturer, is not guaranteed or endorsed by the publisher.

frontiers in Pharmacology

ORIGINAL RESEARCH
published: 06 August 2021
doi: 10.3389/fphar.2021.725341

An Integrated Metabolomic Study of Osteoporosis: Discovery and Quantification of Hyocholic Acids as Candidate Markers

Dawei Deng[1,2,3†], *Chen Pan*[1†], *Zeming Wu*[4], *Yujiao Sun*[2,5], *Chang Liu*[2,5], *Hong Xiang*[2], *Peiyuan Yin*[2,5*] *and Dong Shang*[1,2,5*]

[1]Department of General Surgery, First Affiliated Hospital of Dalian Medical University, Dalian, China, [2]Clinical Laboratory of Integrative Medicine, First Affiliated Hospital of Dalian Medical University, Dalian, China, [3]Department of Hepato-biliary-pancreas, Affiliated Hospital of North Sichuan Medical College, Nanchong, China, [4]iPhenome biotechnology (Yun Pu Kang) Inc, Dalian, China, [5]Institute of Integrative Medicine, Dalian Medical University, Dalian, China

OPEN ACCESS

Edited by:
Bei Cao,
Nanjing Drum Tower Hospital, China

Reviewed by:
Runbin Sun,
Nanjing Drum Tower Hospital, China
Xinwen Wang,
Northeast Ohio Medical University, United States
Hyung-Kyoon Choi,
Chung-Ang University, South Korea

***Correspondence:**
Peiyuan Yin
yinperry@126.com
Dong Shang
shangdong@dmu.edu.cn

[†]These authors have contributed equally to this work and share first authorship

Specialty section:
This article was submitted to Translational Pharmacology, a section of the journal Frontiers in Pharmacology

Received: 15 June 2021
Accepted: 27 July 2021
Published: 06 August 2021

Citation:
Deng D, Pan C, Wu Z, Sun Y, Liu C, Xiang H, Yin P and Shang D (2021) An Integrated Metabolomic Study of Osteoporosis: Discovery and Quantification of Hyocholic Acids as Candidate Markers. Front. Pharmacol. 12:725341. doi: 10.3389/fphar.2021.725341

Osteoporosis is becoming a highly prevalent disease in a large proportion of the global aged population. Serum metabolite markers may be important for the treatment and early prevention of osteoporosis. Serum samples from 32 osteoporosis and 32 controls were analyzed by untargeted metabolomics and lipidomic approaches performed on an ultra-high performance liquid chromatography and high-resolution mass spectrometry (UHPLC-HRMS) system. To find systemic disturbance of osteoporosis, weighted gene correlation network analysis (WGCNA) and statistical methods were employed for data-mining. Then, an in-depth targeted method was utilized to determine potential markers from the family of key metabolites. As a result, 1,241 metabolites were identified from untargeted methods and WGCNA indicated that lipids metabolism is deregulated and glycerol phospholipids, sphingolipids, fatty acids, and bile acids (BA) are majorly affected. As key metabolites of lipids metabolism, 66 bile acids were scanned and 49 compounds were quantified by a targeted method. Interestingly, hyocholic acids (HCA) were found to play essential roles during the occurrence of osteoporosis and may be potential markers. These metabolites may be new therapeutic or diagnosis targets for the screening or treatment of osteoporosis. Quantified measurement of potential markers also enables the establishment of diagnostic models for the following translational research in the clinic.

Keywords: osteoporosis, lipids, bile acids, ageing, metabolomics

INTRODUCTION

Osteoporosis is a progressive systemic bone disease that is characterized by bone loss and microstructural deterioration and results in increased bone fragility, which affects over 200 million people worldwide (Curtis et al., 2017; Compston et al., 2019). Complications of osteoporosis such as chronic pain, fracture and disability seriously affect the quality of life of elderly individuals. Fracture is the most serious complication, with more than 8.9 million osteoporosis-related fractures occurring annually (Cruz-Jentoft and Sayer, 2019). As the global population ages, osteoporosis and its complications are becoming an increasingly serious public health burden (Sànchez-Riera et al., 2014; Tarrant and Balogh, 2020). Osteoporosis is also a highly insidious disease. Due to the absence of obvious symptoms and sensitive biomarkers, many patients

are diagnosed only after a fracture has occurred (Wang et al., 2019; Fang et al., 2020). Furthermore, the first-line drugs used to treat osteoporosis are associated with a substantial number of complications, and the overall therapeutic effects are unsatisfactory (Park et al., 2013; Komm et al., 2015). This indicates that we do not fully understand osteoporosis and the therapeutic targets required.

Metabolites are the ultimate functional products that manifest both genetic and environmental variations, and they combine external stimuli with intracellular signals (Peng et al., 2015). Metabolic profiles obtained using metabolomics techniques under different conditions are closely related to human health (Leslie and Beyan, 2011). Osteoporosis is a metabolic bone disease, and studies have indicated that significant changes in endogenous metabolites modulate bone remodelling in a mouse model of osteoporosis (Nam et al., 2018). Moreover, in the treatment of osteoporosis, oestradiol changed 27 intracellular metabolite levels by correcting lipid and amino acid disorders (Liu et al., 2015). Metabolomics characterizes metabolites in biological samples to provide information on pathway activity, which provides a suitable approach for the study of osteoporosis. Non-targeted metabolomics platforms aim to enlarge the coverage of endogenous metabolites for a better understanding metabolic pathways or screening potential biomarkers. Thus, the challenges for untargeted metabolomics are detection, discovery and identification of differential metabolites. Targeted metabolomics methods focused on a limited number of compounds and provides sensitive and precise measurement of metabolites. The combination of the two approaches has greatly facilitated the discovery of biomarkers and the understanding of pathophysiological mechanisms (Xuan et al., 2020).

Changes in human serum metabolites might reflect pathophysiological alterations caused by various diseases (Shu et al., 2020, 19). Here, metabolic alternations in patients with osteoporosis were analyzed by untargeted metabolomic and lipidomic methods. To better understand the metabolic deregulations occurred in the patients, WGCNA algorithm and multivariate statistical methods were applied. Then targeted metabolomics method performed on a triple quadrupole MS was employed to obtain an in-depth measurement of the key metabolites and their related compounds. The quantitative results may help understanding the metabolic pathway and the establishment of a diagnostic panel, which enables the diagnostic and treatment applications in the clinic.

MATERIALS AND METHODS

Reagents and Solutions

Mass spectrometry level methanol, acetonitrile, isopropanol, formic acid and ammonium acetate were purchased from Fisher Scientific (Fair Lawn, United States). Mass spectrometry level ammonium bicarbonate and methyl tert-butyl ether (MTBE) were purchased from Sigma-Aldrich (St. Louis, United States). Ultra-pure water (18.2 m Ω cm) was used to prepare using Milli-Q purified water system (Merck KGaA, Darmstadt, Germany). Reference bile acid standards and isotope internal standards were purchased from Avanti Polar Lipids (Alabama, United States), Cayman Chemical (Ann Arbor, United States), Cambridge Isotope Laboratories Inc. (Tewksbury, United States), IsoSciences (Ambler, United States), Sigma-Aldrich (St. Louis, United States) and Toronto Research Chemicals (Toronto, Canada). For more information about standards, please referred to **Supplementary Table S1**.

Participants and Criteria

From June 2020 to January 2021, serum samples were collected from osteoporosis patients (OS group, n = 32) at the First Affiliated Hospital of Dalian Medical University. The OS group inclusion criteria were based on the 2014 National Osteoporosis Foundation (NOF) clinical guidelines (Cosman et al., 2014). The exclusion criteria included any mental or organic diseases, cancer, metabolic or hereditary bone disease, and hormone use in the past 6 mo. The serum samples of the control group (Con group, n = 32) were collected from health individuals at an admission physical examination. The age and sex constituent ratio of the control group matched that of the OS group, and the controls did not have any of the above-mentioned OS group exclusion criteria. All patients signed informed consent forms, and the project was approved by the Ethics Committee of First Affiliated hospital of Dalian Medical University.

Serum Sample Collection and Pretreatment

Serum samples were collected from OS patients on the first morning in a fasted state. Likewise, all Con samples were collected at the same time point and under the same fasting conditions as the OS samples were. All samples were immediately stored in a −80°C freezer and thawed at 4°C before pre-treatment. First, 150 μl of each sample was transferred to 1 ml 96-DeepWell plates (Thermo Scientific, United States), and then, 600 μl of methanol was added to the sample to precipitate the protein. Next, the mixture was vortexed for 5 min for better mixing and distribution and centrifuged at 5300 RPM for 20 min (4°C). Two replicates of the 200 μl upper layer were transferred to 450 μl 96-well plates (Thermo Scientific, United States); the samples were concentrated and dried by vacuum centrifugation. The polar metabolite extractions in these two plates were redissolved for positive and negative ion detection with untargeted metabolomics analysis. The remaining upper layers of all samples were mixed and similarly distributed at 200 μl per replicate as quality control (QC) samples (Salem et al., 2016).

To extract lipids from serum, 120 μl methanol was added to 20 μl of sample in a 1.5 ml EP tube (Axygen, United States). Next, the mixture was vortexed for 180 s, and 360 μl of methyl tert-butyl ether (MTBE) and 100 μl of ultrapure water were subsequently added to the solution. The mixture was vortexed for 10 min, kept at room temperature for another 10 min, and finally centrifuged at 13,000 × g for 15 min (4°C). 200 μl of lipid extract from the upper layer was transferred to a 1.5 ml EP tube and dried, similar to the protocol for the polar metabolite extractions described above. The lipid extractions were then redissolved for lipidomics analysis. QC samples of lipids were also prepared.

Moreover, a standard curve configuration was essential for metabolite-targeted quantification. Therefore, we precisely weighed the standards and adjusted the concentration to 1.0 mg ml^{-1} as a stock solution. An appropriate volume of each stock solution was diluted step by step to 465 μg L^{-1}, 232.5 μg L^{-1}, 116.25 μg L^{-1}, 58.125 μg L^{-1}, 29.0625 μg L^{-1}, 14.531 μg L^{-1}, 7.266 μg L^{-1}, 3.633 μg L^{-1}, 1.816 μg L^{-1}, 0.908 μg L^{-1}, 0.454 μg L^{-1}, 0.227 μg L^{-1} and 0.114 μg L^{-1} with the extraction solution. Next, 80 μl of each sample was transferred to 1 ml 96-DeepWell plates, and 320 μl of methanol: acetonitrile (1:1, v:v), which included a 50 ng ml^{-1} bile acid isotope internal standard, was added. After 5 min of vortexing, the mixture was centrifuged at 5300 RPM at 4°C for 20 min. The 260 μl upper layer was transferred to 450 μl 96-well plates and dried as described above. Afterwards, the extraction was redissolved for bile acid-targeted metabolomics analysis. The mixture of QC samples was also distributed at 260 μl per replicate and dried (Choucair et al., 2020).

Untargeted Metabolomic and Lipidomic Analysis

The UHPLC-HRMS system, which was used for untargeted metabolomics analysis, was composed of an Ultimate 3000 ultra-high performance liquid chromatograph and Q Exactive Quadrupole-Orbitrap High-Resolution Mass Spectrometer (Thermo Scientific, United States).

The polar metabolite extracts were separated by reversed-phase chromatography for positive and negative ion detection. Metabolites were separated by using an Excel 2 C18-PFP column (3.0 μm, 2.1 × 100 mm; ACE Co., United Kingdom) for positive detection and eluted with 0.1% formate/water as mobile phase A and acetonitrile as mobile phase B. The linear gradient ramped from 2% mobile phase B to 98% in 10 min. For the negative detection mode, the mobile phases consisted of water (phase A) and acetonitrile/methanol (phase B), both of which contained ammonium bicarbonate buffer salt, and were employed to elute metabolites separated on an Acquity HSS C18 column (1.8 μm, 2.1 × 100 mm; Waters Co., United States). The mobile phase gradient was as follows: 0 min 2% phase B ramped to 100% in 10 min, and another 5 min was used for column washing and equilibration. The flow rate, injection volume and column temperature of both the positive and negative modes were set at the same conditions: 0.4 ml min^{-1}, 5 μl and 50°C.

The chromatographic separation for lipidomic was carried out in positive ionization detection mode. An Accucore C30 core-shell column (2.6 μm, 2.1 × 100 mm; Thermo Scientific, United States) was utilized for lipid molecule separation at 50°C, and the lipids were eluted with 60% acetonitrile in water (phase A) and 10% acetonitrile in isopropanol (phase B), both of which contained 10 mM ammonium formate and 0.1% formate. The separation gradient was optimized as follows: initial 10% B ramping to 50% in 5 min and further increasing to 100% in 23 min. The other 7 min were used for column washing and equilibration using a 0.3 ml min^{-1} flow rate.

For polar metabolite detection, the Quadrupole-Orbitrap mass spectrometer was operated under identical ionization parameters with a heated electrospray ionization source except ionization voltage: sheath gas, 45 arb; aux gas, 10 arb; heater temperature, 355°C; capillary temperature, 320°C and S-Lens RF level, 55%. The metabolomic extracts were profiled in full scan mode under 70,000 FWHM resolution with AGC 1×10^6 and 200 ms max injection time. Data were acquired using a scan range of 70–1,000 m z^{-1}. The lipid molecules were ionized using the same parameters mentioned above. At a 70,000 full width half maximum (FWHM) full scan resolution, the settings differing from those of the polar metabolite analysis included the 300–2000 m z^{-1} scan range and AGC target 3×10^6.

Targeted Metabolomics Analysis

A total of 66 bile acids (**Supplementary Table S2**) were scanned and quantified on a Waters Acquity UPLC (Waters Corp., Milford, United States) coupled with a Sciex 5500+ triple quadrupole (QQQ) mass spectrometer (AB Sciex, Singapore). The bile acids were chromatographically resolved on an C18-PFP column (3 μm, 2.1 × 50 mm; ACE, United Kingdom) after 2.5 μl aliquots of bile acid extract was injected. Water containing 2 mM ammonium acetate was used as phase A, and acetonitrile was used as phase B. The chromatographic gradient ramped from 17% phase B to 30% in 10 min, ramped to 55% in 3 min, rapidly climbed to 95% in 1 min and remained for 3 min; another 5 min was used for column washing and equilibration. The flow rate was set at 0.4 ml min^{-1}. The metabolites were ionized by a TurboV heated electrospray ionization source and then detected by scheduled multiple reaction monitoring mode. The main parameters were optimized as follows: negative ion spray voltage was −4.5 kV, curtain gas pressure was 35 psi, ion gas 1 and 2 pressure were 50 psi, and heater temperature was 550°C.

Date Processing

According to the recommendation of the Metabolomics Standardization Initiative (MSI) (Sumner et al., 2007), first-level annotation required chromatographic retention time, primary mass spectrometry and secondary mass spectrometry information, which was consistent with the standards. At the second level, the polar metabolites were structurally annotated by searching against local databases, mzCloud library (Thermo Scientific, United States), Kyoto Encyclopedia of Genes and Genomes (KEGG) and the Human Metabolome Database (HMDB). On the other hand, untargeted lipid data were processed with LipidSearch (Thermo Scientific, United States) software, including peak picking and lipid identification. For metabolite identification or structural annotation, accuracy of the mass of a precursor within ±10 ppm was a prerequisite. The AUC values were extracted as relative quantification information of polar metabolites and lipids with TraceFinder software (Thermo Scientific, United States). Regarding targeted bile acid detection, internal calibration was conducted with Analyst software and OS-MQ software (AB SCIEX, Singapore) for quantitative analysis of bile acids.

Statistical Analysis

We used R package "pwr" for classical Power Analysis. Next, metabolites with missing value percentages above 50% were

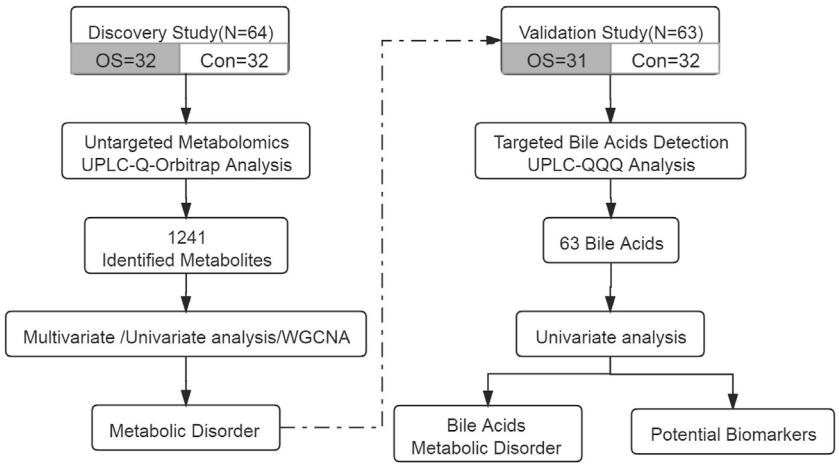

FIGURE 1 | The design and workflow of this study.

excluded, and then the K-nearest algorithm (KNN sample-wise) was employed to impute the missing values. For the purpose of guaranteed uniqueness of metabolites and lipids, molecules detected by multiple methods were retained only once. The normalization of untargeted metabolomics data consisted of three steps: sample calibration, data transformation and data scaling. Firstly, Sample calibration was used to correct sample reproducibility due to batch effects or systematic errors in detection. Secondly, we performed Log transformation on untargeted metabolomics data, which was often used to convert data into normal distribution. Finally, UV scaling was used to pre-process orthogonal projections to latent structures discriminant analysis (OPLS-DA) data. For the bile acid targeted analysis, the mass concentration of serum extraction was transformed to the molar concentration of the original sample based on the molecular weight and dilution factor. Multivariate analysis, such as principal component analysis (PCA) and OPLS-DA, was conducted with SIMCA-P software (Umetrics, Sweden). Univariate analysis including independent samples Student's t-test *p*-value, Benjamini-Hochberg false discovery rate q-value (p-value < 0.05, q-value < 0.2) (Oshansky et al., 2014; Park et al., 2019; Shi et al., 2020, 16) and heatmap drawing was performed on the MetaboAnalyst website (http://www.metaboanalyst.ca) (Xia and Wishart, 2010b, 2010a; Chong et al., 2018). We applied the WGCNA package in the R environment Version 4.0.3 (R Core Team, 2020) to construct co-expression modules of highly correlated metabolites (Langfelder and Horvath, 2008). Moreover, receiver operating characteristic (ROC) curves and box plots were generated with GraphPad Prism 8.0 (GraphPad Software Inc., United States). Binary logistic regression and biomarker model establishment were based on SPSS Statistics 26.0 software (IBM, United States). Cytoscape 3.8.0 (https://cytoscape.org/, Cytoscape Consortium, United States) was used for biological network construction and visualization (Shannon et al., 2003).

RESULTS

Study Design and Clinical Characteristics

Serum samples from 32 patients with osteoporosis and 32 healthy individuals were collected. The annotated serum metabolites were compared and clustered by multivariate analysis, univariate analysis and WGCNA. To clarify the results, targeted analysis of bile acids was performed using another aliquot of the serum samples from the same two groups. Diagnostic model was established using the quantitative BAs' data. The workflow of this study was summarized in **Figure 1**.

No significant differences were found in the clinical characteristics including sex, age, glucose, creatinine, and etc. between the matched groups of Controls and OS. Detailed clinical information is listed in **Supplementary Table S3**.

Untargeted metabolomics was employed to describe the characteristics of serum metabolism among the participants. A total of 1,241 metabolites (1,083 metabolites remaining after data screening and cleaning) were identified. In addition, 366 polar metabolites accounted for 33.8% of the total, and 717 lipids accounted for 66.2%. Among them, 266 triacylglycerols (TGs) accounted for the largest proportion (24.6%). The total ion chromatogram (TIC) displayed the panoramic view of non-targeted metabolomics. The extracted ion chromatogram (XIC) provided a visual presentation of targeted bile acid detection (**Supplementary Figure S1**). The coefficient of variation (CV) distribution of QC, which indicated the reproducibility of the detection method, is shown in **Supplementary Figures S2,S3**.

Metabolic Profiling of Osteoporosis

To illustrate the metabolic alterations between the two groups, OPLS-DA of polar metabolites (**Figure 2A**) and lipids (**Figure 2B**) were used. An overall separation can be observed between the two groups, in both platforms. Volcano plots of polar metabolites (**Figure 2D**) and lipids (**Figure 2E**) show the

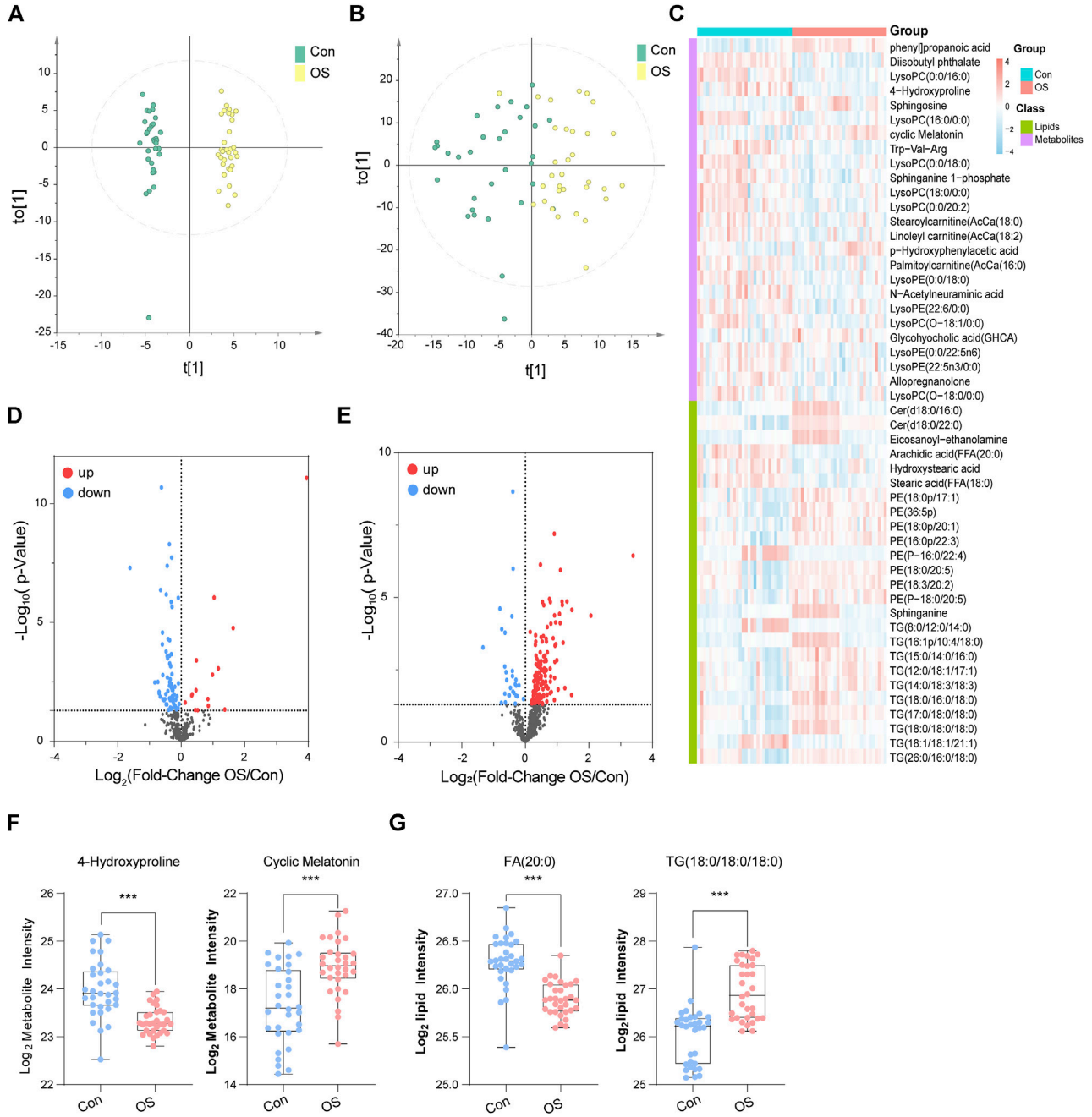

FIGURE 2 | OPLS-DA score plots of metabolites **(A)** and lipids **(B)**. In the heatmap, blue indicates lower relative intensity, and red indicates higher relative intensity **(C)**. The red dots of the metabolites **(D)** and lipids **(E)** in the volcano plots indicated an increase in the OS group, and the blue dots indicate a decrease. 4-Hydroxyproline and cyclic melatonin were representative metabolites **(F)**. FA (20:0) and TG (18:0/18:0/18:0) were representative lipids **(G)**.

differences and average intensity change ratio between the two groups. Most of the polar metabolites decreased, while the lipids increased in the OS group. The relative contents of these metabolites could be visualized by a heat map (**Figure 2C**). The differential metabolites identified mainly included amino acids (AAs), fatty acids (FAs), glycerophosphocholines (PCs), glycerophosphoethanolamine (PE), TGs and BAs. Notably, the serum contents of lysophosphocholines (LPC) in the OS group was significantly lower than that in the Con group, which was in contrast to the trends of other lipids, such as PE and TG. In **Figures 2F,G**, 4-Hydroxyproline and FA (20:0) levels decreased significantly in the OS group, while cyclic Melatonin and TG (18:0/18:0/18:0) levels increased obviously in the OS group (**Supplementary Tables S4,S5**).

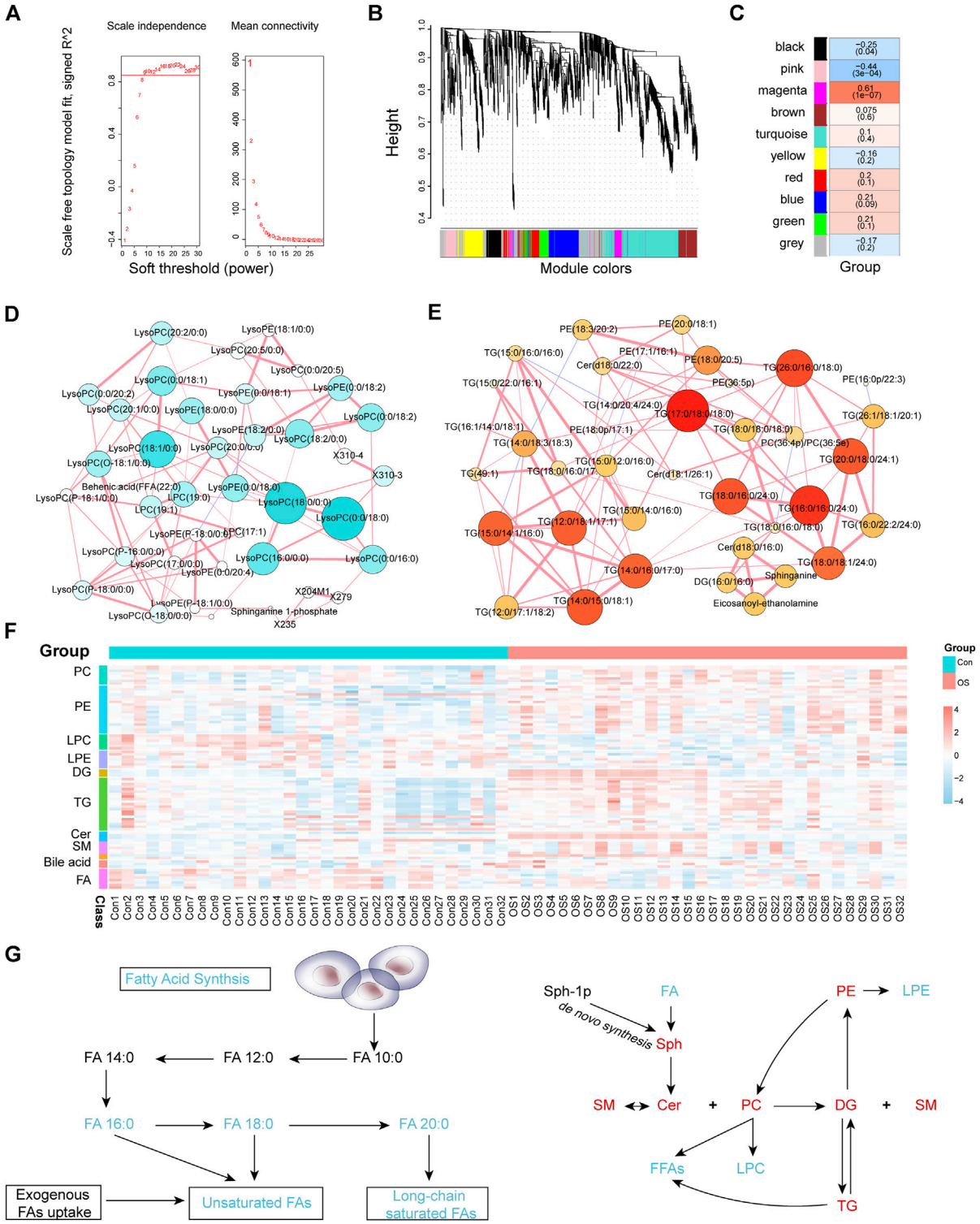

FIGURE 3 | Soft threshold selection was based on scale-free topology R2 and mean connectivity **(A)**. A module cluster tree was used to visualize the distribution of metabolites in each module **(B)**. The correlation coefficients and *p*-values between modules and osteoporosis **(C)**. The MMI networks of the pink **(D)** and magenta **(E)** modules. The correlation of MMI was based on debiased sparse partial correlation (DSPC). The heatmap of osteoporosis-related metabolites and lipids that were differentially expressed between the OS and Con groups **(F)**. Schematic plot of FA synthesis metabolism and the mutual transformation between subclasses of lipids **(G)**. Black text represents undetected metabolites, red text represents significantly enriched metabolites, and green text represents significantly depleted metabolites when the OS group is compared with the Con group.

Construction of Co-expression Modules by WGCNA

To find out the interaction of the differential metabolites, WGCNA, an innovative analysis method, was used to construct a metabolite interaction network considering weighted factors. According to the relative intensity data of 1,083 metabolites, the correlation between the metabolic co-expression module and the clinical phenotype of osteoporosis was analysed by the WGCNA software package. First, the hierarchical clustering method was used to check the outliers, and no outliers were found. The soft threshold was 9 (scale-free topology R2 = 0.882, slope = −1.29, mean connectivity = 20.5); subsequently, the merged cut height was set to 0.2 with a minimum module size of 30. A total of 10 modules were obtained, among which, the grey module was a group of metabolites that could not be included in the co-expression network construction. This module should be reduced as much as possible for the robustness of the model. Pearson correlation analysis was used to evaluate the correlation between modules (**Supplementary Table S6**). The results suggested that there was a significant positive correlation among the green, red and blue modules and that there were no significant negative correlations among modules. The differences between the osteoporosis patients and healthy controls were the clinical features those are concerned about. From **Figure 3C**, we found that the pink (**Supplementary Table S7**) and magenta (**Supplementary Table S8**) modules were significantly related to the occurrence of osteoporosis. The metabolites in pink were expressed at low levels in the OS group, while the change trend of the metabolites in the magenta module was the opposite.

Metabolite-Metabolite Interaction (MMI) Network Construction

The differences between the OS group and Con group were compared in the two modules. The pink module contained 43 metabolites, of which 25 metabolites were significantly downregulated and none upregulated (**Supplementary Figure S4G**). In addition, levels of all 45 metabolites in the magenta module were significantly elevated (**Supplementary Figure S4I**). Furthermore, metabolites with the greatest fold change (FC) ratio between the two groups in each module were selected as representatives. LPC (18:0/0:0) and LPC (16:0/0:0) in the pink module decreased significantly in the OS group. In contrast, TG (17:0/18:0/18:0) and TG (16:0/16:0/24:0) were significantly higher in the OS group than in the Con group. To identify the relationship between the key metabolites in each module, an MMI network was constructed based on the internal connectivity of the metabolites. Surprisingly, the MMI of the pink module (**Figure 3D**; **Supplementary Table S9**) indicated that among the various metabolites downregulated in the OS group, the highly weighted metabolites were mainly LPC. Moreover, the MMI of the magenta module suggested that the upregulated metabolites in the OS group were mainly TG and PE (**Figure 3E**; **Supplementary Table S10**).

Disorders of Lipids Pathways

Patients with osteoporosis had significant abnormal lipid metabolism (**Supplementary Table S11**). As shown in **Figures 3F,G**, levels of PC, PE, diacylglycerols (DG), TG, ceramides (Cer) and sphingomyelins (SM) in the serum of osteoporosis patients were dramatically increased. The relative serum concentrations of LPC, lysophosphatidylethanolamine (LPE), Acetylcarnitine and FA, especially saturated FA, decreased in patients with osteoporosis. In addition, most of the FA chains in TG and PE were long-chain saturated FAs. The changes in different BAs also varied between the two groups. These characteristics indicated that dysregulation of lipid metabolism may contribute to the occurrence of osteoporosis.

Dysregulation of BAs

To validate whether abnormal bile acid metabolism is involved in the occurrence of osteoporosis, a targeted method was carried out on the same batch of serum samples (**Supplementary Table S12**). 49 bile acids were detected from the samples. Similarly, the OPLS-DA score plot showed a significant separation between the OS group and the Con group (**Figure 4A**). The volcano plot indicated that five BAs (or ratios) decreased and that 11 increased in osteoporosis (**Figure 4B**). Furthermore, the concentrations of 16 BAs (or ratios) in each sample are shown in a heatmap (**Figure 4C**).

A diagnostic panel was established based on differentially expressed BAs using binary logistic regression. After variable screening, the box plot of five potential BAs, glycohyocholic acid (GHCA), dehydrocholic acid (DHCA), deoxycholic acid 3-glucuronide (DCA-3G), ursocholic acid (UCA), and deoxycholic acid/cholic acid (DCA/CA), showed that GHCA, DCA-3G, and DCA/CA levels in osteoporosis patients were significantly higher than those in healthy controls. In addition, DHCA and UCA, which were classified as hyocholic acid species (HCAs), were higher in healthy controls (**Figure 4D**). This diagnostic panel for osteoporosis was concluded as follows: $\mathrm{Logit}[P\ ] = 24.063 \times GHCA - 53.524 \times DHCA - 21.971 \times UCA + 54.302 \times DCA - 3G + 0.615 \times DCA/CA - 123.056$ In the equation, P is the predicted probability of osteoporosis, and each BA represents its serum concentration (nmol L^{-1}). The AUC values of the five bile acid biomarkers were as follows: GHCA, AUC = 0.859 (0.7756–0.962); DHCA, AUC = 0.841 (0.744–0.937); DCA-3G, AUC = 0.928 (0.867–0.990); UCA, AUC = 0.741 (0.617–0.864); and DCA/CA, AUC = 0.718 (0.591–0.844). Noticeably, performance of the diagnostic panel in the diagnosis of osteoporosis was superior to that of each bile acid biomarker alone (**Figure 4E**). Moreover, the prediction accuracy of this diagnostic panel was 100% (**Figure 4F**). The results highlighted the diagnostic potential of bile acids.

DISCUSSION

In the present study, we characterized the differences in metabolite and lipid profiles between osteoporosis patients and healthy volunteers using LC-MS metabolomics. WGCNA was utilized to identify metabolites that are closely related to

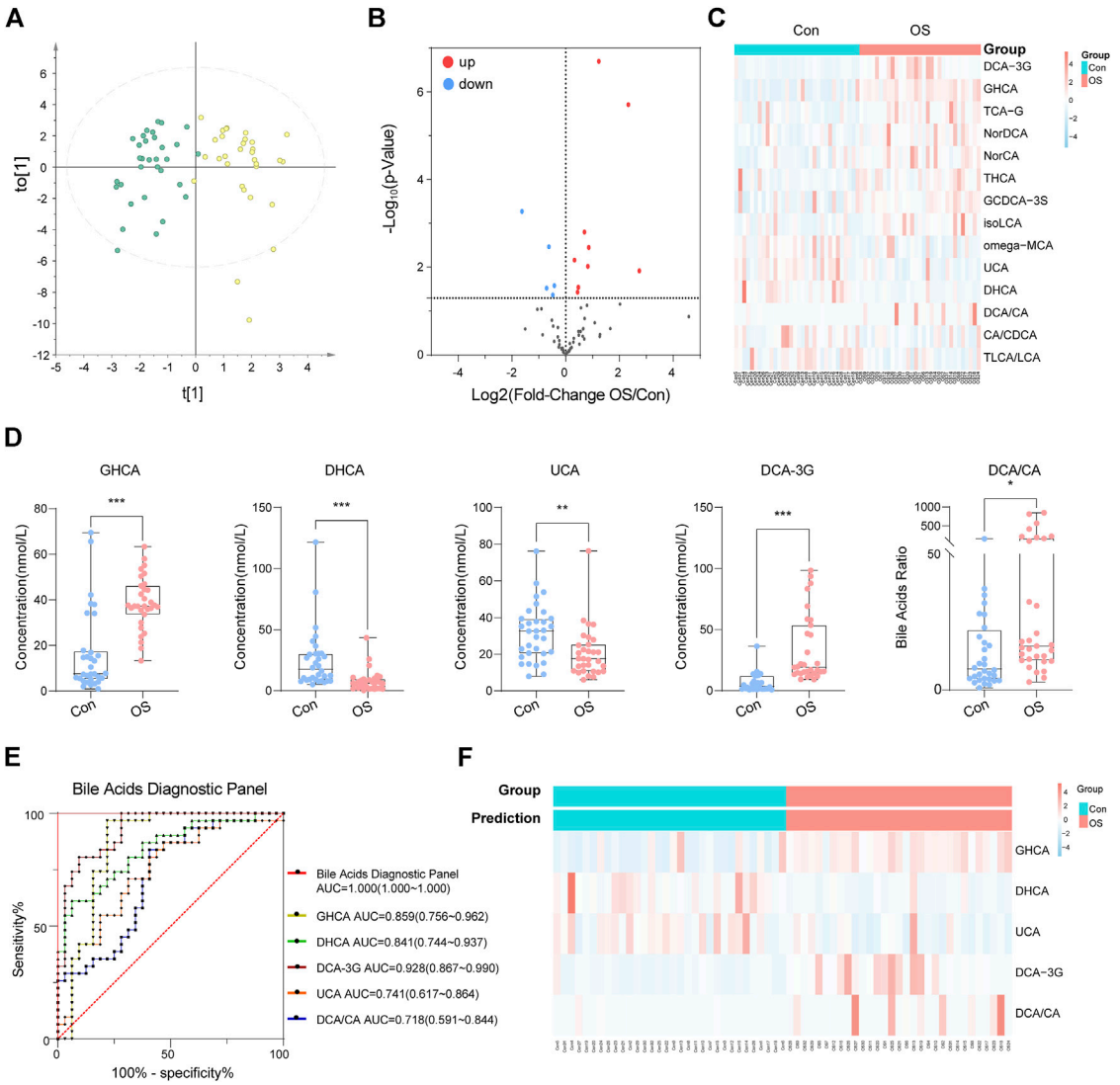

FIGURE 4 | OPLS-DA plot of absolute quantitation of BAs **(A)**. Volcano plot of absolute quantitation of BAs **(B)**. Heatmap of selected BAs that were significantly changed in the volcano plot **(C)**. After analysis by binary logic regression, five BA biomarkers were visualized in the form of box plots **(D)**. The ROC curve of the above five biomarkers and the diagnostic panel **(E)**. The prediction accuracy of the diagnostic panel is shown by a heatmap **(F)**.

osteoporosis onset. Lipid metabolism disorders, mainly abnormalities in fatty acid metabolism, sphingolipid metabolism and BA metabolism, were involved in the initiation of osteoporosis. BAs are involved in lipid digestion and are also important signalling molecules in lipid metabolism. The difference in BAs between osteoporosis patients and healthy volunteers was significant, especially in HCAs. Moreover, the AUC of the 5-metabolite panel provides a promising diagnostic potential. These results demonstrated the role of BAs in osteoporosis.

LPC and LPE are components molecular of membrane and take part in signal transduction (Bai et al., 2014; Rindlisbacher et al., 2018). These compounds are converted from PC and PE by phospholipase A2 (PLA2), a calcium-dependent protein (Hirabayashi et al., 2017). The levels of lyso-lipids were decreased in patients with osteoporosis, while PC and PE levels were increased. The results implied that PLA2 enzyme activity is decreased due to disorders of calcium and phosphorus metabolism, leading to a decrease in LPC, LPE and free fatty acid (FFA) levels. Studies have shown that LPC has pro-inflammatory activity and promotes osteoblast apoptosis (Brys et al., 2019). The accumulation of LPC in bone tissue may lead to the decrease of serum LPC.

Cholesterol is the precursor of vitamin D, bile acids, and steroid hormones, all of which are important regulators of bone metabolism (Hoppel, 2003; Hernandez et al., 2019). BAs regulate the homeostasis of cholesterol, glucose and fat-soluble vitamins, and play a crucial role in maintaining mineral homeostasis (Ma and Patti, 2014; Ruiz-Gaspà et al., 2020). DCA and TCA differed notably in bone tissues of old mice and young mice models of

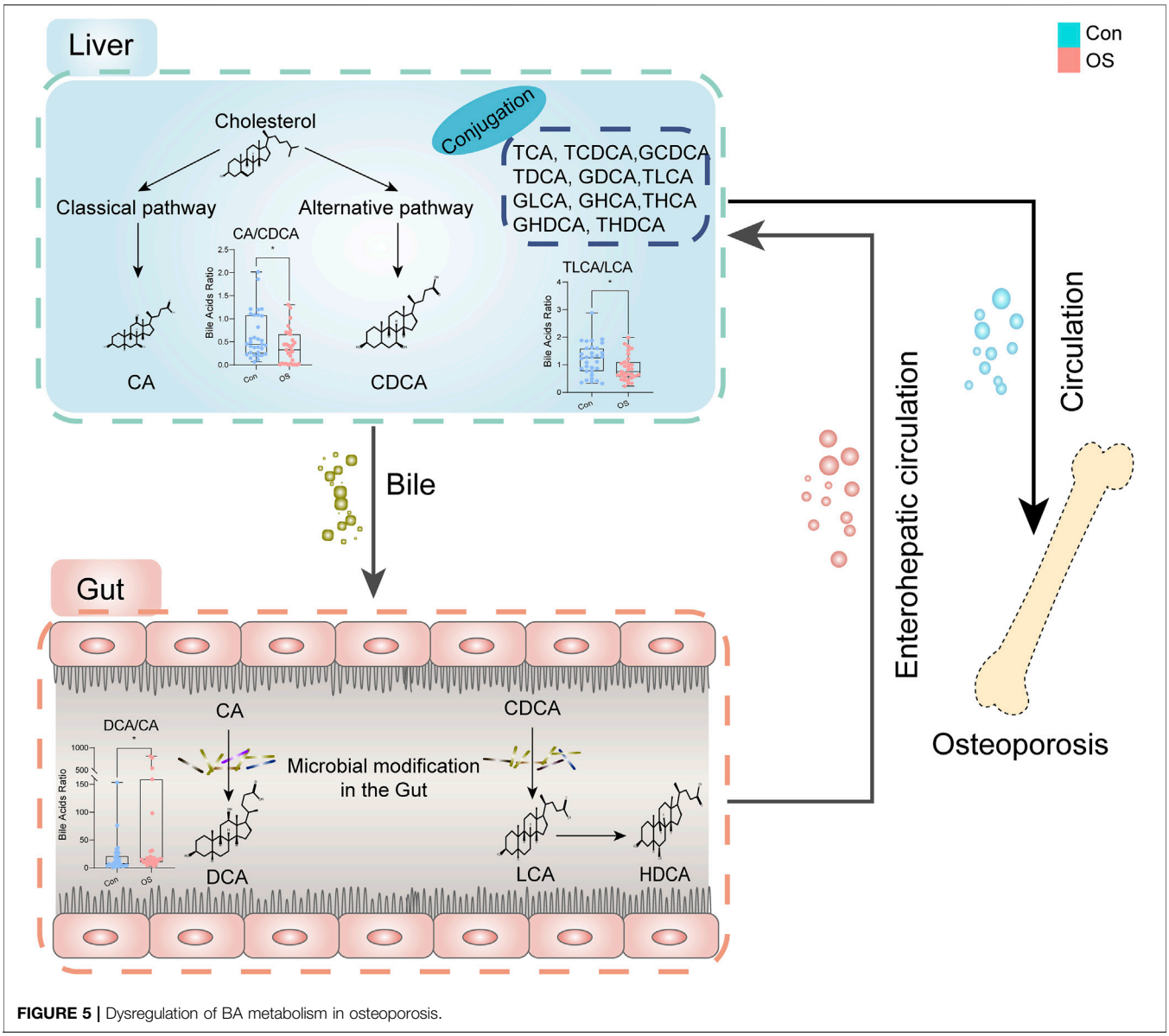

FIGURE 5 | Dysregulation of BA metabolism in osteoporosis.

osteoporosis in the literature (Nam et al., 2018). In our results, BAs changed significantly among osteoporosis patients. However, no significant differences in serum CA, chenodeoxycholic acid (CDCA), DCA and lithocholic acid (LCA). Nevertheless, their derivatives, such as DCA-3G, 23-nordesoxycholic acid (Nor-DCA) and isolithocholic acid (iso-LCA), were significantly different between the two groups. Further exploration of the functions of these BAs is needed.

Interestingly, a significant deregulation of HCAs was found in this study. HCAs are a group of 6a-hydroxylated bile acids that account for a minimal proportion of the total BAs in humans and mice but constitute nearly 80% of BAs in pigs (Spinelli et al., 2016). A recent study reported that HCAs were involved in maintaining glucose homeostasis. HCA promoted glucagon-like peptide-1 (GLP-1) production in enteroendocrine cells by simultaneously activating the membrane G protein-coupled receptor TGR5 and inhibiting farnesoid X receptor (FXR) in a dose-dependent manner, which enhanced insulin secretion and eventually reverted to normoglycaemia (Zheng et al., 2021). Epidemiological investigations found that patients with diabetes have a higher risk of osteoporosis. Succinate enhanced osteoclasts by activating succinic acid receptors in diabetes-associated osteoporosis (Guo et al., 2017). However, in this study, GHCA and taurohyocholic acid (THCA) levels were significantly increased, but there was no significant difference in blood glucose between the two groups. Therefore, the correlations between HCAs and osteoporosis are independent from the occurrence of diabetes.

The molecular ratio of the upstream and downstream of the metabolic pathway is usually used to reflect the catalytic enzymatic activity (MahmoudianDehkordi et al., 2019; Nho et al., 2019). To investigate the mechanisms contributing to

BA alterations in osteoporosis, the ratios of three types of bile acids were compared. The results revealed that bile acid metabolism was converted from the classical pathway to the alternative pathway (CA: CDCA). Since the gut microbiota is believed to be closely connected to osteoporosis, the dysregulation of the gut flora may alter BA levels consequently (Jones et al., 2014; Devlin and Fischbach, 2015; Wahlström et al., 2016). A significant change in secondary BAs was found according to the ratio (DCA:CA). CA is affected by bacterial 7A-dehydroxylase in the gut to produce DCA, which has cytotoxic effects and can result in the destruction of the mitochondrial membrane (Schulz et al., 2013). There was a change in the progression of taurine conjugation of secondary BAs in the liver (taurolithocholic acid (TLCA): LCA). These results indicated that gut microbiota and related BA metabolism may act as an important role in the occurrent osteoporosis (**Figure 5**).

Although our study provided original insights into the pathogenesis of osteoporosis, there were still some limitations. First, the sample size was relatively small, and therefore, we could not stratify the metabolites associated with disease progression according to severity. Second, although the diagnostic model had good diagnostic performance, it still needs to be validated in a larger cohort. Finally, this study was a retrospective study, and the causal relationship between differential metabolites and osteoporosis requires further investigation.

CONCLUSION

Our integrated metabolomic strategy was demonstrated to be practical for the screen of novel biomarkers, which highlights the lipids and bile acids metabolism disorders in patients with osteoporosis. Bile acids change from the classical pathway to the alternative pathway, and HCAs are involved in the occurrence and development of osteoporosis. The deregulation of lipids and the BAs provides a potential basis for the diagnosis and treatment of osteoporosis. Our study confirmed the importance of the combination of untargeted and targeted metabolomic method especially for the trnslational research in the clinic.

DATA AVAILABILITY STATEMENT

The original contributions presented in the study are included in the article/**Supplementary Material**, further inquiries can be directed to the corresponding author/s.

ETHICS STATEMENT

The studies involving human participants were reviewed and approved by Ethics Committee of First Affiliated Hospital of Dalian Medical University. The patients/participants provided their written informed consent to participate in this study.

AUTHOR CONTRIBUTIONS

DD and CP contributed to the design of the study and drafting and revising of the manuscript; ZW directed the LC-MS analysis; YS and CL participated in the collection of serum samples; HX edited the manuscript. PY designed the study and revised the manuscript, DS reviewed the manuscript.

FUNDING

This research was funded by National Key Research and Development Program of China (No. 2018YFE0195200), the National Natural Science Foundation of China (No. 81873156), and Young Science and Technology Talent Project of the Education Department of Liaoning Province China (No. LZ2020075).

SUPPLEMENTARY MATERIAL

The Supplementary Material for this article can be found online at: https://www.frontiersin.org/articles/10.3389/fphar.2021.725341/full#supplementary-material

REFERENCES

Bai, Y., Zhang, H., Sun, X., Sun, C., and Ren, L. (2014). Biomarker Identification and Pathway Analysis by Serum Metabolomics of Childhood Acute Lymphoblastic Leukemia. *Clinica Chim. Acta* 436, 207–216. doi:10.1016/j.cca.2014.05.022

Brys, A. K., Rodriguez-Homs, L. G., Wennerberg, S., Hall, R. P., and Nicholas, M. W. (2019). Anetoderma Associated with a Succinate Dehydrogenase Gene Mutation. *JAMA Dermatol.* 155, 1317–1318. doi:10.1001/jamadermatol.2019.2579

Chong, J., Soufan, O., Li, C., Caraus, I., Li, S., Bourque, G., et al. (2018). MetaboAnalyst 4.0: Towards More Transparent and Integrative Metabolomics Analysis. *Nucleic Acids Res.* 46, W486–W494. doi:10.1093/nar/gky310

Choucair, I., Nemet, I., Li, L., Cole, M. A., Skye, S. M., Kirsop, J. D., et al. (2020). Quantification of Bile Acids: A Mass Spectrometry Platform for Studying Gut Microbe Connection to Metabolic Diseases. *J. Lipid Res.* 61, 159–177. doi:10.1194/jlr.RA119000311

Compston, J. E., McClung, M. R., and Leslie, W. D. (2019). Osteoporosis. *The Lancet* 393, 364–376. doi:10.1016/S0140-6736(18)32112-3

Cosman, F., de Beur, S. J., LeBoff, M. S., Lewiecki, E. M., Tanner, B., Randall, S., et al. (2014). Clinician's Guide to Prevention and Treatment of Osteoporosis. *Osteoporos. Int.* 25, 2359–2381. doi:10.1007/s00198-014-2794-2

Cruz-Jentoft, A. J., and Sayer, A. A. (2019). Sarcopenia. *The Lancet* 393, 2636–2646. doi:10.1016/S0140-6736(19)31138-9

Curtis, E. M., Moon, R. J., Harvey, N. C., and Cooper, C. (2017). The Impact of Fragility Fracture and Approaches to Osteoporosis Risk Assessment Worldwide. *Bone* 104, 29–38. doi:10.1016/j.bone.2017.01.024

Devlin, A. S., and Fischbach, M. A. (2015). A Biosynthetic Pathway for a Prominent Class of Microbiota-Derived Bile Acids. *Nat. Chem. Biol.* 11, 685–690. doi:10.1038/nchembio.1864

Fang, H., Zhang, H., Wang, Z., Zhou, Z., Li, Y., and Lu, L. (2020). Systemic Immune-inflammation Index Acts as a Novel Diagnostic Biomarker for Postmenopausal Osteoporosis and Could Predict the Risk of Osteoporotic Fracture. *J. Clin. Lab. Anal.* 34, e23016. doi:10.1002/jcla.23016

Guo, Y., Xie, C., Li, X., Yang, J., Yu, T., Zhang, R., et al. (2017). Succinate and its G-Protein-Coupled Receptor Stimulates Osteoclastogenesis. *Nat. Commun.* 8, 15621. doi:10.1038/ncomms15621

Hernandez, J. A., Castro, V. L., Reyes-Nava, N., Montes, L. P., and Quintana, A. M. (2019). Mutations in the Zebrafish Hmgcs1 Gene Reveal a Novel Function for Isoprenoids During Red Blood Cell Development. *Blood Adv.* 3, 1244–1254. doi:10.1182/bloodadvances.2018024539

Hirabayashi, T., Anjo, T., Kaneko, A., Senoo, Y., Shibata, A., Takama, H., et al. (2017). PNPLA1 Has a Crucial Role in Skin Barrier Function by Directing Acylceramide Biosynthesis. *Nat. Commun.* 8, 14609. doi:10.1038/ncomms14609

Hoppel, C. (2003). The Role of Carnitine in Normal and Altered Fatty Acid Metabolism. *Am. J. Kidney Dis.* 41, S4–S12. doi:10.1016/s0272-6386(03)00112-4

Jones, M. L., Martoni, C. J., Ganopolsky, J. G., Labbé, A., and Prakash, S. (2014). The Human Microbiome and Bile Acid Metabolism: Dysbiosis, Dysmetabolism, Disease and Intervention. *Expert Opin. Biol. Ther.* 14, 467–482. doi:10.1517/14712598.2014.880420

Komm, B. S., Morgenstern, D., A Yamamoto, L. L., and Jenkins, S. N. (2015). The Safety and Tolerability Profile of Therapies for the Prevention and Treatment of Osteoporosis in Postmenopausal Women. *Expert Rev. Clin. Pharmacol.* 8, 769–784. doi:10.1586/17512433.2015.1099432

Langfelder, P., and Horvath, S. (2008). WGCNA: An R Package for Weighted Correlation Network Analysis. *BMC Bioinformatics* 9, 559. doi:10.1186/1471-2105-9-559

Leslie, R. D., and Beyan, H. (2011). Metabolomics Makes a Mark: Early Changes Associated with Autoimmune Diabetes. *Diabetes* 60, 2688–2690. doi:10.2337/db11-1177

Liu, X., Liu, Y., Cheng, M., Zhang, X., and Xiao, H. (2015). A Metabolomics Study of the Inhibitory Effect of 17-Beta-Estradiol on Osteoclast Proliferation and Differentiation. *Mol. Biosyst.* 11, 635–646. doi:10.1039/c4mb00528g

Ma, H., and Patti, M. E. (2014). Bile Acids, Obesity, and the Metabolic Syndrome. *Best Pract. Res. Clin. Gastroenterol.* 28, 573–583. doi:10.1016/j.bpg.2014.07.004

MahmoudianDehkordi, S., Arnold, M., Nho, K., Ahmad, S., Jia, W., Xie, G., et al. (2019). Altered Bile Acid Profile Associates with Cognitive Impairment in Alzheimer's Disease-An Emerging Role for Gut Microbiome. *Alzheimer's Demen.* 15, 76–92. doi:10.1016/j.jalz.2018.07.217

Nam, M., Huh, J.-E., Kim, M.-S., Ryu, D. H., Park, J., Kim, H.-S., et al. (2018). Metabolic Alterations in the Bone Tissues of Aged Osteoporotic Mice. *Sci. Rep.* 8, 8127. doi:10.1038/s41598-018-26322-7

Nho, K., Kueider-Paisley, A., MahmoudianDehkordi, S., Arnold, M., Risacher, S. L., Louie, G., et al. (2019). Altered Bile Acid Profile in Mild Cognitive Impairment and Alzheimer's Disease: Relationship to Neuroimaging and CSF Biomarkers. *Alzheimer's Demen.* 15, 232–244. doi:10.1016/j.jalz.2018.08.012

Oshansky, C. M., Gartland, A. J., Wong, S.-S., Jeevan, T., Wang, D., Roddam, P. L., et al. (2014). Mucosal Immune Responses Predict Clinical Outcomes During Influenza Infection Independently of Age and Viral Load. *Am. J. Respir. Crit. Care Med.* 189, 449–462. doi:10.1164/rccm.201309-1616OC

Park, J. W., Hwang, S. R., Jeon, O.-C., Moon, H. T., and Byun, Y. (2013). Enhanced Oral Absorption of Ibandronate Via Complex Formation with Bile Acid Derivative. *J. Pharm. Sci.* 102, 341–346. doi:10.1002/jps.23413

Park, S.-M., Cho, H., Thornton, A. M., Barlowe, T. S., Chou, T., Chhangawala, S., et al. (2019). IKZF2 Drives Leukemia Stem Cell Self-Renewal and Inhibits Myeloid Differentiation. *Cell Stem Cell* 24, 153–165. doi:10.1016/j.stem.2018.10.016

Peng, B., Li, H., and Peng, X.-X. (2015). Functional Metabolomics: From Biomarker Discovery to Metabolome Reprogramming. *Protein Cell* 6, 628–637. doi:10.1007/s13238-015-0185-x

Rindlisbacher, B., Schmid, C., Geiser, T., Bovet, C., and Funke-Chambour, M. (2018). Serum Metabolic Profiling Identified A Distinct Metabolic Signature in Patients with Idiopathic Pulmonary Fibrosis - A Potential Biomarker Role for LysoPC. *Respir. Res.* 19, 7. doi:10.1186/s12931-018-0714-2

Ruiz-Gaspà, S., Guañabens, N., Jurado, S., Dubreuil, M., Combalia, A., Peris, P., et al. (2020). Bile Acids and Bilirubin Effects on Osteoblastic Gene Profile. Implications in the Pathogenesis of Osteoporosis in Liver Diseases. *Gene* 725, 144167. doi:10.1016/j.gene.2019.144167

Salem, M. A., Jüppner, J., Bajdzienko, K., and Giavalisco, P. (2016). Protocol: A Fast, Comprehensive and Reproducible One-step Extraction Method for the Rapid Preparation of Polar and Semi-polar Metabolites, Lipids, Proteins, Starch and Cell Wall Polymers from a Single Sample. *Plant Methods* 12, 45. doi:10.1186/s13007-016-0146-2

Sànchez-Riera, L., Carnahan, E., Vos, T., Veerman, L., Norman, R., Lim, S. S., et al. (2014). The Global Burden Attributable to Low Bone Mineral Density. *Ann. Rheum. Dis.* 73, 1635–1645. doi:10.1136/annrheumdis-2013-204320

Schulz, S., Schmitt, S., Wimmer, R., Aichler, M., Eisenhofer, S., Lichtmannegger, J., et al. (2013). Progressive Stages of Mitochondrial Destruction Caused by Cell Toxic Bile Salts. *Biochim. Biophys. Acta (Bba) - Biomembranes* 1828, 2121–2133. doi:10.1016/j.bbamem.2013.05.007

Shannon, P., Markiel, A., Ozier, O., Baliga, N. S., Wang, J. T., Ramage, D., et al. (2003). Cytoscape: A Software Environment for Integrated Models of Biomolecular Interaction Networks. *Genome Res.* 13, 2498–2504. doi:10.1101/gr.1239303

Shi, D., Xia, X., Cui, A., Xiong, Z., Yan, Y., Luo, J., et al. (2020). The Precursor of PI(3,4,5)P3 Alleviates Aging by Activating daf-18(Pten) and Independent of Daf-16. *Nat. Commun.* 11, 4496. doi:10.1038/s41467-020-18280-4

Shu, T., Ning, W., Wu, D., Xu, J., Han, Q., Huang, M., et al. (2020). Plasma Proteomics Identify Biomarkers and Pathogenesis of COVID-19. *Immunity* 53, 1108–1122. doi:10.1016/j.immuni.2020.10.008

Spinelli, V., Lalloyer, F., Baud, G., Osto, E., Kouach, M., Daoudi, M., et al. (2016). Influence of Roux-En-Y Gastric Bypass on Plasma Bile Acid Profiles: A Comparative Study Between Rats, Pigs and Humans. *Int. J. Obes.* 40, 1260–1267. doi:10.1038/ijo.2016.46

Sumner, L. W., Amberg, A., Barrett, D., Beale, M. H., Beger, R., Daykin, C. A., et al. (2007). Proposed Minimum Reporting Standards for Chemical Analysis. *Metabolomics* 3, 211–221. doi:10.1007/s11306-007-0082-2

Tarrant, S. M., and Balogh, Z. J. (2020). The Global Burden of Surgical Management of Osteoporotic Fractures. *World J. Surg.* 44, 1009–1019. doi:10.1007/s00268-019-05237-y

Wahlström, A., Sayin, S. I., Marschall, H.-U., and Bäckhed, F. (2016). Intestinal Crosstalk Between Bile Acids and Microbiota and its Impact on Host Metabolism. *Cel Metab.* 24, 41–50. doi:10.1016/j.cmet.2016.05.005

Wang, J., Yan, D., Zhao, A., Hou, X., Zheng, X., Chen, P., et al. (2019). Discovery of Potential Biomarkers for Osteoporosis Using LC-MS/MS Metabolomic Methods. *Osteoporos. Int.* 30, 1491–1499. doi:10.1007/s00198-019-04892-0

Xia, J., and Wishart, D. S. (2010a). MetPA: A Web-Based Metabolomics Tool for Pathway Analysis and Visualization. *Bioinformatics* 26, 2342–2344. doi:10.1093/bioinformatics/btq418

Xia, J., and Wishart, D. S. (2010b). MSEA: A Web-Based Tool to Identify Biologically Meaningful Patterns in Quantitative Metabolomic Data. *Nucleic Acids Res.* 38, W71–W77. doi:10.1093/nar/gkq329

Xuan, Q., Ouyang, Y., Wang, Y., Wu, L., Li, H., Luo, Y., et al. (2020). Multiplatform Metabolomics Reveals Novel Serum Metabolite Biomarkers in Diabetic Retinopathy Subjects. *Adv. Sci.* 7, 2001714. doi:10.1002/advs.202001714

Zheng, X., Chen, T., Jiang, R., Zhao, A., Wu, Q., Kuang, J., et al. (2021). Hyocholic Acid Species Improve Glucose Homeostasis Through A Distinct TGR5 and FXR Signaling Mechanism. *Cel Metab.* 33, 791–803. doi:10.1016/j.cmet.2020.11.017

Conflict of Interest: Author ZW was employed by the company iPhenome biotechnology (Yun Pu Kang) Inc.

The remaining authors declare that the research was conducted in the absence of any commercial or financial relationships that could be construed as a potential conflict of interest.

Publisher's Note: All claims expressed in this article are solely those of the authors and do not necessarily represent those of their affiliated organizations, or those of the publisher, the editors and the reviewers. Any product that may be evaluated in this article, or claim that may be made by its manufacturer, is not guaranteed or endorsed by the publisher.

frontiers in Pharmacology

ORIGINAL RESEARCH
published: 19 November 2021
doi: 10.3389/fphar.2021.770240

Gas Chromatography–Mass Spectroscopy-Based Metabolomics Analysis Reveals Potential Biochemical Markers for Diagnosis of Gestational Diabetes Mellitus

*Beata A. Raczkowska[1], Patrycja Mojsak[1], David Rojo[2], Beata Telejko[†,3], Magdalena Paczkowska–Abdulsalam[1], Justyna Hryniewicka[3], Anna Zielinska–Maciulewska[3], Malgorzata Szelachowska[3], Maria Gorska[3], Coral Barbas[2], Adam Kretowski[1,3] and Michal Ciborowski[1]**

[1]Clinical Research Centre, Medical University of Bialystok, Bialystok, Poland, [2]Centro de Metabolómica y Bioanálisis (CEMBIO), Facultad de Farmacia, Universidad CEU San Pablo, Campus Montepríncipe, Madrid, Spain, [3]Department of Endocrinology, Diabetology and Internal Medicine, Medical University of Bialystok, Bialystok, Poland

OPEN ACCESS

Edited by:
Ying Zhou,
The First Affiliated Hospital of Nanchang University, China

Reviewed by:
John Punnose,
St. Stephen's Hospital, India
Chin Moi Chow,
The University of Sydney, Australia

***Correspondence:**
Michal Ciborowski
michal.ciborowski@umb.edu.pl

[†]Deceased

Specialty section:
This article was submitted to Translational Pharmacology, a section of the journal Frontiers in Pharmacology

Received: 03 September 2021
Accepted: 28 October 2021
Published: 19 November 2021

Citation:
Raczkowska BA, Mojsak P, Rojo D, Telejko B, Paczkowska–Abdulsalam M, Hryniewicka J, Zielinska–Maciulewska A, Szelachowska M, Gorska M, Barbas C, Kretowski A and Ciborowski M (2021) Gas Chromatography–Mass Spectroscopy-Based Metabolomics Analysis Reveals Potential Biochemical Markers for Diagnosis of Gestational Diabetes Mellitus. Front. Pharmacol. 12:770240. doi: 10.3389/fphar.2021.770240

Due to many adverse effects of gestational diabetes mellitus (GDM) on the mother and fetus, its diagnosis is crucial. The presence of GDM can be confirmed by an abnormal fasting plasma glucose level (aFPG) and/or oral glucose tolerance test (OGTT) performed mostly between 24 and 28 gestational week. Both aFPG and abnormal glucose tolerance (aGT) are used to diagnose GDM. In comparison to measurement of FPG, OGTT is time-consuming, usually inconvenient for the patient, and very often needs to be repeated. Therefore, it is necessary to seek tests that will be helpful and convenient to diagnose GDM. For this reason, we investigated the differences in fasting serum metabolites between GDM women with abnGM and normal FPG (aGT-GDM group), with aFPG and normal glucose metabolism (aFPG-GDM group) as well as pregnant women with normal glucose tolerance (NGT) being a control group. Serum metabolites were measured by an untargeted approach using gas chromatography–mass spectrometry (GC–MS). In the discovery phase, fasting serum samples collected from 79 pregnant women (aFPG-GDM, n = 24; aGT-GDM, n = 26; NGT, n = 29) between 24 and 28 weeks of gestation (gwk) were fingerprinted. A set of metabolites (α–hydroxybutyric acid (α–HB), β–hydroxybutyric acid (β–HB), and several fatty acids) significant in aGT-GDM vs NGT but not significant in aFPG-GDM vs NGT comparison in the discovery phase was selected for validation. These metabolites were quantified by a targeted GC–MS method in a validation cohort consisted of 163 pregnant women (aFPG-GDM, n = 51; aGT-GDM, n = 44; and NGT, n = 68). Targeted analyses were also performed on the serum collected from 92 healthy women in the first trimester (8–14 gwk) who were NGT at this time, but in the second trimester (24–28 gwk) they were diagnosed with GDM. It was found that α–HB, β–HB, and several fatty acids were associated with aGT-GDM. A combination of α–HB, β–HB, and myristic acid was found highly specific and sensitive for the diagnosis of GDM manifested by aGT-GDM (AUC = 0.828) or to select women at a risk of aGT-GDM in the

first trimester (AUC = 0.791). Our findings provide new potential markers of GDM and may have implications for its early diagnosis.

Keywords: gestational diabetes mellitus, biomarkers, metabolomics, serum, quantitative analysis, gas chromatography, mass spectrometry

INTRODUCTION

Gestational diabetes mellitus (GDM), the most common form of metabolic complication in pregnancy (Tenenbaum-Gavish et al., 2020), is defined as any degree of glucose intolerance with the onset or first recognition during pregnancy (Sweeting et al., 2019). GDM affects from 2 to 38% of pregnancies, depending on the diagnostic criteria and population studied (Alesi et al., 2021). Additionally, its prevalence worldwide is rising (Mdoe et al., 2021). In 2017, GDM affected about 204 million women worldwide, with a projection to increase to 308 million by 2045, mostly in developing countries (Yahaya et al., 2020). Several factors can impact the onset of GDM, including immune function disorder, heredity, gene mutations, and especially the effect of hormones (Mdoe et al., 2021). Women who had GDM have an elevated risk to develop diabetes mellitus type 2 (T2DM) or cardiovascular diseases, as well as obesity or hyperlipidemia in later life (Plows et al., 2018). Consequently, the early diagnosis of GDM could be crucial to prevent abovementioned disorders (Buchanan et al., 2012).

Both conditions, abnormal fasting plasma glucose (aFPG) or abnormal results of oral glucose tolerance test (OGTT), which is an indicator of abnormal glucose tolerance (aGT), are used to diagnose GDM. According to Smirnakis et al. (2005) and Riskin-Mashiah et al. (2009), evaluation of fasting plasma glucose (FPG) in the early pregnancy can be used to indicate women at risk for GDM before the 24th week of gestation (gwk). However, recent studies have shown that FPG in early pregnancy was a poor predictor of GDM (Benhalima et al., 2021; Cosson et al., 2021). On the other side, OGTT, in comparison to the single fasting blood collection needed for an FPG measurement, is time-consuming, inconvenient, and may induce nausea and vomiting in some patients (Cosson et al., 2017). However, it is still a "gold standard" for GDM diagnosis (Bogdanet et al., 2020). Finally, even if an abnormal result for FPG is observed in early pregnancy, the OGTT procedure very often needs to be repeated at 24 gwk, which can be refused by some women (Cosson et al., 2017). Consequently, markers allowing for the diagnosis of GDM manifested solely by aGT, without performing OGTT, are needed. Currently an OGTT screening procedure, according to the International Association of Diabetes and Pregnancy Study Groups (IADPSG) criteria (Gupta et al., 2015), should take place between 24 and 28 gwk. Diagnostic or prognostic markers to indicate GDM presence or risk of future development in the early pregnancy are urgently needed. Early diagnosis may allow introduction of effective prevention and care strategies, which may ultimately reduce complications associated with GDM (Brink et al., 2016).

Recent findings have highlighted metabolomics as a prime candidate for evaluating potential markers for GDM (Mao et al., 2017) because of its capacity to detect early deregulations and disruptions in metabolism associated with different diseases (Mojsak et al., 2021). Therefore, it can be used as a potential tool to determine a metabolite or a set of metabolites allowing diagnosis or prediction of GDM (Sakurai et al., 2019). According to reviewed literature reports, several predictive biomarkers of GDM have been suggested, e.g., specific micro-RNAs, amino acids, fatty acids, triglycerides, phosphatidylcholines, or carbohydrates, pyroglutamic, glutamic, phenylacetic and pantothenic acids, xanthine or proteins such as adiponectin, visfatin, omentin-1, fatty acid–binding protein-4, retinol-binding protein-4, globulin, afamin, or fetuin-A (Enquobahrie et al., 2015; Lu et al., 2016; Zhao et al., 2018; Lorenzo-Almorós et al., 2019; Tenenbaum-Gavish et al., 2020; Tian et al., 2021). Numerous serum or plasma metabolites such as α–hydroxybutyric acid (α–HB) (Dudzik et al., 2017), β–hydroxybutyric acid (β–HB) (Scholtens et al., 2014; Dudzik et al., 2017), amino acids (Scholtens et al., 2014; Enquobahrie et al., 2015), sugars (Enquobahrie et al., 2015), and fatty acids (Enquobahrie et al., 2015; Dudzik et al., 2017) have shown to be associated with this disease using various approaches such as gas chromatography–mass spectrometry (GC–MS) (Dudzik et al., 2017; Scholtens et al., 2014; Rahman et al., 2018; O'Neill et al., 2018), liquid chromatography–mass spectrometry (LC–MS) (Liu et al., 2016; Hou et al., 2018; Tian et al., 2021), and nuclear magnetic resonance (NMR) spectroscopy (Pinto et al., 2015; Hou et al., 2018). GC-MS is adequately sensitive to detect subtle differences in the level of serum/plasma metabolites (Dudzik et al., 2017) and was used in the present study.

However, until now, metabolomics studies on GDM were focused on case-control studies, in which the case group comprised women diagnosed with GDM (Pinto et al., 2015; Liu et al., 2016; Hou et al., 2018). There is a lack of studies in which GDM women were divided into separate subgroups depending on the diagnostic scenario, i.e., women with aGT and normal FPG (aGT-GDM group) and women with aFPG and normal glucose tolerance (aFPG-GDM group). To the best of our knowledge, this is the first study conducted to seek differences in metabolic profiles between the abovementioned GDM subgroups of patients and a control group with normal FPG and glucose metabolism. Such an approach has the potential to find the relevance of metabolomics in diagnosis of GDM.

MATERIALS AND METHODS

Study Group

Pregnant women (662) were screened for GDM at the Department of Endocrinology, Diabetology, and Internal Medicine (Medical University of Bialystok, Poland) between

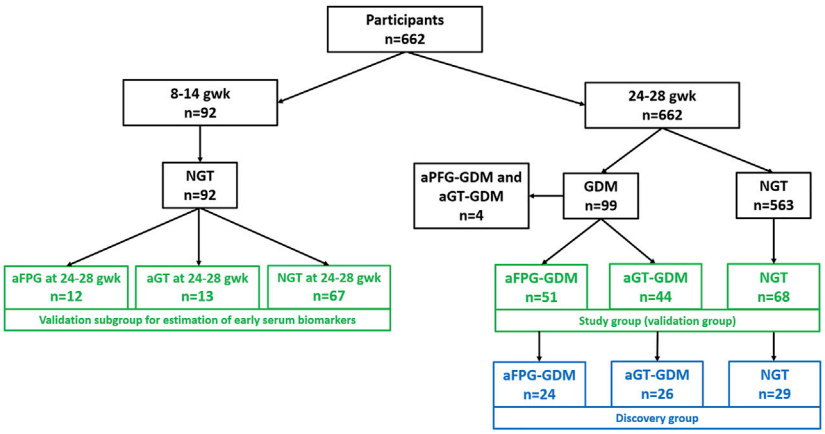

FIGURE 1 | Flow chart presenting participants' selection. Samples selected for the discovery phase are presented in blue rectangles, while those for the validation stage, in green rectangles.

2015 and 2017. For all participants between 24 and 28 gwk, OGTT (75 g) was performed after an overnight fast, with blood samples collected at fasting, 1, and 2 h time points. After clotting at room temperature, fasting serum samples were centrifuged and then separated and frozen at −80°C until the metabolomics assays.

Women were diagnosed with GDM if one of the following criteria was met: fasting glucose ≥92 mg/dl, 1 h glucose ≥180 mg/dl, or 2 h glucose ≥153 mg/dl (Metzger et al., 2010). Women were classified as the aGT-GDM group if they met the following criteria: fasting glucose <92 mg/dl, 1 h glucose ≥180 mg/dl, and/or 2 h glucose ≥153 mg/dl, whilst women were classified as the aFPG-GDM group if they met the following criteria: fasting glucose ≥92 mg/dl, 1 h glucose <180 mg/dl, and 2 h glucose <153 mg/dl. The control group (NGT) comprised participants with the following criteria: fasting glucose <92 mg/dl, 1 h glucose <180 mg/dl, and 2 h glucose <153 mg/dl. All women were characterized by a normal (<5.7%) (Bozkurt et al., 2020) glycated hemoglobin (HbA1c) level.

From the total number of 662 participants, 99 women were diagnosed with GDM between 24–28 gwk; among them, 44 individuals were classified as aGT-GDM, 51 as aFPG-GDM, and only four (excluded from this study) met the criteria to be classified to both–GDM groups. Women from an aGT-GDM group (n = 44) and aFPG-GDM group (n = 51) together with 68 women selected from the NGT group formed a study group (n = 163) which was also a validation cohort. From each subgroup of the validation cohort age- and BMI-matched women were selected for the discovery cohort. A discovery cohort comprised 24 women with aFPG-GDM, 26 with aGT-GDM, and 29 with NGT. Moreover, for the limited set of women (n = 92) fasting serum samples in the first trimester (8–14 gwk) were collected. At that period, all of the selected subjects were characterized by the normal fasting glucose level. However, between 24–28 gwk, some of these women were diagnosed with aGT-GDM (n = 13), others with aFPG–GDM (n = 12), and the rest remained NGT (n = 67). These subjects (n = 92) were included in the present study as the additional independent validation cohort (**Supplementary Table S1**). A flow chart showing classification of participants into specific study groups is presented on **Figure 1**, while the detailed anthropometric and metabolic characteristics of the groups are listed in **Table 1**.

GC–MS-Based Metabolomics

Untargeted and targeted metabolomics analyses were performed on the GC system (Agilent Technologies 7890B) consisting of an autosampler (MultiPurpose Sampler, Gerstel, Germany) and an accurate-mass Q-TOF (Agilent Technologies 7200) detector. Derivative samples (1 µL) were injected into a GC column DB5–MS (30 m length, 0.250 mm i.d., 0.25 µm film 95% dimethyl/5% diphenylpolysiloxane) with a pre–column (10 m J&W integrated with Agilent 122–5532G). The temperature gradient was programmed at 60 °C (held for 1 min), with a ramping increase rate of 10 °C/min up to 325°C (held for 10 min). The total analysis time was 37.5 min. The EI source was operated at 70 eV. The method was RT locked at 19.663 min (elution time of the internal standard–methyl stearate). The mass spectrometer was operated in the scan mode over a mass range of m/z 45–600 at a rate of 10.00 spectra/s. A detailed description of used reagents and applied analytical conditions is available in the **Supplementary Materials File**.

Extraction of serum metabolites was performed as described previously (Mojsak et al., 2021). The derivatization procedure was carried out in two steps. For methoximation, 10 µL of O–methoxyamine hydrochloride (15 mg/ml) in pyridine was added to each vial and vortexed vigorously. The vials were incubated in darkness at room temperature for 16 h. Then, 10 µL of BSTFA with 1% TMCS (v/v) was added, and samples were vortexed for 5 min; silylation was carried out for 1 h at 70°C, and finally, 100 µL of C18:0 methyl ester (10 mg/L in heptane) was added as an internal standard. Samples were mixed again by vortexing gently.

The description of untargeted and targeted GC–MS data treatment is available in the **Supplementary Materials File**.

TABLE 1 | Anthropometric and metabolic characteristics of the subgroups–discovery and validation cohort–second trimester (24–28 weeks of gestation).

Participants' characteristics	Discovery cohort			Validation cohort		
	NGT	aGT-GDM	aFPG-GDM	NGT	aGT-GDM	aFPG-GDM
N	29	26	24	68	44	51
Age [years]	29 (5)	33 (6)^{*,a}	28 (7)	28 (4)	32 (6)^{**,a}	29 (7)
Maternal prepregnancy BMI [kg/m^2]	23.4 (3.7)	23.9 (5.7)	22.4 (7.7)	22.2 (3.2)	22.8 (6.7)	23.2 (5.3)
Maternal pregnancy BMI [kg/m^2]	27 (5)	26.4 (5.4)	26.2 (6.9)	25.6 (3.2)	25.65 (6.4)	26.2 (5)
BMI gain	2.7 (1.6)	2.8 (2.3)	3.4 (1.6)	2.9 (1.8)	2.6 (2.2)	2.8 (2.2)
Total cholesterol [mg/dL]	232 (81)	245.5 (72)	238.5 (54)	231 (48.5)	243 (57)	236 (62)
LDL cholesterol [mg/dL]	130.4 (71)	123 (70.1)	127.7 (48)	111.8 (53.6)	132 (39.6)*	129 (66.2)^{a}
Triglycerides [mg/dL]	183 (68)	173 (60.8)	197.5 (105)	146.5 (55)	185 (89)*	163.5 (79.3)
HDL cholesterol [mg/dL]	73 (21.4)	72.5 (29)	68.5 (23)	90 (28)	77.5 (26.5)^{a}	72.5 (23.8)**
HbA1c (%)	4.7 [0.4]	4.8 [0.4]	4.9 [0.5]	4.7 [0.3]	4.9 [0.3]*	4.9 [0.4]*
HbA1c (mmol/mol)	28 [4.4]	29 [4.4]	30 [5.5]	28 [3.3]	30 [3.3]*	30 [4.4]*
Fasting plasma glucose [mg/dL]	75 (8)	84 (7)^{*,b}	94 (4.2)**	81 (5.5)	84 (6.3)^{*,b}	94 (4)**
Glucose 1 h [mg/dL]	133 (39)	187 (16.3)^{**,b}	138 (24)	114.5 (41.3)	184 (18.8)^{**,b}	131 (26.5)*
Glucose 2 h [mg/dL]	109.5 [19.6]	154 [21.5]^{**,b}	116 [22.8]	104.5 [19.4]	156.6 [22]^{**,b}	111.5 [20.6]
Fasting insulin [μIU/mL]	10.5 (6.4)	14.3 (7.1)*	16.4 (13)*	10.9 (4.3)	13.2 (7.8)*	15.5 (10.7)**
HOMA–IR	2 (1.1)	2.9 (1.6)^{*,a}	3.7 (3.1)**	2.2 (0.9)	2.73 (1.9)*	3.5 (2.7)**
HOMA%β	297.7 (201.5)	279.9 (112.1)^{a}	193.6 (144.5)*	211.4 (103.6)	253.6 (109)^{a}	169 (116.5)*
QUICKI	0.3 (0.03)	0.3 (0.02)^{*,a}	0.3 (0.03)**	0.3 (0.02)	0.3 (0.03)^{*,a}	0.3 (0.03)**

*Data are presented as mean [SD] or median (interquartile range). Abbreviations: NGT, normal glucose tolerance; aGT–GDM, group with diagnosed GDM, based on abnormal OGTT, aFPG–GDM–group with abnormal fasting plasma glucose, HOMA, homeostatic model assessment; IR, insulin resistance; QUICKI, quantitative insulin–sensitivity check index. Statistical significance for NGT vs aGT-GDM, and NGT vs aFPG-GDM, comparisons: * p < 0.05, ** p < 0.0001. Statistical significance for aGT-GDM vs aFPG-GDM, comparison: [a] p < 0.05,[b] p < 0.0001. Continuous data of clinical characteristics were analyzed by Student's t–test for normally distributed data or by the Mann–Whitney U test for the data without the normal distribution.*

STATISTICAL ANALYSIS

Multivariate methods such as principal component analysis (PCA) and partial least squares–discriminant analysis (PLS–DA) were used for data visualization. PCA and PLS–DA models were built using SIMCA–P+ software (13.0.3.0 Umetrics). Statistical significance of the PLS–DA model was validated with permutation testing.

Distribution of the data was assessed by the Shapiro–Wilk test. Student's t–test was used for normally distributed data, whilst the Mann–Whitney *U* test was used for nonparametric data. Benjamini–Hochberg *post hoc* corrections were performed. The threshold for statistical significance was 0.05. Statistical analysis was performed by in-house built scripts for MATLAB (7.10.0.499, MathWorks, Natick, MA, United States). Considering the criteria of the Metabolomics Standards Initiative (Fiehn et al., 2007; Salek et al., 2013), all statistically significant metabolites were identified with the highest confidence level (grade 1). Discovery cohort and both validation cohorts were analyzed independently.

Receiver operating characteristic (ROC) analysis was performed using MedCalc ver. 18 (MedCalc Software, Ostend, Belgium). The performance of the models was compared by applying the nonparametric method of Delong et al. (1988). The specificity and sensitivity were determined according to the sample class prediction using the 7-fold cross-validation predicted values of the fitted *Y–predcv* (implemented in SIMCA–P+ software) for observations in the model.

RESULTS

First, we used GC–MS in an untargeted approach (metabolic fingerprinting) to investigate the differences between aGT-GDM, aFPG-GDM, and NGT groups in the second trimester. Metabolic fingerprinting resulted in a total number of 96 compounds. After data filtering, the matrix was reduced to 50 compounds. As it can be seen in **Supplementary Figure S1**, quality control samples are tightly clustered on the PCA model (panel A), whereas between-group discrimination is displayed (panel B) on the validated (panels C and D) PLS-DA model. In order to evaluate statistically significant differences between the groups aGT-GDM vs NGT, aFPG-GDM vs NGT, and aGT-GDM vs aFPG-GDM, the univariate statistics was performed. The list of 31 statistically significant metabolites is displayed in **Supplementary Table S2**. Metabolites significantly discriminating study groups mainly belong to fatty acids, hydroxy acids, and organooxygen compounds. Only four metabolites (mannitol, cetyl alcohol, arabitol, and p-cresol) were found significantly different in the aFPG-GDM vs NGT comparison. Considering the comparison of aGT-GDM and NGT groups, a great number of compounds was represented by increased saturated fatty acids (caprylic 1.46–fold, capric 2.5–fold, lauric 2.04–fold, myristic 1.81–fold, palmitic 1.46–fold, stearic 1.62–fold, heptadecanoic 1.82–fold, and nonanoic 1.68–fold) and increased unsaturated fatty acids (palmitoleic 1.6–fold, oleic 1.73–fold, and linoleic 1.81–fold) in the aGT-GDM group. Another noticeable group of compounds increased in the subjects with aGT-GDM compared to NGT consisted of hydroxy acids and derivatives, with α–HB and β–HB as the most represented (1.28–fold and 1.76–fold change, respectively).

Fourteen of the most promising metabolites, according to the experimental data and literature (Scholtens et al., 2014; Cobb et al., 2015; Dudzik et al., 2017), significantly discriminating an aGT-GDM group from the NGT group, were chosen for quantification in both validation cohorts. Metabolites found as

TABLE 2 | Statistically significant metabolites for NGT vs aGT-GDM comparison based on the validation study results.

Metabolite	1st trimester			2nd trimester		
	NGT	aGT-GDM	aFPG-GDM	NGT	aGT-GDM	aFPG-GDM
α-Hydroxybutyric acid [mg/L]	1.45 (0.35)	1.8 (0.45)*	1.54 (0.3)	1.26 (0.25)	1.42 (0.24)***	1.36 (0.32)
B-Hydroxybutyric acid [mg/L]	1.28 (0.72)	1.63 (0.71)*	1.45 (0.44)	1.29 (0.46)	1.69 (1.07)**	1.47 (0.68)
Capric acid [mg/L]	0.24 (0.07)	0.32 (0.08)*	0.26 (0.07)	-	-	-
Nonanoic acid [mg/L]	-	-	-	0.24 (0.08)	0.27 (0.11)**	0.26 (0.11)
Lauric acid [mg/L]	0.21 (0.09)	0.28 (0.11)*	0.26 (0.08)	0.23 (0.08)	0.28 (0.11)**	0.24 (0.15)
Myristic acid [mg/L]	0.42 (0.27)	0.59 (0.13)*	0.57 (0.21)	0.47 (0.23)	0.69 (0.25)****	0.53 (0.3)
Palmitic acid [mg/L]	13.32 (2.85)	14.75 (1.97)*	13.52 (2.67)	13.41 (2.34)	14.93 (2.7)***	14.18 (2.36)
Oleic acid [mg/L]	38.77 (23.19)	47.7 (33.45)*	45.6 (23.73)	40.33 (16.36)	48.45 (18.15)**	39.55 (18.63)

*Classification of the subgroups in the 1st trimester study group was based on the OGTT results obtained in the 2nd trimester. Data are presented as a median and interquartile range in brackets. Statistical significance for aGT–group vs NGT, comparison: * - p <0.05, ** - p <0.01, *** - p <0.0001, **** - p <0.00001 by Mann–Whitney U test. Abbreviations: NGT, normal glucose tolerance; aGT-GDM, group with diagnosed GDM, based on abnormal OGTT, aFPG-GDM, group with abnormal fasting plasma glucose.*

significant in the validation study for NGT vs aGT-GDM comparison in any of validation cohorts are presented in **Table 2**.

We observed an increased level for all of the metabolites in the subjects with the aGT-GDM group in comparison to NGT individuals, which also confirms the results of fingerprinting analysis. Interestingly, the majority of compounds (i.e., α–HB, β–HB, myristic, lauric, palmitic, and oleic acids) were statistically significant and shared a similar change in the concentration level between the aGT–group and NGT in both the first and second trimester. The only difference between the trimesters was found for nonanoic acid and capric acid, statistically significant only in the second or first trimester, respectively. α–HB (p = 0.00005) and myristic acid (p = 0.000005) were found to be strongly associated with the aGT–group. To evaluate the clinical usefulness and predictive ability of potential biomarkers to distinguish the aGT–group from NGT, a ROC curve analysis was performed for all of the metabolites that passed the validation independently as well as for the combinations of different metabolites (**Supplementary Table S3**). Considering each metabolite independently, the best predictive power to discriminate aGT-GDM patients, characterized by fair accuracy of the test, was found for myristic acid (Area Under Curve, AUC = 0.787 in the second trimester and AUC = 0.759 in the first trimester), α–HB (AUC = 0.745 in the second trimester and AUC = 0.797 in the first trimester), and palmitic acid (AUC = 0.754 in the second trimester and AUC = 0.745 in the first trimester). The ROC curve and the corresponding AUC were significantly improved when combining the selected metabolites into different models. The combination of fatty acids myristic, lauric, palmitic, oleic, and nonanoic (in case of the second trimester) or capric (first trimester) acid was found to have a good predictive ability (AUC = 0.775 in the second trimester and AUC = 0.747 in the first trimester). Furthermore, an addition of α–HB and β–HB to the combination of fatty acids improved its predictive value (AUC = 0.815 in the second trimester and AUC = 0.772 in the first trimester) (**Supplementary Table S3**). However, the best diagnostic power considering its accuracy, sensitivity, and specificity was found for the model consisting of α–HB, β–HB, and myristic acid (AUC = 0.828 in the second trimester and AUC = 0.791 in the first trimester) (**Figure 2**).

DISCUSSION

The discussion on the most appropriate screening strategy for GDM with OGTT at 24–28 weeks of pregnancy is ongoing (Gupta et al., 2015). Detection in the early pregnancy of metabolites showing subtle metabolic perturbations indicating GDM presence or risk of development has clinical significance for early diagnosis or prognosis (Tenenbaum-Gavish et al., 2020), which is crucial to prevent subsequent damage in both the mother and fetus (Brink et al., 2016). Metabolomics research can not only propose novel diagnostic or prognostic GDM biomarkers but may also allow monitoring of pregnancy complications for better GDM management (Donovan et al., 2018).

Therefore, in the discovery phase of this study, we have evaluated differences in serum metabolic profiles between the patients with GDM diagnosed solely with aFPG or aGT in comparison to pregnant women with NGT. Among significant metabolites (**Table 2**), mainly fatty acids (palmitic, stearic, capric, lauric, oleic, caprylic, myristic, nonanoic, heptadecanoic, and palmitoleic acids) and both hydroxybutyric acids (α and β) were observed. The same metabolites or metabolites from the same classes have already been proposed by other authors as characteristic to GDM. For instance, in the study conducted by (Hou et al., 2018), almost a half of FFAs were elevated in GDM patients. Dudzik et al. (2017) reported an increased level of several fatty acids in the GDM group compared to NGT, with stearic acid as the most represented. Enquobahrie et al. (2015) presented the results of untargeted GC–MS analysis of serum samples collected in the early pregnancy. Out of 17 discovered metabolites distinguishing GDM from NGT individuals, myristic and oleic acids were among the most abundant metabolites within the GDM group. Despite the fact that the diagnostic criteria used by Enquobahrie et al. (2015) were different than in the presented study, the results for myristic acid are consistent with ours.

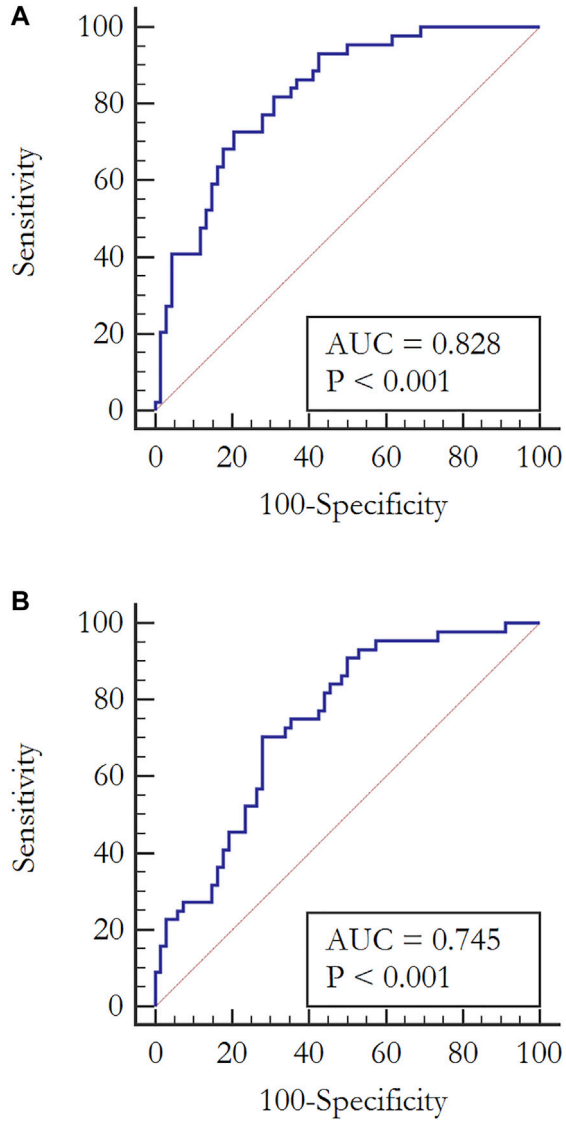

FIGURE 2 | ROC curves analyses evaluating the clinical usefulness of potential biomarkers to diagnose pregnant women with aGT–group from a fasting serum sample in the second trimester. **(A)** Combination of α–HB, β–HB, and myristic acid: AUC = 0.828, CI (0.745–0.892), Sensitivity = 72.7, Specificity = 79.4, $p < 0.0001$ **(B)** α–HB: AUC = 0.745, CI (0.654–0.823), Sensitivity = 70.5, Specificity = 72, $p < 0.0001$.

Oxidation of free fatty acids and excess acetyl-CoA production lead to an increase in the β–HB level (Lu et al., 2021). Increased levels of α–HB and β–HB in GDM patients in comparison to those of NGT women were also observed by others. In the recent study conducted by Lu et al. (2021) on the Chinese population, an elevated level of β–HBA in the second or third trimester was found associated with GDM. In the already mentioned study of Dudzik et al. (2017), increased levels of α–HB and β–HB in the GDM group as compared to NGT were also noted. Moreover, Scholtens et al. (2014) demonstrated broad-scale perturbations in hyperglycemic pregnant women and compared metabolic profiles of mothers with high and low FPG levels. Among significant metabolites, α–HB and β–HB were noted. The study was focused largely on the differences between high and normal fasting plasma glucose subjects. Nevertheless, according to the clinical characteristics presented in this report, among the individuals defined as high–FPG, subjects with increased plasma glucose level at 1 h or 2 h in OGTT were also present.

The elevated level of α–HB can be associated with oxidative stress or increased insulin resistance (Meigs et al., 2007). Oxidative stress is a result of enhanced mitochondrial activity. To manage the resulting oxidative stress, glutathione biosynthesis is activated, and consequently, a demand for cysteine is increased. During the conversion of cystathionine to cysteine, α–ketobutyric acid (α–KB) is produced, whereas α–HB is a by–product of α–KB formation (Dudzik et al., 2014). Another important metabolite associated with aGT–GDM individuals is β–HB. Besides its known role as an important ketone body, which carries energy from the liver to peripheral tissues during fasting or exercise, β–HB plays a significant role in cellular processes regulation by altering the level of other regulatory metabolites such as acetyl-CoA, succinyl-CoA, and NAD^+ (Newman and Verdin, 2014). Moreover, insulin resistance is characterized by increased lipolysis and increased fatty acid oxidation (Bronisz et al., 2018). IR is observed in normal pregnancy, but in the case of excessive IR and significant β-cell dysfunction, GDM develops (Chen et al., 2019; Kampmann et al., 2019). Increased circulating free fatty acids (also observed in our study) have been recognized as one of the most critical factors contributing to IR and altering insulin secretion (Chen et al., 2019).

However, none of the abovementioned metabolomics studies on GDM considered the differences among the women diagnosed solely with either aGT or aFPG. These two distinct metabolic states, but described as isolated impaired glucose tolerance (iIGT) and isolated impaired fasting glucose (iIFG), were previously investigated in pre-T2DM nonpregnant individuals (Gall et al., 2010; Ferrannini et al., 2013; Cobb et al., 2015; Cobb et al., 2016). These reports demonstrate some consistency with the results of our study, particularly for iIGT individuals. For instance, Gall et al. (2010) proposed that α–HB can serve as an early biomarker of insulin resistance and IGT in nondiabetic individuals. Its increased level was associated with increased lipid oxidation and oxidative stress. Furthermore, the role of α–HB in the pathophysiology of the prediabetes state was proved by Cobb et al. (2015; 2016). Besides the elevated concentration of α–HB in the individuals with IGT, they also found an increase of β–HB together with an increased free fatty acids level, which supports the concept of using α–HB, β–HB, and free fatty acids as biomarkers of iIGT without performing an OGTT. As the aim of this study was to find biomarkers that could replace OGTT, but in the case of GDM diagnosis, we evaluated the diagnostic potential of metabolites statistically significant for the aGT-GDM vs NGT comparison using data obtained in the validation phase. It was confirmed that a combination of α–HB, β–HB, and myristic acid was highly

specific and sensitive for the diagnosis of GDM manifested by abnormal glucose tolerance with AUC = 0.828 (**Figure 2**).

Samples belonging to the other validation group were collected in the first trimester (8–14 gwk) from women with normal FPG. However, some of these women (**Figure 1**) were diagnosed with GDM between 24–28 gwk. Performed targeted analyses revealed a similar metabolite profile in the first and the second trimester of pregnancy, considering the change in the concentration level of significant metabolites between aGT-GDM and NGT individuals. Despite the fact that the number of samples from the first trimester was limited, the comparable tendency in both time points of pregnancy shows that α–HB, β–HB, and myristic acid may serve as early biomarkers of later-onset GDM (AUC = 0.791, Table S3). However, we are aware that normoglycemic women in the first trimester did not undergo OGTT. According to the diagnostic strategy (International Association of Diabetes and Pregnancy Study Groups Consensus Panel et al., 2010), if the fasting plasma glucose level at the first prenatal visit is below 92 mg/dl, women should be screened for GDM with 75 g OGTT between 24 and 28 gwk. Therefore, because of a lack of data, we cannot reject the possibility of the already existing aGT-GDM. Further investigations are needed to evaluate whether the proposed markers are strictly related to the presence of IFG or can be considered predictive. Nevertheless, diagnosing individuals at high risk would potentially allow the prevention of GDM development by implementing lifestyle modifications with adequate diet and physical activity (Tobias et al., 2011; Zhang et al., 2016).

Based on the literature review, there are only few reports in the literature (Ravnsborg et al., 2016; Leitner et al., 2017; Corcoran et al., 2018; Yin et al., 2018) where the GDM predictive metabolites found in metabolomics are subjected to further validation. For example, Leitner et al. (2017) received similar results for α–HBA and β–HBA as strong markers in the prediction of GDM. This hypothesis was additionally tested by targeted profiling of serotonin-derived metabolites, also in urine samples, and went one step further with the integration of plasma and urine metabolic markers to improve the prediction accuracy of GDM in this study. Due to this fact, the continuation of our study should be the replication of the findings in a large cohort study and developing methods for other matrices, which may improve the understanding of GDM pathogenesis and may have implications for its early diagnosis.

CONCLUSION

Our study explored differences in the serum metabolic profile in pregnancy, firstly by untargeted, and finally by quantitative analysis with the GC–MS technique. In the first part of the study, we identified and confirmed a set of metabolites representative for GDM women with abnormal glucose tolerance but a normal FPG level (aGT-GDM group). A combination of three metabolites (α–HB, β–HB, and myristic acid) was found strongly associated with aGT-GDM. Measurement of the concentrations of the proposed panel of metabolites in the fasting serum sample has the potential to be a useful clinical test to diagnose GDM in the second trimester of pregnancy without the need to perform OGTT. Moreover, these metabolites can potentially be used to identify, in the early pregnancy, subjects with aGT-GDM or at high risk for developing GDM manifested by abnormal glucose metabolism in the near future. The proposed panel of metabolites can potentially be used instead of OGTT. However, measurement of FPG is still needed to indicate women with aFPG-GDM. Consequently, fasting plasma glucose measurement should be accompanied by the measurement of α–HB, β–HB, and myristic acid in the fasting serum sample. From the perspective of pregnant women, it will facilitate the diagnostic procedure, as only a single fasting blood collection will be needed. Measurement of these GDM markers can be easily performed using a method based on chromatographic separation and MS detection. The application of MS in clinical laboratories has developed very well in the last decade, and this technology is already used for such routine applications as therapeutic drug monitoring, newborn screening, or steroid analysis (Honour et al., 2018; Cui et al., 2020; Seger and Salzmann, 2020). Consequently, MS combined with a separation technique can be easily adapted to measure metabolites significant in this study. Our work contributes to the design of novel diagnostic targets that may facilitate precision medicine and lead to the development of personalized diagnostics of aGT-GDM based on the three biomarkers (α–HB, β–HB, and myristic acid).

DATA AVAILABILITY STATEMENT

The original contributions presented in the study are included in the article/**Supplementary Files**; further inquiries can be directed to the corresponding author.

ETHICS STATEMENT

The studies involving human participants were reviewed and approved by the Bioethical Committee of the Medical University of Bialystok (R–I–002/369/2014). The patients/participants provided their written informed consent to participate in this study.

AUTHOR CONTRIBUTIONS

BR researched data, contributed to the study design, performed the metabolome analysis, the data interpretation, and wrote the manuscript. PM provided analytic and intellectual input on the metabolome data, performed data interpretation, and wrote the manuscript. DR contributed to the study design, metabolome analysis, data interpretation, and manuscript revision. MP-A contributed to data analysis. BT contributed to the study design, patients' recruitment, and provided an intellectual input on the clinical data. JH and AZ-M contributed to patients' recruitment and sample collection. MS and MG provided an intellectual input on the clinical data. MC provided analytic and intellectual input on the

metabolome data, contributed to the study design, data analysis, and the manuscript preparation and revision. AK provided an intellectual input on the clinical data and revised the manuscript. CB provided analytic and intellectual input on the metabolome data and revised the manuscript. CB, AK, and MC are the guarantors of this work and, as such, had full access to all the data in the study and took responsibility for the integrity of the data and the accuracy of the data analysis.

FUNDING

This study was supported by funds from the Leading National Research Centre in Bialystok (KNOW 2012–2017).

ACKNOWLEDGMENTS

CB and DR would like to acknowledge funding from the Spanish Ministry of Economy and Competitiveness (CTQ 2014–55279–R). All the authors acknowledge Monika Davis, Christopher Davis, and Katarzyna Miniewska for English proofreading.

SUPPLEMENTARY MATERIAL

The Supplementary Material for this article can be found online at: https://www.frontiersin.org/articles/10.3389/fphar.2021.770240/full#supplementary-material

REFERENCES

Alesi, S., Ghelani, D., Rassie, K., and Mousa, A. (2021). Metabolomic Biomarkers in Gestational Diabetes Mellitus: A Review of the Evidence. *Int. J. Mol. Sci.* 22 (11), 5512. doi:10.3390/ijms22115512

Benhalima, K., Van Crombrugge, P., Moyson, C., Verhaeghe, J., Vandeginste, S., Verlaenen, H., et al. (2021). Women with Mild Fasting Hyperglycemia in Early Pregnancy Have More Neonatal Intensive Care Admissions. *J. Clin. Endocrinol. Metab.* 106 (2), e836–e854. doi:10.1210/clinem/dgaa831

Bogdanet, D., O'Shea, P., Lyons, C., Shafat, A., and Dunne, F. (2020). The Oral Glucose Tolerance Test-Is it Time for a Change?-A Literature Review with an Emphasis on Pregnancy. *J. Clin. Med.* 9 (11), 3451. doi:10.3390/jcm9113451

Bozkurt, L., Göbl, C. S., Leitner, K., Pacini, G., and Kautzky-Willer, A. (2020). HbA1c during Early Pregnancy Reflects Beta-Cell Dysfunction in Women Developing GDM. *BMJ Open Diabetes Res. Care* 8 (2), e001751. doi:10.1136/bmjdrc-2020-001751

Brink, H. S., van der Lely, A. J., and van der Linden, J. (2016). The Potential Role of Biomarkers in Predicting Gestational Diabetes. *Endocr. Connect.* 5 (5), R26–R34. doi:10.1530/EC-16-0033

Bronisz, A., Ozorowski, M., and Hagner-Derengowska, M. (2018). Pregnancy Ketonemia and Development of the Fetal Central Nervous System. *Int. J. Endocrinol.* 2018, 1242901. doi:10.1155/2018/1242901

Buchanan, T. A., Xiang, A. H., and Page, K. A. (2012). Gestational Diabetes Mellitus: Risks and Management during and after Pregnancy. *Nat. Rev. Endocrinol.* 8 (11), 639–649. doi:10.1038/nrendo.2012.96

Chen, X., Stein, T. P., Steer, R. A., and Scholl, T. O. (2019). Individual Free Fatty Acids Have Unique Associations with Inflammatory Biomarkers, Insulin Resistance and Insulin Secretion in Healthy and Gestational Diabetic Pregnant Women. *BMJ Open Diabetes Res. Care* 7 (1), e000632. doi:10.1136/bmjdrc-2018-000632

Cobb, J., Eckhart, A., Motsinger-Reif, A., Carr, B., Groop, L., and Ferrannini, E. (2016). α-Hydroxybutyric Acid Is a Selective Metabolite Biomarker of Impaired Glucose Tolerance. *Diabetes Care* 39 (6), 988–995. doi:10.2337/dc15-2752

Cobb, J., Eckhart, A., Perichon, R., Wulff, J., Mitchell, M., Adam, K. P., et al. (2015). A Novel Test for IGT Utilizing Metabolite Markers of Glucose Tolerance. *J. Diabetes Sci. Technol.* 9 (1), 69–76. doi:10.1177/1932296814553622

Corcoran, S. M., Achamallah, N., Loughlin, J. O., Stafford, P., Dicker, P., Malone, F. D., et al. (2018). First Trimester Serum Biomarkers to Predict Gestational Diabetes in a High-Risk Cohort: Striving for Clinically Useful Thresholds. *Eur. J. Obstet. Gynecol. Reprod. Biol.* 222, 7–12. doi:10.1016/j.ejogrb.2017.12.051

Cosson, E., Carbillon, L., and Valensi, P. (2017). High Fasting Plasma Glucose during Early Pregnancy: A Review about Early Gestational Diabetes Mellitus. *J. Diabetes Res.* 2017, 8921712. doi:10.1155/2017/8921712

Cosson, E., Vicaut, E., Berkane, N., Cianganu, T. L., Baudry, C., Portal, J. J., et al. (2021). Prognosis Associated with Initial Care of Increased Fasting Glucose in Early Pregnancy: A Retrospective Study. *Diabetes Metab.* 47 (3), 101197. doi:10.1016/j.diabet.2020.08.007

Cui, J. J., Wang, L. Y., Tan, Z. R., Zhou, H. H., Zhan, X., and Yin, J. Y. (2020). MASS SPECTROMETRY-BASED PERSONALIZED DRUG THERAPY. *Mass. Spectrom. Rev.* 39 (5-6), 523–552. doi:10.1002/mas.21620

DeLong, E. R., DeLong, D. M., and Clarke-Pearson, D. L. (1988). Comparing the Areas under Two or More Correlated Receiver Operating Characteristic Curves: a Nonparametric Approach. *Biometrics* 44 (3), 837–845. doi:10.2307/2531595

Donovan, B. M., Nidey, N. L., Jasper, E. A., Robinson, J. G., Bao, W., Saftlas, A. F., et al. (2018). First Trimester Prenatal Screening Biomarkers and Gestational Diabetes Mellitus: A Systematic Review and Meta-Analysis. *PLoS One* 13 (7), e0201319. doi:10.1371/journal.pone.0201319

Dudzik, D., Zorawski, M., Skotnicki, M., Zarzycki, W., García, A., Angulo, S., et al. (2017). GC-MS Based Gestational Diabetes Mellitus Longitudinal Study: Identification of 2-and 3-hydroxybutyrate as Potential Prognostic Biomarkers. *J. Pharm. Biomed. Anal.* 144, 90–98. doi:10.1016/j.jpba.2017.02.056

Dudzik, D., Zorawski, M., Skotnicki, M., Zarzycki, W., Kozlowska, G., Bibik-Malinowska, K., et al. (2014). Metabolic Fingerprint of Gestational Diabetes Mellitus. *J. Proteomics* 103, 57–71. doi:10.1016/j.jprot.2014.03.025

Enquobahrie, D. A., Denis, M., Tadesse, M. G., Gelaye, B., Ressom, H. W., and Williams, M. A. (2015). Maternal Early Pregnancy Serum Metabolites and Risk of Gestational Diabetes Mellitus. *J. Clin. Endocrinol. Metab.* 100 (11), 4348–4356. doi:10.1210/jc.2015-2862

Ferrannini, E., Natali, A., Camastra, S., Nannipieri, M., Mari, A., Adam, K. P., et al. (2013). Early Metabolic Markers of the Development of Dysglycemia and Type 2 Diabetes and Their Physiological Significance. *Diabetes* 62 (5), 1730–1737. doi:10.2337/db12-0707

Fiehn, O., Sansone, S. A., Fan, T., Goodacre, R., Griffin, J. L., Hardy, N. W., et al. (2007). The Metabolomics Standards Initiative. *Nat. Biotechnol.* 25 (3), 846–848. doi:10.1007/s11306-007-0070-610.1038/nbt0807-846b

Gall, W. E., Beebe, K., Lawton, K. A., Adam, K. P., Mitchell, M. W., Nakhle, P. J., et al. (2010). Alpha-Hydroxybutyrate Is an Early Biomarker of Insulin Resistance and Glucose Intolerance in a Nondiabetic Population. *PLoS ONE* 5 (5), e10883. doi:10.1371/journal.pone.0010883

Gupta, Y., Kalra, B., Baruah, M. P., Singla, R., and Kalra, S. (2015). Updated Guidelines on Screening for Gestational Diabetes. *Int. J. Womens Health* 7, 539–550. doi:10.2147/IJWH.S82046

Honour, J. W., Conway, E., Hodkinson, R., and Lam, F. (2018). The Evolution of Methods for Urinary Steroid Metabolomics in Clinical Investigations Particularly in Childhood. *J. Steroid Biochem. Mol. Biol.* 181, 28–51. doi:10.1016/j.jsbmb.2018.02.013

Hou, W., Meng, X., Zhao, A., Zhao, W., Pan, J., Tang, J., et al. (2018). Development of Multimarker Diagnostic Models from Metabolomics Analysis for Gestational Diabetes Mellitus (GDM). *Mol. Cel Proteomics* 17 (3), 431–441. doi:10.1074/mcp.RA117.000121

International Association of Diabetes and Pregnancy Study Groups Consensus PanelMetzger, B. E., Gabbe, S. G., Persson, B., Buchanan, T. A., Catalano, P. A., et al. (2010). International Association of Diabetes and Pregnancy Study Groups Recommendations on the Diagnosis and Classification of Hyperglycemia in Pregnancy. *Diabetes Care* 33 (3), 676–682. doi:10.2337/dc09-1848

Kampmann, U., Knorr, S., Fuglsang, J., and Ovesen, P. (2019). Determinants of Maternal Insulin Resistance during Pregnancy: An Updated Overview. *J. Diabetes Res.* 2019, 5320156. doi:10.1155/2019/5320156

Leitner, M., Fragner, L., Danner, S., Holeschofsky, N., Leitner, K., Tischler, S., et al. (2017). Combined Metabolomic Analysis of Plasma and Urine Reveals AHBA, Tryptophan and Serotonin Metabolism as Potential Risk Factors in Gestational Diabetes Mellitus (GDM). *Front. Mol. Biosci.* 4, 84. doi:10.3389/fmolb.2017.00084

Liu, T., Li, J., Xu, F., Wang, M., Ding, S., Xu, H., et al. (2016). Comprehensive Analysis of Serum Metabolites in Gestational Diabetes Mellitus by UPLC/Q-TOF-MS. *Anal. Bioanal. Chem.* 408 (4), 1125–1135. doi:10.1007/s00216-015-9211-3

Lorenzo-Almorós, A., Hang, T., Peiró, C., Soriano-Guillén, L., Egido, J., Tuñón, J., et al. (2019). Predictive and Diagnostic Biomarkers for Gestational Diabetes and its Associated Metabolic and Cardiovascular Diseases. *Cardiovasc. Diabetol.* 18 (1), 140. doi:10.1186/s12933-019-0935-9

Lu, L., Koulman, A., Petry, C. J., Jenkins, B., Matthews, L., Hughes, I. A., et al. (2016). An Unbiased Lipidomics Approach Identifies Early Second Trimester Lipids Predictive of Maternal Glycemic Traits and Gestational Diabetes Mellitus. *Diabetes Care* 39 (12), 2232–2239. doi:10.2337/dc16-0863

Lu, W., Luo, M., Fang, X., Zhang, R., Li, S., Tang, M., et al. (2021). Discovery of Metabolic Biomarkers for Gestational Diabetes Mellitus in a Chinese Population. *Nutr. Metab. (Lond)* 18 (1), 79. doi:10.1186/s12986-021-00606-8

Mao, X., Chen, X., Chen, C., Zhang, H., and Law, K. P. (2017). Metabolomics in Gestational Diabetes. *Clin. Chim. Acta* 475, 116–127. doi:10.1016/j.cca.2017.10.019

Mdoe, M. B., Kibusi, S. M., Munyogwa, M. J., and Ernest, A. I. (2021). Prevalence and Predictors of Gestational Diabetes Mellitus Among Pregnant Women Attending Antenatal Clinic in Dodoma Region, Tanzania: an Analytical Cross-Sectional Study. *BMJ Nutr. Prev. Health* 4, 69–79. doi:10.1136/bmjnph-2020-000149

Meigs, J. B., Larson, M. G., Fox, C. S., Keaney, J. F., Vasan, R. S., and Benjamin, E. J. (2007). Association of Oxidative Stress, Insulin Resistance, and Diabetes Risk Phenotypes: the Framingham Offspring Study. *Diabetes Care* 30 (10), 2529–2535. doi:10.2337/dc07-0817

Metzger, B. E., Metzger, B. E., Gabbe, S. G., Persson, B., Buchanan, T. A., Catalano, P. A., et al. (2010). International Association of Diabetes and Pregnancy Study Groups Recommendations on the Diagnosis and Classification of Hyperglycemia in Pregnancy. *Diabetes Care* 33 (3), 676–682. doi:10.2337/dc09-1848

Mojsak, P., Miniewska, K., Godlewski, A., Adamska-Patruno, E., Samczuk, P., Rey-Stolle, F., et al. (2021). A Preliminary Study Showing the Impact of Genetic and Dietary Factors on GC-MS-Based Plasma Metabolome of Patients with and without PROX1-Genetic Predisposition to T2DM up to 5 Years Prior to Prediabetes Appearance. *Curr. Issues Mol. Biol.* 43 (2), 513–528. doi:10.3390/cimb43020039

Newman, J. C., and Verdin, E. (2014). β-Hydroxybutyrate: Much More Than a Metabolite. *Diabetes Res. Clin. Pract.* 106 (2), 173–181. doi:10.1016/j.diabres.2014.08.009

O'Neill, K., Alexander, J., Azuma, R., Xiao, R., Snyder, N. W., Mesaros, C. A., et al. (2018). Gestational Diabetes Alters the Metabolomic Profile in 2nd Trimester Amniotic Fluid in a Sex-Specific Manner. *Int. J. Mol. Sci.* 19 (9), 2696. doi:10.3390/ijms19092696

Pinto, J., Almeida, L. M., Martins, A. S., Duarte, D., Barros, A. S., Galhano, E., et al. (2015). Prediction of Gestational Diabetes through NMR Metabolomics of Maternal Blood. *J. Proteome Res.* 14 (6), 2696–2706. doi:10.1021/acs.jproteome.5b00260

Plows, J. F., Stanley, J. L., Baker, P. N., Reynolds, C. M., and Vickers, M. H. (2018). The Pathophysiology of Gestational Diabetes Mellitus. *Int. J. Mol. Sci.* 19 (11), 3342. doi:10.3390/ijms19113342

Rahman, M. L., Anne Feng, Y.-C., Fiehn, O., Tsai, M. Y., Tekola-Ayele, F., Liang, L., et al. (2018). Plasma Lipidomics and Gestational Diabetes-A Longitudinal Study in a Multiracial Cohort. *Diabetes* 67 (Suppl. 1), 174. doi:10.2337/db18-174-LB

Ravnsborg, T., Andersen, L. L., Trabjerg, N. D., Rasmussen, L. M., Jensen, D. M., and Overgaard, M. (2016). First-trimester Multimarker Prediction of Gestational Diabetes Mellitus Using Targeted Mass Spectrometry. *Diabetologia* 59 (5), 970–979. doi:10.1007/s00125-016-3869-8

Riskin-Mashiah, S., Younes, G., Damti, A., and Auslender, R. (2009). First-trimester Fasting Hyperglycemia and Adverse Pregnancy Outcomes. *Diabetes Care* 32 (9), 1639–1643. doi:10.2337/dc09-0688

Sakurai, K., Eguchi, A., Watanabe, M., Yamamoto, M., Ishikawa, K., and Mori, C. (2019). Exploration of Predictive Metabolic Factors for Gestational Diabetes Mellitus in Japanese Women Using Metabolomic Analysis. *J. Diabetes Investig.* 10 (2), 513–520. doi:10.1111/jdi.12887

Salek, R. M., Steinbeck, C., Viant, M. R., Goodacre, R., and Dunn, W. B. (2013). The Role of Reporting Standards for Metabolite Annotation and Identification in Metabolomic Studies. *GigaScience* 2, 13. doi:10.1186/2047-217X-2-13

Scholtens, D. M., Muehlbauer, M. J., Daya, N. R., Stevens, R. D., Dyer, A. R., Lowe, L. P., et al. (2014). Metabolomics Reveals Broad-Scale Metabolic Perturbations in Hyperglycemic Mothers during Pregnancy. *Diabetes Care* 37 (1), 158–166. doi:10.2337/dc13-0989

Seger, C., and Salzmann, L. (2020). After Another Decade: LC-MS/MS Became Routine in Clinical Diagnostics. *Clin. Biochem.* 82, 2–11. doi:10.1016/j.clinbiochem.2020.03.004

Smirnakis, K. V., Martinez, A., Blatman, K. H., Wolf, M., Ecker, J. L., and Thadhani, R. (2005). Early Pregnancy Insulin Resistance and Subsequent Gestational Diabetes Mellitus. *Diabetes Care* 28 (5), 1207–1208. doi:10.2337/diacare.28.5.1207

Sweeting, A. N., Wong, J., Appelblom, H., Ross, G. P., Kouru, H., Williams, P. F., et al. (2019). A Novel Early Pregnancy Risk Prediction Model for Gestational Diabetes Mellitus. *Fetal Diagn. Ther.* 45 (2), 76–84. doi:10.1159/000486853

Tenenbaum-Gavish, K., Sharabi-Nov, A., Binyamin, D., Møller, H. J., Danon, D., Rothman, L., et al. (2020). First Trimester Biomarkers for Prediction of Gestational Diabetes Mellitus. *Placenta* 101, 80–89. doi:10.1016/j.placenta.2020.08.020

Tian, M., Ma, S., You, Y., Long, S., Zhang, J., Guo, C., et al. (2021). Serum Metabolites as an Indicator of Developing Gestational Diabetes Mellitus Later in the Pregnancy: A Prospective Cohort of a Chinese Population. *J. Diabetes Res.* 2021, 8885954. doi:10.1155/2021/8885954

Tobias, D. K., Zhang, C., van Dam, R. M., Bowers, K., and Hu, F. B. (2011). Physical Activity before and during Pregnancy and Risk of Gestational Diabetes Mellitus: A Meta-Analysis. *Diabetes Care* 34 (1), 223–229. doi:10.2337/dc10-1368

Yahaya, T. O., Salisu, T., Abdulrahman, Y. B., and Umar, A. K. (2020). Update on the Genetic and Epigenetic Etiology of Gestational Diabetes Mellitus: a Review. *Egypt. J. Med. Hum. Genet.* 21 (1), 13. doi:10.1186/s43042-020-00054-8

Yin, L., Huai, Y., Zhao, C., Ding, H., Jiang, T., and Shi, Z. (2018). Early Second-Trimester Peptidomic Identification of Serum Peptides for Potential Prediction of Gestational Diabetes Mellitus. *Cell Physiol. Biochem.* 51 (3), 1264–1275. doi:10.1159/000495538

Zhang, C., Rawal, S., and Chong, Y. S. (2016). Risk Factors for Gestational Diabetes: Is Prevention Possible? *Diabetologia* 59 (7), 1385–1390. doi:10.1007/s00125-016-3979-3

Zhao, B., Han, X., Meng, Q., and Luo, Q. (2018). Early Second Trimester Maternal Serum Markers in the Prediction of Gestational Diabetes Mellitus. *J. Diabetes Investig.* 9 (4), 967–974. doi:10.1111/jdi.12798

Conflict of Interest: The authors declare that the research was conducted in the absence of any commercial or financial relationships that could be construed as a potential conflict of interest.

Publisher's Note: All claims expressed in this article are solely those of the authors and do not necessarily represent those of their affiliated organizations, or those of the publisher, the editors, and the reviewers. Any product that may be evaluated in this article, or claim that may be made by its manufacturer, is not guaranteed or endorsed by the publisher.

frontiers in Pharmacology

ORIGINAL RESEARCH
published: 22 November 2021
doi: 10.3389/fphar.2021.754185

HR-MS Based Untargeted Lipidomics Reveals Characteristic Lipid Signatures of Wilson's Disease

Yixiao Zhi[1,2†], Yujiao Sun[1,3†], Yonggeng Jiao[4†], Chen Pan[1,5], Zeming Wu[6], Chang Liu[1,3], Jie Su[2], Jie Zhou[2], Dong Shang[1,2,5], Junqi Niu[2], Rui Hua[2] and Peiyuan Yin[1,3]**

[1]Clinical Laboratory of Integrative Medicine, First Affiliated Hospital of Dalian Medical University, Dalian, China, [2]Department of Hepatology, The First Hospital of Jilin University, Changchun, China, [3]Institute of Integrative Medicine, Dalian Medical University, Dalian, China, [4]Department of Anesthesiology Jilin Province FAW General Hospital, Changchun, China, [5]Department of General Surgery, First Affiliated Hospital of Dalian Medical University, Dalian, China, [6]iPhenome biotechnology Inc. Dalian (Yun Pu Kang), Dalian, China

OPEN ACCESS

Edited by:
Hiu Yee Kwan, Hong Kong Baptist University, Hong Kong, SAR China

Reviewed by:
Niroshika Keppetipola, California State University, Fullerton, United States
Chin Moi Chow, The University of Sydney, Australia

***Correspondence:**
Rui Hua
huar@jlu.edu.cn
Peiyuan Yin
yinperry@126.com
yinpeiyuan@dm.edu.cn

†These authors have contributed equally to this work

Specialty section:
This article was submitted to Translational Pharmacology, a section of the journal Frontiers in Pharmacology

Received: *06 August 2021*
Accepted: *02 November 2021*
Published: *22 November 2021*

Citation:
Zhi Y, Sun Y, Jiao Y, Pan C, Wu Z, Liu C, Su J, Zhou J, Shang D, Niu J, Hua R and Yin P (2021) HR-MS Based Untargeted Lipidomics Reveals Characteristic Lipid Signatures of Wilson's Disease. Front. Pharmacol. 12:754185. doi: 10.3389/fphar.2021.754185

Background and Aims: The diagnosis of Wilson's disease (WD) is challenging by clinical or genetic criteria. A typical early pathological change of WD is the increased liver lipid deposition and lowered serum triglyceride (TG). Therefore, the contents of serum lipids may provide evidence for screening of biomarkers for WD.

Methods: 34 WD patients, 31 WD relatives, and 65 normal controls were enrolled in this study. Serum lipidomics data was acquired by an ultra-high-performance liquid chromatography high-resolution mass spectrometry system, and the data were analyzed by multivariate statistical methods.

Results: Of all 510 identified lipids, there are 297 differential lipids between the WD and controls, 378 differential lipids between the relatives and controls, and 119 differential lipids between the patients and relatives. In WD, the abundances of most saturated TG were increased, whereas other unsaturated lipids decreased, including phosphatidylcholine (PC), sphingomyelin (SM), lysophosphatidylcholine (LPC), ceramide (Cer), and phosphatidylserine (PS). We also found many serum lipid species may be used as biomarkers for WD. The areas under the receiver operating characteristic curve (AUC) of PS (35:0), PS (38:5), and PS (34:0) were 0.919, 0.843, and 0.907. The AUCs of TG (38:0) and CerG1 (d42:2) were 0.948 and 0.915 and the AUCs of LPC (17:0) and LPC (15:0) were 0.980 and 0.960, respectively. The lipid biomarker panel exhibits good diagnostic performance for WD. The correlation networks were built among the different groups and the potential mechanisms of differential lipids were discussed. Interestingly, similar lipid profile of WD is also found in their relatives, which indicated the changes may also related to the mutation of the ATP7B gene.

Conclusions: Lipid deregulation is another important hallmark of WD besides the deposition of copper. Our lipidomic results provide new insights into the diagnostic and therapeutic targets of WD.

Keywords: Wilson disease, lipidomics, biomarkers, triglyceride, metabolomic

INTRODUCTION

Wilson's disease (WD) is an autosomal recessive genetic disease, which is due to a mutation of the ATP7B gene that leads to a copper metabolism disorder (Ala et al., 2007; Członkowska et al., 2018). WD presents most commonly between ages 5 and 35 (Xie and Wu, 2017). Copper ions are deposited in the liver, brain, cornea, kidneys and bone, which progressively aggravates organ damage (Cumings, 1948; Mounajjed et al., 2013; Bandmann et al., 2015). The most prominent clinical presentations of WD are liver disease and cirrhosis, neurologic symptoms and psychiatric features (Mulligan and Bronstein, 2020). Available treatments include zinc salts and chelators, which allow for sufficient control of symptoms. But these drugs do not cure the disease and develop severe side effects (Ranucci et al., 2017).

The diagnosis of WD is often delayed. There is no gold standard because of the nonspecific clinical features (Ryan et al., 2019). The diagnosis of the disease primarily depends on clinical manifestations, laboratory test results, decreases in ceruloplasmin content, increases in 24-h urine copper excretion, liver biopsy findings (increase in liver copper content) and ATP7B gene mutation (Steindl et al., 1997; Ferenci et al., 2019). When low serum ceruloplasmin content was used as a screening test for WD, its positive predictive value was only 6% (Ferenci, 2014). Twenty-four-hour urinary copper excretion may be lower or even normal in 16–23% of WD patients, especially in children and asymptomatic siblings (European Association for Study of Liver, 2012). Hepatic copper content >250 μg/g dry weight is an important indicator of WD, but liver biopsy is an invasive procedure (Ferenci et al., 2005). Comprehensive molecular genetic screening is expensive and difficult because of more than 700 possible mutations (Ferenci, 2005; Mak and Lam, 2008).

Defective ATP7B function results in pathological copper accumulation, which leads to hepatic steatosis and liver injury in WD (Stättermayer et al., 2015). Copper accumulation markedly alters lipid metabolism, and the lipid peroxidation system that produces free redicals, changes enzyme activity and inhibits mitochondrial functions. These changes have been reported in patients and animal models (Gerosa et al., 2019). Our clinical observations indicated that the serum TG levels in WD patients are generally lower than that in healthy controls. The mean TG level in WD patients was 0.85 mmol/L, whereas the level was 1.19 mmol/L in the control group (normal level: 0.28–1.8 mmol/L). Although the TG level is within the normal range for both groups, it remains significantly lower in WD patients. Performing lipidomics to analyze WD metabolic disturbance will contribute to the elucidation of WD diagnosis and understanding of the pathogenesis of WD.

Lipidomics emerged in 2003 as an approach to study the metabolism of the cellular lipidome and has greatly advanced in recent years (Blanksby and Mitchell, 2010). The development of mass spectrometry (MS) has accelerated this emerging discipline (Han et al., 2012). Clinical lipidomics provides a powerful tool to investigate the links between lipids and corresponding diseases, which will play a critical role in prevention, diagnosis, and potential therapies (Cortes et al., 2014; Zhang et al., 2018). Although the development of disease-specific biomarkers provides noninvasive diagnosis for various diseases, it remains a challenge to identify and develop lipid-based and disease-specific biomarkers (Loomba et al., 2015).

In this study, WD patients, their immediate family or relatives and healthy subjects were enrolled. An ultra-high-performance liquid chromatography high-resolution mass spectrometry (UHPLC-HRMS) based method was used to acquire the lipidomic data. We aimed to describe the metabolic deregulations of WD and identify the characteristics of lipids for the disease. These lipidomic findings may help to explore the mechanisms that change in lipid molecules, which may serve as potential diagnostic or therapeutic biomarkers for WD.

MATERIALS AND METHODS

Participants

In this study, 34 WD patients (WD group) were recruited from the Department of Hepatology at the First Hospital of Jilin University from January 2012 to February 2019. The diagnosis of WD was made according to the 2012 European Society for Wilson's Disease guidelines in this study (European Association for Study of Liver, 2012). Patients who had viral type B or C liver disease, drug-induced liver disease, alcoholic liver disease, autoimmune liver disease, overlap syndrome, hemochromatosis, original or secondary malignant tumor or were pregnant or lactating were excluded. Another group included 31 relatives, who were WD patients' immediate family or relatives (WDIR group). The clinical and laboratory tests were normal in the WDIR. Sixty-five healthy controls (HC group) were matched for age and sex. This study was approved by the ethics committees of the First Hospital of Jilin University (No. 2019-346). After obtaining informed consent from patients or their legal guardians, clinical records and plasma were tested and analyzed.

Lipid Extraction

Serum samples were collected from participants on the early morning after an overnight fast (12 h). Then the serum samples were immediately stored at −80°C. The serum samples were thawed at 4°C for 60 min and an aliquot of 50 μl sample was added into a 1.5 ml Eppendorf (EP) tube (Axygen, United States). Then, 250 μl methanol and 750 μl methyl tert-butyl ether (MTBE) were added to the samples, and the samples were vortexed for 5 min. Next, 250 μl of water was added to the mixture, and the samples were shaken using Rotational Incubator QB-128 (Kylin-Bell, China) at 60 rpm/min for 30 min at room temperature and then kept at 4°C for 30 min to promote separation. The samples were then centrifuged at 4°C and 13,000 ×g for 15 min. The upper (lipid extract) phase was quantitatively transferred to a 96-well plate, dried under reduced pressure (Labconco, United States), and stored at −20°C. Before analysis, the lipid extract was redissolved in 500 μl of acetonitrile/isopropanol solution and transferred to a tube for ultra-high-performance liquid chromatography-high-resolution mass spectrometry (UHPLC-HRMS) detection. A pooled quality control (QC) sample was prepared by mixing equal amounts of all the samples.

Untargeted Lipidomics Analysis

Liquid chromatography-mass spectrometry (LC-MS) was performed on a UHPLC system coupled with a Q-Exactive mass spectrometer (Thermo Scientific, United States). Chromatographic separation was performed on an Accucore C30 column (Thermo Scientific Inc., United States, 2.6 μm, 100 mm), with a column temperature of 50°C, a mobile phase A (60% acetonitrile, 40% water, 10 mM ammonium formate and 0.1% formic acid) and mobile phase B (90% isopropanol +10% acetonitrile, 10 mM ammonium formate and 0.1% formic acid), a gradient elution (0–1 min 100% B, 1–6 min 100–50% B, 6–30 min 50–0% B, 30–38 min column washing and re-equilibration), a flow rate of 0.3 ml·min-1, and an injection volume of 5 μl.

Ionization conditions of MS were positive ion spray (ESI+) mode detection, spray voltage of 4000 V, sheath gas and auxiliary gas of 45 and 10 arb, heater temperature of 350°C, capillary temperature of 320°C, and S-Lens RF level of 50%. When the negative ion spray (ESI-) mode was detected, the spray voltage was adjusted to 3500 V, and the other parameters remained the same as those for ESI + mode.

The sample analysis was carried out in two steps. First, full-scan-data-dependent tandem MS (MS^2) was performed on all QC samples, and the obtained primary and secondary MS data were used to identify lipid molecular structures. Then, all samples were tested by high-resolution first-order MS full-scan detection with positive and negative ionization switching, and the data obtained were used to determine the relative quantification of lipids.

MS parameters of the lipid molecular structure were full-scan data dependent MS^2 data acquisition carried out in ESI+ and ESI- modes. The resolution ratio of the first-order MS was 70,000 full widths at half maximum (FWHM); the mass scanning range was 300–1,400 m/z; the automatic gain control threshold target was 1×10^5; the maximum ion implantation time (IT) was 100 ms; the resolution ratio of secondary MS was 17,500 FWHM; the automatic gain control target was 10^5; the maximum IT was 80 ms; the dynamic exclusion time was 5 s; the parent ion isolation window was 1.0 Da, and the loop count was 10. The MS fragmentation energies of the stepped normalized collision energy (NCE) of ESI+ and ESI- MS were 25% + 40 and 35%, respectively.

The parameters of full-scan analysis were as follows: ESI+ and ESI- ionization were switched in real time; the resolution ratio of the first-order MS was 70,000 FWHM; the mass scanning range was 300–1,400 m/z; and the automatic gain control target was 3×10^6.

Data Analysis

LipidSearch software (Thermo Scientific, United States) was used to process the ddMS^2 lipidomics data collected by UPLC-HRMS, including peak detection and lipid structure identification. The main setting parameters were as follows: The retrieval accuracy of primary class parent ion MS was 5 ppm, and the secondary fragment mass spectrum was 5 mDa.

For peak integration and relative quantification of lipid molecules, the qualitative list of lipids produced by LipidSearch software was imported into TraceFinder software (Thermo Scientific, United States) for peak integration. The obtained peak area was used for analyzing lipid relative quantification, and finally, a data matrix containing fragment ion information was output. The missing values in the data matrix were processed using the 80% devaluation principle. Then, the data were imported into Metaboanalyst 4.0 online software (https://www.metaboanalyst.ca/) and SIMCA-P 14.1 (Umetrics, Sweden) for mode discrimination analysis. Principal component analysis (PCA), partial least squares-discriminant analysis (PLS-DA), and orthogonal PLS-DA (OPLS-DA) were used to construct a group-based model and discover differentially abundant metabolites between groups. The false discovery rate (FDR; adjusted $p < 0.05$) and fold change (FC; adjusted $p < 0.05$) were obtained by univariate T-test and ANOVA, and a volcano map was drawn to find differentially abundant metabolites. The obtained differentially abundant metabolites were uploaded to Metaboanalyst.

Normal distribution of the quantitative data was confirmed by independent sample t-tests and was expressed as the mean ± SD. For each independent metabolite, the receiver operating characteristic (ROC) curve was used to calculate the area under the curve (AUC), 95% confidence interval (95% CI), cutoff value, sensitivity and specificity to evaluate the predictive value of each metabolite. For the combined indicators, logistic regression analysis and ROC curve analysis were used to calculate the AUC and the 95% CI. In this study, a two-sided test was used, and differences with $p < 0.05$ were considered statistically significant.

RESULTS

Study Design and Data Acquisition

The flow diagram of this research design is illustrated in **Figure 1**. A total of 130 serum samples (from 65 healthy controls, 34 WD patients, and 31 WD patients' immediate family or relatives) was analyzed by lipidomics to reveal lipid profiles in WD, followed by preprocessing of metabolomics data, including peak detection, alignment, filtering and normalization and then various statistical analyses were performed, including PCA, OPLS-DA, univariate T-test and ANOVA. Our lipidomics profiling identified 512 lipids, of which 510 passed QC procedures and were eligible for analysis (**Table 1**). 89.6% peaks had coefficients of variation (CV) below 10% and the CV value of 98.8% of the lipids was less than 30%, indicating that this experiment had good quantitative accuracy. (**Supplementary Figure S1**).

Clinical Profiles

WD patients were at the age of 8–50, with a large age span. The sex ratio of 1:1 conformed to the patterns of autosomal inheritance and the epidemiological characteristics of the disease. The most common clinical manifestations were single-system involvement; 52% of adolescents had hepatic involvement, whereas 28% had multisystem involvement, and middle-aged patients had mostly multisystem involvement. The concentration of serum ceruloplasmin (normal value: 0.2–0.5 g/L) less than 0.1 g/L is considered as strong evidence for diagnosis of WD (Bandmann et al., 2015).

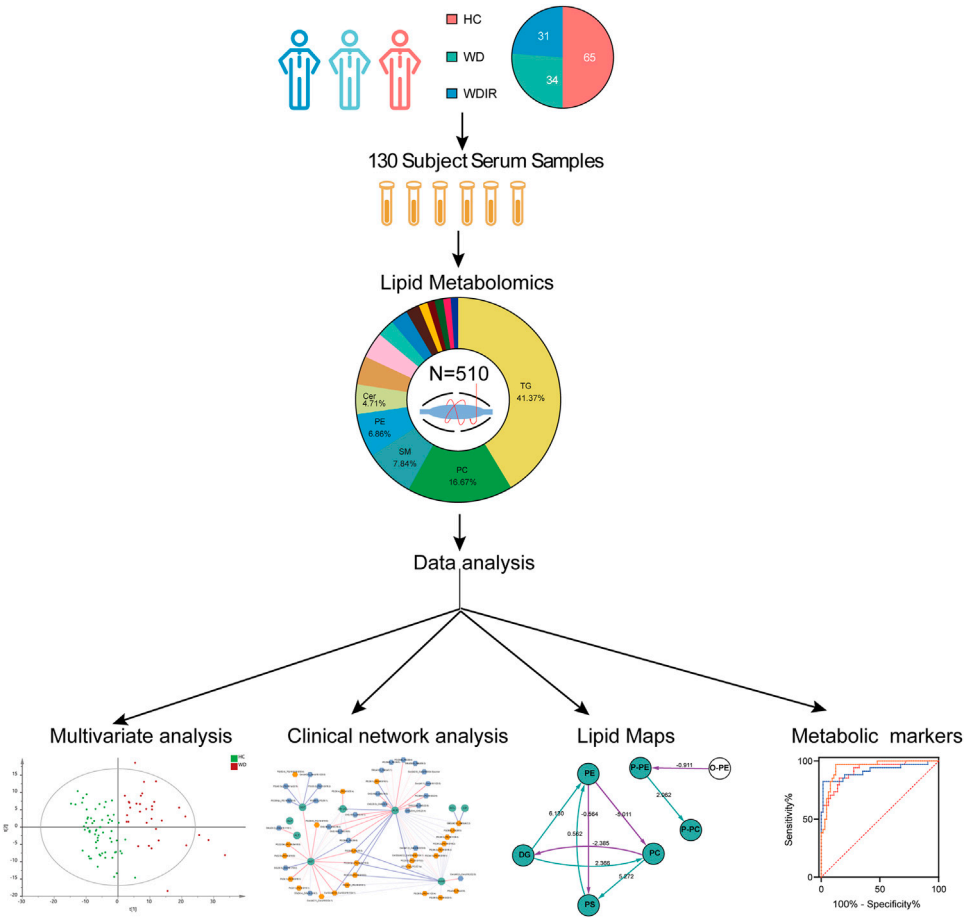

FIGURE 1 | Workflow of WD serum analysis. This figure depicts the design and steps of this study, beginning with sample collection for the three cohorts, followed by untargeted lipidomic analysis, and then the various data analyses employed, including PCA, OPLS-DA, univariate T-test and ANOVA.

TABLE 1 | Baseline characteristics of subjects.

Characteristics	Patient (n = 34)	Control (n = 65)
Age (years)	27.5 ± 10.9	29.3 ± 11.1
Sex (male/female)	16/18	36/29
Manifestation (cerebral/hepatic/mixed)	6/16/12	—
Ceruloplasmin (g/L)	0.1 ± 0.04	—
Serum copper level (μmol/L)	5.8 ± 3.8	—
Urinary copper level (μmol/24 h)	10.1 ± 26.8	—
Acetylcholine esterase (U/L)	5048.2 ± 2360.1	—
Alanine aminotransferase (U/L)	55.8 ± 96.1	18.5 ± 11.0
Aspartate aminotransferase (U/L)	45.5 ± 47.2	21.4 ± 5.5
Gamma-glutamyl aminotransferase (U/L)	54.2 ± 43.8	20.0 ± 11.2
Alkaline phosphatase (U/L)	99.6 ± 63.7	79.3 ± 51.7
Albumin (g/L)	36.9 ± 8.1	46.6 ± 2.7
Triglyceride (mmol/L)	0.8 ± 0.4	1.2 ± 0.4

Data are presented as mean as the mean ± SD.

Ceruloplasmin content was significantly reduced (less than 0.1 g/L) in most patients, but 21% of patients still had a mildly reduced level of ceruloplasmin between 0.1 and 0.2 g/L. These patients were distributed in the adolescent stage, and 2/3 of them had liver-type symptoms. Serum TG levels were tested in patients, with an average value of 0.85 mmol/L (normal value: 0.28–1.8 mmol/L). Serum TG levels in controls were tested, with an average value of 1.19 mmol/L and generally higher than those of the patients. A T-test was performed for the differences between the two groups, with $p < 0.05$. The clinical details of the WD patients are shown in **Table 1**.

Differential Lipids Analysis

SIMCA-P 14.1 software was used to model the lipidomic data of 130 serum samples. A PCA model was established for all participants (**Figure 2A**). The QC samples were clustered tightly together, and HC, WDIR, and WD could be clearly distinguished, which showed a trend of intergroup separation on the score plots. Given that WD is a genetic disease, the intersection between WD and WDIR conforms to genetic regulations. The results of the PLS-DA method showed better separation into separate clusters (**Figure 2B**). Furthermore, PLS-DA model validation with permutation tests (999 times) reflected that the metabolic alteration in each score plot was reliable and had clinical prediction significance (**Supplementary Figure S2**).

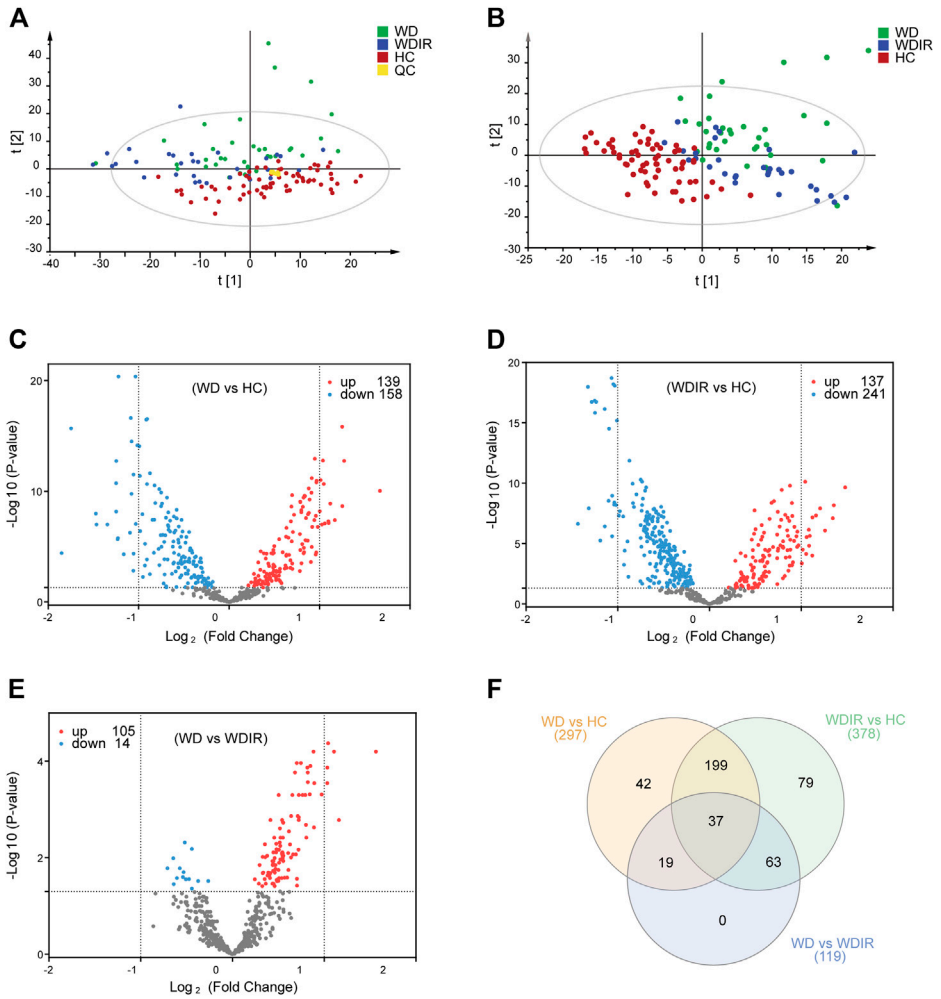

FIGURE 2 | Overview of differential lipid profiles in three groups. **(A)** Principal component analysis (PCA) was used to test the samples of the WD, WDIR and HC (R2X = 0.893, Q2 = 0.772). **(B)** Partial least squares discriminant analysis (PLS-DA) was used to cluster the samples of the three groups (R2X = 0.524, R2X = 0.676, Q2 = 0.506). **(C)** A volcano plot showing the dysregulated features between WD and HC (Student's t-test, FDR<0.05). **(D)** A volcano plot for the different lipids of WDIR and HC. **(E)** A volcano plot for the WD and WDIR. **(F)** Venn diagram displaying the number of differentially abundant metabolites that overlapped in the WD versus HC comparison (WD vs HC), WD versus WDIR comparison (WD vs WDIR), and WDIR versus HC comparison (WDIR vs HC).

A Venn diagram displayed the overlap of the differential metabolites in WD vs HC and WDIR vs HC (**Figure 2F**).

Differential Lipids Between Wilson's Disease and Healthy Controls

We further analyzed the relationship between WD and HC. PLS-DA was used to classify the two groups, and clear separation between the two groups (**Supplementary Figure S2**). 297 differential lipids were identified (**Figure 2C**) which mainly included TG, phosphatidylcholine (PC), sphingomyelin (SM), lysophosphatidylcholine (LPC), ceramide (Cer), and phosphatidylserine (PS). Differences in metabolites were observed between WD and HC: 14 metabolites (**Figure 3A**) were significantly increased with an absolute log2 FC ≥ 1 and FDR<0.05 and 22 significantly downregulated (**Figure 3A**) with absolute log2 FC ≤ 1 and FDR<0.05. A heat map shows the 36 significantly differentially abundant metabolites (**Figure 3A**). The ultra-long-chain ceramides, phosphatidylethanolamine (PE) and LPC were all downregulated compared with HC. PC was mainly decreased, while TG was mainly increased. Eight TGs with saturated fatty acids (TG(8:0/10:0/10:0), TG(12:0/12:0/14:0), TG(16:0/12:0/12:0), TG(18:1/12:0/12:0), TG(16:0/14:0/14:0), TG(16:0/14:0/16:0), TG(16:0/14:0/17:0), TG(16:0/16:0/16:0)) were significantly increased (**Figure 3A**), and two TGs with unsaturated fatty acids [TG(16:0/18:1/20:3), TG(18:3/18:3/18:3)] were significantly decreased (**Figures 3A**, **Figure 5H,I**) in WD patients compared with healthy controls. PC is mainly distributed on the outer side of the cell membrane. In our results, the unsaturated PC (**Figure 3A**) showed a downward trend. PE is mainly distributed in the inner membrane of the cell membrane. In our results, the acyl structure of PE (PE(16:0/18:1), PE(16:0/18:2), PE(18:0/18:1), PE(18:0/18:2),

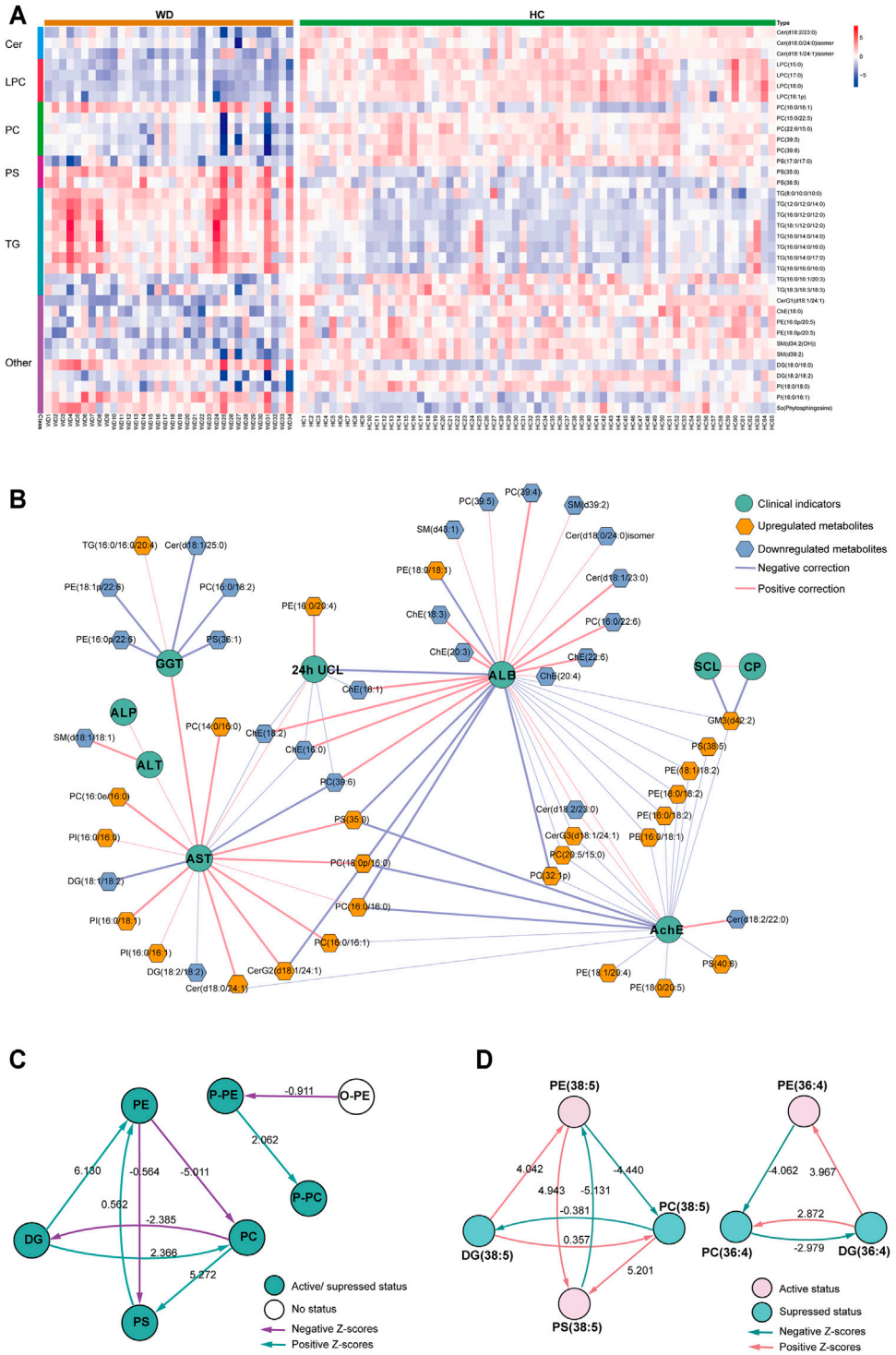

FIGURE 3 | Metabolomic profiles differ between WD and HC. **(A)** Heat map of the 36 differential lipids between WD and HC. **(B)** Correlation network of differential metabolites and clinical indicators in WD and HC. The connections between two nodes were established by Pearson correlation (Student's t-test, FDR <0.05). CP = ceruloplasmin; SCL = serum copper level; 24-h UCL = 24-h urinal copper level; ALT = alanine transaminase; AST = aspartate transaminase; GGT = γ-glutamyltransferase; ALP = alkaline phosphatase; AchE = acetylcholine esterase; ALB = albumin. **(C)** Lipid subclass correlation network of differentially abundant metabolites in WD and HC. **(D)** Lipid molecular species correlation network of differentially abundant metabolites in WD and HC.

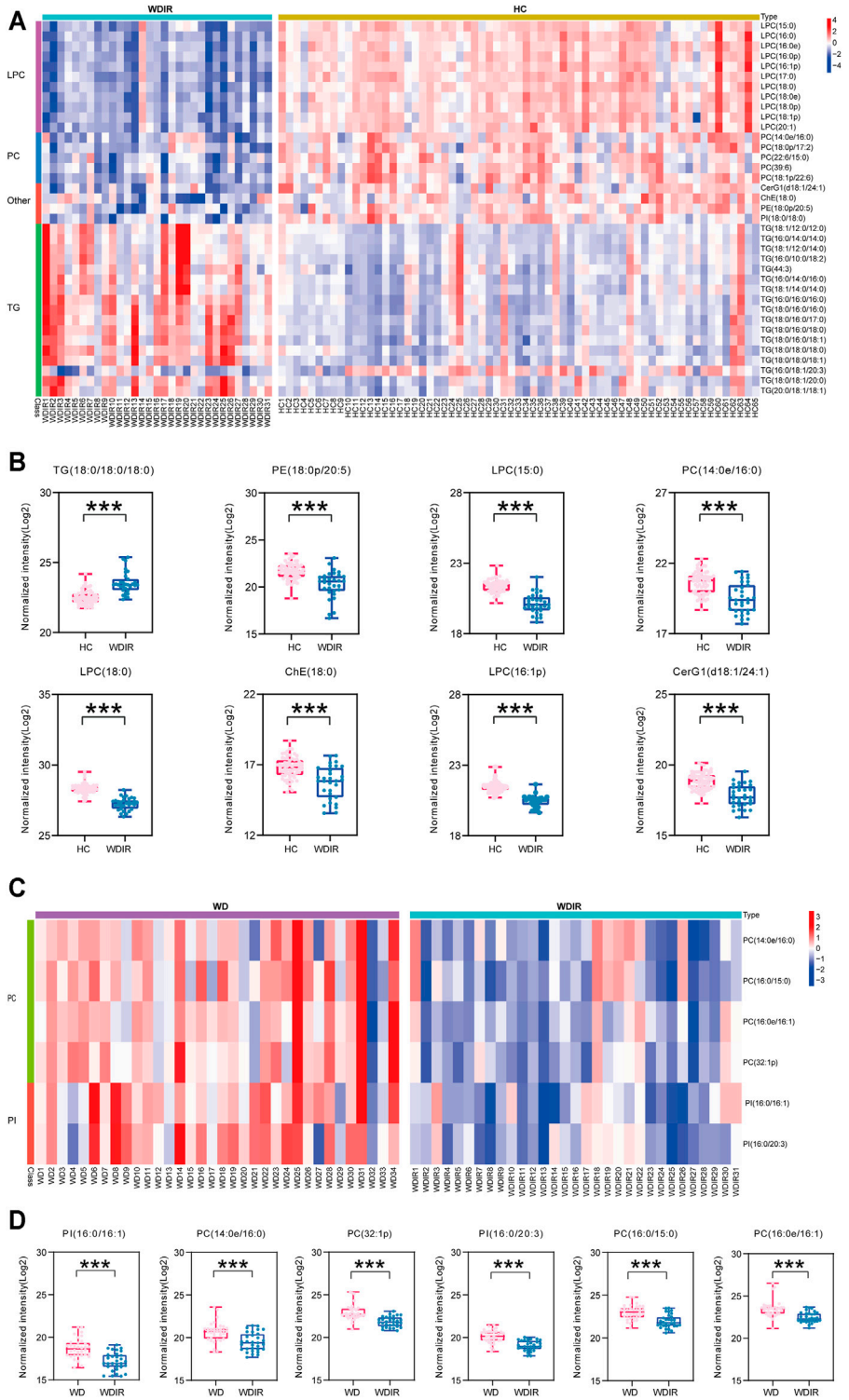

FIGURE 4 | Metabolomic profiles differ between WDIR vs HC and WD vs WDIR. **(A)** Heat map of the 37 differential metabolites between WDIR and HC. **(B)** Relative concentration of differential metabolites screened by LASSO in WDIR and HC. **(C)** Heat map of the 6 differential metabolites between WD and WDIR. **(D)** Relative concentration of differential metabolites in WD and WDIR.

PE(18:1/18:2), PE(18:1/20:4), PE(18:0/20:5)) was increased, while the acetal structure of PE [PE(16:0p/20:5), PE(16:0p/22:6), PE(18:1p/22:6), PE(18:0p/20:5)] was decreased (**Figures 3A,B**). Reduction in acetal PE content causes the destruction of the mitochondrial membrane (Maeba and Ueta, 2003), increases the generation of oxygen free radicals, causes mitochondrial dysfunction and energy metabolism failure, and causes cell apoptosis and even focal necrosis (Zoeller et al., 2002).

A correlation network based on the data of significantly differential metabolites and clinical factors in WD and HC revealed a change in the metabolic profile in WD patients (**Figure 3B**). Metabolites associated with γ-glutamyltransferase (GGT) or albumin (ALB), such as Cholesterol ester (ChE) and Cer, were mainly decreased, and the metabolites associated with aspartate transaminase (AST) and acetylcholine esterase (AchE), such as PC and PE, were mainly increased. Alkaline phosphatase (ALP), alanine transaminase (ALT), serum copper level (SCL) and ceruloplasmin had low correlations with differentially abundant metabolites in WD vs HC. Metabolic pathway analysis was conducted with BioPAN (Gaud et al., 2021) to further explore the metabolite–metabolite correlation between WD and HC (**Figures 3C,D**). The lipid-class active reactions were PC→PS→PE, DG→PE→PS, DG→PC and P-PE→P-PC. The lipid-class suppressed reaction chains were PE→PC→DG and PC→DG (**Figure 3C**). The synthesis of PS (38:5) was active, whereas decomposition was suppressed. The synthesis of DG (36:4) was suppressed, whereas decomposition was active (**Figure 3D**). **Figure 3D** indicates why PS (38:5) was a significantly increased metabolite and why DG (36:4) was a significantly decreased metabolite, as shown in **Figure 3A**.

Differential Lipids Between WDIR and Healthy Controls

To explore the metabolic differences between WDIR and the HC, a PLS-DA model was established. As is shown in **Supplementary Figure. S2C**, a clear separation was observed between WDIR and HC. A total of 378 dysregulated metabolic features were discovered between the two groups, including 16 significantly up-regulated lipids and 21 significantly decreased lipids (**Figure 2D**). **Figure 4A** shows the 37 significantly differential lipids between WDIR and HC. Among the top 37 lipids, those decreased included PC and LPC. In contrast, the top metabolites that increased were mostly TGs. According to LASSO regression selection (**Supplementary Figure S3**), there were 7 metabolites for which the levels were significantly changed in WDIR compared to those in the controls, including PE (18:0p/20:5), PC (14:0e/16:0), ChE (18:0), LPC (15:0), LPC (18:0), LPC (16:1p), and CerG1(d18:1/24:1) (**Figure 4B**). Moreover, the level of TG (18:0/18:0/18:0) was found to be significantly elevated in WD patients' immediate family or relatives. Interestingly, LPC (15:0) and CerG1(d18:1/24:1) were also decreased in WD patients compared with controls.

Differential Lipids Between Wilson's Disease and WDIR

Then, the differences between WD and WDIR were analyzed. A PLS-DA model was set up to show the overall metabolic differences between the two groups. The model demonstrated remarkable separation between WD patients and their relatives (**Supplementary Figure S2**). A total of 119 dysregulated metabolic features were identified between the two groups, including PC, SM, PI and TG (**Figure 2E**). The heat map showed that PC and PI were significantly upregulated in WD patients (**Figure 4C**). The levels of 6 significantly increased metabolites were higher in WD than in HC (**Figure 4D**).

Potential Lipid Biomarkers for Wilson's Disease

Seven important lipids were selected via least absolute shrinkage and selection operator (LASSO) regression significantly contributed to the diagnostic value for WD (**Figures 5A–G**, **Supplementary Figure S3**). The ROC curve was plotted for the 7 lipids to discriminate the WD patients and healthy controls. Among them, the AUC of the 7 lipids was greater than 0.8, with high sensitivity and specificity. PS (35:0) (95% CI: 0.862-0.976), PS (38:5) (95% CI: 0.763-0.922) and TG (38:0) (95% CI: 0.905-0.990) were increased differentially abundant metabolites (**Figure 5J**). CerG1(d42:2) (95% CI: 0.844-0.987), LPC(15:0) (95% CI: 0.926-0.993), LPC (17:0) (95% CI: 0.958-1.000) and PS (34:0) (95% CI: 0.842-0.972) were decreased (**Figure 5K**). LPC (17:0) and LPC (15:0) were shown to have the greatest chance of appearing in the biomarker panel. Binary Logistic regression analysis was performed on the biomarker panel and the AUC is 1.000 (**Figure 5L**).

DISCUSSION

WD occurs in siblings (25%) but rarely in the previous generation (0.5%) or offspring (0.5%) because of the autosomal recessive mode of transmission (Brunet et al., 2012). The patients' family members may have late onset and be asymptomatic and may have different phenotypes even with the same genotype. Important diagnostic indicators for WD, including ceruloplasmin, 24 h urine copper excretion, Kayser Fleischer (KF) ring, and hepatic copper concentration, are all limited and not appropriate for screening in populations or newborns (Członkowska et al., 2018). Despite the potential devastating course of WD, the time of onset is not predictable. Thus, we aimed to identify potential lipid biomarkers that can provide an early warning for WD onset. Early diagnosis of WD is crucial for effective treatments that can prevent many manifestations of WD.

At the early stages of the disease, copper accumulation in the liver has a major effect on the dysregulation of lipid metabolism (Huster et al., 2007). In our study, there were common changes in TG molecules in WD patients and their relatives compared to those in controls. There were 297 differential lipids between WD and HC, of which TG, PC, SM, PE and LPC accounted for the majority. TG molecules except TG (16:0/18:1/20:3) were significantly upregulated in WDIR compared with HC. The detected TG molecules among the differential metabolites between WD and HC mostly had saturated fatty acid chains. However, only a few TGs containing unsaturated fatty acid chains were decreased in WD.

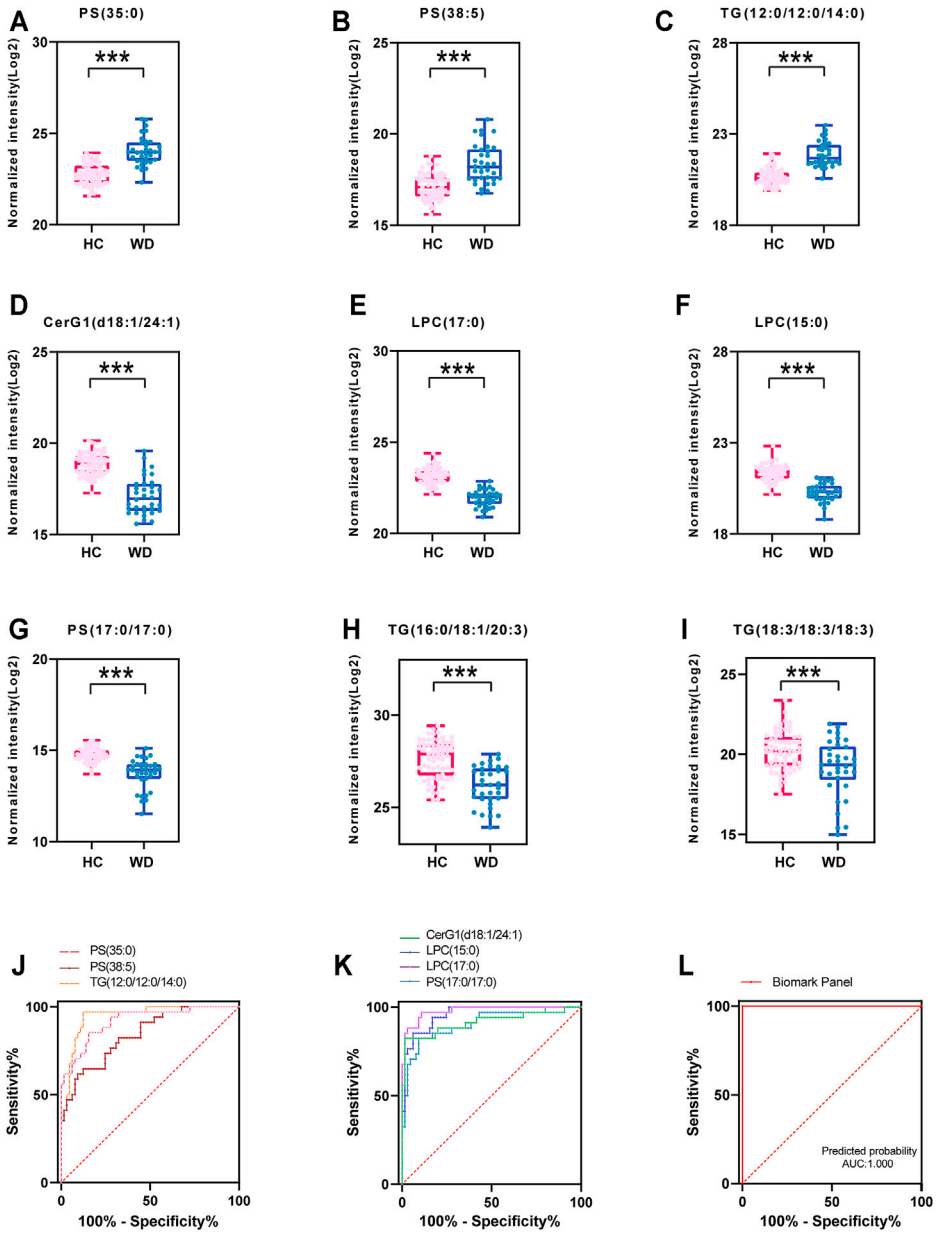

FIGURE 5 | Fitting prediction of WD biomarkers. **(A–G)** Relative concentration of significantly differentially abundant metabolites screened by LASSO in WD and HC. **(H–I)** Relative unsaturated TG concentration of significantly differentially abundant metabolites in WD and HC. **(J–K)** ROC curve analysis of increased metabolites in WD and HC. **(L)** ROC curve analysis of the biomarker panel in WD and HC.

In the human body, most of the total TG has unsaturated fatty acid chains (Kawano and Cohen, 2013). Therefore, when testing the total TG content in serum, the change would be consistent with most TGs containing unsaturated fatty acid chains showing a downward trend. In this study, although the serum TG contents of WD (0.85 mmol/L) were at lower range of normal, there is still a significant decrease compared with the controls (1.19 mmol/L), clearly indicative of lipid metabolism disorder with pathology in the liver in which fat droplets are deposited (Lutsenko, 2014). The extent of the accumulation of these saturated fatty acids in the steatotic liver parallels the liver disease severity in nonalcoholic steatohepatitis (Chiappini et al., 2016; Zhou et al., 2016; Chiappini et al., 2017). We speculated that hepatic steatosis was related not only to the amount of lipids but also to their specific composition and proportion. The accumulated copper in WD is assumed to lead to the development of chronic hepatitis by stimulating the production of reactive oxygen species and accelerating the formation of harmful hydroxyl radicals (Du et al., 2004). Unsaturated fatty acids containing multiple double bonds play a protective role in liver by redox reaction and reaction with free radicals (DeLany et al., 2000; Barber et al., 2021). Animal studies suggest PUFAs could reduce hepatic TG deposition (Sekiya et al., 2003). In our study, saturated fatty acids

were upregulated and unsaturated fatty acids were downregulated in WD patients, resulting in a reduction of hepatoprotective effect and WD exacerbations. Unsaturated fatty acids were upregulated in their asymptomatic relatives. We speculated that unsaturated fatty acids could protect the liver against lipid accumulation.

It is well-known that dietary fat, along with adipose tissue lipolysis and hepatic *de novo* lipogenesis, affects hepatic lipogenesis (Luukkonen et al., 2018). There is evidence that saturated fatty acids derived from the diets may influence liver fat content (Allard et al., 2008; Petersson et al., 2010). Liver TGs may be derived from the plasma or be newly synthesized from glucose (Kawano and Cohen, 2013). Consumption of low glycemic index diets could improve liver lipid metabolism and disease prognosis, since glucose promotes lipogenesis by activation of carbohydrate response element binding protein (ChREBP) (Kawano and Cohen, 2013). Additionally, dietary (n-6) and (n-3) PUFAs are potent inhibitors of hepatic lipogenesis (Jump, 2011). But n-3 PUFAs cannot be synthesized by the human body and must be extracted from exogenous food (fish oil, flax seeds, etc.). Our results implied that the imbalance of intrahetapic lipid in WD patients could be corrected by supplementation with unsaturated fatty acids, since dietary PUFAs are able to regulate hepatic glycolysis and *de novo* lipogenesis and to limit TG deposition in the liver (Jump, 2008; Di Minno et al., 2012). Dietary supplementation with unsaturated fatty acids, especially PUFAs, and consumption of low glycemic index diets before the onset of WD may be of for protecting liver and delay the progression of cirrhosis. Further work is warranted to understand the role of unsaturated fatty acids in WD pathogenesis and therapeutics.

The result that LPCs were downregulated in both WD patients and WDIR compared with HC is intriguing. To date, it has been found that LPC is decreased in drug-induced liver injury, viral hepatitis, alcoholic hepatitis, nonalcoholic fatty liver, liver failure and liver cirrhosis (Huang et al., 2013; Saito et al., 2014; Sherriff et al., 2016). However, there is no report on the pathogenic mechanisms of LPCs in WD. The mechanisms underlying LPC lipotoxicity include lipoapoptosis triggered by c-Jun NH2-terminal kinase (JNK) and endoplasmic reticulum (ER) stress activation, causing mitochondrial dysfunction, and LPC impairs hepatic mitochondrial oxidative phosphorylation, inducing hepatocyte lipoapoptosis (Kakisaka et al., 2012; Hollie et al., 2014). Most of these lipotoxic mechanisms overlap those of saturated fatty acids, suggesting that LPC depletion could be a major downstream effector of saturated fatty acid toxicity.

Our study showed that the levels of PS (35:0) and PS (38:5) increased, whereas the levels of PS (34:0) decreased in WD patients. PS, accounting for 13–15% of the phospholipids in the human cerebral cortex, is an important precursor for the two major phospholipids PE and PC (Kim et al., 2014). It has also been found that PS can reduce oxidative stress in the brain and stimulate neurotransmitter release (Suzuki et al., 2001; Chaung et al., 2013). The significantly differential abundance of PS may be associated with the neurological presentation in WD. The lack of ATP7B-mediated hepatic efflux of copper contributes to the failure of mitochondria to handle massive copper accumulation (Zischka and Lichtmannegger, 2014; Polishchuk et al., 2019). Disruption of ER-mitochondrial PS transfer is a newly reported new mechanism involved in the development of liver disease (Hernández-Alvarez et al., 2019). It has also been found that PS on blood cells and endothelial cells plays an important role in the hypercoagulable state in cirrhotic patients (Wu et al., 2016).

We found a significant decrease of ultra-long-chain ceramides and glycosphingolipids. Ceramides containing long side chains such as palmitic (CER 16:0) and stearic (CER 18:0) are suspected to be linked to hepatic steatosis (Wasilewska et al., 2018). Cer-derived C22:0-24:0 ceramides are crucial for regulating hepatic function. C16:0 ceramides is suspected to correlate with hepatosteatosis (Turpin et al., 2014). Meanwhile, ceramide can induce hepatocyte apoptosis in WD patients, which is an important cause of hepatocyte loss (Lang et al., 2007; Engin, 2017). It is well known that increased and uncontrolled death of hepatocytes results in hepatic steatosis and cirrhosis, which are the most commonly described dysfunctions in WD (Wooton-Kee et al., 2020). Previous studies have shown that ceramide content decreased in the early stages of the disease and increased when liver cell apoptosis begins to exhibit pathological changes, such as liver cirrhosis. The reduction in Cer-mediated mitochondrial division may product the mitochondrial fatty acid oxidation capacity, which is almost certainly key to reducing hepatic steatosis (Samuel and Shulman, 2019). For a potential application of WD diagnosis, we established a biomarker panel that comprised 7 lipids (PS(35:0), PS (38:5), TG (38:0), CerG1(d42:2), LPC (17:0), LPC (15:0), and PS (34:0)). However, there are still some limitations in our study. Since WD is a rare disease, only 34 patients from one medical center were enrolled in our study during 7 years of sample collection. The diagnostic performance of the lipid biomarkers requires further validations in a larger cohort and a multiple-center study.

CONCLUSION

Based on our lipidomics data, we found an interesting metabolic profile of WD patients. Our results highlight lipids deregulations with the deposition of copper. The abnormal lipid metabolism provides possible biomarkers for the diagnosis of WD, as a complementary of ceruloplasmin. More importantly, lipid metabolism may also be an effective therapeutic target for WD, which may alleviate the hepatic steatosis and liver injury among the patients.

DATA AVAILABILITY STATEMENT

The original contributions presented in the study are included in the article/**Supplementary Material**, further inquiries can be directed to the corresponding authors.

ETHICS STATEMENT

The study involving human participants were reviewed and approved by the ethics committees of the First Hospital of Jilin University. Written informed consent to participate in this study was provided by the participants' legal guardian/ next of kin.

AUTHOR CONTRIBUTIONS

PY designed the study and revised the manuscript. YZ and YS were involved in data analysis and wrote the manuscript. YJ, CP and CL collected the data. ZW directed the LC-MS analysis. JS and JZ collected the samples and clinical data. JN and RH design the study and review the manuscript.

FUNDING

This research was funded by the National Natural Science Foundation of China (No. 81873156), and Young Science and Technology Talent Project of the Education Department of Liaoning Province China (No. LZ2020075). National Key Research and Development Program of China (No. 2018YFE0195200), Jilin Provincial Department of science and technology (20200201499JC). The open-access publication fees were funded by the first affiliated hospital of Dalian medical university.

SUPPLEMENTARY MATERIAL

The Supplementary Material for this article can be found online at: https://www.frontiersin.org/articles/10.3389/fphar.2021.754185/full#supplementary-material

REFERENCES

Ala, A., Walker, A. P., Ashkan, K., Dooley, J. S., and Schilsky, M. L. (2007). Wilson's Disease. *Lancet* 369, 397–408. doi:10.1016/S0140-6736(07)60196-2

Allard, J. P., Aghdassi, E., Mohammed, S., Raman, M., Avand, G., Arendt, B. M., et al. (2008). Nutritional Assessment and Hepatic Fatty Acid Composition in Non-Alcoholic Fatty Liver Disease (NAFLD): a Cross-Sectional Study. *J. Hepatol.* 48, 300–307. doi:10.1016/j.jhep.2007.09.009

Bandmann, O., Weiss, K. H., and Kaler, S. G. (2015). Wilson's Disease and Other Neurological Copper Disorders. *Lancet Neurol.* 14, 103–113. doi:10.1016/S1474-4422(14)70190-5

Barber, R. G., Grenier, Z. A., and Burkhead, J. L. (2021). Copper Toxicity Is Not Just Oxidative Damage: Zinc Systems and Insight from Wilson Disease. *Biomedicines* 9, 316. doi:10.3390/biomedicines9030316

Blanksby, S. J., and Mitchell, T. W. (2010). Advances in Mass Spectrometry for Lipidomics. *Annu. Rev. Anal. Chem. Palo Alto Calif.* 3, 433–465. doi:10.1146/annurev.anchem.111808.073705

Brunet, A. S., Marotte, S., Guillaud, O., and Lachaux, A. (2012). Familial Screening in Wilson's Disease: Think at the Previous Generation!. *J. Hepatol.* 57, 1394–1395. doi:10.1016/j.jhep.2012.07.011

Chaung, H. C., Chang, C. D., Chen, P. H., Chang, C. J., Liu, S. H., and Chen, C. C. (2013). Docosahexaenoic Acid and Phosphatidylserine Improves the Antioxidant Activities *In Vitro* and *In Vivo* and Cognitive Functions of the Developing Brain. *Food Chem.* 138, 342–347. doi:10.1016/j.foodchem.2012.10.082

Chiappini, F., Desterke, C., Bertrand-Michel, J., Guettier, C., and Le Naour, F. (2016). Hepatic and Serum Lipid Signatures Specific to Nonalcoholic Steatohepatitis in Murine Models. *Sci. Rep.* 6, 31587. doi:10.1038/srep31587

Chiappini, F., Coilly, A., Kadar, H., Gual, P., Tran, A., Desterke, C., et al. (2017). Metabolism Dysregulation Induces a Specific Lipid Signature of Nonalcoholic Steatohepatitis in Patients. *Sci. Rep.* 7, 46658. doi:10.1038/srep46658

Cortes, M., Pareja, E., García-Cañaveras, J. C., Donato, M. T., Montero, S., Mir, J., et al. (2014). Metabolomics Discloses Donor Liver Biomarkers Associated with Early Allograft Dysfunction. *J. Hepatol.* 61, 564–574. doi:10.1016/j.jhep.2014.04.023

Cumings, J. N. (1948). The Copper and Iron Content of Brain and Liver in the normal and in Hepato-Lenticular Degeneration. *Brain* 71, 410–415. doi:10.1093/brain/71.4.410

Członkowska, A., Litwin, T., Dusek, P., Ferenci, P., Lutsenko, S., Medici, V., et al. (2018). Wilson Disease. *Nat. Rev. Dis. Primers* 4, 21. doi:10.1038/s41572-018-0018-3

DeLany, J. P., Windhauser, M. M., Champagne, C. M., and Bray, G. A. (2000). Differential Oxidation of Individual Dietary Fatty Acids in Humans. *Am. J. Clin. Nutr.* 72, 905–911. doi:10.1093/ajcn/72.4.905

Di Minno, M. N., Russolillo, A., Lupoli, R., Ambrosino, P., Di Minno, A., and Tarantino, G. (2012). Omega-3 Fatty Acids for the Treatment of Non-alcoholic Fatty Liver Disease. *World J. Gastroenterol.* 18, 5839–5847. doi:10.3748/wjg.v18.i41.5839

Du, C., Fujii, Y., Ito, M., Harada, M., Moriyama, E., Shimada, R., et al. (2004). Dietary Polyunsaturated Fatty Acids Suppress Acute Hepatitis, Alter Gene Expression and Prolong Survival of Female Long-Evans Cinnamon Rats, a Model of Wilson Disease. *J. Nutr. Biochem.* 15, 273–280. doi:10.1016/j.jnutbio.2003.11.005

Engin, A. (2017). Non-Alcoholic Fatty Liver Disease. *Adv. Exp. Med. Biol.* 960, 443–467. doi:10.1007/978-3-319-48382-5_19

European Association for Study of Liver (2012). EASL Clinical Practice Guidelines: Wilson's Disease. *J. Hepatol.* 56, 671–685. doi:10.1016/j.jhep.2011.11.007

Ferenci, P., Steindl-Munda, P., Vogel, W., Jessner, W., Gschwantler, M., Stauber, R., et al. (2005). Diagnostic Value of Quantitative Hepatic Copper Determination in Patients with Wilson's Disease. *Clin. Gastroenterol. Hepatol. Off. Clin. Pract. J. Am. Gastroenterol. Assoc.* 3, 811–818. doi:10.1016/s1542-3565(05)00181-3

Ferenci, P., Stremmel, W., Członkowska, A., Szalay, F., Viveiros, A., Stättermayer, A. F., et al. (2019). Age and Sex but Not ATP7B Genotype Effectively Influence the Clinical Phenotype of Wilson Disease. *Hepatology* 69, 1464–1476. doi:10.1002/hep.30280

Ferenci, P., Steindl-Munda, P., Vogel, W., Jessner, W., Gschwantler, M., Stauber, R., et al. (2005). Diagnostic Value of Quantitative Hepatic Copper Determination in Patients with Wilson's Disease. *Clin. Gastroenterol. Hepatol.* 3, 811–818. doi:10.1016/s1542-3565(05)00181-3

Ferenci, P. (2014). Whom and How to Screen for Wilson Disease. *Expert Rev. Gastroenterol. Hepatol.* 8, 513–520. doi:10.1586/17474124.2014.899898

Gaud, C., C Sousa, B., Nguyen, A., Fedorova, M., Ni, Z., O'Donnell, V. B., et al. (2021). BioPAN: a Web-Based Tool to Explore Mammalian Lipidome Metabolic Pathways on LIPID MAPS. *F1000Res* 10, 4. doi:10.12688/f1000research.28022.2

Gerosa, C., Fanni, D., Congiu, T., Piras, M., Cau, F., Moi, M., et al. (2019). Liver Pathology in Wilson's Disease: From Copper Overload to Cirrhosis. *J. Inorg. Biochem.* 193, 106–111. doi:10.1016/j.jinorgbio.2019.01.008

Han, X., Yang, K., and Gross, R. W. (2012). Multi-dimensional Mass Spectrometry-Based Shotgun Lipidomics and Novel Strategies for Lipidomic Analyses. *Mass. Spectrom. Rev.* 31, 134–178. doi:10.1002/mas.20342

Hernández-Alvarez, M. I., Sebastián, D., Vives, S., Ivanova, S., Bartoccioni, P., Kakimoto, P., et al. (2019). Deficient Endoplasmic Reticulum-Mitochondrial Phosphatidylserine Transfer Causes Liver Disease. *Cell* 177, 881–895.e17. doi:10.1016/j.cell.2019.04.010

Hollie, N. I., Cash, J. G., Matlib, M. A., Wortman, M., Basford, J. E., Abplanalp, W., et al. (2014). Micromolar Changes in Lysophosphatidylcholine Concentration Cause Minor Effects on Mitochondrial Permeability but Major Alterations in Function. *Biochim. Biophys. Acta* 1841, 888–895. doi:10.1016/j.bbalip.2013.11.013

Huang, H. J., Zhang, A. Y., Cao, H. C., Lu, H. F., Wang, B. H., Xie, Q., et al. (2013). Metabolomic Analyses of Faeces Reveals Malabsorption in Cirrhotic Patients. *Dig. Liver Dis.* 45, 677–682. doi:10.1016/j.dld.2013.01.001

Huster, D., Purnat, T. D., Burkhead, J. L., Ralle, M., Fiehn, O., Stuckert, F., et al. (2007). High Copper Selectively Alters Lipid Metabolism and Cell Cycle Machinery in the Mouse Model of Wilson Disease. *J. Biol. Chem.* 282, 8343–8355. doi:10.1074/jbc.M607496200

Jump, D. B. (2008). N-3 Polyunsaturated Fatty Acid Regulation of Hepatic Gene Transcription. *Curr. Opin. Lipidol.* 19, 242–247. doi:10.1097/MOL.0b013e3282ffaf6a

Jump, D. B. (2011). Fatty Acid Regulation of Hepatic Lipid Metabolism. *Curr. Opin. Clin. Nutr. Metab. Care* 14, 115–120. doi:10.1097/MCO.0b013e328342991c

Kakisaka, K., Cazanave, S. C., Fingas, C. D., Guicciardi, M. E., Bronk, S. F., Werneburg, N. W., et al. (2012). Mechanisms of Lysophosphatidylcholine-Induced Hepatocyte Lipoapoptosis. *Am. J. Physiol. Gastrointest. Liver Physiol.* 302, G77–G84. doi:10.1152/ajpgi.00301.2011

Kawano, Y., and Cohen, D. E. (2013). Mechanisms of Hepatic Triglyceride Accumulation in Non-alcoholic Fatty Liver Disease. *J. Gastroenterol.* 48, 434–441. doi:10.1007/s00535-013-0758-5

Kim, H. Y., Huang, B. X., and Spector, A. A. (2014). Phosphatidylserine in the Brain: Metabolism and Function. *Prog. Lipid Res.* 56, 1–18. doi:10.1016/j.plipres.2014.06.002

Lang, P. A., Schenck, M., Nicolay, J. P., Becker, J. U., Kempe, D. S., Lupescu, A., et al. (2007). Liver Cell Death and Anemia in Wilson Disease Involve Acid Sphingomyelinase and Ceramide. *Nat. Med.* 13, 164–170. doi:10.1038/nm1539

Loomba, R., Quehenberger, O., Armando, A., and Dennis, E. A. (2015). Polyunsaturated Fatty Acid Metabolites as Novel Lipidomic Biomarkers for Noninvasive Diagnosis of Nonalcoholic Steatohepatitis. *J. Lipid Res.* 56, 185–192. doi:10.1194/jlr.P055640

Lutsenko, S. (2014). Modifying Factors and Phenotypic Diversity in Wilson's Disease. *Ann. N. Y. Acad. Sci.* 1315, 56–63. doi:10.1111/nyas.12420

Luukkonen, P. K., Sädevirta, S., Zhou, Y., Kayser, B., Ali, A., Ahonen, L., et al. (2018). Saturated Fat Is More Metabolically Harmful for the Human Liver Than Unsaturated Fat or Simple Sugars. *Diabetes Care* 41, 1732–1739. doi:10.2337/dc18-0071

Maeba, R., and Ueta, N. (2003). Ethanolamine Plasmalogen and Cholesterol Reduce the Total Membrane Oxidizability Measured by the Oxygen Uptake Method. *Biochem. Biophys. Res. Commun.* 302, 265–270. doi:10.1016/s0006-291x(03)00157-8

Mak, C. M., and Lam, C. W. (2008). Diagnosis of Wilson's Disease: a Comprehensive Review. *Crit. Rev. Clin. Lab. Sci.* 45, 263–290. doi:10.1080/10408360801991055

Mounajjed, T., Oxentenko, A. S., Qureshi, H., and Smyrk, T. C. (2013). Revisiting the Topic of Histochemically Detectable Copper in Various Liver Diseases with Special Focus on Venous Outflow Impairment. *Am. J. Clin. Pathol.* 139, 79–86. doi:10.1309/AJCPDZR4OHDQNG3L

Mulligan, C., and Bronstein, J. M. (2020). Wilson Disease: An Overview and Approach to Management. *Neurol. Clin.* 38, 417–432. doi:10.1016/j.ncl.2020.01.005

Petersson, H., Arnlöv, J., Zethelius, B., and Risérus, U. (2010). Serum Fatty Acid Composition and Insulin Resistance Are Independently Associated with Liver Fat Markers in Elderly Men. *Diabetes Res. Clin. Pract.* 87, 379–384. doi:10.1016/j.diabres.2009.11.019

Polishchuk, E. V., Merolla, A., Lichtmannegger, J., Romano, A., Indrieri, A., Ilyechova, E. Y., et al. (2019). Activation of Autophagy, Observed in Liver Tissues from Patients with Wilson Disease and from ATP7B-Deficient Animals, Protects Hepatocytes from Copper-Induced Apoptosis. *Gastroenterology* 156, 1173–1189.e5. doi:10.1053/j.gastro.2018.11.032

Ranucci, G., Polishchuck, R., and Iorio, R. (2017). Wilson's Disease: Prospective Developments towards New Therapies. *World J. Gastroenterol.* 23, 5451–5456. doi:10.3748/wjg.v23.i30.5451

Ryan, A., Nevitt, S. J., Tuohy, O., and Cook, P. (2019). Biomarkers for Diagnosis of Wilson's Disease. *Cochrane Database Syst. Rev.* 2019, CD012267. doi:10.1002/14651858.cd012267.pub2

Saito, K., Maekawa, K., Ishikawa, M., Senoo, Y., Urata, M., Murayama, M., et al. (2014). Glucosylceramide and Lysophosphatidylcholines as Potential Blood Biomarkers for Drug-Induced Hepatic Phospholipidosis. *Toxicol. Sci.* 141, 377–386. doi:10.1093/toxsci/kfu132

Samuel, V. T., and Shulman, G. I. (2019). Nonalcoholic Fatty Liver Disease, Insulin Resistance, and Ceramides. *N. Engl. J. Med.* 381, 1866–1869. doi:10.1056/NEJMcibr1910023

Sekiya, M., Yahagi, N., Matsuzaka, T., Najima, Y., Nakakuki, M., Nagai, R., et al. (2003). Polyunsaturated Fatty Acids Ameliorate Hepatic Steatosis in Obese Mice by SREBP-1 Suppression. *Hepatology* 38, 1529–1539. doi:10.1016/j.hep.2003.09.028

Sherriff, J. L., O'Sullivan, T. A., Properzi, C., Oddo, J. L., and Adams, L. A. (2016). Choline, its Potential Role in Nonalcoholic Fatty Liver Disease, and the Case for Human and Bacterial Genes. *Adv. Nutr.* 7, 5–13. doi:10.3945/an.114.007955

Stättermayer, A. F., Traussnigg, S., Dienes, H. P., Aigner, E., Stauber, R., Lackner, K., et al. (2015). Hepatic Steatosis in Wilson Disease--Role of Copper and PNPLA3 Mutations. *J. Hepatol.* 63, 156–163. doi:10.1016/j.jhep.2015.01.034

Steindl, P., Ferenci, P., Dienes, H. P., Grimm, G., Pabinger, I., Madl, C., et al. (1997). Wilson's Disease in Patients Presenting with Liver Disease: a Diagnostic challenge. *Gastroenterology* 113, 212–218. doi:10.1016/s0016-5085(97)70097-0

Suzuki, S., Yamatoya, H., Sakai, M., Kataoka, A., Furushiro, M., and Kudo, S. (2001). Oral Administration of Soybean Lecithin Transphosphatidylated Phosphatidylserine Improves Memory Impairment in Aged Rats. *J. Nutr.* 131, 2951–2956. doi:10.1093/jn/131.11.2951

Turpin, S. M., Nicholls, H. T., Willmes, D. M., Mourier, A., Brodesser, S., Wunderlich, C. M., et al. (2014). Obesity-Induced CerS6-Dependent C16:0 Ceramide Production Promotes Weight Gain and Glucose Intolerance. *Cell Metab* 20, 678–686. doi:10.1016/j.cmet.2014.08.002

Wasilewska, N., Bobrus-Chociej, A., Harasim-Symbor, E., Tarasów, E., Wojtkowska, M., Chabowski, A., et al. (2018). Increased Serum Concentration of Ceramides in Obese Children with Nonalcoholic Fatty Liver Disease. *Lipids Health Dis.* 17, 216. doi:10.1186/s12944-018-0855-9

Wooton-Kee, C. R., Robertson, M., Zhou, Y., Dong, B., Sun, Z., Kim, K. H., et al. (2020). Metabolic Dysregulation in the Atp7b -/- Wilson's Disease Mouse Model. *Proc. Natl. Acad. Sci. U. S. A.* 117, 2076–2083. doi:10.1073/pnas.1914267117

Wu, X., Yao, Z., Zhao, L., Zhang, Y., Cao, M., Li, T., et al. (2016). Phosphatidylserine on Blood Cells and Endothelial Cells Contributes to the Hypercoagulable State in Cirrhosis. *Liver Int.* 36, 1800–1810. doi:10.1111/liv.13167

Xie, J. J., and Wu, Z. Y. (2017). Wilson's Disease in China. *Neurosci. Bull.* 33, 323–330. doi:10.1007/s12264-017-0107-4

Zhang, L., Han, X., and Wang, X. (2018). Is the Clinical Lipidomics a Potential Goldmine? *Cell Biol. Toxicol.* 34, 421–423. doi:10.1007/s10565-018-9441-1

Zhou, Y., Orešič, M., Leivonen, M., Gopalacharyulu, P., Hyysalo, J., Arola, J., et al. (2016). Noninvasive Detection of Nonalcoholic Steatohepatitis Using Clinical Markers and Circulating Levels of Lipids and Metabolites. *Clin. Gastroenterol. Hepatol.* 14, 1463–1472.e6. doi:10.1016/j.cgh.2016.05.046

Zischka, H., and Lichtmannegger, J. (2014). Pathological Mitochondrial Copper Overload in Livers of Wilson's Disease Patients and Related Animal Models. *Ann. N. Y. Acad. Sci.* 1315, 6–15. doi:10.1111/nyas.12347

Zoeller, R. A., Grazia, T. J., LaCamera, P., Park, J., Gaposchkin, D. P., and Farber, H. W. (2002). Increasing Plasmalogen Levels Protects Human Endothelial Cells during Hypoxia. *Am. J. Physiol. Heart Circ. Physiol.* 283, H671–H679. doi:10.1152/ajpheart.00524.2001

Conflict of Interest: Author ZW is employed by iPhnome (Yun Pu Kang) biotechnology Inc. Dalian.

The remaining authors declare that the research was conducted in the absence of any commercial or financial relationships that could be construed as a potential conflict of interest.

Publisher's Note: All claims expressed in this article are solely those of the authors and do not necessarily represent those of their affiliated organizations, or those of the publisher, the editors and the reviewers. Any product that may be evaluated in this article, or claim that may be made by its manufacturer, is not guaranteed or endorsed by the publisher.

frontiers in Pharmacology

ORIGINAL RESEARCH
published: 30 November 2021
doi: 10.3389/fphar.2021.760474

Prediction of Liver Weight Recovery by an Integrated Metabolomics and Machine Learning Approach After 2/3 Partial Hepatectomy

Runbin Sun[1,2†], Haokai Zhao[1†], Shuzhen Huang[1], Ran Zhang[1], Zhenyao Lu[1], Sijia Li[1], Guangji Wang[1], Jiye Aa[1]* and Yuan Xie[1]**

[1]Jiangsu Province Key Laboratory of Drug Metabolism and Pharmacokinetics, State Key Laboratory of Natural Medicines, China Pharmaceutical University, Nanjing, China, [2]Phase I Clinical Trials Unit, Nanjing University Medical School Affiliated Drum Tower Hospital, Nanjing, China

OPEN ACCESS

Edited by:
Pei Jiang,
Jining First People's Hospital, China

Reviewed by:
HuaLin Cai,
Central South University, China
Chunmei Geng,
Jining First People's Hospital, China

***Correspondence:**
Guangji Wang
guangjiwang@hotmail.com
Jiye Aa
jiyea@cpu.edu.cn
Yuan Xie
yuanxie58@yahoo.com

[†]These authors have contributed equally to this work

Specialty section:
This article was submitted to Translational Pharmacology, a section of the journal Frontiers in Pharmacology

Received: 18 August 2021
Accepted: 01 November 2021
Published: 30 November 2021

Citation:
Sun R, Zhao H, Huang S, Zhang R, Lu Z, Li S, Wang G, Aa J and Xie Y (2021) Prediction of Liver Weight Recovery by an Integrated Metabolomics and Machine Learning Approach After 2/3 Partial Hepatectomy. Front. Pharmacol. 12:760474. doi: 10.3389/fphar.2021.760474

Liver has an ability to regenerate itself in mammals, whereas the mechanism has not been fully explained. Here we used a GC/MS-based metabolomic method to profile the dynamic endogenous metabolic change in the serum of C57BL/6J mice at different times after 2/3 partial hepatectomy (PHx), and nine machine learning methods including Least Absolute Shrinkage and Selection Operator Regression (LASSO), Partial Least Squares Regression (PLS), Principal Components Regression (PCR), k-Nearest Neighbors (KNN), Support Vector Machines (SVM), Random Forest (RF), eXtreme Gradient Boosting (xgbDART), Neural Network (NNET) and Bayesian Regularized Neural Network (BRNN) were used for regression between the liver index and metabolomic data at different stages of liver regeneration. We found a tree-based random forest method that had the minimum average Mean Absolute Error (MAE), Root Mean Squared Error (RMSE) and the maximum R square (R^2) and is time-saving. Furthermore, variable of importance in the project (VIP) analysis of RF method was performed and metabolites with VIP ranked top 20 were selected as the most critical metabolites contributing to the model. Ornithine, phenylalanine, 2-hydroxybutyric acid, lysine, etc. were chosen as the most important metabolites which had strong correlations with the liver index. Further pathway analysis found Arginine biosynthesis, Pantothenate and CoA biosynthesis, Galactose metabolism, Valine, leucine and isoleucine degradation were the most influenced pathways. In summary, several amino acid metabolic pathways and glucose metabolism pathway were dynamically changed during liver regeneration. The RF method showed advantages for predicting the liver index after PHx over other machine learning methods used and a metabolic clock containing four metabolites is established to predict the liver index during liver regeneration.

Keywords: liver regeneration, partial hepatectomy, metabolomics, machine learning, GC/MS

INTRODUCTION

The liver is the largest internal solid organ (by mass) and has various essential functions for body homeostasis, including digestion, balancing glucose and storing glycogen, regulating blood amino acids, carrying away wastes, detoxifying chemicals, and metabolizing drugs. The liver has a mysterious ability to regenerate. It is the only organ that can regenerate itself to 100% of original weight in mammals (Miyaoka and Miyajima, 2013; Michalopoulos and Bhushan, 2020). It is known that the liver can restore to its original weight from as little as 25% of the original liver mass to guarantee the stability of liver weight about body weight. Based on this feature of the liver, partial hepatectomy (PHx) is widely used in the clinic for liver trauma, intrahepatic gallstones, hepatic cyst, hepatic neoplasms (both benign and malignant), and liver transplantation (Orcutt and Anaya, 2018; O'Grady, 2000; Xia et al., 2014; Nuzzo et al., 2008). Liver regeneration is a highly complex process. Different types of cells and many signaling pathways are involved, including hepatocyte proliferation, reprogramming of extracellular matrix, inflammation, immune and metabolic regulation, etc. (Preziosi and Monga, 2017; Michalopoulos and Bhushan, 2020).

It is important to obtain accurate liver weight for major hepatic resection and living donor liver transplantation. Simply, the total liver volume can be predicted based on body surface area and body weight (Vauthey et al., 2002). However, this method cannot be used to measure liver volume after liver resection. Imaging-based liver volumetric methods include anatomical structure imaging method and functional imaging method. Anatomical structure imaging includes computed tomography (CT) (Ogasawara et al., 1995; Alonso-Torres et al., 2005; Lim et al., 2014; Kim et al., 2019), magnetic resonance imaging (MRI) (Hockings et al., 2002; Sahin et al., 2003; Inderbitzin et al., 2004), ultrasonography (Kitajima et al., 2008; Kasuya et al., 2011), and functional imaging including single-photon emission computed tomography (SPECT) (De Graaf et al., 2008; Stinauer et al., 2012; Yoshida et al., 2014). These methods have shown reliable liver volume measurements and have been widely utilized to evaluate postoperative liver regeneration and assess liver function recovery (Bassignani et al., 2001; Zamboni et al., 2008; de Graaf et al., 2010; Spira et al., 2012). These image-based evaluation methods can achieve the liver weight and the shape of the liver, and functional-based image methods can further evaluate the liver function. However, these methods have a certain degree of error and overestimate the actual liver volume (D'Onofrio et al., 2014). There still remains an urgent need to develop a new method to evaluate liver regeneration and liver function after PHx.

Several non-image methods for liver volumetry have been developed. From a systemic biology view, the microarray data of rat liver during regeneration and the adaptive logistic regression identified M6PR→IGF2R and MCM5→STAT1 pathways as biomarkers for liver regeneration (Chen et al., 2016). Metabolomics is the profile of endogenous small molecules. It is widely used in the early detection of hepatocellular carcinoma (Zhang et al., 2013; Safaei et al., 2016), identification of subtypes and different stages of non-alcoholic steatohepatitis (Alonso et al., 2017; Dong et al., 2017), investigation of hepatitis virus infection (Du Preez and Sithebe, 2013; Huang et al., 2016; Naggie et al., 2020), prediction of and identification of drug-induced liver injury (Xie et al., 2019), and reveal the mode of action of natural products in the treatment of liver disease (Beyoğlu and Idle, 2020). The metabolomics technique is used for liver transplantation to discover biomarkers associated with donor-recipient matching and early allograft dysfunction (Cortes et al., 2014; Faitot et al., 2018). Specifically, bile salt and triglyceride levels are proposed to be early predictors of liver volume and functional increase after liver resection (Hoekstra et al., 2012a; Hoekstra et al., 2012b). The hepatic ratio of phosphatidylcholine to phosphatidylethanolamine is also a survival predictor following partial hepatectomy (Ling et al., 2012). Hyaluronic acid is metabolized by liver sinusoid endothelial cells. Its level can be used to evaluate functional liver reserve after liver resection and prediction of complications associated with liver resection (Nanashima et al., 2001; Nanashima et al., 2004). The L-[1–^{13}C]Methionine breath test and the production of $^{13}CO_2$ are considered valuable indicators for evaluating liver regeneration (Ishii et al., 2001). These biomarker-based methods can predict the regeneration of the liver as well as liver function recovery.

Several models have been proposed to characterize the process of liver regeneration. A liver growth model based on general growth law has been introduced to accurately predict liver transplants' growth (Shestopaloff and Sbalzarini, 2014). Furchtgott et al. developed a mathematical model of rat liver regeneration based on the interplay of cytokines and growth factors, and Periwal et al. further transferred this model to humans (Furchtgott et al., 2009; Periwal et al., 2014). These studies used a single approach and are usually limited by moderate accuracy. Machine learning is a subset of artificial intelligence used for clinical diagnostics, prognosis prediction, precision treatments, health monitoring, and drug discovery and development (Vamathevan et al., 2019; Goecks et al., 2020). Machine learning approaches have large flexibility and are free from prior assumptions, and they are particularly suitable for datasets with few observations and many variables, especially for omics data. Traditional statistical methods aim to infer relationships between variables, while machine learning algorithms focus on making predictions as accurate as possible even though some of them are difficult to interpret. Machine learning disentangles the complex relationships between numerous variables of omics studies in determining their effect on the main outcome (Rajula et al., 2020). However, there is no study about predicting the liver index after PHx by integrating metabolomics and machine learning algorithms in our knowledge. Here we use nine machine learning methods including Least Absolute Shrinkage and Selection Operator Regression (LASSO), Partial Least Squares Regression (PLS), Principal Components Regression (PCR), k-Nearest Neighbors (KNN), Support Vector Machines (SVM), Random Forest (RF), eXtreme Gradient Boosting (xgbDART), Neural Network (NNET), and Bayesian Regularized Neural Networks (BRNN) to select the best regression model between the liver index and metabolomics data from serum, discover the main metabolic

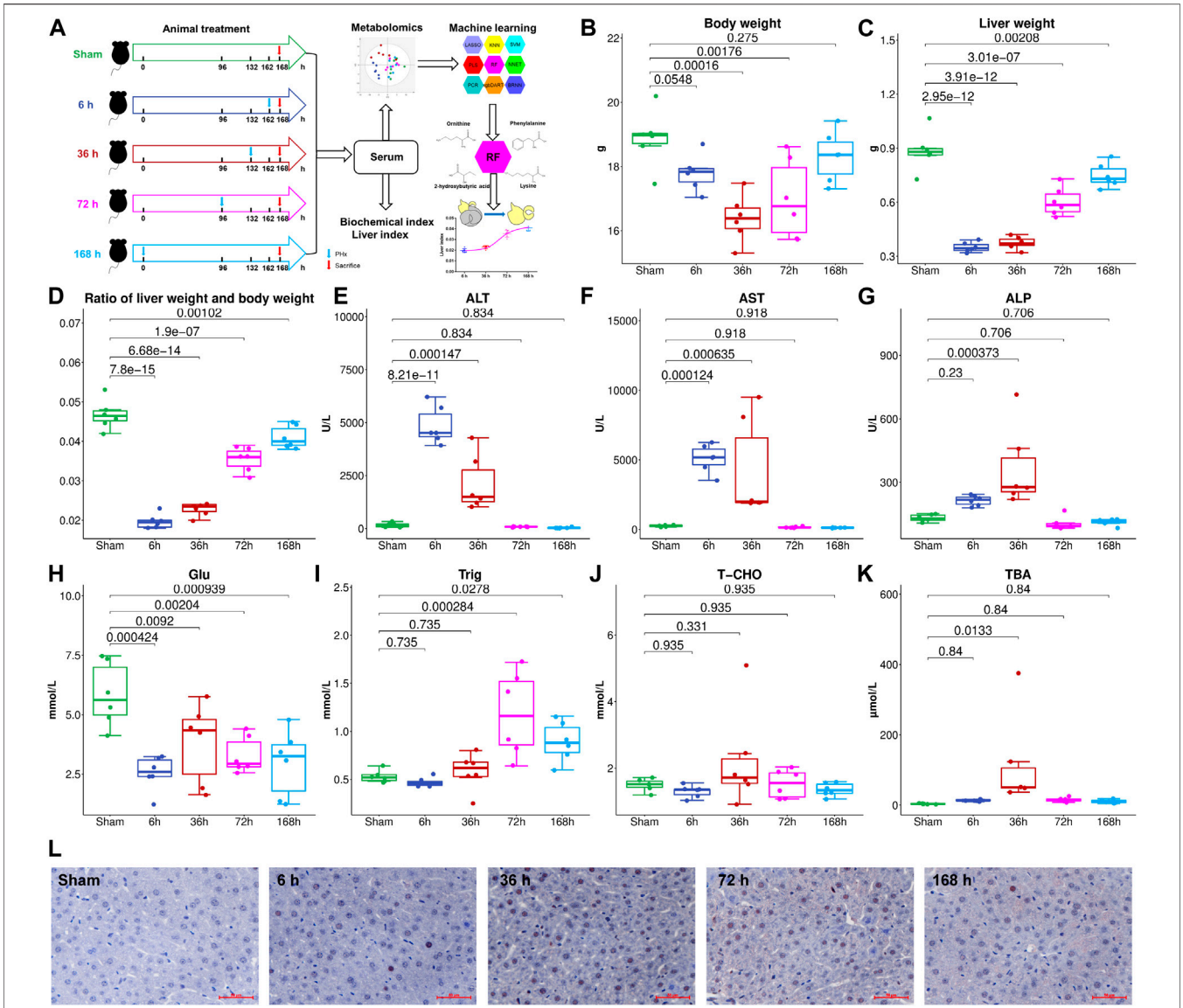

FIGURE 1 | (A), Flowchart of the animal experiment. Liver weight **(B)**, Body weight **(C)**, and liver index **(D)** change at different stages after 2/3 PHx. Liver function index, alanine aminotransferase (ALT) **(E)**, aspartate aminotransferase (AST) **(F)**, and alkaline phosphatase (AKP) **(G)** were measured for the Sham group and 6, 36, 72, and 168 h after PHx, serum glucose **(H)**, triglyceride **(I)**, total cholesterol **(J)**, and total bile acids (TBA) **(K)** were measured. **(L)**, PCNA expression in the livers of mice before and after PHx.

pathways during liver regeneration, and finally establish a prediction model with a metabolite set to predict the liver index during liver regeneration.

MATERIALS AND METHODS

Chemicals

Methanol (chromatography grade), n-Heptane (chromatography grade), methoxyamine, pyridine, and N-methyl-N-trimethylsilyl-trifluoroacetamide+1% trimethylchlorosilane (MSTFA+1% TMCS) were purchased from Merck KGaA (Darmstadt, Germany). Stable-isotope-labeled [$^{13}C_2$]-myristic acid was purchased from Cambridge Isotope Laboratories (Andover, MA, United States).

Animal Studies

Thirty male C57BL/6J mice (5 weeks old, purchased from Changzhou Cavens Laboratory Animal Co., Changzhou, China) were housed under a 12 h light/12 h dark condition (lights on at 6:00 and lights off at 18:00). All animal care and experimental procedures protocols were approved by the Animal Ethics Committee of China Pharmaceutical University (2018-DMPK-12-06). All mice were fed with a standard chow diet (AIN-93M, Trophic Animal Feed High-Tech Co., Ltd, Nantong, China) and tap water *ad libitum* for 1 week to acclimate the

environment. The mice were divided into five groups (n = 6), Sham group (Sham), 6 h after PHx group (6 h), 36 h after PHx group (36 h), 72 h after PHx group (72 h), and 168 h after PHx group (168 h). The mice were anesthetized with isofluorane when doing the PHx surgery. For the Sham group, the abdominal cavity was opened without cutting the liver and then sewed; for PHx groups, the left lateral and median liver lobes, including gall bladder, were resected according to the procedure in literature. The mice were sacrificed 0 h (Sham group), 6, 36, 72 and 168 h after PHx. At the time of sacrifice, mice were weighed and anesthetized by avertin; the whole blood was centrifuged at 8,000 rpm for 5 min to get the serum and was stored at −80°C for further analysis. Livers were harvested and weighed, and the liver index was calculated (liver weight/body weight). The proliferative cell nuclear antigen (PCNA) expression was measured, and images were collected using an inverted microscope (Leica DMI 3000B, Germany). A flowchart of the animal experiment is shown in **Figure 1A**.

Measurement of Serum Biochemical Index

Levels of serum glucose, triglyceride, cholesterol, total bile acids (TBA), alanine aminotransferase (ALT), aspartate aminotransferase (AST), and alkaline phosphatase (AKP) were measured using kits purchased from Nanjing Jiancheng Bioengineering Institute (Nanjing, China) according to the manufacturer's instructions.

Sample Preparation for GC/MS and Compound Identification

The metabolites in serum were profiled by a GC/MS-based metabolomics method as previously reported (A et al., 2005). Briefly, 50 μL of serum was extracted with 200 μL of methanol containing 5 μg/ml [$^{13}C_2$]-myristic acid; after oximation and derivatization, 0.5 μL of the sample were injected into a SHIMADZU QP2010Ultra/SE GC/MS system (Kyoto, Japan) with an RTx-5MS fused silica capillary column (30 m × 0.25 mm ID, J&W Scientific, United States). The raw data acquired were processed by GCMSSolution (version 4.11). The metabolites were identified using NIST 14 (National Institute of Standards and Technology, Gaithersburg, MD, United States), Wiley 9 (Wiley–VCH Verlag GmbH & Co KGaA, Weinheim, Germany), and an in-house mass spectra library database (A et al., 2005; Sun et al., 2019).

The Regression of Liver Index and Metabolites by Nine Machine Learning Methods

PCA was performed for dimension reduction using SIMCA-P 13.0 software (Umetrices, Umeå, Sweden). Nine machine learning methods including LASSO, PLS, PCR, KNN, SVM, RF, xgbDART, NNET, and BRNN were used for regression between the liver index and metabolites. The code used was shown in **Supplementary Data Sheet S2**. Models were evaluated by the parameters, including the Mean Absolute Error (MAE), the Root Mean Squared Error (RMSE), and R square (R^2). All of the machine learning methods were performed and tuned using the "caret" package in the R project (version 3.6.3). Variable importance in the projection (VIP) analysis was used to evaluate metabolites' contribution to the model.

Pathway Analysis

Metabolomics pathway analysis of the metabolites with VIP >1 was carried out using MetaboAnalyst (www.metaboanalyst.ca). Hypergeometric test for over-representation analysis and relative-betweenness centrality for pathway topology analysis was selected, and Mus musculus (KEGG) library was chosen.

Selection of Metabolite Set for the Prediction of the Liver Index

Correlation coefficients between liver index, ALT, and metabolites at different time points were calculated. To further evaluate the RF method's ability to predict the liver index after 2/3 PHx, the dataset was split into the training set and testing set (5:1). The metabolite with the most significant VIP value, the metabolites ranked top 4, 8, 12, 20, 40, 59 and the whole dataset without one metabolite whose VIP is 0 (**Supplementary Data Sheet S1**) was further used to train the RF model and predict the liver index in the testing set, and their performance was also compared. Models were evaluated by the parameters including MAE, RMSE, and R^2.

Statistical Analysis

For statistical analysis of MAE, RMSE, and R^2 in each model, Kruskal–Wallis Test followed by Wilcox test was used; for statistical analysis of metabolites among groups, One-way ANOVA followed by Fisher's LSD multiple comparison test and corrected by the Benjamini-Hochberg method to control the False Discovery Rate (FDR) was conducted by R project (version 3.6.3). The correlation coefficients were calculated by the "corrplot" package in the R project. $p < 0.05$ was considered statistically different.

RESULTS

Regeneration of Liver After 2/3 Partial Hepatectomy

To investigate liver regeneration progress and the associated metabolic change after partial hepatectomy, 2/3 PHx in C57BL/6J mice was performed and samples were collected at five time points (Sham group, 6, 36, 72, and 168 h after PHx, the total sample size is 30). The liver index was calculated using liver weight and body weight. The remaining liver exhibited an elevated growth rate in the first 3 days and returned to nearly 90% of the original weight after 7 days (**Figures 1B–D**). During liver regeneration, ALT (**Figure 1E**), AST (**Figure 1F**), and AKP (**Figure 1G**) all showed a significant increase at the early stage and returned to normal after 72 h. Serum glucose (**Figure 1H**) was reduced after PHx. Serum triglyceride (**Figure 1I**) and total cholesterol (**Figure 1J**) showed a slight decrease at 6 h after 2/3 PHx, increased at 36 and 72 h after 2/3 PHx, and fell at the late phase of liver regeneration. Total bile acids (TBA) (**Figure 1K**) in the serum significantly increased after 2/3 PHx. PCNA staining

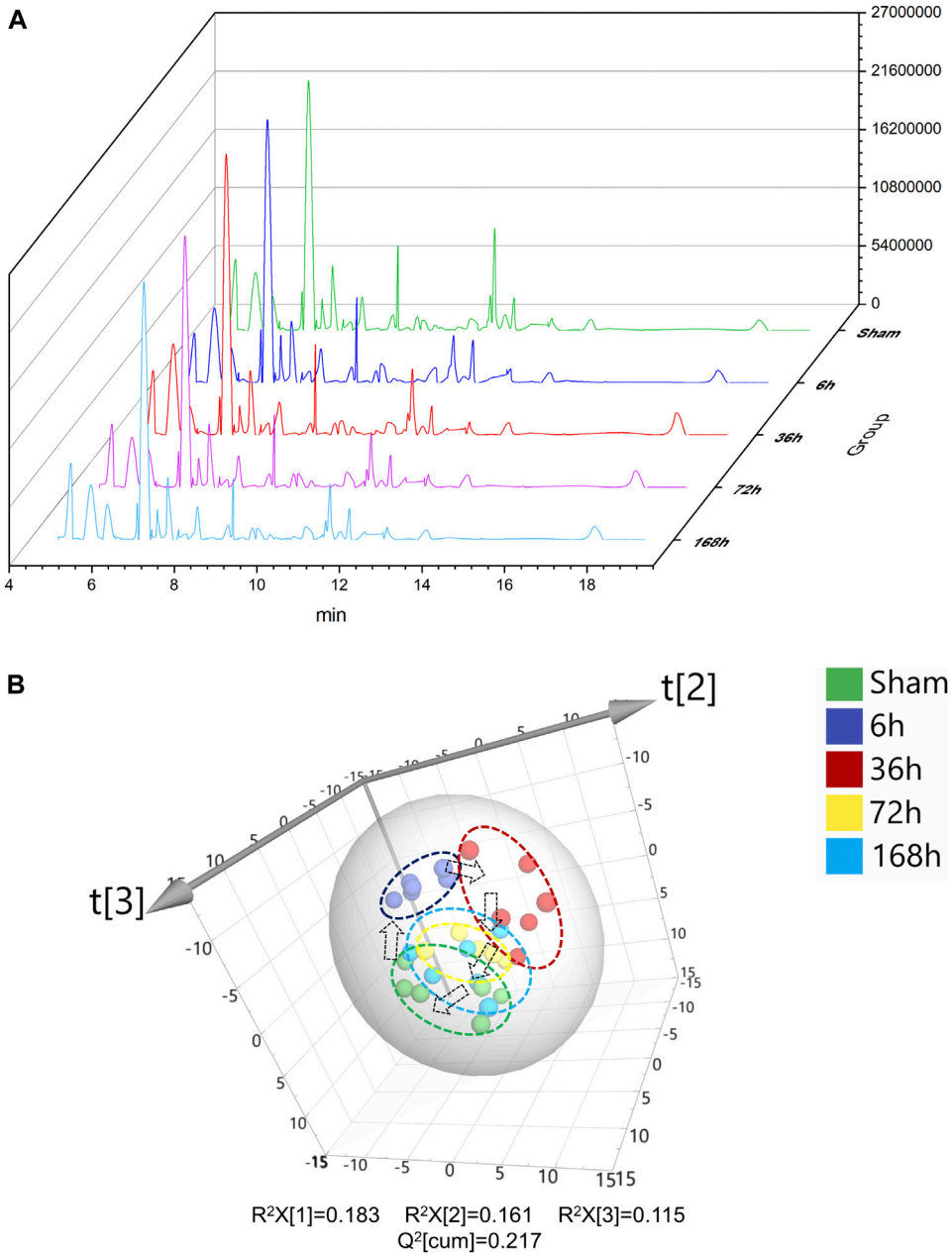

FIGURE 2 | (A) Typical GC/MS chromatograms of serum from Sham group and 6, 36, 72, and 168 h after PHx. **(B)** 3D scoress plot of principal components analysis of mouse serum from Sham group, 6 h group, 36 h group, 72 h group, and 168 h group, respectively. Each point represents a metabolite profile of a biological replicate.

on the livers of sham-operated mice and the livers of mice following operation revealed apparent DNA replication, and there were most positive cells at 36 h after 2/3 PHx (**Figure 1L**).

GC/MS Chromatograms and Overview of the Metabolomics Data

Typical serum GC/MS chromatograms from each time point after PHx are shown in **Figure 2A**. One hundred eighteen compounds were identified, including organic acids, amino acids, carbohydrates, purines and fatty acids, the representative mass spectrum, and the comparison with mass spectrum in the library were shown in **Supplementary Data Sheet S1**. Unsupervised principal component analysis (PCA) was applied to gain an overview of the metabolomics data. From the scatter plot (**Figure 2B**), no outlier was found in the PCA analysis. A clear separation between the 6 h group, 36 h group, and sham group was observed, whereas the 72 h

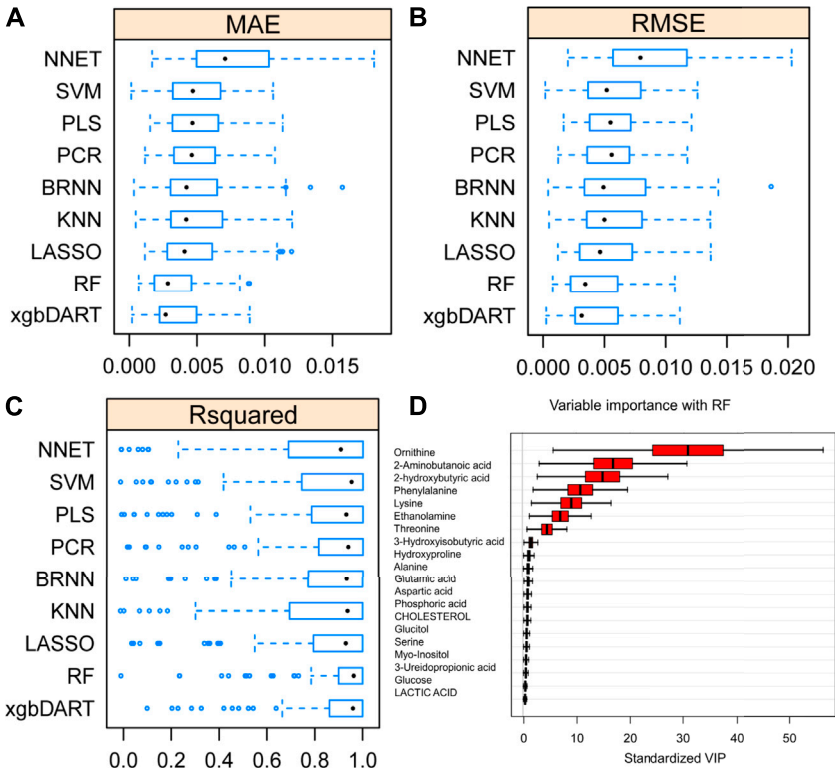

FIGURE 3 | Average MAE **(A)**, RMSE **(B)** and R^2 **(C)** on 10 repeated 10-fold cross-validation of nine machine learning algorithms for prediction of the liver index from metabolomics data. **(D)** Variable importance revealed by random forest (RF) method.

group and 168 h group were closer to the Sham group; this suggested that PHx induced significant metabolic change at the early stage and returned to normal during the liver regeneration process.

Comparison of Machine Learning Methods and Selection of Important Features

To select the most suitable machine learning model of the regression between the liver index and metabolites, we performed and compared nine machine learning methods: LASSO, PLS, PCR, KNN, SVM, RF, xgbDART, NNET, and BRNN. We performed 10-fold cross-validation 10 times on the dataset, and MAE, RMSE, and R^2 were calculated to evaluate the model performance. As shown in **Figures 3A–C**, the tree-based methods RF method and xgbDART method had the minimum average MAE, RMSE, and the maximum average R^2. xgbDART method is rather time-consuming and showed no obvious superiority over the RF method; thus, we selected the RF method for further analysis. To choose the most important metabolites contributing to the RF model, we performed VIP analysis and the metabolites which ranked top 20 were selected. Ornithine, phenylalanine, 2-aminobutanoic acid, 2-hydroxybutyric acid, and lysine had the highest VIP values (**Figure 3D**). The relative amounts of these metabolites were shown in **Figure 4A–L**.

Pathway Analysis

To reveal the key pathways changed during liver regeneration, the selected most important metabolites in serum were further analyzed by the online tool MetaboAnalyst (http://www.metaboanalyst.ca). The chosen metabolites were mapped to KEGG metabolic pathways for over-representation and pathway analyses. The pathway was considered to be significantly related which had a p value of less than 0.05. Arginine biosynthesis, Pantothenate and CoA biosynthesis, Galactose metabolism, Valine, leucine and isoleucine degradation, and beta-Alanine metabolism, etc. were the most influenced pathways, **Figure 5**.

Random Forest Model With a Set of Four Metabolites Were Selected for the Prediction of the Liver Index After 2/3 PHx

To further validate the most important metabolites, correlation analysis was performed and shown by heatmap in **Figure 6**. Metabolites including ornithine (**Figure 7A**), phenylalanine (**Figure 7B**), 2-aminobutanoic acid (**Figure 7C**), 2-hydroxybutyric acid (**Figure 7D**), lysine (**Figure 7E**), glutamic acid (**Figure 7F**), ethanolamine (**Figure 7G**), and threonine (**Figure 7H**) all showed an apparent positive correlation with the liver index. They showed obvious negative correlations with ALT, **Figures 7I–P**. The metabolomics data were partitioned into the training set and testing set, containing 25 samples and five

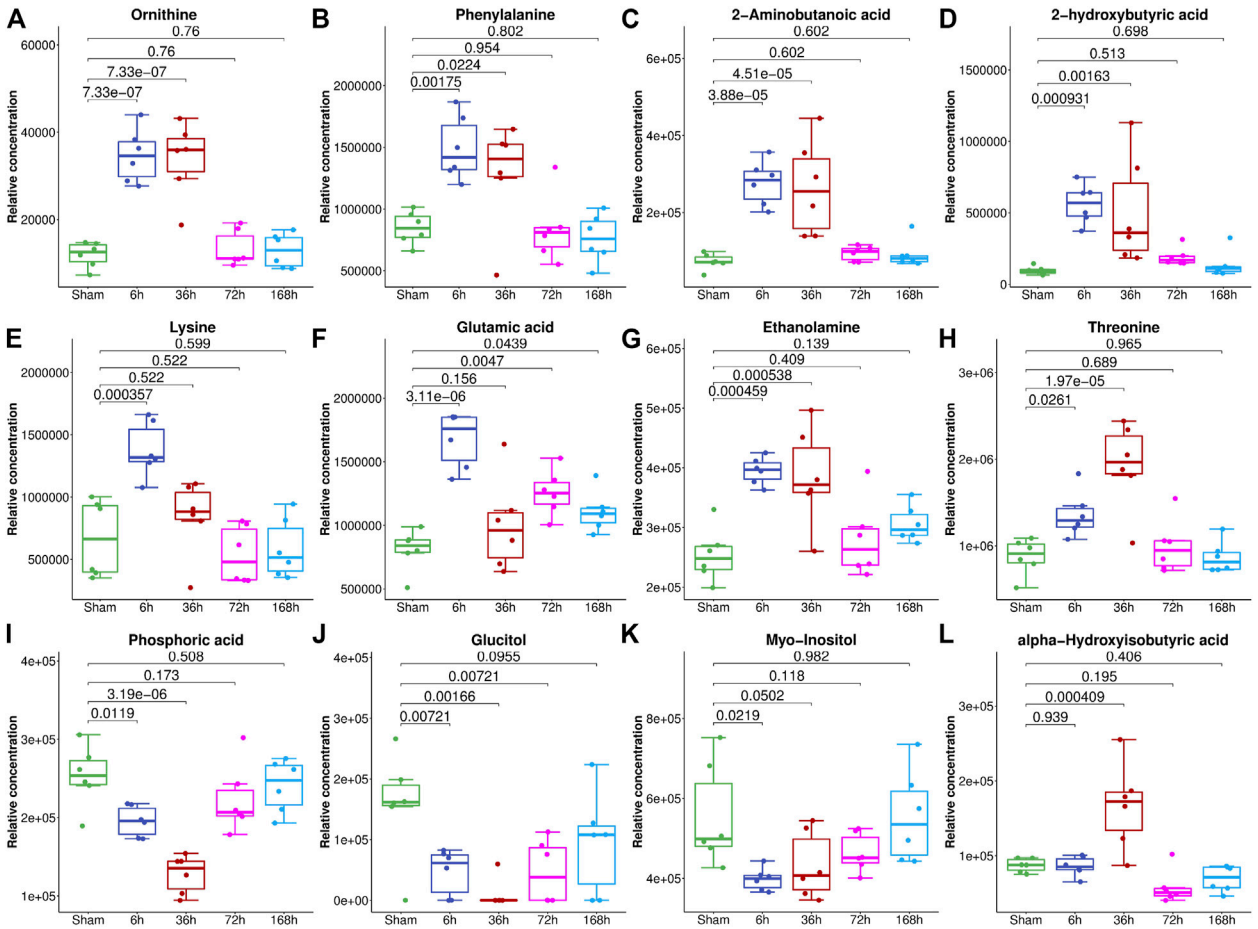

FIGURE 4 | The relative abundance of metabolites with the highest VIP values in the serum of mice from the Sham group and 6, 36, 72, and 168 h after PHx. The box plot shows the relative abundance of metabolites, including ornithine **(A)**, phenylalanine **(B)**, 2-aminobutanoic acid **(C)**, 2-hydroxybutyric acid **(D)**, lysine **(E)**, glutamic acid **(F)**, ethanolamine **(G)**, threonine **(H)**, phosphoric acid **(I)**, glucitol **(J)**, myo-inositol **(K)** and alpha-hydroxyisobutyric acid **(L)**. Data were represented as mean ± S.D.

samples, respectively. The comparison of RF methods using a different number of metabolites showed a significant difference in RAE, RMSE, and R_2 among other models (**Figures 8A–C**). Then the models were tested on the testing set, and the regression of actual liver index and predicted liver index were performed. The model RF05 containing metabolites ranked top 20 had the minimum MAE and RMSE. Considering the accuracy of prediction with as few metabolites as possible, we selected model RF02 with a set of 4 metabolites including ornithine, phenylalanine, lysine, and 2-hydroxybutyric acid as the final prediction model, and the MAE, RMSE, and R^2 of the testing set were 0.002, 0.003, and 0.948, respectively (**Figure 8D**). The metabolic map of these metabolites was shown in **Supplementary Figures S1–S4**.

DISCUSSION

After 2/3 PHx, the remnant liver initiates the progress of regeneration and the liver cells would undergo the resting state of the cell cycle (G0) to G1 transition, then S phase, and ultimately mitosis. The progress of liver regeneration includes initiation, progression, and termination, and each of these phases was tightly regulated by numerous signaling pathways (Caldez et al., 2018). To explore the metabolic change and then establish a regression method to predict the liver index at each phase by metabolites in the serum during liver regeneration, we select four time points after 2/3 PHx representing different stages. The liver index at different time points showed a typical growth curve and indicated that these time points could represent the growth of the remaining liver. The serum biochemical indexes representing the liver function and staining results representing the growth of liver cells also indicated the different phases during liver regeneration.

Machine learning has variable applications in healthcare. The main functions of machine learning algorithms include classification, regression, and dimensional reduction. Here we aimed to establish a relationship between metabolites in the serum and liver index at a different time of liver regeneration by regression and select the potential biomarkers of liver regeneration. We compared nine machine learning algorithms for regression, LASSO, PLS, PCR, KNN, SVM, RF, xgbDART, NNET, and BRNN. LASSO is a regression model originally

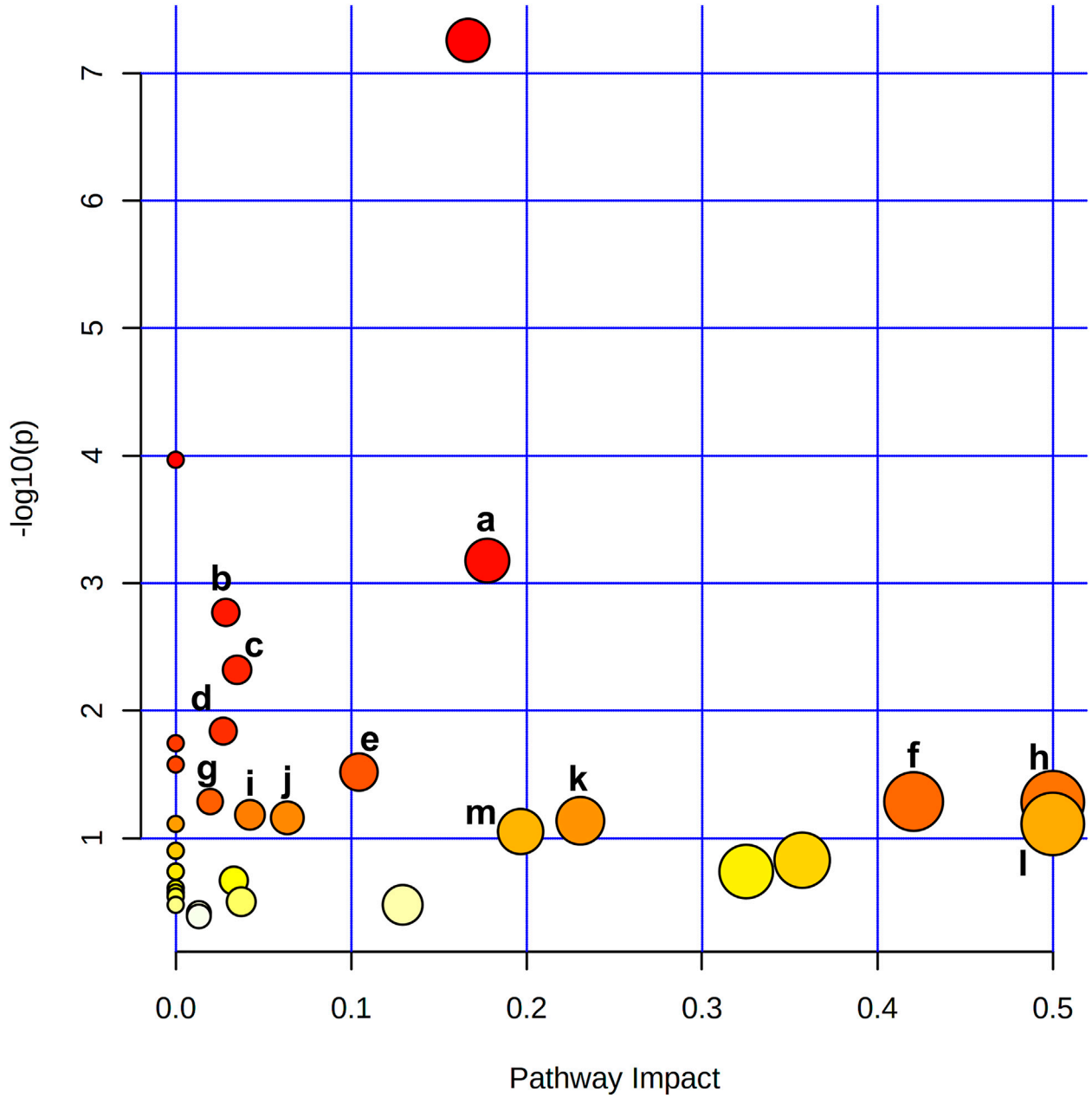

FIGURE 5 | Metabolite pathway analysis based on metabolites displayed significant variation in the serum revealed that a. Arginine biosynthesis, b. Pantothenate and CoA biosynthesis, c. Galactose metabolism, d. Valine, leucine and isoleucine degradation, e. beta-Alanine metabolism, f. Alanine, aspartate and glutamate metabolism, g. Glutathione metabolism, h. Phenylalanine, tyrosine and tryptophan biosynthesis, i. Glyoxylate and dicarboxylate metabolism, j. Cysteine and methionine metabolism, k. Glycine, serine and threonine metabolism, l. D-Glutamine and D-glutamate metabolism, m. Arginine and proline metabolism were the most affected pathways after 2/3 PHx.

formulated from the linear regression model and performed both for variable selection and regression. PLS and PCR are methods where multivariate data is projected into a smaller coordinate space (dimensional reduction) before regression. SVM method constructs hyperplanes that can be used for classification and regression. RF and xgbDART are both tree-based models which construct a multitude of decision trees. NNET and BRNN are considered deep learning methods and they simulate biological neural networks that constitute animal brains. These methods are more complex non-linear machine learning methods applicable for analyzing high-dimensional metabolomics data. The comparison of MAE, RMSE, and R^2 of the methods used showed RF and xgbDART are the most accurate methods. xgbDART is much more time-consuming than RF, whereas it offers no significant advantage. Thus we select RF as the method used for further optimization and analysis. From the VIP analysis

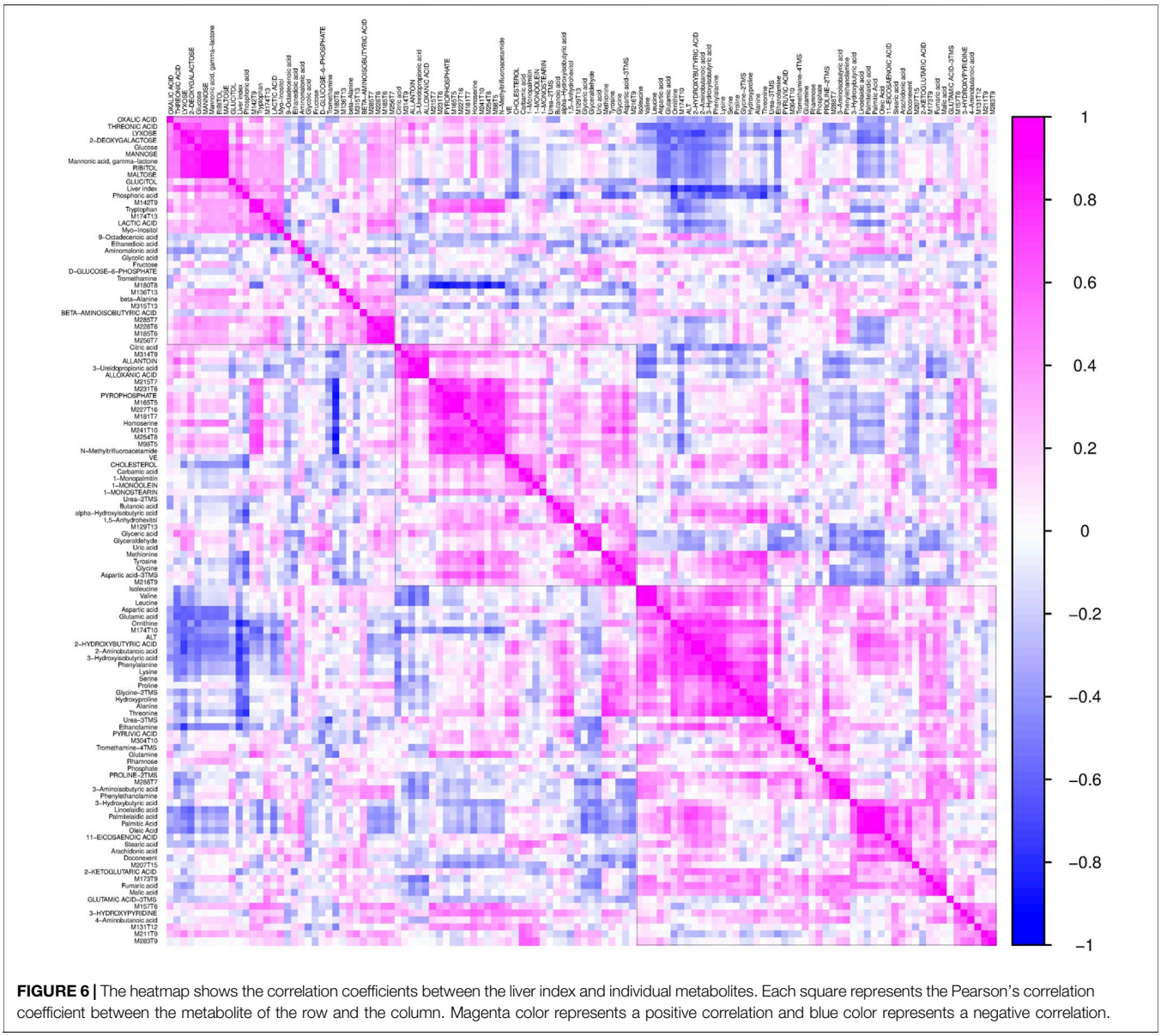

FIGURE 6 | The heatmap shows the correlation coefficients between the liver index and individual metabolites. Each square represents the Pearson's correlation coefficient between the metabolite of the row and the column. Magenta color represents a positive correlation and blue color represents a negative correlation.

of RF, we choose different amounts of metabolites to validate the model performance further and evaluate its prediction ability. A metabolite set containing ornithine, phenylalanine, lysine, and 2-hydroxybutyric acid was selected as the potential metabolite set for predicting the liver index after 2/3 PHx.

Networks, including cytokine, growth factor, and metabolic, are the essential circuitry required for liver regeneration (Fausto et al., 2006). Metabolic alteration is proposed to occur immediately after PHx. The previous gene expression data implied that metabolic genes are suppressed during liver regeneration, which is considered paradoxical because it maintains metabolic homeostasis and supports regeneration (Fausto et al., 2006). Currently, there is more understanding of metabolic changes during liver regeneration. Glucose metabolism, lipid metabolism, bile acid metabolism, amino acid metabolism, and one-carbon metabolism are essential for liver regeneration (Huang and Rudnick, 2014; Preziosi and Monga, 2017). We also observed a significant elevation of triglycerides and bile acids and the reduction of glucose in the serum during liver regeneration. It has been reported that glucose supplementation impairs liver regeneration, and preventing the accumulation of hepatic fat also suppresses liver regeneration (Huang and Rudnick, 2014). Dietary caloric restriction accelerates the initiation of regenerative hepatocellular proliferation (Cuenca et al., 2001). These studies revealed the importance of nutrient metabolism in liver regeneration. Bile acids are important for liver regeneration following partial hepatectomy, the extra bile acids cause activation of bile acid receptors including TGR5 and FXR thus preventing hepatotoxicity and providing signals to the regenerative process (Fan et al., 2015; van de Laarschot et al., 2016; Kong et al., 2018). Protein synthesis and amino acid metabolism are

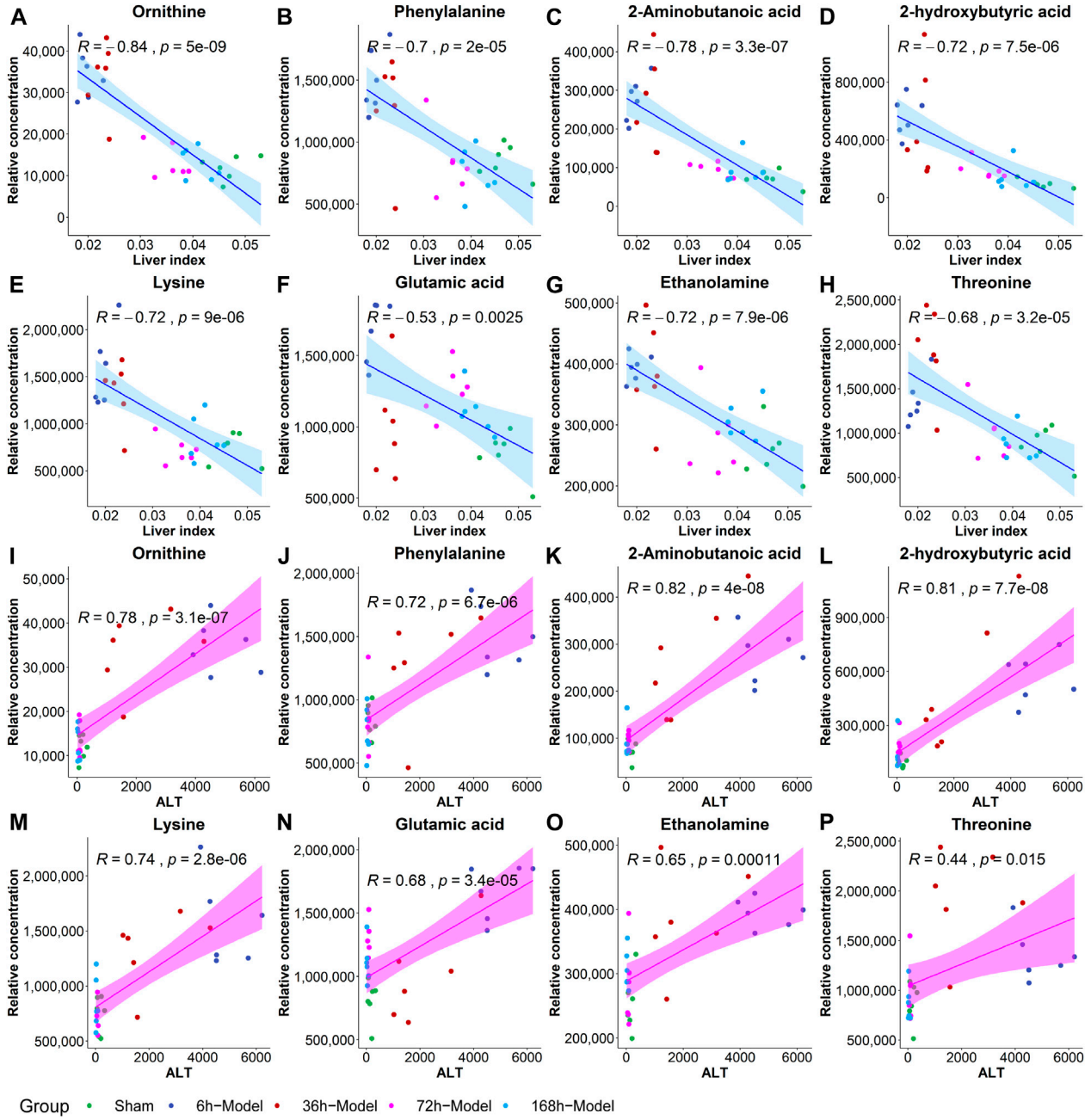

FIGURE 7 | The correlation coefficients between the liver index and metabolites including ornithine **(A)**, phenylalanine **(B)**, 2-aminobutanoic acid **(C)**, 2-hydroxybutyric acid **(D)**, lysine **(E)**, glutamic acid **(F)**, ethanolamine **(G)** and threonine **(H)**, and the correlations between ALT and metabolites including ornithine **(I)**, phenylalanine **(J)**, 2-aminobutanoic acid **(K)**, 2-hydroxybutyric acid **(L)**, lysine **(M)**, glutamic acid **(N)**, ethanolamine **(O)**, and threonine **(P)**.

essential functions of the liver, and altered amino acid metabolism is observed during liver regeneration. Amino acids are not only components of protein but also work as endogenous signaling molecules. Ornithine is an amino acid that plays a vital role in the urea cycle. A previous study found that urea cycle enzymes were significantly perturbated during liver regeneration, which enhanced urea cycle capacity and increased ammonia elimination (Meier et al., 2019). 2-hydroxybutyric acid is an organic acid derived from alpha-ketobutyrate, and alpha-ketobutyrate is produced by threonine and methionine catabolism and glutathione anabolism. 2-aminobutyric acid is a byproduct of cysteine biosynthesis from cystathionine and it can modulate glutathione homeostasis (Irino et al., 2016). Glutathione is a critical intracellular antioxidant and participates in many critical cellular functions including defense against toxins and free radicals, modulation of cell cycle, and

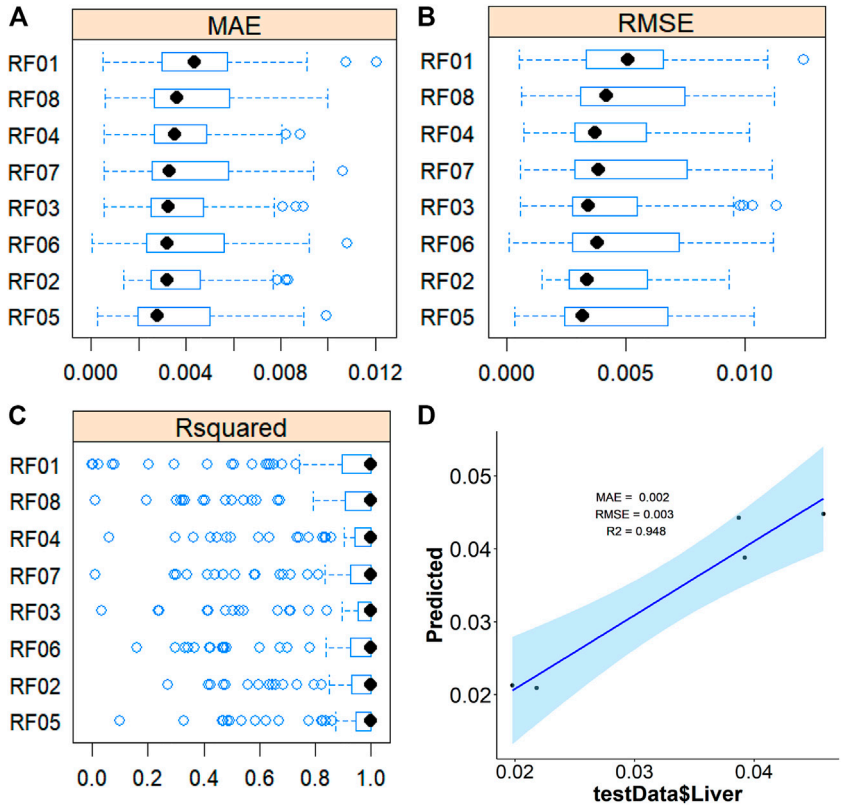

FIGURE 8 | Average MAE **(A)**, RMSE **(B)**, and R^2 **(C)** on 10 repeated 10-fold cross-validation of random forest method with a different subset of the metabolomics data for prediction of the liverindex from the train data set. **(D)**, the linear regression between the original liver index with the predicted liver index by the RF method in the testing data set.

maintenance of immune system homeostasis. Previous literature reported that glutathione, oxidized glutathione, and cysteine levels were doubled after PHx (Huang et al., 1998). Further study confirmed that glutathione plays a role in hepatic NF-κB activation *in vivo* and is necessary for the accurate timing of liver regeneration (Riehle et al., 2013). Urea cycle disorder was reported to be associated with a reduced level of glutathione, increased superoxide radical, and diminished activity of antioxidant mechanisms that may lead to cell damage. We found endogenous metabolites including ornithine, 2-hydroxybutyric acid, and 2-aminobutyric acid, the metabolites involved in the urea cycle and glutathione metabolism, all showed significant change during liver regeneration, and this may be associated with the down-regulated expression of glutamine synthase enzyme and specific activities of urea cycle metabolic pathways (Huang and Rudnick, 2014), and the cytochrome P450 system was down-regulated (Solangi et al., 1988). However, the precise mechanisms behind remain to be verified by further research.

There remain some shortages in this study. Firstly, four time points were selected to represent the initiation, progression, and termination phase of liver regeneration. More time points constituting a complete curve should be evaluated to establish the mathematical model and accurately predict liver weight. Secondly, due to the limitation of GC/MS, many metabolites had not been measured; further use of LC-QTOF/MS is essential to cover more metabolites. Thirdly, a mechanism study to reveal the change of metabolic pathways should be performed. Last but not least, although our model showed good performance in mice, there remains a gap between animals and humans; thus, the transformation from mouse to human should be considered for benefit in the clinic.

CONCLUSION

In conclusion, by using a high-throughput GC/MS-based metabolomics technology and machine learning algorithms, we establish mathematical models of liver index and metabolites to predict liver regeneration after 2/3 PHx and compared their performance. We finally choose a time-saving RF method and a set of 4 metabolites containing ornithine, phenylalanine, lysine, and 2-hydroxybutyric acid as a metabolic clock for the accurate prediction of liver index during liver regeneration. Glucose metabolism and amino acid metabolism pathways, including Arginine biosynthesis, Pantothenate and CoA biosynthesis, Galactose metabolism, Valine, leucine, and isoleucine degradation and beta-Alanine metabolism were the most influenced pathways. In the future, we are planning to utilize LC-QTOF/MS based metabolomics to cover more metabolites, and liver regeneration under different circumstances in animals

and humans will be performed to validate our model and transform the model into clinic.

DATA AVAILABILITY STATEMENT

The raw data supporting the conclusion of this article will be made available by the authors, without undue reservation.

ETHICS STATEMENT

The animal study was reviewed and approved by Animal Ethics Committee of China Pharmaceutical University.

AUTHOR CONTRIBUTIONS

YX, JA, and RS designed the study, RS, SH, RZ, ZL, and SL performed the majority of the experiments, RS and HZ statistically analyzed the data, YX and RS prepared the original draft, GW and JA reviewed and edited the manuscript. All authors have read and agreed to the published version of the manuscript.

FUNDING

This research was funded by the National Natural Science Foundation of the People's Republic of China (Grant numbers 81872932, 81703601, 81530098, 81421005), the Key Technology Projects of China "Creation of New Drugs" (Grant number 2017ZX09301013), Leading technology foundation research project of Jiangsu Province (BK20192005), Six Talent Peaks Project in Jiangsu Province (SWYY-061), Sanming Project of Medicine in Shenzhen (SZSM201801060).

SUPPLEMENTARY MATERIAL

The Supplementary Material for this article can be found online at: https://www.frontiersin.org/articles/10.3389/fphar.2021.760474/full#supplementary-material

Supplementary Data Sheet S1 | The comparison of the representative mass spectrum with mass spectrum in the library.

Supplementary Data Sheet S2 | Original data of metabolomics and VIPs in each model.

Supplementary Figure S1 | The code of machine learning models.

Supplementary Figure S2 | The metabolic pathway of ornithine: arginine and ornithine metabolism.

Supplementary Figure S3 | The metabolic pathway of ornithine: glutathione metabolism.

Supplementary Figure S4 | The metabolic pathway of phenylalanine and lysine: tropane, piperidine, and pyridine alkaloid biosynthesis.

Supplementary Figure S5 | The metabolic pathway of 2-hydroxybutyrate: propanoate metabolism.

REFERENCES

A, J., Trygg, J., Gullberg, J., Johansson, A. I., Jonsson, P., Antti, H., et al. (2005). Extraction and GC/MS Analysis of the Human Blood Plasma Metabolome. *Anal. Chem.* 77 (24), 8086–8094. doi:10.1021/ac051211v

Alonso, C., Fernández-Ramos, D., Varela-Rey, M., Martínez-Arranz, I., Navasa, N., Van Liempd, S. M., et al. (2017). Metabolomic Identification of Subtypes of Nonalcoholic Steatohepatitis. *Gastroenterology* 152 (6), 1449–e7. doi:10.1053/j.gastro.2017.01.015

Alonso-Torres, A., Fernández-Cuadrado, J., Pinilla, I., Parrón, M., de Vicente, E., and López-Santamaría, M. (2005). Multidetector CT in the Evaluation of Potential Living Donors for Liver Transplantation. *Radiographics* 25 (4), 1017–1030. doi:10.1148/rg.254045032

Bassignani, M. J., Fulcher, A. S., Szucs, R. A., Chong, W. K., Prasad, U. R., and Marcos, A. (2001). Use of Imaging for Living Donor Liver Transplantation. *Radiographics* 21 (1), 39–52. doi:10.1148/radiographics.21.1.g01ja0739

Beyoğlu, D., and Idle, J. R. (2020). Metabolomic Insights into the Mode of Action of Natural Products in the Treatment of Liver Disease. *Biochem. Pharmacol.* 180, 114171. doi:10.1016/j.bcp.2020.114171

Caldez, M. J., Van Hul, N., Koh, H. W. L., Teo, X. Q., Fan, J. J., Tan, P. Y., et al. (2018). Metabolic Remodeling during Liver Regeneration. *Dev. Cel* 47 (4), 425–e5. doi:10.1016/j.devcel.2018.09.020

Chen, L.-Y., Yang, J., Xu, G.-G., Liu, Y.-Q., Li, J.-T., and Xu, C.-S. (2016). Biomarker Identification of Rat Liver Regeneration via Adaptive Logistic Regression. *Int. J. Autom. Comput.* 13 (2), 191–198. doi:10.1007/s11633-015-0919-5

Cortes, M., Pareja, E., García-Cañaveras, J. C., Donato, M. T., Montero, S., Mir, J., et al. (2014). Metabolomics Discloses Donor Liver Biomarkers Associated with Early Allograft Dysfunction. *J. Hepatol.* 61 (3), 564–574. doi:10.1016/j.jhep.2014.04.023

Cuenca, A. G., Cress, W. D., Good, R. A., Marikar, Y., and Engelman, R. W. (2001). Calorie Restriction Influences Cell Cycle Protein Expression and DNA Synthesis during Liver Regeneration. *Exp. Biol. Med. (Maywood)* 226 (11), 1061–1067. doi:10.1177/153537020122601114

D'Onofrio, M., De Robertis, R., Demozzi, E., Crosara, S., Canestrini, S., and Pozzi Mucelli, R. (2014). Liver Volumetry: Is Imaging Reliable? Personal Experience and Review of the Literature. *World J. Radiol.* 6 (4), 62–71. doi:10.4329/wjr.v6.i4.62

de Graaf, W., Bennink, R. J., Veteläinen, R., and van Gulik, T. M. (2010). Nuclear Imaging Techniques for the Assessment of Hepatic Function in Liver Surgery and Transplantation. *J. Nucl. Med.* 51 (5), 742–752. doi:10.2967/jnumed.109.069435

De Graaf, W., Veteläinen, R. L., De Bruin, K., Van Vliet, A. K., Van Gulik, T. M., and Bennink, R. J. (2008). 99mTc-GSA Scintigraphy with SPECT for Assessment of Hepatic Function and Functional Volume during Liver Regeneration in a Rat Model of Partial Hepatectomy. *J. Nucl. Med.* 49 (1), 122–128. doi:10.2967/jnumed.107.044255

Dong, S., Zhan, Z. Y., Cao, H. Y., Wu, C., Bian, Y. Q., Li, J. Y., et al. (2017). Urinary Metabolomics Analysis Identifies Key Biomarkers of Different Stages of Nonalcoholic Fatty Liver Disease. *World J. Gastroenterol.* 23 (15), 2771–2784. doi:10.3748/wjg.v23.i15.2771

Du Preez, I., and Sithebe, N. P. (2013). The Use of Metabolomics as a Tool to Investigate Hepatitis C. *Metabolomics* 9 (2), 497–505. doi:10.1007/s11306-012-0467-8

Faitot, F., Besch, C., Battini, S., Ruhland, E., Onea, M., Addeo, P., et al. (2018). Impact of Real-Time Metabolomics in Liver Transplantation: Graft Evaluation and Donor-Recipient Matching. *J. Hepatol.* 68 (4), 699–706. doi:10.1016/j.jhep.2017.11.022

Fan, M., Wang, X., Xu, G., Yan, Q., and Huang, W. (2015). Bile Acid Signaling and Liver Regeneration. *Biochim. Biophys. Acta* 1849 (2), 196–200. doi:10.1016/j.bbagrm.2014.05.021

Fausto, N., Campbell, J. S., and Riehle, K. J. (2006). Liver Regeneration. *Hepatology* 43 (S1), S45–S53. doi:10.1002/hep.20969

Furchtgott, L. A., Chow, C. C., and Periwal, V. (2009). A Model of Liver Regeneration. *Biophys. J.* 96 (10), 3926–3935. doi:10.1016/j.bpj.2009.01.061

Goecks, J., Jalili, V., Heiser, L. M., and Gray, J. W. (2020). How Machine Learning Will Transform Biomedicine. *Cell* 181 (1), 92–101. doi:10.1016/j.cell.2020.03.022

Hockings, P. D., Roberts, T., Campbell, S. P., Reid, D. G., Greenhill, R. W., Polley, S. R., et al. (2002). Longitudinal Magnetic Resonance Imaging Quantitation of Rat Liver Regeneration after Partial Hepatectomy. *Toxicol. Pathol.* 30 (5), 606–610. doi:10.1080/01926230290105811

Hoekstra, L. T., Rietkerk, M., van Lienden, K. P., van den Esschert, J. W., Schaap, F. G., and van Gulik, T. M. (2012). Bile Salts Predict Liver Regeneration in Rabbit Model of portal Vein Embolization. *J. Surg. Res.* 178 (2), 773–778. doi:10.1016/j.jss.2012.06.038

Hoekstra, L. T., van Lienden, K. P., Schaap, F. G., Chamuleau, R. A., Bennink, R. J., and van Gulik, T. M. (2012). Can Plasma Bile Salt, Triglycerides, and apoA-V Levels Predict Liver Regeneration? *World J. Surg.* 36 (12), 2901–2908. doi:10.1007/s00268-012-1770-2

Huang, H., Sun, Z., Pan, H., Chen, M., Tong, Y., Zhang, J., et al. (2016). Serum Metabolomic Signatures Discriminate Early Liver Inflammation and Fibrosis Stages in Patients with Chronic Hepatitis B. *Sci. Rep.* 6, 30853. doi:10.1038/srep30853

Huang, J., and Rudnick, D. A. (2014). Elucidating the Metabolic Regulation of Liver Regeneration. *Am. J. Pathol.* 184 (2), 309–321. doi:10.1016/j.ajpath.2013.04.034

Huang, Z. Z., Li, H., Cai, J., Kuhlenkamp, J., Kaplowitz, N., and Lu, S. C. (1998). Changes in Glutathione Homeostasis during Liver Regeneration in the Rat. *Hepatology* 27 (1), 147–153. doi:10.1002/hep.510270123

Inderbitzin, D., Gass, M., Beldi, G., Ayouni, E., Nordin, A., Sidler, D., et al. (2004). Magnetic Resonance Imaging Provides Accurate and Precise Volume Determination of the Regenerating Mouse Liver. *J. Gastrointest. Surg.* 8 (7), 806–811. doi:10.1016/j.gassur.2004.07.013

Irino, Y., Toh, R., Nagao, M., Mori, T., Honjo, T., Shinohara, M., et al. (2016). 2-Aminobutyric Acid Modulates Glutathione Homeostasis in the Myocardium. *Sci. Rep.* 6, 36749. doi:10.1038/srep36749

Ishii, Y., Asai, S., Kohno, T., Takahashi, Y., Nagata, T., Suzuki, S., et al. (2001). Evaluation of Liver Regeneration Using the L-[1-13C]methionine Breath Test. *J. Surg. Res.* 95 (2), 195–199. doi:10.1006/jsre.2000.6012

Kasuya, K., Sugimoto, K., Kyo, B., Nagakawa, Y., Ikeda, T., Mori, Y., et al. (2011). Ultrasonography-guided Hepatic Tumor Resection Using a Real-Time Virtual Sonography with Indocyanine green Navigation (With Videos). *J. Hepatobiliary Pancreat. Sci.* 18 (3), 380–385. doi:10.1007/s00534-010-0356-3

Kim, J. E., Kim, J. H., Park, S. J., Choi, S. Y., Yi, N. J., and Han, J. K. (2019). Prediction of Liver Remnant Regeneration after Living Donor Liver Transplantation Using Preoperative CT Texture Analysis. *Abdom. Radiol. (Ny)* 44 (5), 1785–1794. doi:10.1007/s00261-018-01892-2

Kitajima, K., Taboury, J., Boleslawski, E., Savier, E., Vaillant, J. C., and Hannoun, L. (2008). Sonographic Preoperative Assessment of Liver Volume before Major Liver Resection. *Gastroenterol. Clin. Biol.* 32 (4), 382–389. doi:10.1016/j.gcb.2008.02.007

Kong, B., Sun, R., Huang, M., Chow, M. D., Zhong, X. B., Xie, W., et al. (2018). Fibroblast Growth Factor 15-Dependent and Bile Acid-independent Promotion of Liver Regeneration in Mice. *Hepatology* 68 (5), 1961–1976. doi:10.1002/hep.30041

Lim, M. C., Tan, C. H., Cai, J., Zheng, J., and Kow, A. W. (2014). CT Volumetry of the Liver: where Does it Stand in Clinical Practice? *Clin. Radiol.* 69 (9), 887–895. doi:10.1016/j.crad.2013.12.021

Ling, J., Chaba, T., Zhu, L. F., Jacobs, R. L., and Vance, D. E. (2012). Hepatic Ratio of Phosphatidylcholine to Phosphatidylethanolamine Predicts Survival after Partial Hepatectomy in Mice. *Hepatology* 55 (4), 1094–1102. doi:10.1002/hep.24782

Meier, M., Knudsen, A. R., Andersen, K. J., Ludvigsen, M., Eriksen, P. L., Pedersen, A. K. N., et al. (2019). Perturbations of Urea Cycle Enzymes during Posthepatectomy Rat Liver Failure. *Am. J. Physiol. Gastrointest. Liver Physiol.* 317 (4), G429–G440. doi:10.1152/ajpgi.00293.2018

Michalopoulos, G. K., and Bhushan, B. (2020). Liver Regeneration: Biological and Pathological Mechanisms and Implications. *Nat. Rev. Gastroenterol. Hepatol.* 18, 1–16. doi:10.1038/s41575-020-0342-4

Miyaoka, Y., and Miyajima, A. (2013). To divide or Not to divide: Revisiting Liver Regeneration. *Cell Div* 8 (1), 8–12. doi:10.1186/1747-1028-8-8

Naggie, S., Lusk, S., Thompson, J. W., Mock, M., Moylan, C., Lucas, J. E., et al. (2020). Metabolomic Signature as a Predictor of Liver Disease Events in Patients with HIV/HCV Co-infection. *J. Infect. Dis.* 222(12), 2012–2020. doi:10.1093/infdis/jiaa316

Nanashima, A., Yamaguchi, H., Shibasaki, S., Sawai, T., Yamaguchi, E., Yasutake, T., et al. (2001). Measurement of Serum Hyaluronic Acid Level during the Perioperative Period of Liver Resection for Evaluation of Functional Liver reserve. *J. Gastroenterol. Hepatol.* 16 (10), 1158–1163. doi:10.1046/j.1440-1746.2001.02599.x

Nanashima, A., Yamaguchi, H., Tanaka, K., Shibasaki, S., Tsuji, T., Ide, N., et al. (2004). Preoperative Serum Hyaluronic Acid Level as a Good Predictor of Posthepatectomy Complications. *Surg. Today* 34 (11), 913–919. doi:10.1007/s00595-004-2845-y

Nuzzo, G., Clemente, G., Giovannini, I., De Rose, A. M., Vellone, M., Sarno, G., et al. (2008). Liver Resection for Primary Intrahepatic Stones: a Single-center Experience. *Arch. Surg.* 143 (6), 570–574. doi:10.1001/archsurg.143.6.570

O'Grady, J. G. (2000). Treatment Options for Other Hepatic Malignancies. *Liver Transpl.* 6 (6B), s23–9. doi:10.1053/jlts.2000.18687

Ogasawara, K., Une, Y., Nakajima, Y., and Uchino, J. (1995). The Significance of Measuring Liver Volume Using Computed Tomographic Images before and after Hepatectomy. *Surg. Today* 25 (1), 43–48. doi:10.1007/BF00309384

Orcutt, S. T., and Anaya, D. A. (2018). Liver Resection and Surgical Strategies for Management of Primary Liver Cancer. *Cancer Control* 25 (1), 1073274817744621. doi:10.1177/1073274817744621

Periwal, V., Gaillard, J. R., Needleman, L., and Doria, C. (2014). Mathematical Model of Liver Regeneration in Human Live Donors. *J. Cel Physiol* 229 (5), 599–606. doi:10.1002/jcp.24482

Preziosi, M., and Monga, S. (2017). Update on the Mechanisms of Liver Regeneration. *Semin. Liver Dis.* 37, 141–151. doi:10.1055/s-0037-1601351

Rajula, H. S. R., Verlato, G., Manchia, M., Antonucci, N., and Fanos, V. (2020). Comparison of Conventional Statistical Methods with Machine Learning in Medicine: Diagnosis, Drug Development, and Treatment. *Medicina (Kaunas)* 56 (9), 455. doi:10.3390/medicina56090455

Riehle, K. J., Haque, J., McMahan, R. S., Kavanagh, T. J., Fausto, N., and Campbell, J. S. (2013). Sustained Glutathione Deficiency Interferes with the Liver Response to TNF-α and Liver Regeneration after Partial Hepatectomy in Mice. *J. Liver Dis. Transpl.* 1 (2).

Safaei, A., Arefi Oskouie, A., Mohebbi, S. R., Rezaei-Tavirani, M., Mahboubi, M., Peyvandi, M., et al. (2016). Metabolomic Analysis of Human Cirrhosis, Hepatocellular Carcinoma, Non-alcoholic Fatty Liver Disease and Non-alcoholic Steatohepatitis Diseases. *Gastroenterol. Hepatol. Bed Bench* 9 (3), 158–173.

Sahin, B., Emirzeoglu, M., Uzun, A., Incesu, L., Bek, Y., Bilgic, S., et al. (2003). Unbiased Estimation of the Liver Volume by the Cavalieri Principle Using Magnetic Resonance Images. *Eur. J. Radiol.* 47 (2), 164–170. doi:10.1016/s0720-048x(02)00152-3

Shestopaloff, Y. K., and Sbalzarini, I. F. (2014). A Method for Modeling Growth of Organs and Transplants Based on the General Growth Law: Application to the Liver in Dogs and Humans. *PLoS One* 9 (6), e99275. doi:10.1371/journal.pone.0099275

Solangi, K., Sacerdoti, D., Goodman, A. I., Schwartzman, M. L., Abraham, N. G., and Levere, R. D. (1988). Differential Effects of Partial Hepatectomy on Hepatic and Renal Heme and Cytochrome P450 Metabolism. *Am. J. Med. Sci.* 296 (6), 387–391. doi:10.1097/00000441-198812000-00004

Spira, D., Schulze, M., Sauter, A., Brodoefel, H., Brechtel, K., Claussen, C., et al. (2012). Volume Perfusion-CT of the Liver: Insights and Applications. *Eur. J. Radiol.* 81 (7), 1471–1478. doi:10.1016/j.ejrad.2011.04.010

Stinauer, M. A., Diot, Q., Westerly, D. C., Schefter, T. E., and Kavanagh, B. D. (2012). Fluorodeoxyglucose Positron Emission Tomography Response and normal Tissue Regeneration after Stereotactic Body Radiotherapy to Liver Metastases. *Int. J. Radiat. Oncol. Biol. Phys.* 83 (5), e613–8. doi:10.1016/j.ijrobp.2012.02.008

Sun, R., Huang, J., Yang, N., He, J., Yu, X., Feng, S., et al. (2019). Purine Catabolism Shows a Dampened Circadian Rhythmicity in a High-Fat Diet-Induced Mouse Model of Obesity. *Molecules* 24 (24), 4524. doi:10.3390/molecules24244524

Vamathevan, J., Clark, D., Czodrowski, P., Dunham, I., Ferran, E., Lee, G., et al. (2019). Applications of Machine Learning in Drug Discovery and

Development. *Nat. Rev. Drug Discov.* 18 (6), 463–477. doi:10.1038/s41573-019-0024-5

van de Laarschot, L. F., Jansen, P. L., Schaap, F. G., and Olde Damink, S. W. (2016). The Role of Bile Salts in Liver Regeneration. *Hepatol. Int.* 10 (5), 733–740. doi:10.1007/s12072-016-9723-8

Vauthey, J. N., Abdalla, E. K., Doherty, D. A., Gertsch, P., Fenstermacher, M. J., Loyer, E. M., et al. (2002). Body Surface Area and Body Weight Predict Total Liver Volume in Western Adults. *Liver Transpl.* 8 (3), 233–240. doi:10.1053/jlts.2002.31654

Xia, H. T., Dong, J. H., Yang, T., Zeng, J. P., and Liang, B. (2014). Extrahepatic Cyst Excision and Partial Hepatectomy for Todani Type IV-A Cysts. *Dig. Liver Dis.* 46 (11), 1025–1030. doi:10.1016/j.dld.2014.07.007

Xie, Z., Chen, E., Ouyang, X., Xu, X., Ma, S., Ji, F., et al. (2019). Metabolomics and Cytokine Analysis for Identification of Severe Drug-Induced Liver Injury. *J. Proteome Res.* 18 (6), 2514–2524. doi:10.1021/acs.jproteome.9b00047

Yoshida, M., Shiraishi, S., Sakamoto, F., Beppu, T., Utsunomiya, D., Okabe, H., et al. (2014). Assessment of Hepatic Functional Regeneration after Hepatectomy Using (99m)Tc-GSA SPECT/CT Fused Imaging. *Ann. Nucl. Med.* 28 (8), 780–788. doi:10.1007/s12149-014-0872-3

Zamboni, G. A., Pedrosa, I., Kruskal, J. B., and Raptopoulos, V. (2008). Multimodality Postoperative Imaging of Liver Transplantation. *Eur. Radiol.* 18 (5), 882–891. doi:10.1007/s00330-007-0840-6

Zhang, A., Sun, H., Yan, G., Han, Y., Ye, Y., and Wang, X. (2013). Urinary Metabolic Profiling Identifies a Key Role for Glycocholic Acid in Human Liver Cancer by Ultra-performance Liquid-Chromatography Coupled with High-Definition Mass Spectrometry. *Clin. Chim. Acta* 418, 86–90. doi:10.1016/j.cca.2012.12.024

Conflict of Interest: The authors declare that the research was conducted in the absence of any commercial or financial relationships that could be construed as a potential conflict of interest.

Publisher's Note: All claims expressed in this article are solely those of the authors and do not necessarily represent those of their affiliated organizations, or those of the publisher, the editors, and the reviewers. Any product that may be evaluated in this article, or claim that may be made by its manufacturer, is not guaranteed or endorsed by the publisher.

frontiers in Pharmacology

ORIGINAL RESEARCH
published: 03 January 2022
doi: 10.3389/fphar.2021.794103

Comparative Evaluation of the Effect of Metformin and Insulin on Gut Microbiota and Metabolome Profiles of Type 2 Diabetic Rats Induced by the Combination of Streptozotocin and High-Fat Diet

Nan Hu[1], Qi Zhang[2], Hui Wang[3], Xuping Yang[1], Yan Jiang[1], Rong Chen[1] and Liying Wang[1]**

[1]Department of Pharmacy, The Third Affiliated Hospital of Soochow University/The First People's Hospital of Changzhou, Changzhou, China, [2]Department of Pharmacy, Changzhou No. 7 People's Hospital, Changzhou, China, [3]Department of Pathology, The Third Affiliated Hospital of Soochow University/The First People's Hospital of Changzhou, Changzhou, China

OPEN ACCESS

Edited by:
Linsheng Liu,
The First Affiliated Hospital of Soochow University, China

Reviewed by:
Xinwen Wang,
Northeast Ohio Medical University, United States
Zhixiang Yan,
Sun Yat-sen University, China
Yun-Li Yu,
Second Affiliated Hospital of Soochow University, China

***Correspondence:**
Rong Chen
pharmacy_czyy@163.com
Liying Wang
wlyzqcz@163.com

Specialty section:
This article was submitted to Translational Pharmacology, a section of the journal Frontiers in Pharmacology

Received: 13 October 2021
Accepted: 22 November 2021
Published: 03 January 2022

Citation:
Hu N, Zhang Q, Wang H, Yang X, Jiang Y, Chen R and Wang L (2022) Comparative Evaluation of the Effect of Metformin and Insulin on Gut Microbiota and Metabolome Profiles of Type 2 Diabetic Rats Induced by the Combination of Streptozotocin and High-Fat Diet. Front. Pharmacol. 12:794103. doi: 10.3389/fphar.2021.794103

Lately, an increasing number of studies have investigated the relationship between metformin and gut microbiota, suggesting that metformin exerts part of its hypoglycemic effect through the microbes. However, its underlying mechanism remains largely undetermined. In the present study, we investigated the effects of metformin on gut microbiota and metabolome profiles in serum and compared it with insulin treatment in rats with type 2 diabetes mellitus (T2DM). Diabetic rats (DM group) were induced by a combination of streptozotocin and high-fat diet (HFD). After 7 days, DM rats were treated with metformin (MET group) or insulin (INS group) for 3 weeks. The 16S rRNA sequencing of the gut microbiota and non-targeted metabolomics analysis of serum were conducted. A total of 13 bile acids (BAs) in serum were further determined and compared among different groups. The rat model of T2DM was well established with the typical diabetic symptoms, showing significantly increased blood glucose, AUC of OGTT, HOMA-IR, TC, TG, LDL-C and TBA. Metformin or insulin treatment could ameliorate symptoms of diabetes and partly recover the abnormal biochemical indicators. Compared with DM rats, the relative abundances of 13 genera were significantly changed after metformin treatment, while only three genera were changed after insulin treatment. The metformin and insulin treatments also exhibited different serum metabolome profiles in T2DM rats. Moreover, 64 differential metabolites were identified between MET and DM groups, whereas 206 were identified between INS and DM groups. Insulin treatment showed greater influence on amino acids, glycerophospholipids/glycerolipids, and acylcarnitine compared with the metformin treatment, while metformin had an important impact on BAs. Furthermore, metformin could significantly decrease the serum levels of CA, GCA, UDCA, and GUDCA, but increase the level of TLCA in DM rats. Insulin treatment significantly decreased the levels of CA, UDCA, and CDCA. Besides, several metabolites in serum or microbiota were positively or negatively correlated with some bacteria. Collectively, our findings indicated that metformin had a stronger effect on gut microbiota than insulin, while

insulin treatment showed greater influence on serum metabolites, which provided novel insights into the therapeutic effects of metformin on diabetes.

Keywords: type 2 diabetes, metformin, insulin, microbiota, metabolome, bile acids

INTRODUCTION

As a chronic metabolic disease with complex pathogenesis, type 2 diabetes mellitus (T2DM) refers to a spectrum of systemic illnesses related to glucose metabolism, lipid metabolism, and amino acid metabolism. Moreover, T2DM often has high rates of death and disability, and it is accompanied by severe complications. For more than 2 decades, metformin is a first-line treatment regimen to increase insulin sensitivity in T2DM patients although its underlying mechanisms of action remain largely undetermined. It is believed that metformin improve patients' hyperglycemia by suppressing hepatic gluconeogenesis, decreasing hepatic glucose output, elevating glucose uptake and utilization in peripheral tissues, and enhancing the energy metabolism in several organs, such as muscle, fat, and liver through activating of AMP-activated protein kinase (Kristófi and Eriksson, 2021). The concentration of metformin in the bowel is 100–300 times greater compared with the serum, and about 50% of its intake is detected in the stool. The half-life of metformin is approximately 3–4 h once orally administered, which is significantly shorter than the duration of its hypoglycemic effect. Besides, metformin can not decrease blood glucose when intravenously administered. The above-mentioned findings all indicate that metformin has key impacts on the digestive tract.

Recently, with the advance of detection technology, it has been found that gut microbiota plays a fundamental role in the pathogenesis of diabetes. Accordingly, a great deal of attention has been paid to the relationship between metformin and gut microbiota. We have previously reviewed the literature concerning the effects of metformin on the gut microbiota of various species, including mice, rats, and humans with obesity or T2DM, and the compositional changes of the gut microbiota have been summarized. Accumulating evidence has indicated that metformin may change the composition of gut microbiota, through which its hypoglycemic effects are exerted (Zhang and Hu, 2020). Nevertheless, it remains largely unknown how metformin alters the gut microbiota.

To clarify the complex interaction between microbial ecosystems and host, it is necessary to adopt comprehensive analytical methods that capture the dynamic interplays among metformin, gut microbiota and diabetes. Metabolomics can determine alterations in absolute and/or relative contents of hundreds to thousands of small elements in blood and tissue, and offer valuable insights into disease diagnosis and the mechanisms of pathogenesis and drug intervention. Several metagenomic and metabolomic methods have been exploited to evaluate the phenotype of diabetic individuals and to represent decisive metabolic processes. Nevertheless, the association between gut microbiota and metformin-regulated metabolites remains largely unclear in the pathogenesis of diabetes.

In our current work, 16S rRNA gene sequencing analysis was used to assess the alterations of the gut microbiota in T2DM rats induced by a combination of streptozotocin (STZ) and high-fat diet (HFD). Moreover, we also evaluated the intervention effect of metformin and insulin. Besides, differential metabolites in serum were identified by non-targeted and targeted metabolomics analyses. Furthermore, the interplay between the gut microbiota and host metabolism was investigated to unravel the mechanism of metformin in the treatment of T2DM.

MATERIALS AND METHODS

Materials and Reagents

Methanol, acetonitrile and formic acid of HPLC-grade were provided by Merck (Dannstadt, Germany). STZ, reference bile acid (BA) standards, including cholic acid (CA), glycocholic acid (GCA), deoxycholic acid (DCA), chenodeoxycholic acid (CDCA), ursodeoxycholic acid (UDCA), glycochenodeoxycholic acid (GCDCA), taurocholic acid (TCA), tauroursodeoxycholic acid (TUDCA), glycoursodeoxycholic acid (GUDCA), taurochenodeoxycholic acid (TCDCA), taurodeoxycholic acid (TDCA), lithocholic acid (LCA), and taurolithocholic acid (TLCA), and isotope internal standards were supplied by Sigma-Aldrich (St. Louis, MO, United States). Metformin (purity > 95%) was purchased from Aladdin Reagent Co., Ltd. (China). Insulin (NovoLet®N) was applied by Novo Nordisk Pharmaceutical Industries, Inc. Normal and high-fat chow were obtained from TROPHIC Animal Feed High-Tech Co., Ltd. (Nantong, China). Deionized water was purified using a MilliQ system (Millipore Corporation, MA, United States).

Animals

Sprague-Dawley rats (male, 110–150 g) were purchased from Cavens Experimental Animal Co., Ltd. (Changzhou, China), and the animals were bred in a facility under the controlled conditions (22–24°C, relative humidity 55–60%, and a 12-h light/dark photoperiod). The rats were given free access to water and food and acclimatized to the animal facility for 3 days before the experiment.

Animal Experiments

T2DM was induced by a combination of low-dose STZ via intraperitoneal injection and HFD as previously described (Wang et al., 2019). Briefly, the rats were divided into CON (n = 6) and DM (n = 40) groups. The rats in the CON group were fed on normal chow, while DM rats were fed on HFD

containing 15% lard (w/w), 20% sucrose, 5% sesame oil, 2.5% cholesterol, and 57.5% normal chow for 5 weeks. Following overnight fasting, DM rats were intraperitoneally injected with a single dose of STZ (35 mg/kg). CON rats only received the vehicle solution. At 7 days after the administration of STZ, the level of fasting blood glucose (FBG) was measured. Only rats with an FBG level higher than 11.1 mM were considered as successful DM rats and used for the subsequent experiments. The DM rats were then randomly divided into three groups: 1) DM group (n = 7), continually fed with HFD; 2) MET group (n = 7), fed with HFD and intragastrically administered with 300 mg/kg body weight metformin once daily for 3 weeks; and 3) INS group (n = 7), fed with HFD and subcutaneously injected with insulin (2–4 U/day) according to glucose levels for 3 weeks. FBG and body weight were monitored and recorded during the experiments. Animal protocols complied with institutional guidelines for the care and the use of laboratory animals and were authenticated by the Ethics Committee of the Third Affiliated Hospital of Soochow University.

Oral Glucose Tolerance Test and Sample Collection

OGTT was conducted 3 days before the end of the animal experiment. Briefly, 12-h fasting-adapted rats were orally administered with glucose solution (2 g/kg). The blood glucose levels were measured at 0, 15, 30, 60, and 120 min after the glucose administration, the corresponding curves were plotted, and the areas under the curve (AUCs) of OGTT were calculated. After 9 weeks, rats were sacrificed under ether anesthesia, and blood specimens were harvested from the abdominal aorta. The blood samples were allowed to stand at room temperature for 2 h and centrifuged at 3, 500 rpm for 10 min. The liver and colon were collected. The contents of the colon were placed in sterile Falcon tubes, followed by storage at −80°C before DNA isolation. An automatic biochemistry analyzer (AU5800, Beckman Coulter, United States) was adopted to analyze the serum biochemical parameters, including fasting serum glucose (GLU), total cholesterol (TC), triglycerides (TGs), high-density lipoprotein cholesterol (HDL-C), low-density lipoprotein cholesterol (LDL-C), total bile acid (TBA), urea, creatinine (Cr), alanine aminotransferase (ALT), and aspartate aminotransferase (AST). Serum insulin was measured using an electrochemiluminescence immunoassay. The homeostasis model of assessment for insulin resistance index (HOMA-IR) was calculated as [fasting serum glucose (mmol/L) × fasting serum insulin (mIU/L)]/22.5.

Histological Assessment

The liver and colon were collected, followed by fixation in 10% buffered formaldehyde. After being rinsed with tap water, the specimens were dehydrated in increasing concentrations of alcohol (70% alcohol for 1 h, then 96% alcohol for 1 h three times). The paraffin-embedded tissues were cut into 4-mm sections using a microtome (Leica RM 2015, Germany), followed by hematoxylin-eosin (H&E) staining. An Olympus CX31 microscope (Olympus Hamburg, Germany) was adopted to examine the sections.

Gut Microbiota Analysis

An E.Z.N.A. Stool DNA Kit (Omega Bio-tek, Norcross, GA, United States) was adopted to extract microbial DNA according to the manufacturer's instructions. The primers 338F (5′-ACTCCTACGGGAGGCAGCAG-3′) and 806R (5′-GGACTACHVGGGTWTCTAAT-3′) were used to amplify the V3-V4 region of the bacterial 16S ribosomal RNA gene using a GeneAmp 9,700 thermocycler (ABI, United States) as previously described (Hu et al., 2021). The structure of the gut microbiota was assessed by dual-indexing amplification and sequencing on the Illumina MiSeq platform, followed by QIIME (version 1.6.0) bioinformatic analysis.

Raw files of Fastq format were quality-filtered by Trimmomatic and merged by FLASH based on the criteria as follows. The reads were truncated at any site receiving an average quality score <20 over a 50 bp sliding window. Sequences greater than 10 bp were amalgamated based on their overlap with no more than 2 bp. Sequences of each sample were separated according to barcodes (exactly matching) and primers (allowing 2 nucleotide mismatching), while reads consisting of ambiguous bases were discarded. A novel "greedy" algorithm that performs chimera filtering and operational taxonomic unit (OTU) clustering simultaneously was used to cluster OUT with a similarity cutoff of 97% using UPARSE (version 7.1 http://drive5.com/uparse/). The RDP Classifer algorithm (http://rdp.cme.msu.edu/) was used to analyze the taxonomy of each 16S rRNA gene sequence against the Silva (SSU123) 16S rRNA database, and the confidence threshold was set at 70%. Alpha diversity (ACE and Chao index, which were used to assess the community richness) and beta diversity were calculated using QIIME. OTUs were analyzed by unweighted UniFrac distance-metrics analysis for each sample. Principal component analysis (PCA) was then carried out according to the matrix-of-distance.

Non-Targeted Metabolomics Analysis

Briefly, 100 μL of serum sample was mixed with 400 μL acetonitrile/methanol (v/v, 1:1) containing the internal standard of L-2-chlorophenylalanine (2 μg/ml), followed by extractions of metabolites. Subsequently, the specimens were vortexed for 30 s, sonicated for 10 min in an ice-water bath, incubated at −40°C for 1 h, and centrifuged at 10,000 rpm for 15 min at 4°C. Next, 425 μL of supernatant was dried at 37°C, and the residuals were reconstituted in 200 μL of 50% acetonitrile by sonication on ice for 10 min. The sample was then centrifuged at 12,000 rpm for 15 min at 4°C, and 75 μL of supernatant was subjected to LC/MS/MS. Equal aliquots of the supernatants from all of the samples were mixed, which were used as quality control (QC) samples.

The metabolites were separated using a UHPLC system (1,290, Agilent Technologies), which was equipped with a UPLC BEH Amide column (2.1*100 mm, 1.7 μm, Waters) coupled to a TripleTOF6600 (Q-TOF, AB Sciex) at Biotree Biotech Co., Ltd. (Shanghai, China). The mobile phase was composed of 25 mM ammonium acetate and 25 mM ammonia hydroxide in

water (pH = 9.75) (A) and acetonitrile (B). The elution program was conducted as follows: 0–0.5 min, 95%B; 0.5–7.0 min, 95–65% B; 7.0–8.0 min, 65–40% B; 8.0–9.0 min, 40% B; 9.0–9.1 min, 40–95% B; 9.1–12.0 min, 95% B. The volume of injection was 1 μL (pos) or 1 μL (neg). The column temperature was maintained at 25°C. The conditions of electrospray ionization (ESI) source were set as follows: gas 1 at 60 psi, gas 2 at 30 psi, curtain gas at 35 psi, source temperature as 600°C, declustering potential at 60 V, and ion spray voltage floating (ISVF) at 5,000 V or −4,000 V in positive or negative modes, respectively.

MS raw data (wiff) files were transformed to the mzXML format by ProteoWizard and processed by R package XCMS (version 3.2). Such a process included peak deconvolution, alignment, and integration. Minfrac and cut-off values were set as 0.5 and 0.6, respectively. An in-house MS2 database was applied for the identification of metabolites. Subsequently, multivariate statistical analyses were carried out using the SIMCA-P software (version 14.1, Umetrics AB, Umea, Sweden), including PCA and OPLS-DA. The clusters, differences, and outliners in different groups were assessed using PCA, and the metabolic difference between the two groups was analyzed using the OPLS-DA. Differential metabolites were defined as those metabolites with an adjusted $p < 0.05$ and variable importance (VIP) > 1. R2 (goodness of fit parameter) and Q2 (goodness of prediction parameter) values were used for the quality evaluation of each model. Besides, cross-validation and testing with 200 permutations were adopted to avoid the over-fitting of the OPLS-DA model.

Serum Bile Acids Measurement

To a 50 μL aliquot of each serum sample, 20 μL (100 ng/ml) of internal standard (TCA-d4, GCA-d5, CDCA-d4, DCA-d5, GCDCA-d7, and LCA-d4) and 150 μL of acetonitrile solution were added. The mixture was then vortexed for 30 s and centrifuged at 16,400 rpm for 10 min. An aliquot (100 μL) of the supernatant was diluted by 100 μL ultrapure water and then analyzed. The levels of 13 serum BAs, including TUDCA, TCA, GUDCA, GCA, TCDCA, TDCA, CA, UDCA, GCDCA, CDCA, LCA, TLCA, and DCA, were determined using a validated high-performance liquid chromatography-tandem mass spectrometry (HPLC-MS/MS) method. The chromatographic system (Jasper™ HPLC system) consisted of a vacuum degasser, a binary pump, an autosampler, and a Kinetex EVO C18 column (50 × 2.1 mm, 2.6 μm, Phenomenex, United States) and was operated at 40°C. The mobile phase consisted of water containing 0.1% formic acid and 0.5% ammonia (A) and acetonitrile (B). The gradient elution started at 25%B, increased to 35%B (0.01–4.50 min), 50%B (4.50–6.00 min), and 95%B (6.00–6.10 min), maintained at 95%B (6.10–7.40 min), and then restored to 25% (7.50–9.00 min). The flow rate was fixed at 0.4 ml/min. The injection volume was 10 μL. The AB SCIEX Triple Quad™ 4500MD mass spectrometer (Applied Biosystem Sciex, Ontario, Canada) was used for qualitative and quantitative analysis. The mass spectrometer was operated in multiple reaction monitoring (MRM) and negative ESI mode (−3500 V) with the following parameters: ion source temperature, 500°C; nebulizer gas (gas 1), nitrogen, 55 psi; turbo gas (gas 2), nitrogen, 45 psi; and curtain gas, nitrogen, 30 psi. The precursor ion and product ion mass, declustering potentials (DP), collision energies (CE), and retention time of each bile acid were summarized in **Supplementary Table S1**.

Among these 13 BAs, primary BAs included CA and CDCA, as well as their glycine-conjugates and taurine-conjugates, such as GCA, GCDCA, TCA, and TCDCA, while secondary BAs produced by deconjugation and/or dehydroxylation of primary BAs by gut bacteria included DCA, UDCA, and LCA, as well as their glycine-conjugates and taurine-conjugates, such as TLCA, TDCA, GUDCA, and TUDCA.

Statistical Analysis

GraphPad Prism software v 9.0 was employed for all statistical assays. The results were expressed as mean ± SD. The difference between the two groups was compared using unpaired Student's t-test, and multiple comparisons were performed using one-way ANOVA, followed by Dunnett's post hoc test. The relationship between differential metabolites and the relative abundance of the intestinal microbiome at the genus level was evaluated by Pearson's correlation analysis. Corrections of p values for multiple comparisons were controlled by FDR, and $p < 0.05$ was considered statistically significant.

RESULTS

T2DM Modeling

After STZ injection, diabetic symptoms were observed in most rats, including polyuria, polydipsia, and polyphagia. The FBG levels of 21 rats were higher than 11.1 mM after 7 days, which were chosen for the following experiment. However, because of severe diabetes, two rats in the DM group died in the eighth and ninth weeks of the experiments. After STZ injection (the fifth week), the levels of FBG were remarkably increased in the DM group compared with the CON group. Metformin and insulin treatment could reduce the levels of FBG, and insulin exhibited higher hypoglycemic effect than metformin during the experiment (**Figure 1A**). Because HFD influenced the appetite of rats, the body weight of rats in the DM, MET, and INS groups was significantly decreased from the first week of the experiment. Metformin and insulin treatment could both increase the body weight of DM rats (**Figure 1B**). OGTT was performed in different groups, and the corresponding AUC was also analyzed (**Figures 1C,D**). The results of OGTT were ameliorated to some extent in the MET and INS groups. The levels of fasting insulin were comparable among CON, DM, MET and INS groups (**Figure 1E**). HOMA-IR index was markedly greater in the DM group compared with the CON group, implying that the islet function of the DM group was affected. The HOMA-IR index was remarkably decreased in the MET group and INS group compared with the DM group, indicating that the treatment of metformin and insulin significantly improved the insulin resistance of diabetic rats (**Figure 1F**).

Histological Assessment

Histological assessments were conducted in the liver and colon of rats from different groups (**Figure 1G**). The liver lobule had a clear

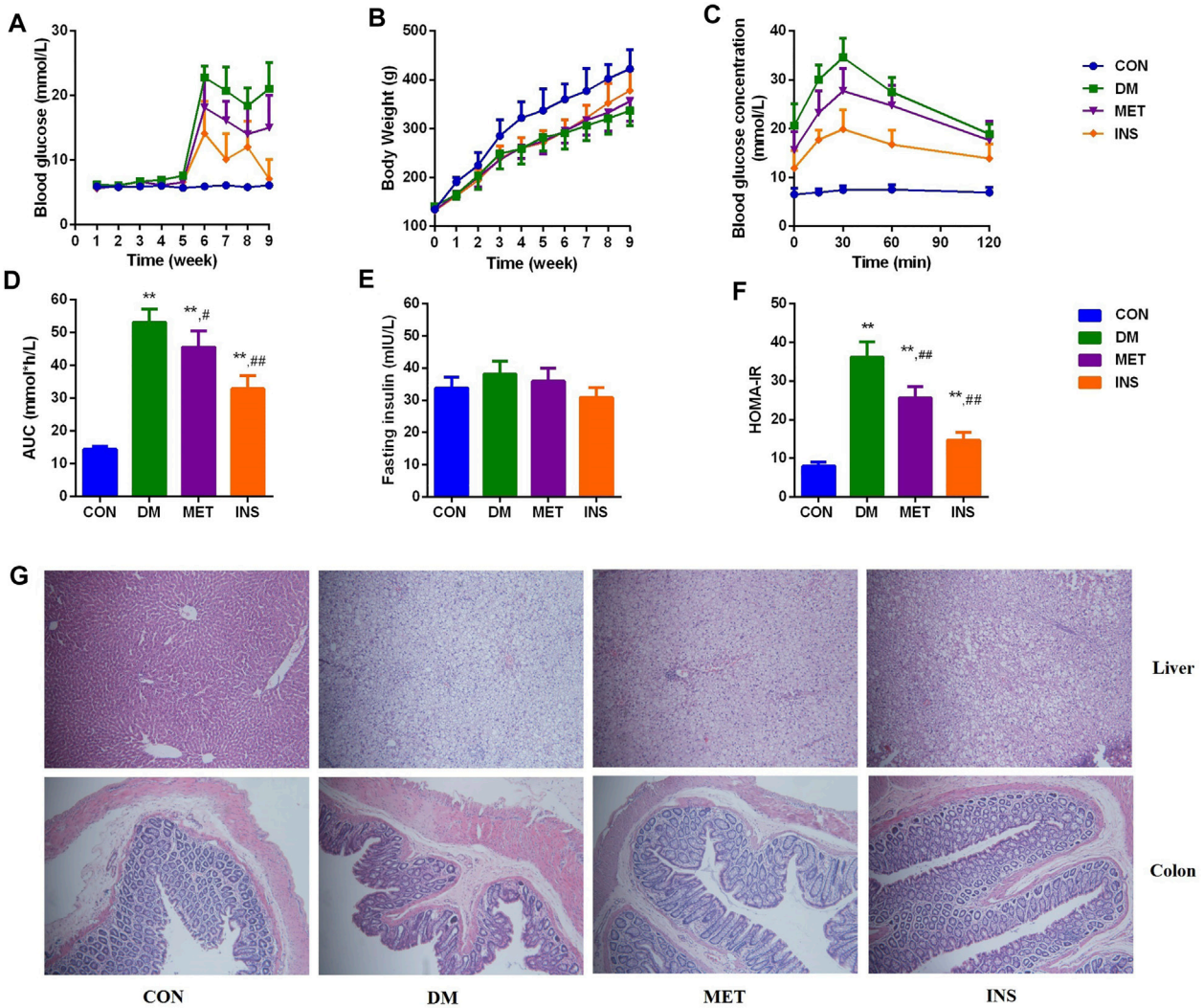

FIGURE 1 | Effects of metformin and insulin on **(A)** Blood glucose; **(B)** Body weight; **(C)** Oral glucose tolerance test (OGTT); **(D)** Area under the curve (AUC) of OGTT; **(E)** Fasting insulin; **(F)** HOMA-IR index; **(G)** Histological structure of liver and colon (HE staining) $^{*}p < 0.05$, $^{**}p < 0.01$ vs. CON group. $\#p < 0.05$, $\#\#p < 0.01$ vs. DM group.

structure, and the liver cells exhibited a radial distribution around the central vein in the CON group. The structure of the liver lobule in the DM group disappeared, and the liver cord showed disordered arrangement, exhibiting widened hepatic sinusoids. Hepatocytes appeared swelling, and the size was increased. Moreover, we observed lipid droplets of different sizes in the cytoplasm with focal steatosis in hepatocytes. In the MET group, the hepatocellular cord showed a clear structure with normal liver sinusoids, mild steatosis was observed in the cytoplasm of the liver cells, and lipid droplets were decreased. The hepatocellular cord in the INS group displayed a clear structure, and mild steatosis was observed in the cytoplasm of the liver cells. The swelling of hepatocytes was relieved. Compared with the CON group, DM rats showed damaged mucosal architecture in the colon. The epithelium was slightly hyperplastic with villus atrophy. Taken together, metformin and insulin treatment significantly improved these pathological conditions.

Biochemical Parameters

Compared with the CON group, the levels of TC, TG, and LDL-C were significantly increased in the DM group, indicating dyslipidemia in diabetic rats. Metformin and insulin could suppress the levels of TC, TG, and LDL-C in different degrees (**Table 1**). Compared with the CON group, the level of TBA was markedly higher in DM rats, and both metformin and insulin treatment could decrease the TBA level. There was no difference in urea, Cr, ALT, and AST among the four groups.

Effect of Metformin and Insulin on the Gut Microbiota

A total of 1,178 012 sequences were obtained from 32 samples, and averagely 36,812 sequences were recovered for each sample and

TABLE 1 | Biochemical parameters.

Parameters	CON(n = 6)	DM(n = 5)	MET (n = 7)	INS(n = 7)
TC (mmol/L)	1.81 ± 0.42	7.92 ± 3.70**	6.64 ± 2.76**	6.05 ± 2.22**
TG (mmol/L)	1.26 ± 0.28	1.66 ± 0.07*	1.11 ± 0.25##	0.50 ± 0.17**,##
HDL-C (mmol/L)	0.86 ± 0.14	0.63 ± 0.27	0.62 ± 0.13**	0.44 ± 0.17**
LDL-C (mmol/L)	0.42 ± 0.14	5.36 ± 2.94**	4.26 ± 2.09**	3.45 ± 0.73**
TBA (μmol/L)	11.18 ± 7.19	20.22 ± 3.14*	15.84 ± 4.42#	10.29 ± 3.96##
Urea (mmol/L)	5.44 ± 0.65	5.21 ± 1.57	5.29 ± 1.75	4.67 ± 1.08
Cr (μmol/L)	51.00 ± 4.98	48.40 ± 10.97	53.43 ± 5.35	49.43 ± 5.38
ALT (U/L)	59.50 ± 18.43	65.80 ± 15.71	94.57 ± 60.44	62.71 ± 9.72
AST (U/L)	165.33 ± 21.42	154.40 ± 72.57	186.43 ± 54.46	135.14 ± 14.06*

*Values were presented as means ± SD; TC, total cholesterol; TG, triglycerides; HDL, high-density lipoprotein; LDL, low-density lipoprotein; TBA, total bile acid; Cr, creatinine; ALT, alanine aminotransferase; AST, aspartate transaminase. *p < 0.05, **p < 0.01 vs. CON group. #p < 0.05, ##p < 0.01 vs. DM group.*

used for comparative analysis. The Good's coverage for the observed OTUs was 99.76 ± 0.02%, and the rarefaction curves displayed clear asymptotes (**Figure 2A**), together indicating a near-complete sampling of the community. **Figure 2B** shows the ACE and Chao index of four groups, and metformin significantly decreased the ACE and Chao indexes compared with the DM group. A total of 703 OTUs were yielded from 32 samples, including 342 shared OTUs for four groups, and there were 40, 8, 19 and 5 special OTUs for the CON, DM, MET, and INS groups, respectively (**Figure 2C**). Weighted UniFrac PCoA distances showed separation among the CON, DM, MET, and INS groups. Based on the PCoA analysis, different trends were observed from the intestinal microbiota structure of the MET and INS groups, and both of them were clearly separated from the DM and CON groups (**Figure 2D**). **Figure 2E** shows the top six phyla in four groups. The dominant phyla included Firmicutes and Bacteroidetes. DM rats had a greater abundance of Firmicutes and a lower abundance of Bacteroidetes compared with the CON group, and thus the ratio of Bacteroidetes/Firmicutes was significantly lower in the DM (0.31) group compared with the CON (0.56) group ($p < 0.05$). Both metformin and insulin treatment could reduce the abundance of Firmicutes and elevate the abundance of Bacteroidetes in DM rats, and the ratio of Bacteroidetes/Firmicutes was 0.47 and 0.89 in the MET and INS groups, respectively. In addition, DM rats showed a significantly higher abundance of the phyla Actinobacteria ($p < 0.01$) compared with the CON group. Metformin treatment further increased such abundance, while insulin treatment decreased the abundance of Actinobacteria (**Figure 2F**).

Figure 3A shows a heatmap presenting the detailed intestinal microbiota composition (top 50) at the genus level. The relatively predominant taxa at the genus level were *Lactobacillus*, *norank_f_Bacteroidales_S24-7_group*, *Lachnospiraceae_NK4A136_group*, and *Alloprevotella*. Compared with the CON group, the abundances of *Roseburia*, *Christensenellaceae_R-7_group*, and (*Ruminococcus*) *_gnavus_group* were significantly increased, while the abundances of *Alloprevotella*, *Prevotella_1*, and *Prevotellaceae_Ga6A1_group* were significantly decreased in the DM group. After metformin treatment, the composition of intestinal microbiota changed a lot at the genus level. The abundances of *Phascolarctobacterium*, *Anaerotruncus*, (*Eubacterium*)*_hallii_group*, and (*Ruminococcus*) *_torques_group* were significantly higher, while the abundances of *Lactobacillus*, *unclassified_f_Lachnospiraceae*, *norank_f_Ruminococcaceae*, *unclassified_f_Ruminococcaceae*, *Ruminiclostridium_6*, *Quinella*, *Oscillibacter*, *Lachnospiraceae_UCG-006*, and *Ruminiclostridium* were significantly lower in the MET group compared with the DM group. However, insulin treatment showed little impact on the intestinal microbiota at the genus level. The abundance of *norank_f_Bacteroidales_S24-7_group* was increased, and the abundance of *Lactobacillu* and *unclassified_f_Peptostreptococcaceae* was decreased in the INS group compared with the DM group (**Figure 3B**).

Non-targeted Metabolomics Analysis

To further elucidate the therapeutic mechanisms of metformin and insulin on T2DM, we assessed the serum metabolites in CON, DM, MET, and INS groups according to metabolomics. We first applied the PCA model for data interpretation to explore the general trend of the four groups. The generalized separation of variations was primarily conducted according to PCA, and the variations of all groups were calculated using the OPLS-DA method based on the VIP values. **Figures 4A,B** show that a superior separation existed among the CON, DM, MET, and INS groups in both ESI^+ and ESI^- modes. PCA score plots showed that significant differences were observed between the CON group and DM group in the positive and negative ions, indicating that the serum metabolites in T2DM rats were remarkably altered. The PCA loading diagram showed that metformin and insulin could affect the serum metabolic composition of DM rats in different degrees, indicating that the abnormal metabolism in DM rats was ameliorated after metformin and insulin treatment.

To further identify differential metabolites and to increase the number of representative latent biomarkers, we applied the OPLS-DA to distinguish the two groups. A more clear separation among different groups was achieved using the supervised OPLS-DA model. **Figures 4C,D** show that there was a clearly distinction between the CON group and DM group in ESI+ and ESI- modes (C: R2X = 0.802, R2Y = 0.998, Q2 = 0.863; D: R2X = 0.750, R2Y = 0.996, Q2 = 0.969). **Figures 4E,F**, display that the MET group and DM group were obviously separated in the ESI+ and ESI- modes (E: R2X = 0.506, R2Y = 0.996, Q2 = 0.524; F: R2X = 0.438, R2Y =

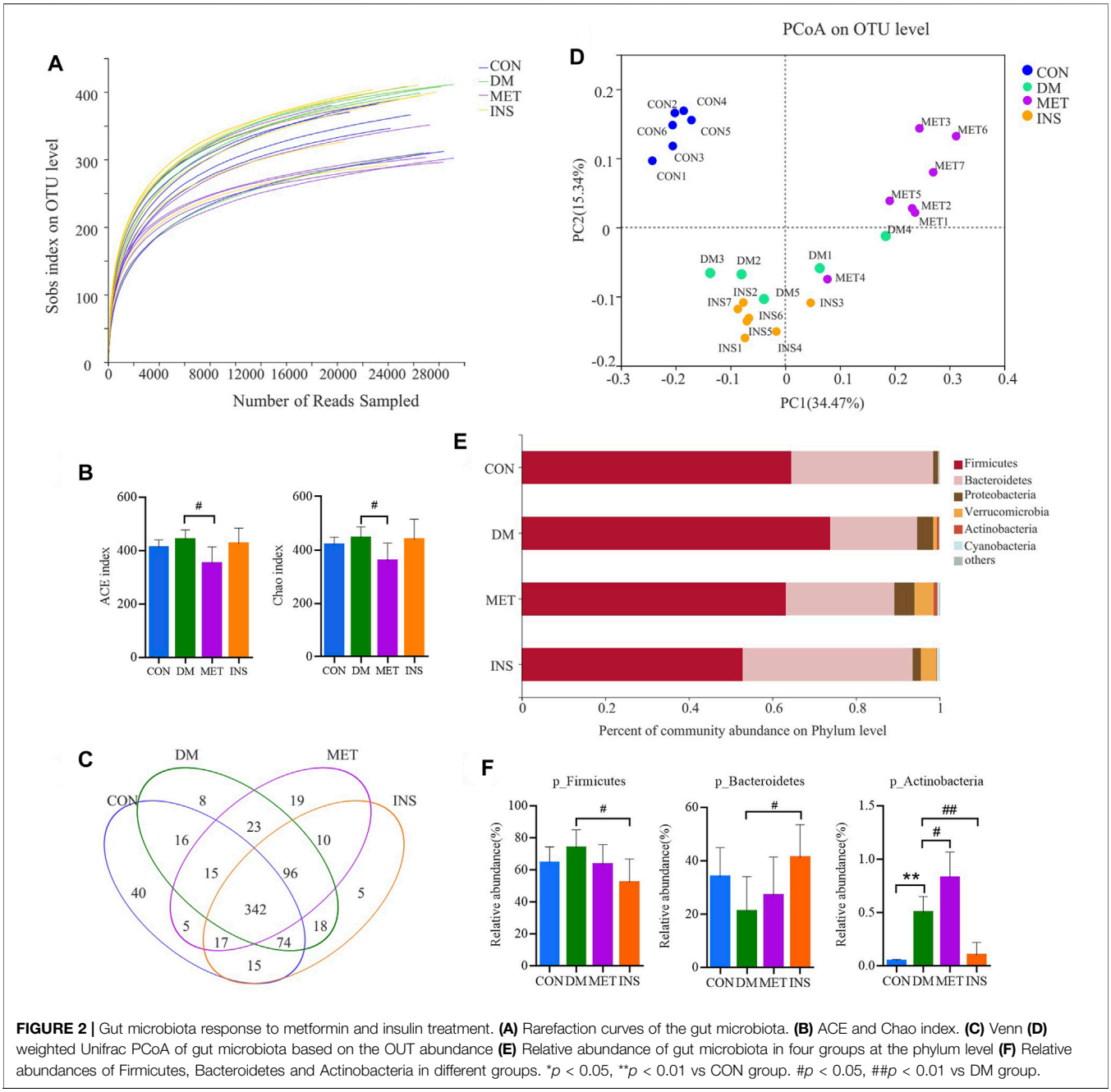

FIGURE 2 | Gut microbiota response to metformin and insulin treatment. **(A)** Rarefaction curves of the gut microbiota. **(B)** ACE and Chao index. **(C)** Venn **(D)** weighted Unifrac PCoA of gut microbiota based on the OUT abundance **(E)** Relative abundance of gut microbiota in four groups at the phylum level **(F)** Relative abundances of Firmicutes, Bacteroidetes and Actinobacteria in different groups. *$p < 0.05$, **$p < 0.01$ vs CON group. #$p < 0.05$, ##$p < 0.01$ vs DM group.

0.954, Q2 = 0.318). **Figures 4G,H** show that the INS group and DM group also had an obvious variation in the ESI+ and ESI- modes (G: R2X = 0.841, R2Y = 0.997, Q2 = 0.787; H: R2X = 0.843, R2Y = 0.997, Q2 = 0.751).

Identification of Differential Metabolites

In our current work, we adopted the supervised OPLS-DA model to identify the biomarkers based on the $p < 0.05$ and VIP > 1. Next, we searched the accurate mass to charge ratio (m/z) of the positive and negative ions in the online library (http://www.hmdb.ca/) to identify the qualified elements. In addition, the potential biomarkers were surmised by the fragmentation behaviors of MS/MS. According to the criteria of $p < 0.05$ and VIP > 1, a few metabolites were identified as the latent biomarkers. Moreover, 328, 64, and 206 differential metabolites were identified among DM/CON, MET/DM, and INS/DM groups, respectively (**Supplementary Table S2**). Four types of (amino acids, BAs, glycerophospholipids/glycerolipids, and acylcarnitines) and 47 metabolites related to glucose metabolism were screened and identified as potential biomarkers in the MET or INS group (**Table 2**). Specifically, compared with the DM group, the levels of L-glutamine, L-citrulline, CA, GCA, 3a,7a-dihydroxycholanoic acid, 3a, 6b, 7b-trihydroxy-5b-cholanoic acid, MG [0:0/18:2 (9Z, 12Z)/0:0], PE [22:6 (4Z,7Z,10Z,13Z,16Z, 19Z)/15:0], PG [18:3 (9Z,12Z, 15Z)/22:5 (4Z,7Z,10Z,13Z, 16Z)], TG [18:0/o-

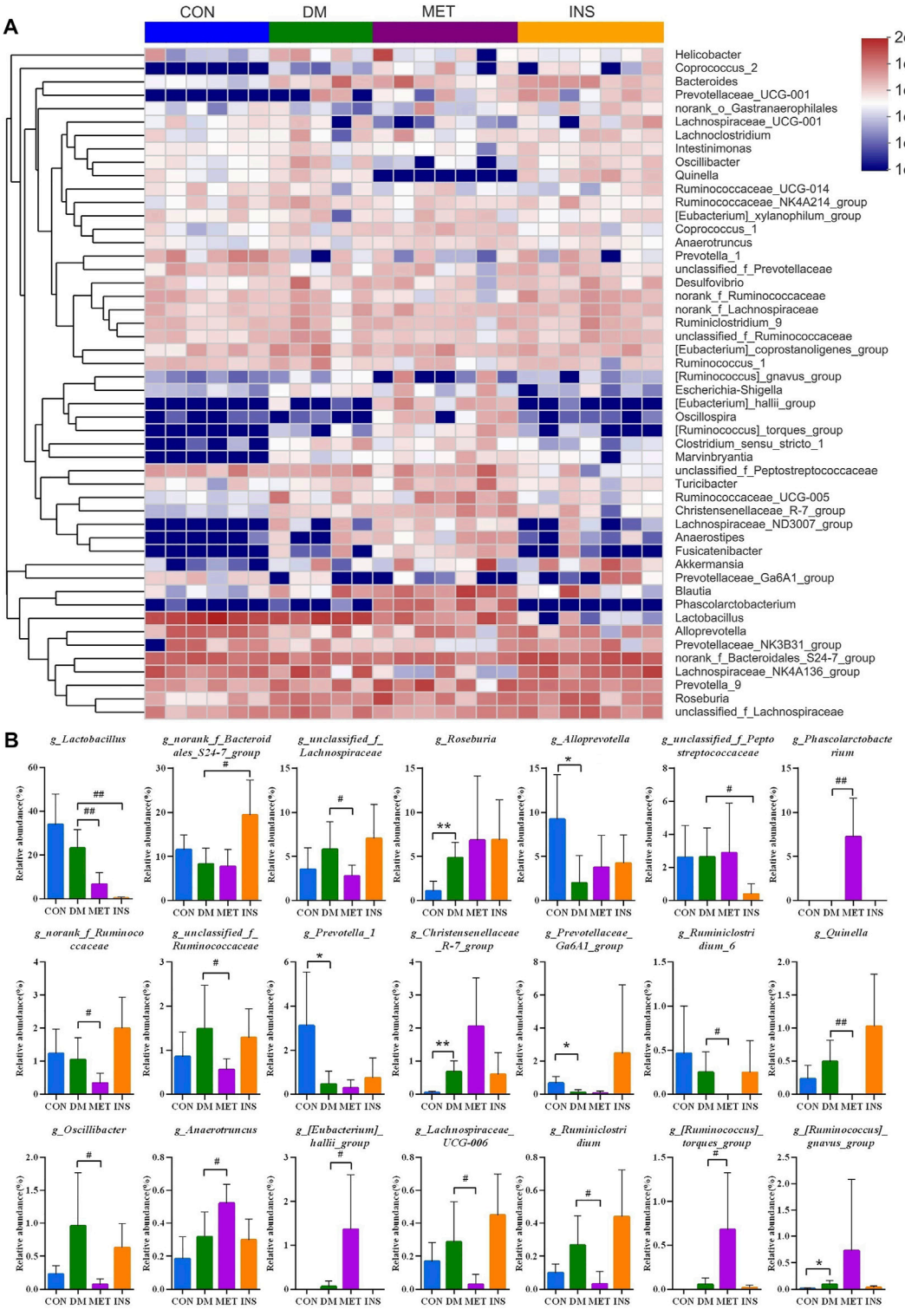

FIGURE 3 | The detailed effects of metformin on the gut microbiota of diabetic rats at the genus level. **(A)** the relative abundances of 50 dominant genera in the gut microbiota of four groups are presented in a heatmap. **(B)** Relative abundances of *g_Lactobacillus*, *g_norank_f_Bacteroidales_S24-7_group*, *g_unclassified_f_Lachnospiraceae*, *g_Roseburia*, *g_Alloprevotella*, *g_unclassified_f_Peptostreptococcaceae*, *g_Phascolarctobacterium*, *g_Ruminiclostridium_9*, *g_norank_f_Ruminococcaceae*, *g_Desulfovibrio*, *g_Turicibacter*, *g_unclassified_f_Ruminococcaceae*, *g_Prevotella_1*, *g_Christensenellaceae_R-7_group*, *g_Prevotellaceae_Ga6A1_group*, *g_Ruminiclostridium_6*, *g_Quinella*, *g_Prevotellaceae_UCG-001*, *g_Oscillibacter*, *g_Clostridium_sensu_stricto_1*, *g_Anaerotruncus*, *g_(Eubacterium)_hallii_group*, *g_Lachnospiraceae_UCG-006*, *g_Ruminiclostridium*, *g_(Ruminococcus)_torques_group* and *g_(Ruminococcu)_gnavus_group* in the gut microbiota of four groups. *$p < 0.05$, **$p < 0.01$ vs. CON group. #$p < 0.05$, ##$p < 0.01$ vs. DM group.

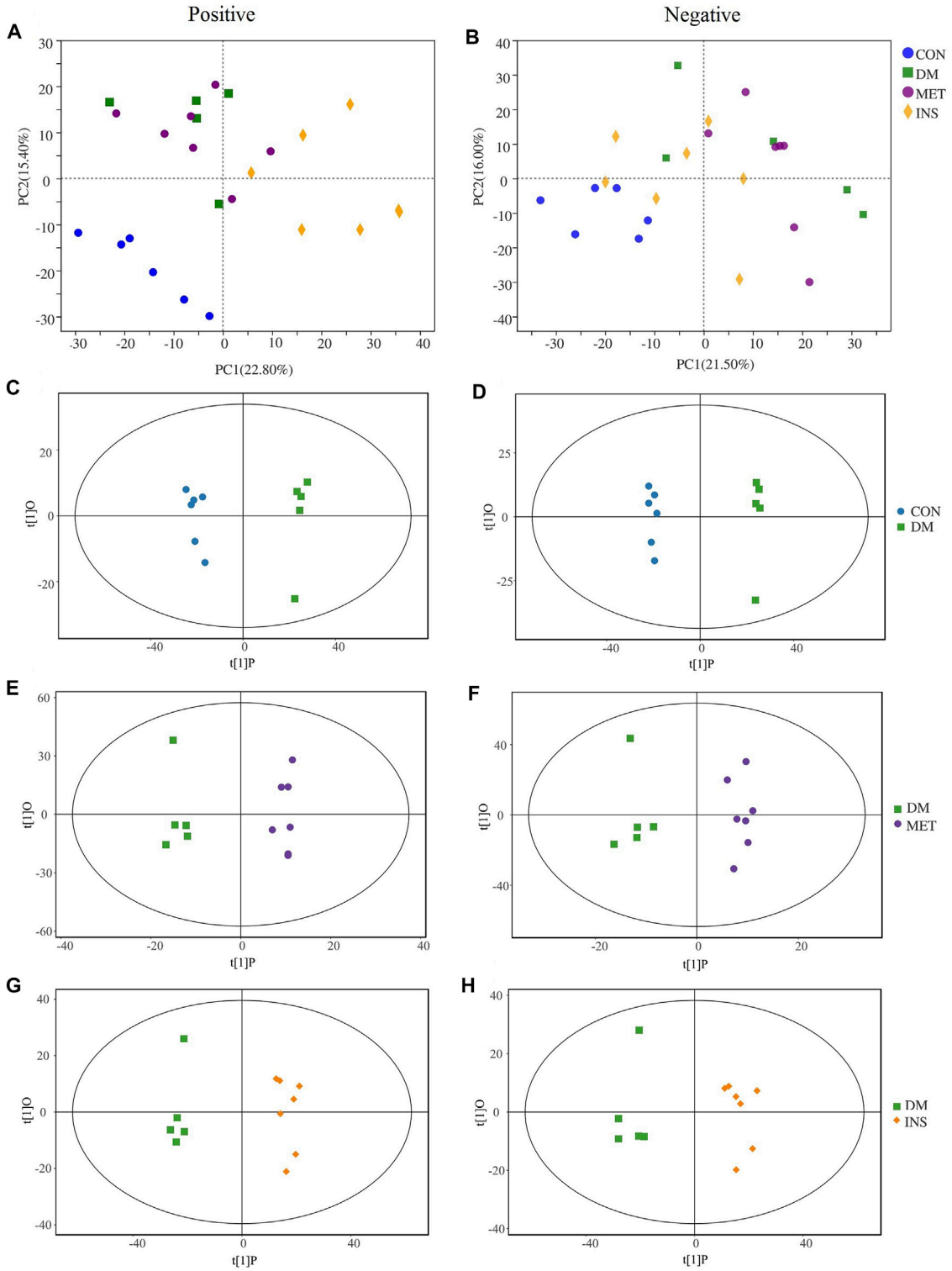

FIGURE 4 | PCA and OPLS-DA score plots in positive mode and negative mode. PCA score plot of each group in positive mode **(A)** and negative mode **(B)**. OPLS-DA score plots from CON group vs DM group in positive mode **(C)** and negative mode **(D)**; MET group vs DM group in positive mode **(E)** and negative mode **(F)**; INS group vs DM group in positive mode **(G)** and negative mode **(H)**.

TABLE 2 | The information of metabolites selected as biomarkers characterized in serum profiles and their taxonomy.

Metabolites	m/z	Rt	DM/CON	MET/DM	INS/DM	Taxonomy
L-Glutamic acid	148.0590	420.2050	↑*	—	↓#	L-alpha-amino acids
L-Glutamine	169.0572	355.0700	↑*	↓##	—	L-alpha-amino acids
L-Isoleucine	130.0860	295.5550	↑*	—	↓##	L-alpha-amino acids
L-Leucine	132.1004	276.8655	↑*	—	↓##	L-alpha-amino acids
L-Valine	159.1111	249.4830	↑*	—	↓##	L-alpha-amino acids
L-Citrulline	176.1022	371.7170	↑*	↓#	—	L-alpha-amino acids
Cholic acid	373.2724	209.8450	↑*	↓#	↓#	Bile acids and derivatives
Deoxycholic acid	391.2828	148.0540	↑*	—	↓#	Bile acids and derivatives
Glycocholic acid	466.3147	234.0415	↑**	↓#	—	Bile acids and derivatives
3a,7a-Dihydroxycholanoic acid	427.2578	159.4030	↑*	↓#	↓#	Bile acids and derivatives
3a,6b,7b-Trihydroxy-5b-cholanoic acid	409.2925	209.7790	↑*	↓#	↓##	Bile acids and derivatives
3-Oxocholic acid	405.2613	136.9160	↑**	—	↓##	Bile acids and derivatives
LysoPC [16:1 (9Z)]	494.3207	111.2680	↑*	—	↓#	Glycerophospholipids
LysoPC (17:0)	544.3123	175.0980	↓**	—	↓##	Glycerophospholipids
LysoPC (P-16:0)	480.3422	167.6570	↓**	—	↓##	Glycerophospholipids
LysoPE (24:0/0:0)	566.4144	168.4340	↓*	—	↓##	Glycerophospholipids
MG [0:0/18:2 (9Z,12Z)/0:0]	337.2718	233.2635	—	↓##	↓##	Monoacylglycerides
PC [18:1 (11Z)/18:1 (11Z)]	844.5764	123.3900	↑*	—	↓##	Glycerophospholipids
PC [18:1 (11Z)/18:3 (9Z,12Z,15Z)]	782.5684	119.1020	↑**	—	↓##	Glycerophospholipids
PC [18:4 (6Z, 9Z, 12Z, 15Z)/18:4 (6Z, 9Z, 12Z, 15Z)]	812.4455	39.7520	↑*	—	↓#	Glycerophospholipids
PC [20:5 (5Z, 8Z, 11Z, 14Z, 17Z)/14:0]	752.5187	124.7615	↑**	—	↓##	Glycerophospholipids
PE [18:4 (6Z, 9Z, 12Z, 15Z)/20:5 (5Z, 8Z, 11Z, 14Z, 17Z)]	794.9319	340.0400	↑**	—	↓#	Glycerophospholipids
PE [22:1 (13Z)/22:2 (13Z, 16Z)]	417.3330	47.3170	↑*	↑#	—	Glycerophospholipids
PE [22:6 (4Z, 7Z, 10Z, 13Z, 16Z, 19Z)/15:0]	750.5032	125.3440	↑*	↓#	—	Glycerophospholipids
PE [P-16:0/14:1 (9Z)]	646.9096	338.7110	↑**	—	↓##	Glycerophospholipids
PE (P-16:0e/0:0)	460.2674	36.5820	↑*	—	↓#	Glycerophospholipids
PE-NMe2 [16:0/18:1 (9Z)]	745.0469	26.0570	↑*	—	↓#	Glycerophospholipids
PG (16:0/16:0)	721.9525	339.4390	↑*	—	↓#	Glycerophospholipids
PG [16:0/18:3 (9Z, 12Z, 15Z)]	745.5051	239.5230	—	↑##	—	Glycerophospholipids
PG [18:3 (6Z, 9Z, 12Z)/16:1 (9Z)]	741.9493	340.0140	↑*	—	↓#	Glycerophospholipids
PG [18:3 (9Z, 12Z, 15Z)/22:5 (4Z, 7Z, 10Z, 13Z, 16Z)]	820.0494	338.6380	—	↓##	↓##	Glycerophospholipids
PI[16:1 (9Z)/18:1 (11Z)]	852.5577	180.2530	↓**	—	↓#	Glycerophospholipids
PI[18:1 (9Z)/18:3 (9Z,12Z,15Z)]	876.5553	176.5865	↓*	—	↓#	Glycerophospholipids
PS(14:0/16:0)	730.8923	339.1120	↑*	—	↓##	Glycerophospholipids
TG [14:1 (9Z)/15:0/20:4 (8Z,11Z,14Z,17Z)]	811.6628	155.8800	↓*	—	↓#	Glycerolipids
TG [16:1 (9Z)/18:0/20:0] (iso6)	940.8009	344.5030	↑*	—	↓#	Glycerolipids
TG [18:0/o-18:0/22:5 (7Z,10Z,13Z,16Z,19Z)]	924.5365	209.4260	—	↓#	↓#	Glycerolipids
TG [18:1 (9Z)/24:0/18:3 (6Z,9Z,12Z)]	984.9234	338.6735	↑**	—	↓##	Glycerolipids
TG (20:0/14:0/o-18:0)	850.4403	338.6760	↑*	—	↓#	Glycerolipids
TG [20:0/18:3 (9Z,12Z,15Z)/20:2n6]	922.4837	114.7160	↓*	↑#	—	Glycerolipids
TG (22:0/22:0/o-18:0)	1,103.8635	338.7090	↑**	—	↓##	Glycerolipids
11Z-Octadecenylcarnitine	426.3567	152.4600	↑*	—	↓#	Acylcarnitine
2-Hydroxylauroylcarnitine	360.2727	191.5340	↑**	—	↓##	Acylcarnitine
2-Methylbutyroylcarnitine	246.1686	223.4530	↓*	↓#	—	Acylcarnitine
3,5-Tetradecadiencarnitine	368.2777	162.5400	↑*	↓##	↓##	Acylcarnitine
3-Hydroxy-9-hexadecenoylcarnitine	414.3194	179.6235	↑**	—	↓##	Acylcarnitine
Trans-2-Tetradecenoylcarnitine	370.2937	159.9770	↑**	—	↓##	Acylcarnitine

18:0/22:5 (7Z,10Z,13Z,16Z, 19Z)], 2-methylbutyroylcarnitine, and 3,5-tetradecadiencarnitine were significantly decreased, while the levels of PE [22:1 (13Z)/22:2 (13Z, 16Z)], PG [16:0/18:3 (9Z,12Z, 15Z)], and TG [20:0/18:3 (9Z,12Z,15Z)/20:2n6] were significantly increased in the MET group. More differential metabolites were found between INS and DM groups, such as L-glutamic acid, L-isoleucine, L-leucine, L-valine, CA, DCA, 3a,7a-ddihydroxycholanoic acid, 3a,6b, 7b-trihydroxy-5b-cholanoic acid, 3-oxocholic acid, lysoPC [16:1 (9Z)], lysoPC(17:0), lysoPC(P-16:0), lysoPE (24:0/0:0), PC [18:1 (11Z)/18:1 (11Z)], PC[18:1 (11Z)/18:3 (9Z,12Z, 15Z)], PC [18:4 (6Z,9Z,12Z, 15Z)/18:4 (6Z,9Z,12Z, 15Z)], PC[20:5 (5Z,8Z,11Z,14Z, 17Z)/14:0], PE [18:4 (6Z,9Z,12Z, 15Z)/20:5 (5Z,8Z,11Z,14Z, 17Z)], PE [P-16:0/14:1 (9Z)], PE (P-16:0e/0:0), PE-NMe2 [16:0/18:1 (9Z)], PG (16:0/16:0), PG [18:3 (6Z,9Z, 12Z)/16:1 (9Z)], PI[16:1 (9Z)/18:1 (11Z)], PI[18:1 (9Z)/18:3 (9Z,12Z, 15Z)], PS(14:0/16:0), TG (16:1 (9Z)/18:0/20:0)(iso6),TG [18:1 (9Z)/24:0/18:3 (6Z,9Z, 12Z)], TG (20:0/14:0/o-18:0), TG (22:0/22:0/o-18:0), 11Z-octadecenylcarnitine, 2-hydroxymyristoylcarnitine, 2-hydroxylauroylcarnitine, 3,5-tetradecadiencarnitine, 3-hydroxy-9-hexadecenoylcarnitine, and trans-2-tetradecenoylcarnitine.

Serum Bile Acids

Thirteen BAs were detected in four groups, including both primary BAs (CA, CDCA, GCA, GCDCA, TCA and TCDCA) and secondary BAs (DCA, UDCA, LCA, TLCA, TDCA, GUDCA, and TUDCA) (**Figure 5**). Compared with the CON group, the serum levels of both

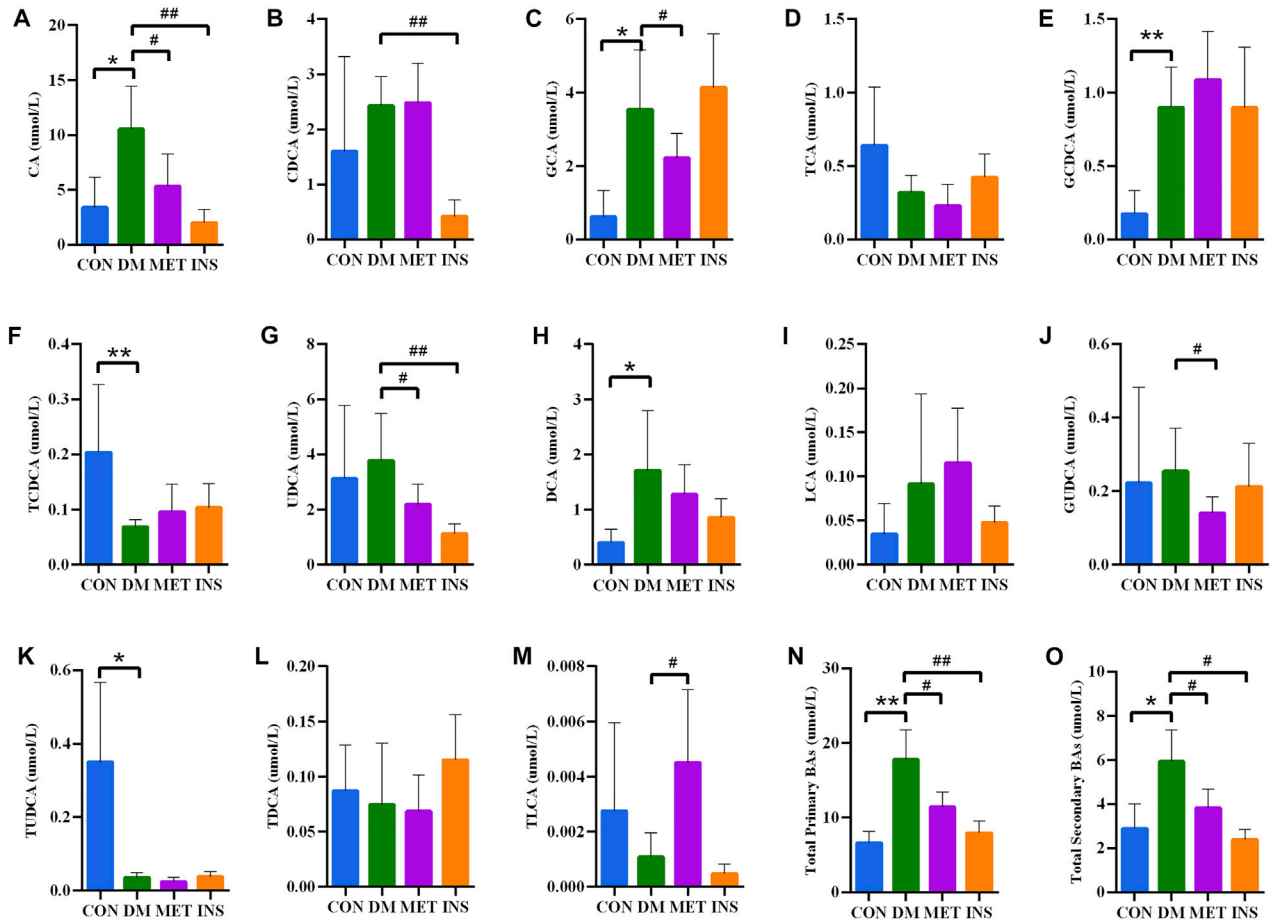

FIGURE 5 | Serum BA concentrations in rats of four groups. **(A)** CA, cholic acid; **(B)** CDCA, chenodeoxycholic acid; **(C)** GCA, glycocholic acid; **(D)** TCA, taurocholic acid; **(E)** GCDCA, glycochenodeoxycholic acid; **(F)** TCDCA, taurochenodeoxycholic acid; **(G)** UDCA, ursodeoxycholic acid; **(H)** DCA, deoxycholic acid; **(I)** LCA, lithocholic acid; **(J)** GUDCA, glycoursodeoxycholic acid; **(K)** TUDCA, Tauroursodeoxycholic acid; **(L)** TDCA, taurodeoxycholic acid; **(M)** TLCA, taurolithocholic acid; **(N)** Total primary BAs; **(O)** Total secondary BAs. *$p < 0.05$, **$p < 0.01$ vs. CON group. # $p < 0.05$, ## $p < 0.01$ vs. DM group.

primary and secondary BAs were remarkably increased in the DM group. In particular, serum levels of CA, GCA, GCDCA, and DCA were significantly higher, while the levels of TUDCA and TCDCA were lower in the DM group compared with the CON group. No significant differences were detected in serum levels of UDCA, CDCA, TCA, GUDCA, TDCA, LCA, and TLCA between the DM and CON groups. Metformin treatment could significantly decrease the serum levels of CA, GCA, UDCA, and GUDCA, while such treatment increased the level of TLCA in DM rats. Insulin treatment also significantly decreased the level of CA, UDCA, and CDCA.

Associations Between the Intestinal Microbiota and Serum Metabolites

In the present study, we assessed the relationships between the intestinal microbiota and serum differential metabolites identified between DM and MET rats using Spearman's correlation analysis (**Figure 6**). L-glutamine and L-citrulline were positively associated with the relative abundance of *Lactobacillus* ($p < 0.05$), and the corresponding r values were 0.68 and 0.66, respectively. Besides, L-citrulline also exhibited a positive correlation with the relative abundances of *Ruminiclostridium*, *norank_f_Ruminococcaceae*, *unclassified_f_Ruminococcaceae*, *Quinella*, *Ruminiclostridium_6*, *Oscillibacter*, and *Lachnospiraceae_UCG-006* ($p < 0.05$, r = 0.60–0.75), and it had a negative correlation with *Phascolarctobacteriu* ($p < 0.05$, $r = -0.70$). CA, GCA, and 3a,6b, 7b-trihydroxy-5b-cholanoic acid showed significant positive correlations with the relative abundance of *Lactobacillus* ($p < 0.05$, $r = 0.61$–0.69). CA, 3a,7a-dihydroxycholanoic acid and 3a, 6b, 7b-trihydroxy-5b-cholanoic acid showed negative correlations with the relative abundances of (*Ruminococcus*)*_torques_group*, (*Eubacterium*)*_hallii_group*, and *Phascolarctobacterium*. LPA (0:0/18:2 (9Z, 12Z)), MG (0:0/18:2 (9Z, 12Z)/0:0), PG [18:3 (9Z,12Z, 15Z)/22:5 (4Z,7Z,10Z,13Z, 16Z)] and PE [22:6 (4Z,7Z,10Z,13Z,16Z, 19Z)/15:0] showed moderate-to-high positive association with the abundance of *Quinella* ($p < 0.05$, r = 0.60–0.87), while PE [22:1 (13Z)/22:2 (13Z, 16Z)] and PG [16:0/18:3 (9Z,12Z, 15Z)] showed high negative correlation with *Quinella* ($p < 0.01$, r = −0.74–0.76). Moreover, 3, 5-tetradecadiencarnitine displayed high positive associations with

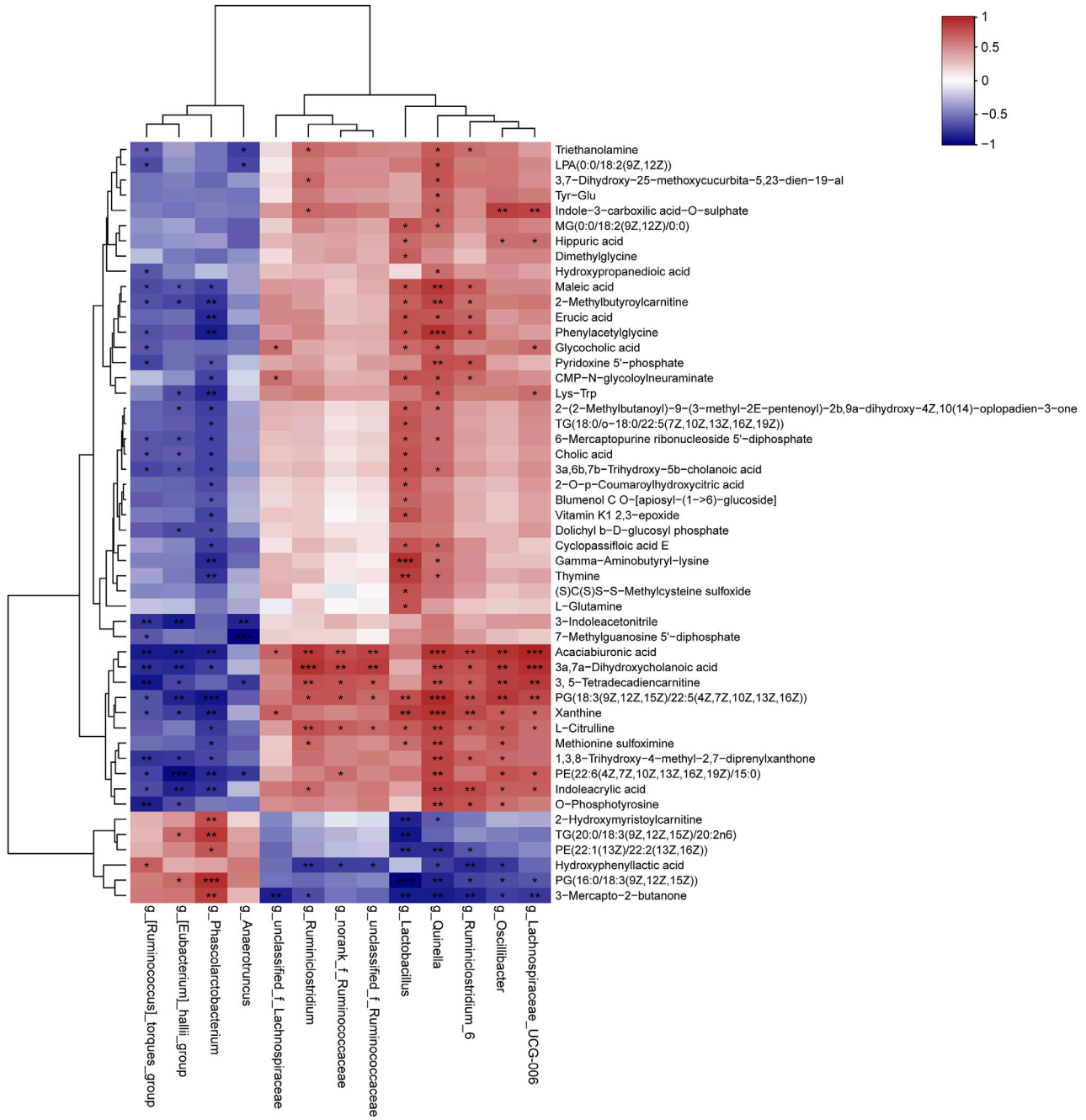

FIGURE 6 | Correlation analysis of the gut microbiome and serum metabolites. The results of Spearman's correlation between 13 differential genera (MET vs. DM) and 50 differential metabolites (MET vs. DM) were presented as a heatmap. *$p < 0.05$, **$p < 0.01$, ***$p < 0.001$ denoted statistical significance between bacterial taxa and metabolites.

Ruminiclostridium_6, *Quinella*, *Oscillibacter* and *Lachnospiraceae_UCG-006* ($p < 0.01$, r = 0.71–0.80), while they had negative association with (*Ruminococcus*)*_torques_group* ($p < 0.01$, r = −0.82).

The relationships between the intestinal microbiota and serum BAs in DM and MET rats were also assessed using Spearman's correlation analysis (**Figure 7**). CA and total primary BAs were positively associated with the relative abundances of *Quinella* and *Lachnospiraceae_UCG-006* ($p < 0.05$), while they were negatively associated with (*Ruminococcus*)*_torques_group* ($p < 0.01$, r = 0.71–0.75). TCA exhibited a negative correlation with the relative abundances of *Phascolarctobacteriu.* GCA showed sigenificant positive correlation with the relative abundance of *unclassified_f_Lachnospiraceae* ($p < 0.01$, r = 0.72). TUDCA,

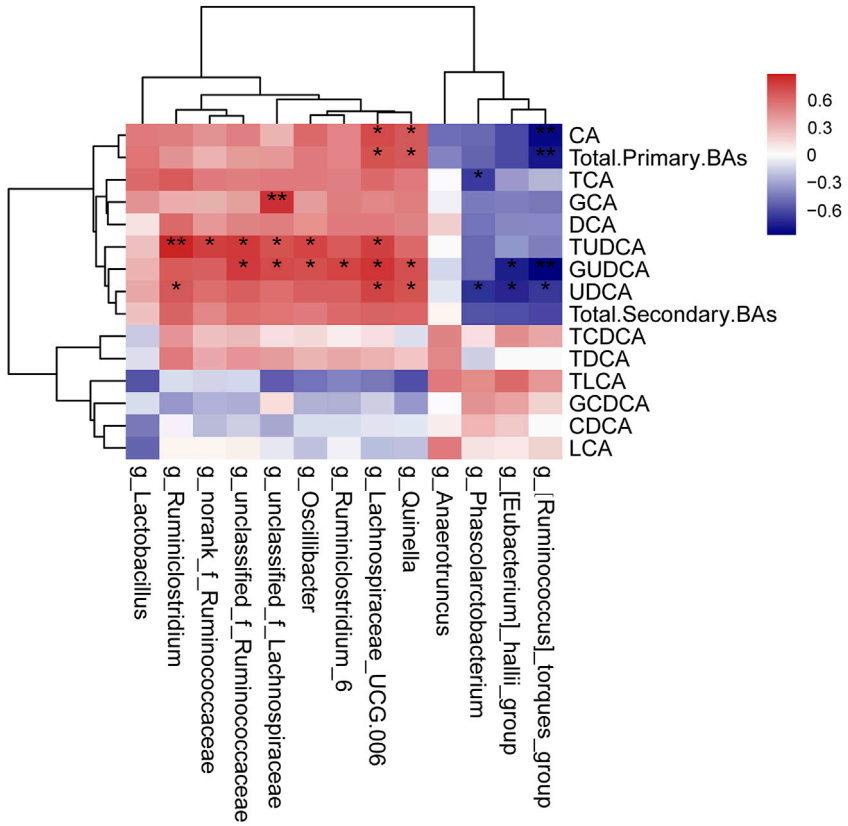

FIGURE 7 | Correlation analysis of the gut microbiome and serum BAs. The results of Spearman's correlation between 13 differential genera (MET vs. DM) and BAs (MET vs. DM) were presented as a heatmap. *$p < 0.05$, **$p < 0.01$ denoted statistical significance between bacterial taxa and BAs.

GUDCA, and UDCA displayed positivecorrelation with the relative abundances of several genera, such as *Ruminiclostridium*, *norank_f_Ruminococcaceae*, *unclassified_f_Ruminococcaceae*, *unclassified_f_Lachnospiraceae*, *Oscillibacter*, *Ruminiclostridium_6*, *Lachnospiraceae_UCG-006*, and *Quinella*. Besides, GUDCA and UDCA had negative correlations with the relative abundances of (*Ruminococcus*)*_torques_group* and (*Eubacterium*)*_hallii_group*.

DISCUSSION

In the present study, we showed that both metformin and insulin treatment reduced the blood glucose level, ameliorated the lipid metabolism, changed the composition of gut microbiota, and altered the serum metabolome in T2DM rats induced by the combination of STZ and HFD. Metformin treatment for 3 weeks partially decreased the levels of blood glucose, TC, TG, and LDL-C in DM rats, and the effectiveness was weaker compared with the insulin treatment. Metformin and insulin treatment altered the gut microbiota and metabolome profiles differently, indicating that different mechanisms were involved in the two types of pharmacotherapy.

Firmicutes and Bacteroidetes are the two dominant phyla in the gut microbiota, and the Bacteroidetes/Firmicutes ratio has been previously suggested as a marker of metabolic disease. Accumulating evidence has confirmed that diabetes and obesity can decrease the ratio of Bacteroidetes/Firmicutes in humans and animals (Everard and Cani, 2013; Gurung et al., 2020). Several investigations have shown that metformin treatment can elevate the ratio of Bacteroidetes/Firmicutes (Ryan et al., 2020; Zhang and Hu, 2020). In the present study, we also found that metformin and insulin both increased the ratio of Bacteroidetes/Firmicutes. It was noticeable that the relative abundance of phylum Actinobacteria was remarkably different among the four groups. Diabetes elevated the relative abundance of phylum Actinobacteria, which was regulated oppositely by the treatment of metformin or insulin. Metformin further increased the abundance, while insulin decreased the relative abundance of Actinobacteria. A study regarding the intestinal microbiome of Chinese T2DM patients has shown that the relative abundance of Actinobacteria in T2DM patients treated with metformin is markedly greater compared with the untreated T2DM patients, which is in agreement with our data (Zhang F. et al., 2019).

At the genus level, 13 genera changed significantly after metformin treatment, while only three changed after insulin treatment, indicating the greater influence of metformin on the gut microbiota. Among these genera, the abundances of short-chain fatty acid (SCFA)-producing bacteria, such as *Phascolarctobacterium*, *Anaerotruncus*, (*Eubacterium*)

_hallii_group, and (*Ruminococcus*)*_torques_group* were significantly increased after metformin treatment. SCFAs can activate intestinal gluconeogenesis and have beneficial effects on glucose and energy homeostasis (Larsen et al., 2010). SCFAs can be produced by certain bacteria. For example, propionic acid can be produced by *Phascolarctobacterium* (Reichardt et al., 2014), and butyric acid can be produced by *Eubacterium*, *Roseburia*, and *Faecalibacterium* (Louis et al., 2004). A lot of studies have reported that metformin regimen can elevate the abundances of SCFA-producing bacteria in diabetic animals and patients (Lee and Ko, 2014; Shin et al., 2014; Forslund et al., 2015; De La Cuesta-Zuluaga et al., 2017; Wu et al., 2017; Lee et al., 2018). The abundance of *Ruminococcus* was also found increased in db/db mice and C57BL/6J mice by metformin treatment (Bornstein et al., 2017; Zhang W. et al., 2019; Ahmadi et al., 2020). Zhang et al. have reported that metformin treatment can increase the abundance of *Phascolarctobacterium* in Wistar rats fed with HFD (Zhang et al., 2015). We also found that the abundances of two genera *unclassified_f_Lachnospiraceae* and *Lachnospiraceae_UCG-006*, which belong to the family *Lachnospiraceae,* were decreased in the MET group compared with the CON group. It has been reported that the abundance of *Lachnospiraceae* is increased in obese mice fed by HFD (Li et al., 2021), while it is decreased in women with a vegetarian diet (Barrett et al., 2018). Liraglutide, a glucagon-like peptide-1 (GLP-1) analog, significantly increases the abundances of *Lachnospiraceae_UCG-001* and *Lachnospiraceae_NK4A136_group nonalcoholic* in db/db mice with nonalcoholic fatty liver (Liu et al., 2020), suggesting that the decrease of *Lachnospiraceae* is beneficial for T2DM. The abundance of *unclassified Lachnospiraceae* is markedly decreased in metformin-treated obese patients compared with the metformin-naive obese patients (Hiel et al., 2020). Similar results are also observed in Wistar rats fed with HFD and T2DM Sprague-Dawley rats, showing that the abundances of *Lachnospiraceae_incertae_sedis* and *Lachnospiraceae NK4A136* are decreased after metformin administration (Zhang et al., 2015; Cui et al., 2019). Ryan et al. have reported that the abundance of *Ruminococcus* is decreased by metformin treatment in C57BL/6 mice fed with HFD (Ryan et al., 2020). We also found that the abundances of *norank_f_Ruminococcaceae* and *unclassified_f_Ruminococcaceae* were reduced by metformin. Elbere et al. have shown that the metformin treatment can elevate the abundance of *Oscillibacter* in both healthy nondiabetic individuals and T2DM patients (Elbere et al., 2020), which is opposite to our results. The alteration of *Lactobacillus* in our present work was also inconsistent with previous findings, in which its abundance is increased by metformin treatment in obese or diabetic rodents (Zhang et al., 2015; Zhang M. et al., 2019; Cui et al., 2019).

Amino acids promote the production of endogenous glucose as substrates of gluconeogenesis (Schutz, 2011). Insulin resistance is associated with higher levels of branched-chain amino acids (BCAAs), aromatic amino acids, and glutamate/glutamine (Tai et al., 2010). Among the serum differential metabolites between CON and DM groups, the levels of L-glutamic acid, L-glutamine, L-citrulline, and BCAAs (L-isoleucine, L-leucine, and L-valine) were all remarkably increased in the DM group compared with the CON group. After metformin treatment, the serum levels of L-glutamine and L-citrulline were decreased. It has been reported that metformin regulates ammonia homeostasis by controlling glutamine metabolism in the enterocyte, exerting an indirect regulatory effect on both the uptake and degradation of glutamine (Gil-GÓmez et al., 2018). Adam et al. have assessed 353 metabolites in fasting serum samples from T2DM patients who are treated with metformin or without anti-diabetic medication and found that citrulline is significantly lower in metformin-treated T2DM patients compared with those not receiving anti-diabetic medication. Citrulline is also confirmed to be significantly reduced in patients receiving metformin treatment for 7 years. Furthermore, lower citrulline levels in plasma, skeletal muscle, and adipose tissue are validated in mice receiving metformin (Adam et al., 2016). Moreover, the plasma concentrations of citrulline and arginine in overweight/obese adults with impaired fasting glucose can be decreased after 3 months of metformin plus pioglitazone regimen (Irving et al., 2015). Besides, acute administration of metformin decreases the concentration of plasma citrulline in non-diabetic African Americans (Rotroff et al., 2016). Citrulline plays a prominent role in nitric oxide biosynthesis and the urea cycle. The potential mechanism underlying metformin's effect on citrulline metabolism is related to the role of metformin in cellular and systemic nitric oxide and/or urea biosynthesis in individuals with T2DM (Irving and Spielmann, 2016). Many studies have confirmed that obesity and insulin resistance are associated with elevated circulating levels of BCAAs. BCAA and related metabolites are widely accepted as the most efficient biomarkers of obesity, insulin resistance, and T2DM in human (Knebel et al., 2016; Bloomgarden, 2018; White et al., 2021). In the present study, diabetes dramatically elevated the levels of BCAAs, which was consistent with previous studies. The change of BCAA level was not significant between the DM and MET groups, indicating that the metformin treatment might not affect on the BCAA metabolism. However, after insulin treatment, the levels of all three BCAAs, including L-isoleucine, L-leucine, and L-valine, were significantly decreased. The difference in effect on BCAA metabolism might be one of the distinctions in the action mechanism between metformin and insulin.

Acylcarnitines (ACs) function as carnitine esters of fatty acids that have entered the mitochondria. Lately, ACs are suggested as biomarkers of insulin resistance and metabolic inflexibility in humans (Mihalik et al., 2010; Ramos-Roman et al., 2012). Previous studies have indicated that the fatty acid oxidation rate exceeds the tricarboxylic acid cycle, thus resulting in the deposition of intermediary metabolites such as ACs (Muoio and Neufer, 2012; Schooneman et al., 2013). Makarova et al. have reported that insulin secretion upon glucose treatment reduces the plasma levels of long-chain acylcarnitin of normal mice by 30% (Makarova et al., 2019). We found that several ACs exhibited significant differences between the DM and CON groups. The serum levels of 2-methylbutyroylcarnitine, 11Z-octadecenylcarnitine, 2-hydroxylauroylcarnitine, 3,5-tetradecadiencarnitine, 3-hydroxy-9-hexadecenoylcarnitine and trans-2-tetradecenoylcarnitine were higher in diabetic rats compared with the control rats, and insulin treatment could

decrease the levels of all these ACs. The effect of metformin on ACs seemed weaker compared with insulin, and metformin treatment only decreased the levels of 2-methylbutyroylcarnitine and 3,5-tetradecadiencarnitine. Paul et al. have also reported that metformin reduces the levels of several ACs in metabolically dysfunctional mice (Ryan et al., 2020).

Lipid metabolism plays a fundamental role in the pathogenesis of diabetes. Dyslipidemia can promote the insulin resistance process, and further aggravate T2DM. Many studies have shown that elevated lipotoxicity, such as enhanced synthesis of fatty acids, sphingolipids and phospholipids, is associated with the pathogenesis of diabetes (Zhu et al., 2011; Floegel et al., 2013; Meikle et al., 2013; Shui et al., 2013; Zhao et al., 2013; Knebel et al., 2016; Tonks et al., 2016). It has been reported that there is a positive correlation between T2DM ceramide, and its precursor dihydroceramide, as well as phosphatidylethanolamine, phosphatidylglycerol and phosphatidylinositol (Meikle et al., 2013). TG is one of the high-risk factors for T2DM, the level of which should be strictly controlled in T2DM patients. We found that a lot of lipids, including PC, PE, PG, PI, PS and TG, were all significantly higher in T2DM rats compared with the normal rats, and insulin treatment could alleviate most of them. Metformin has beneficial effects on improving lipid metabolism, resulting in a reduction of chylomicrons by up to 50% in T2DM patients (He, 2020). Controversial conclusions have been obtained on the effects of metformin on lipid metabolism. For instance, Safai et al. have shown that T2DM patients treated with metformin have higher levels of five lysophosphatidylethanolamines (LysoPEs) compared with metformin-naïve patients (Safai et al., 2018), while Wanninger et al. have found that the levels of PC, lysoPC, phosphatidylserine, and sphingomyelin (derived from PC) were lower in metformin-exposed hepatocytes (Wanninger et al., 2008). It has been believed that metformin reduces the content of hepatic lipid by activating AMPK, thereby ameliorating the situation in hyperglycemia and insulin resistance (Viollet et al., 2012). However, in our present study, metformin treatment showed a weaker influence on this dyslipidemia, and only very few types of lipid were reversed. It was possibly attributed to the short course of metformin treatment, and the effect of metformin on lipid metabolism disorders has not been shown.

As the main element of bile, BAs not only facilitate the digestion and absorption of fat but also are involved in glycolipid and energy metabolism. BAs are cholesterol catabolites that are mainly synthesized in the liver, in which CA and CDCA are the two primary BAs generated. Following hepatic synthesis, BAs are secreted into bile as glycine or taurine conjugates. BAs are actively reabsorbed by enterocytes in the terminal ileum to hepatocytes, where they are taken up and reused. A small proportion of BAs is modified by intestinal microbiota and passively reabsorbed in the colon. Primary BAs can be metabolized to secondary BAs by gut bacteria. In the intestine, a part of conjugated CA and CDCA is de-conjugated by gut bacterial bile salt hydroxylase (BSH) to form DCA and LCA. In addition, small amounts of CDCA are converted to UDCA by gut bacterial 7β-hydroxysteroid dehydrogenase (Ferrell and Chiang, 2019). It has been demonstrated that BAs can take part in both glucose metabolism and energy regulation, mostly via the activation of the farnesoid X receptor (FXR) and the G protein-coupled BA receptor 1 (BA membrane-type receptor TGR5). A lot of studies have shown that hepatic insulin resistance and hyperglycemia increase BA synthesis, resulting in alterations in BA composition. For example, it has been reported that diabetic (db/db) mice have a larger total BA pool size than wild-type control animals (Chen et al., 2016). The levels of postprandial TBA, CA, CDCA, DCA and UDCA were greater in T2DM patients compared with healthy controls (Sonne et al., 2016). In our current work, both metformin and insulin could partially recover the increased TBA in diabetic rats. Moreover, several BAs changed significantly among different groups. For example, the levels of CA, DCA, GCA, CDCA, 3a,7a-dihydroxycholanoic acid, 3a,6b,7b-trihydroxy-5b-cholanoic acid and 3-oxocholic acid were higher in the DM group compared with the CON group. The level of CA, GCA, 3a,7a-dihydroxycholanoic acid and 3a,6b,7b-trihydroxy-5b-cholanoic acid were lower in the MET group compared with the DM group. Besides, we further determine the levels of 13 types of BAs, including six primary BAs and seven secondary BAs, using LC-MS/MS. Compared with the DM group, metformin and insulin treatment could both decrease the levels of total primary BAs and total secondary BAs. In addition, metformin could decrease the levels of CA, GCA, UDCA, and GUDCA, while it increased the level of TLCA. The levels of CA, CDCA and UDCA in DM rats were decreased after insulin administration. Metformin can ameliorate glucose metabolism by modulating the TBA level in the serum of diabetic animals. It has been reported that metformin treatment increases the level of BSH produced by the gut microbiota in diabetic mice (Wu et al., 2017). Sun et al. have shown that metformin changed the level of GUDCA by modulating the gut microbiota (such as inhibition of *Bacteroides fragilis* growth), thereby suppressing the FXR signaling pathway to decrease blood glucose and maintain blood glucose homeostasis. It has been hypothesized that metformin reduces the reabsorption of BA in the distal ileum, resulting in increased bile salt concentration within the colon, which may explain the impacts of metformin on the colonic microbiota (Carter et al., 2003).

Collectively, we, for the first time, evaluated the impacts of metformin on the gut microbiota and assessed the interplay between gut microbiota and host metabolism in T2DM rats induced by a combination of STZ and HFD. The above-mentioned effects of metformin were also compared with insulin treatment to further investigate the different therapeutic mechanisms between metformin and insulin. Compared with insulin treatment, metformin showed greater influences on the composition of the gut microbiota, while it had a weaker impact on serum metabolites. The therapeutic mechanisms of metformin on diabetic rats were likely associated with restoration of the dysbiosis of gut microbiota and regulation of the disorder of amino acids (L-glutamine and L-citrulline), glycerophospholipids/glycerolipids, acylcarnitine (3,5-tetradecadiencarnitine), and BAs. Taken together, regulating the BA levels might be a critical mechanism underlying the therapeutic effects of metformin on diabetes.

Our findings provided valuable insights in to the latent mechanism of metformin.

DATA AVAILABILITY STATEMENT

The raw sequencing data in our study have been deposited in the BioProject: PRJNA774924, https://www.ncbi.nlm.nih.gov/bioproject/?term=PRJNA774924.

ETHICS STATEMENT

The animal study was reviewed and approved by the Ethics Committee of the Third Affiliated Hospital of Soochow University.

AUTHOR CONTRIBUTIONS

NH and RC designed the study. XY directed the LC-MS/MS analysis. WH conducted the histological assay. NH, QZ, YJ, and RC were responsible for the animal experiment. NH and RC were the major contributors in drafting and revising the manuscript. LW reviewed the manuscript. All authors read and approved the final manuscript.

FUNDING

This work was funded by National Natural Science Foundation of China (No. 81503136), Changzhou High Level Medical Talents Training Project (No. 2016CZBJ010), and Science and Technology Project of Changzhou Health Commission (QN 202005).

SUPPLEMENTARY MATERIAL

The Supplementary Material for this article can be found online at: https://www.frontiersin.org/articles/10.3389/fphar.2021.794103/full#supplementary-material

REFERENCES

Adam, J., Brandmaier, S., Leonhardt, J., Scheerer, M. F., Mohney, R. P., Xu, T., et al. (2016). Metformin Effect on Nontargeted Metabolite Profiles in Patients with Type 2 Diabetes and in Multiple Murine Tissues. *Diabetes* 65, 3776–3785. doi:10.2337/db16-0512

Ahmadi, S., Razazan, A., Nagpal, R., Jain, S., Wang, B., Mishra, S. P., et al. (2020). Metformin Reduces Aging-Related Leaky Gut and Improves Cognitive Function by Beneficially Modulating Gut Microbiome/Goblet Cell/Mucin Axis. *J. Gerontol. A. Biol. Sci. Med. Sci.* 75, e9–e21. doi:10.1093/gerona/glaa056

Barrett, H. L., Gomez-Arango, L. F., Wilkinson, S. A., Mcintyre, H. D., Callaway, L. K., Morrison, M., et al. (2018). A Vegetarian Diet Is a Major Determinant of Gut Microbiota Composition in Early Pregnancy. *Nutrients* 10. doi:10.3390/nu10070890

Bloomgarden, Z. (2018). Diabetes and Branched-Chain Amino Acids: What Is the Link? *J. Diabetes* 10, 350–352. doi:10.1111/1753-0407.12645

Bornstein, S., Moschetta, M., Kawano, Y., Sacco, A., Huynh, D., Brooks, D., et al. (2017). Metformin Affects Cortical Bone Mass and Marrow Adiposity in Diet-Induced Obesity in Male Mice. *Endocrinology* 158, 3369–3385. doi:10.1210/en.2017-00299

Carter, D., Howlett, H. C., Wiernsperger, N. F., and Bailey, C. J. (2003). Differential Effects of Metformin on Bile Salt Absorption from the Jejunum and Ileum. *Diabetes Obes. Metab.* 5, 120–125. doi:10.1046/j.1463-1326.2003.00252.x

Chen, C., Hu, B., Wu, T., Zhang, Y., Xu, Y., Feng, Y., et al. (2016). Bile Acid Profiles in Diabetic (Db/db) Mice and Their Wild Type Littermates. *J. Pharm. Biomed. Anal.* 131, 473–481. doi:10.1016/j.jpba.2016.09.023

Cui, H. X., Zhang, L. S., Luo, Y., Yuan, K., Huang, Z. Y., and Guo, Y. (2019). A Purified Anthraquinone-Glycoside Preparation from Rhubarb Ameliorates Type 2 Diabetes Mellitus by Modulating the Gut Microbiota and Reducing Inflammation. *Front. Microbiol.* 10, 1423. doi:10.3389/fmicb.2019.01423

De La Cuesta-Zuluaga, J., Mueller, N. T., Corrales-Agudelo, V., Velásquez-Mejía, E. P., Carmona, J. A., Abad, J. M., et al. (2017). Metformin Is Associated with Higher Relative Abundance of Mucin-Degrading Akkermansia Muciniphila and Several Short-Chain Fatty Acid-Producing Microbiota in the Gut. *Diabetes Care* 40, 54–62. doi:10.2337/dc16-1324

Elbere, I., Silamikelis, I., Dindune, Ii., Kalnina, I., Ustinova, M., Zaharenko, L., et al. (2020). Baseline Gut Microbiome Composition Predicts Metformin Therapy Short-Term Efficacy in Newly Diagnosed Type 2 Diabetes Patients. *PLoS One* 15, e0241338. doi:10.1371/journal.pone.0241338

Everard, A., and Cani, P. D. (2013). Diabetes, Obesity and Gut Microbiota. *Best Pract. Res. Clin. Gastroenterol.* 27, 73–83. doi:10.1016/j.bpg.2013.03.007

Ferrell, J. M., and Chiang, J. Y. L. (2019). Understanding Bile Acid Signaling in Diabetes: From Pathophysiology to Therapeutic Targets. *Diabetes Metab. J.* 43, 257–272. doi:10.4093/dmj.2019.0043

Floegel, A., Stefan, N., Yu, Z., Mühlenbruch, K., Drogan, D., Joost, H. G., et al. (2013). Identification of Serum Metabolites Associated with Risk of Type 2 Diabetes Using a Targeted Metabolomic Approach. *Diabetes* 62, 639–648. doi:10.2337/db12-0495

Forslund, K., Hildebrand, F., Nielsen, T., Falony, G., Le Chatelier, E., Sunagawa, S., et al. (2015). Disentangling Type 2 Diabetes and Metformin Treatment Signatures in the Human Gut Microbiota. *Nature* 528, 262–266. doi:10.1038/nature15766

Gil-GÓmez, A., Gómez-Sotelo, A. I., Ranchal, I., RojasGarcía-Valdecasas, M., Muñoz-Hernández, R., et al. (2018). Metformin Modifies Glutamine Metabolism in an *In Vitro* and *In Vivo* Model of Hepatic Encephalopathy. *Rev. Esp Enferm Dig.* 110, 427–433. doi:10.17235/reed.2018.5004/2017

Gurung, M., Li, Z., You, H., Rodrigues, R., Jump, D. B., Morgun, A., et al. (2020). Role of Gut Microbiota in Type 2 Diabetes Pathophysiology. *EBioMedicine* 51, 102590. doi:10.1016/j.ebiom.2019.11.051

He, L. (2020). Metformin and Systemic Metabolism. *Trends Pharmacol. Sci.* 41, 868–881. doi:10.1016/j.tips.2020.09.001

Hiel, S., Gianfrancesco, M. A., Rodriguez, J., Portheault, D., Leyrolle, Q., Bindels, L. B., et al. (2020). Link between Gut Microbiota and Health Outcomes in Inulin -treated Obese Patients: Lessons from the Food4Gut Multicenter Randomized Placebo-Controlled Trial. *Clin. Nutr.* 39, 3618–3628. doi:10.1016/j.clnu.2020.04.005

Hu, N., Liu, X., Mu, Q., Yu, M., Wang, H., Jiang, Y., et al. (2021). The Gut Microbiota Contributes to the Modulation of Intestinal CYP3A1 and P-Gp in Streptozotocin-Induced Type 1 Diabetic Rats. *Eur. J. Pharm. Sci.* 162, 105833. doi:10.1016/j.ejps.2021.105833

`Irving, B. A., Carter, R. E., Soop, M., Weymiller, A., Syed, H., Karakelides, H., et al. (2015). Effect of Insulin Sensitizer Therapy on Amino Acids and Their Metabolites. *Metabolism* 64, 720–728. doi:10.1016/j.metabol.2015.01.008

Irving, B. A., and Spielmann, G. (2016). Does Citrulline Sit at the Nexus of Metformin's Pleotropic Effects on Metabolism and Mediate its Salutatory Effects in Individuals with Type 2 Diabetes? *Diabetes* 65, 3537–3540. doi:10.2337/dbi16-0050

Knebel, B., Strassburger, K., Szendroedi, J., Kotzka, J., Scheer, M., Nowotny, B., et al. (2016). Specific Metabolic Profiles and Their Relationship to Insulin Resistance in Recent-Onset Type 1 and Type 2 Diabetes. *J. Clin. Endocrinol. Metab.* 101, 2130–2140. doi:10.1210/jc.2015-4133

Kristófi, R., and Eriksson, J. W. (2021). Metformin as an Anti-inflammatory Agent: a Short Review. *J. Endocrinol.* 251 (2), R11–R22. doi:10.1530/JOE-21-0194

Larsen, N., Vogensen, F. K., Van Den Berg, F. W., Nielsen, D. S., Andreasen, A. S., Pedersen, B. K., et al. (2010). Gut Microbiota in Human Adults with Type 2 Diabetes Differs from Non-diabetic Adults. *PLoS One* 5, e9085. doi:10.1371/journal.pone.0009085

Lee, H., and Ko, G. (2014). Effect of Metformin on Metabolic Improvement and Gut Microbiota. *Appl. Environ. Microbiol.* 80, 5935–5943. doi:10.1128/AEM.01357-14

Lee, H., Lee, Y., Kim, J., An, J., Lee, S., Kong, H., et al. (2018). Modulation of the Gut Microbiota by Metformin Improves Metabolic Profiles in Aged Obese Mice. *Gut Microbes* 9, 155–165. doi:10.1080/19490976.2017.1405209

Li, A., Wang, N., Li, N., Li, B., Yan, F., Song, Y., et al. (2021). Modulation Effect of Chenpi Extract on Gut Microbiota in High-Fat Diet-Induced Obese C57BL/6 Mice. *J. Food Biochem.* 45, e13541. doi:10.1111/jfbc.13541

Liu, Q., Cai, B. Y., Zhu, L. X., Xin, X., Wang, X., An, Z. M., et al. (2020). Liraglutide Modulates Gut Microbiome and Attenuates Nonalcoholic Fatty Liver in Db/db Mice. *Life Sci.* 261, 118457. doi:10.1016/j.lfs.2020.118457

Louis, P., Duncan, S. H., Mccrae, S. I., Millar, J., Jackson, M. S., and Flint, H. J. (2004). Restricted Distribution of the Butyrate Kinase Pathway Among Butyrate-Producing Bacteria from the Human colon. *J. Bacteriol.* 186, 2099–2106. doi:10.1128/jb.186.7.2099-2106.2004

Makarova, E., Makrecka-Kuka, M., Vilks, K., Volska, K., Sevostjanovs, E., Grinberga, S., et al. (2019). Decreases in Circulating Concentrations of Long-Chain Acylcarnitines and Free Fatty Acids during the Glucose Tolerance Test Represent Tissue-specific Insulin Sensitivity. *Front. Endocrinol. (Lausanne)* 10, 870. doi:10.3389/fendo.2019.00870

Meikle, P. J., Wong, G., Barlow, C. K., Weir, J. M., Greeve, M. A., Macintosh, G. L., et al. (2013). Plasma Lipid Profiling Shows Similar Associations with Prediabetes and Type 2 Diabetes. *PLoS One* 8, e74341. doi:10.1371/journal.pone.0074341

Mihalik, S. J., Goodpaster, B. H., Kelley, D. E., Chace, D. H., Vockley, J., Toledo, F. G., et al. (2010). Increased Levels of Plasma Acylcarnitines in Obesity and Type 2 Diabetes and Identification of a Marker of Glucolipotoxicity. *Obesity (Silver Spring)* 18, 1695–1700. doi:10.1038/oby.2009.510

Muoio, D. M., and Neufer, P. D. (2012). Lipid-induced Mitochondrial Stress and Insulin Action in Muscle. *Cell Metab* 15, 595–605. doi:10.1016/j.cmet.2012.04.010

Ramos-Roman, M. A., Sweetman, L., Valdez, M. J., and Parks, E. J. (2012). Postprandial Changes in Plasma Acylcarnitine Concentrations as Markers of Fatty Acid Flux in Overweight and Obesity. *Metabolism* 61, 202–212. doi:10.1016/j.metabol.2011.06.008

Reichardt, N., Duncan, S. H., Young, P., Belenguer, A., Mcwilliam Leitch, C., Scott, K. P., et al. (2014). Phylogenetic Distribution of Three Pathways for Propionate Production within the Human Gut Microbiota. *Isme j* 8, 1323–1335. doi:10.1038/ismej.2014.14

Rotroff, D. M., Oki, N. O., Liang, X., Yee, S. W., Stocker, S. L., Corum, D. G., et al. (2016). Pharmacometabolomic Assessment of Metformin in Non-diabetic, African Americans. *Front. Pharmacol.* 7, 135. doi:10.3389/fphar.2016.00135

Ryan, P. M., Patterson, E., Carafa, I., Mandal, R., Wishart, D. S., Dinan, T. G., et al. (2020). Metformin and Dipeptidyl Peptidase-4 Inhibitor Differentially Modulate the Intestinal Microbiota and Plasma Metabolome of Metabolically Dysfunctional Mice. *Can. J. Diabetes* 44, 146–155. doi:10.1016/j.jcjd.2019.05.008

Safai, N., Suvitaival, T., Ali, A., Spégel, P., Al-Majdoub, M., Carstensen, B., et al. (2018). Effect of Metformin on Plasma Metabolite Profile in the Copenhagen Insulin and Metformin Therapy (CIMT) Trial. *Diabet Med.* 35, 944–953. doi:10.1111/dme.13636

Schooneman, M. G., Vaz, F. M., Houten, S. M., and Soeters, M. R. (2013). Acylcarnitines: Reflecting or Inflicting Insulin Resistance? *Diabetes* 62, 1–8. doi:10.2337/db12-0466

Schutz, Y. (2011). Protein Turnover, Ureagenesis and Gluconeogenesis. *Int. J. Vitam Nutr. Res.* 81, 101–107. doi:10.1024/0300-9831/a000064

Shin, N. R., Lee, J. C., Lee, H. Y., Kim, M. S., Whon, T. W., Lee, M. S., et al. (2014). An Increase in the Akkermansia Spp. Population Induced by Metformin Treatment Improves Glucose Homeostasis in Diet-Induced Obese Mice. *Gut* 63, 727–735. doi:10.1136/gutjnl-2012-303839

Shui, G., Lam, S. M., Stebbins, J., Kusunoki, J., Duan, X., Li, B., et al. (2013). Polar Lipid Derangements in Type 2 Diabetes Mellitus: Potential Pathological Relevance of Fatty Acyl Heterogeneity in Sphingolipids. *Metabolomics* 9, 786–799. doi:10.1007/s11306-013-0494-0

Sonne, D. P., Van Nierop, F. S., Kulik, W., Soeters, M. R., Vilsbøll, T., and Knop, F. K. (2016). Postprandial Plasma Concentrations of Individual Bile Acids and FGF-19 in Patients with Type 2 Diabetes. *J. Clin. Endocrinol. Metab.* 101, 3002–3009. doi:10.1210/jc.2016-1607

Tai, E. S., Tan, M. L., Stevens, R. D., Low, Y. L., Muehlbauer, M. J., Goh, D. L., et al. (2010). Insulin Resistance Is Associated with a Metabolic Profile of Altered Protein Metabolism in Chinese and Asian-Indian Men. *Diabetologia* 53, 757–767. doi:10.1007/s00125-009-1637-8

Tonks, K. T., Coster, A. C., Christopher, M. J., Chaudhuri, R., Xu, A., Gagnon-Bartsch, J., et al. (2016). Skeletal Muscle and Plasma Lipidomic Signatures of Insulin Resistance and Overweight/obesity in Humans. *Obesity (Silver Spring)* 24, 908–916. doi:10.1002/oby.21448

Viollet, B., Guigas, B., Sanz Garcia, N., Leclerc, J., Foretz, M., and Andreelli, F. (2012). Cellular and Molecular Mechanisms of Metformin: an Overview. *Clin. Sci. (Lond)* 122, 253–270. doi:10.1042/CS20110386

Wang, Z., Yang, H., Xu, J., Zhao, K., Chen, Y., Liang, L., et al. (2019). Prediction of Atorvastatin Pharmacokinetics in High-Fat Diet and Low-Dose Streptozotocin-Induced Diabetic Rats Using a Semiphysiologically Based Pharmacokinetic Model Involving Both Enzymes and Transporters. *Drug Metab. Dispos* 47, 1066–1079. doi:10.1124/dmd.118.085902

Wanninger, J., Neumeier, M., Weigert, J., Liebisch, G., Weiss, T. S., Schäffler, A., et al. (2008). Metformin Reduces Cellular Lysophosphatidylcholine and Thereby May Lower Apolipoprotein B Secretion in Primary Human Hepatocytes. *Biochim. Biophys. Acta* 1781, 321–325. doi:10.1016/j.bbalip.2008.04.012

White, P. J., Mcgarrah, R. W., Herman, M. A., Bain, J. R., Shah, S. H., and Newgard, C. B. (2021). Insulin Action, Type 2 Diabetes, and Branched-Chain Amino Acids: A Two-Way Street. *Mol. Metab.* 52, 101261. doi:10.1016/j.molmet.2021.101261

Wu, H., Esteve, E., Tremaroli, V., Khan, M. T., Caesar, R., Mannerås-Holm, L., et al. (2017). Metformin Alters the Gut Microbiome of Individuals with Treatment-Naive Type 2 Diabetes, Contributing to the Therapeutic Effects of the Drug. *Nat. Med.* 23, 850–858. doi:10.1038/nm.4345

Zhang, F., Wang, M., Yang, J., Xu, Q., Liang, C., Chen, B., et al. (2019a). Response of Gut Microbiota in Type 2 Diabetes to Hypoglycemic Agents. *Endocrine* 66, 485–493. doi:10.1007/s12020-019-02041-5

Zhang, M., Feng, R., Yang, M., Qian, C., Wang, Z., Liu, W., et al. (2019b). Effects of Metformin, Acarbose, and Sitagliptin Monotherapy on Gut Microbiota in Zucker Diabetic Fatty Rats. *BMJ Open Diabetes Res. Care* 7, e000717. doi:10.1136/bmjdrc-2019-000717

Zhang, Q., and Hu, N. (2020). Effects of Metformin on the Gut Microbiota in Obesity and Type 2 Diabetes Mellitus. *Diabetes Metab. Syndr. Obes.* 13, 5003–5014. doi:10.2147/dmso.s286430

Zhang, W., Xu, J. H., Yu, T., and Chen, Q. K. (2019c). Effects of Berberine and Metformin on Intestinal Inflammation and Gut Microbiome Composition in Db/db Mice. *Biomed. Pharmacother.* 118, 109131. doi:10.1016/j.biopha.2019.109131

Zhang, X., Zhao, Y., Xu, J., Xue, Z., Zhang, M., Pang, X., et al. (2015). Modulation of Gut Microbiota by Berberine and Metformin during the Treatment of High-Fat Diet-Induced Obesity in Rats. *Sci. Rep.* 5, 14405. doi:10.1038/srep14405

Zhao, C., Mao, J., Ai, J., Shenwu, M., Shi, T., Zhang, D., et al. (2013). Integrated Lipidomics and Transcriptomic Analysis of Peripheral Blood Reveals Significantly Enriched Pathways in Type 2 Diabetes Mellitus. *BMC Med. Genomics* 6 (Suppl. 1), S12. doi:10.1186/1755-8794-6-S1-S12

Zhu, C., Liang, Q. L., Hu, P., Wang, Y. M., and Luo, G. A. (2011). Phospholipidomic Identification of Potential Plasma Biomarkers Associated

with Type 2 Diabetes Mellitus and Diabetic Nephropathy. *Talanta* 85, 1711–1720. doi:10.1016/j.talanta.2011.05.036

Conflict of Interest: The authors declare that the research was conducted in the absence of any commercial or financial relationships that could be construed as a potential conflict of interest.

Publisher's Note: All claims expressed in this article are solely those of the authors and do not necessarily represent those of their affiliated organizations, or those of the publisher, the editors and the reviewers. Any product that may be evaluated in this article, or claim that may be made by its manufacturer, is not guaranteed or endorsed by the publisher.

frontiers in Pharmacology

ORIGINAL RESEARCH
published: 27 January 2022
doi: 10.3389/fphar.2022.835359

Integrative Metabolomics, Proteomics and Transcriptomics Analysis Reveals Liver Toxicity of Mesoporous Silica Nanoparticles

Jing Li[1], *Runbin Sun*[2], *Hui Xu*[1,2]* *and Guangji Wang*[2]

[1]Lab of Nano-Biology Technology, School of Physics and Electronics, Institute of Super-Microstructure and Ultrafast Process in Advanced Materials, Central South University, Changsha, China, [2]Key Laboratory of Drug Metabolism and Pharmacokinetics, State Key Laboratory of Natural Medicines, China Pharmaceutical University, Nanjing, China

OPEN ACCESS

Edited by:
Linsheng Liu,
The First Affiliated Hospital of Soochow University, China

Reviewed by:
Bin Wei,
Zhejiang University of Technology, China
Xinwen Wang,
Northeast Ohio Medical University, United States

***Correspondence:**
Hui Xu
xuhui@csu.edu.cn

Specialty section:
This article was submitted to Translational Pharmacology, a section of the journal Frontiers in Pharmacology

Received: 14 December 2021
Accepted: 07 January 2022
Published: 27 January 2022

Citation:
Li J, Sun R, Xu H and Wang G (2022) Integrative Metabolomics, Proteomics and Transcriptomics Analysis Reveals Liver Toxicity of Mesoporous Silica Nanoparticles. Front. Pharmacol. 13:835359. doi: 10.3389/fphar.2022.835359

As pharmaceutical excipients, mesoporous silica nanoparticles (MSNs) have attracted considerable concern based on potential risks to the public. The impact of MSNs on biochemical metabolism is poorly understood, and few studies have compared the effects of MSNs administered via different routes. To evaluate the hepatotoxicity of MSNs, metabolomics, proteomics and transcriptomic analyses were performed in mice after intravenous (20 mg/kg/d) or oral ad-ministration (200 mg/kg/d) of MSNs for 10 days. Intravenous injection induced significant hepatic injury based on pathological inspection and increased the levels of AST/ALT and the inflammatory factors IL-6, IL-1β and TNF-a. Omics data suggested intravenous administration of MSNs perturbed the following metabolites: succinate, hypoxanthine, GSSG, NADP+, NADPH and 6-phosphogluconic acid. In addition, increases in GPX, SOD3, G6PD, HK, and PFK at proteomic and transcriptomic levels suggested elevation of glycolysis and pentose phosphate pathway, synthesis of glutathione and nucleotides, and antioxidative pathway activity, whereas oxidative phosphorylation, TCA and mitochondrial energy metabolism were reduced. On the other hand, oral administration of MSNs disturbed inflammatory factors and metabolites of ribose-5-phosphate, 6-phosphogluconate, GSSG, and NADP+ associated with the pentose phosphate pathway, glutathione synthesis and oxidative stress albeit to a lesser extent than intravenous injection despite the administration of a ten-fold greater dose. Overall, systematic biological data suggested that intravenous injection of nanoparticles of pharmaceutical excipients substantially affected hepatic metabolism function and induced oxidative stress and inflammation, whereas oral administration exhibited milder effects compared with intravenous injection.

Keywords: mesoporous silica nanoparticle, metabolomics, proteomics, transcriptomic, hepatotoxicity, oxidative stress, oxidative phosphorylation, inflammation

1 INTRODUCTION

Mesoporous silica nanoparticles (MSNs) have been widely used in biology (Rosenholm et al., 2016) and medicine (Tang et al., 2012) due to their high pore volume, large specific surface area, easy surface modification, biocompatibility, and degradability features, such as slow drug release (He et al., 2016; Song et al., 2016). MSNs have been used in cancer treatment (Baeza et al., 2015; Birault et al., 2020), biological diagnosis (Lee et al., 2013), and imaging (Trewyn et al., 2007). Although MSNs exhibit some special, ideal properties as traditional preparation excipient materials, including both degradable or nondegradable produces, these materials are generally considered inert and harmless to the body. However, an increasing number of studies have demonstrated that these tiny nanoparticles can affect the tissues and cells of the body, causing inflammation and histopathological changes (Liu et al., 2012; Peeters et al., 2013; Nemmar et al., 2016; Zhang et al., 2018). Therefore, the assessment of their safety *in vivo* becomes indispensable.

Nanomaterials and porous adsorption particles for pharmacies are generally prepared as injections, oral dosage forms or powder sprays, which enter the body through intravenous, gavage or atomization, respectively (Fu et al., 2013). Nanoparticles easily enter the body through injection and impact the body (Cho et al., 2009; Zhao et al., 2012; Nemmar et al., 2016). In addition, studies have suggested that after orally administered nanoparticles enter the intestine, these nanoparticles can further pass through the intestinal membrane barrier, enter into the circulation system and subsequently tissues and cells, and thus impact the body (He et al., 2011; Li et al., 2015; Chen et al., 2019, 2020). Similar to the processes of solid particles in the atmosphere and in sprays, these solid particles mainly enter the lungs through breathing via the respiratory tract, adhere to the oral cavity and nasal cavity, enter the gastrointestinal tract through drinking or eating, or enter the cells in the oral mucosa of the nasal cavity (Griese, 1999; Patton and Byron, 2007; Park et al., 2010; Garbuzenko et al., 2014; Shin et al., 2017; Pietroiusti et al., 2018; Rosário et al., 2021).

The liver bears the brunt as the target organ of the particles. Lu et al. (2010), (2015) reported that intravenous injection (IV) of silica nanoparticles showed significant capture of the particles in the liver and induced hepatic injury. Huang et al. (2011), Li et al. (2015) administered MSN (particle size over 100 nm) suspensions to ICR mice at a dose of 20 mg/kg by intravenous injection and found increased accumulation in the liver after 7 days. Moreover, oral administration (IG) of MSN suspensions to ICR mice at a dose of 40 mg/kg and spherical MSNs yielded high liver accumulation after 7 days. Mohamed et al. found that acute and subacute oral administration of graphene oxide nanoparticles induced genomic instability and mutagenicity in the mouse liver (Mohamed et al., 2020), which are closely involved in oxidative stress.

Despite sporadic reports on the effects of MSNs on the body, tissues or organs, there is a lack of systematic evaluation on the metabolism, gene and protein levels of the damage to the body, tissues or organs under the conditions of two different dosage forms based on different administration modes, namely injection and oral administration. Considering that the liver is the key primary organ responsible for systematic metabolism and the turnover of small molecules, metabolomics combined with transcriptomics and proteomics was used in this study to assess the effects of intravenous and intragastric administration of MSNs on the function of the liver and to further clarify the effects of administration mode on the body and system. We aim to provide insight into improved assessment of the safety of intravenous injection or oral administration of MSNs and further understanding of the underlying mechanism of hepatotoxicity.

2 MATERIALS AND METHODS

2.1 Fabrication and Characterization of Mesoporous Silica Nanoparticles

Mesoporous silica nanoparticles were synthesized according to our previous reports (He et al., 2014, 2017). Briefly, N-octadecyltrimethoxysilanem (C18TMS, 95%) and tetraethyl orthosilicate (TEOS, 98%) were mixed in 50 ml ethanol and sonicated for 10 min. Then, the mixture was transferred into solutions of ethanol, ammonia and deionized water with stirring for 2 h at room temperature. The C18TMS-incorporated particles were collected by filtration, washed with ethanol and deionized water and dried at room temperature. Finally, the collections were calcined at 550°C for 6 h. The morphology and structure of MSNs were observed by scanning electron microscopy (SEM, Hitachi S-4800) and electron microscopy (TEM, JEM-2100F). The surface area, pore volume and pore diameter were calculated by Brunauer-Emmett-Teller (BET) and Barrett-Joyner-Halenda (BJH) methods using a Quantachrome Autosorb-1C apparatus.

2.2 Animal Administration and Sample Collection

All animal experiments were performed in accordance with Institutional Animal Care and Use Committee guidelines of China Pharmaceutical University. Male ICR mice (5–7 weeks of age, 20–25 g) were used in our experiments and were purchased from Shanghai Xipu-Bikai Experimental Animal Co., Ltd. All animals were kept on a 12-h light-dark cycle, fed ad libitum and acclimated to our research environment at least 1 week before the experimental manipulation.

Thirty healthy ICR mice were randomly allocated into three groups (n = 10 for each group): the control group, IV group and IG group. The MSN suspension (in physiological saline solution) at concentrations of 0.6 mg/ml and 6 mg/ml was ultrasonicated for 20 min before experiments. The suspension was injected through the tail vein (20 mg/kg/d) or administered by gavage (200 mg/kg/d) every day. The treatment period was 10 days.

After fasting overnight on the tenth day, blood samples were collected via the ocular vein, centrifuged twice at 3,000 rpm for 10 min to separate serum and stored at −80°C. After blood collection, the mice were sacrificed immediately. The livers were separated, rinsed in cold phosphate buffer solution, and filter paper was used to soak up water. The hepatic lobes were split into two

parts for GC-MS and LC-MS metabolomics. One portion of hepatic lobules was collected for RT–PCR, and the other portion was fixed in 10% formalin for histopathological examination. During the sampling process, all but blood and pathology samples were immediately placed in dry ice and stored at −80°C.

Twenty-four healthy ICR mice were randomly allocated into three groups (n = 8 for each group): the control group, IV group and IG group. The previous administration procedure was repeated. After 10 days, the mice were sacrificed, the livers were separated, rinsed in cold phosphate buffer solution, and filter paper was used to soak up water. The hepatic lobes were split into two parts for proteomics and transcriptomics, and all samples were immediately placed in dry ice and stored at −80°C.

2.3 Metabolomics Analysis

2.3.1 GC-MS Analysis

The liver samples were pretreated for GC-MS or LC-MS analysis as reported previously (Aa et al., 2021). In brief, 900 μl methanol solution containing [1,2-$^{13}C_2$] myristic acid (12.5 μg/ml) as the internal standard (IS) was added to 20 mg of liver tissue samples (n = 8–9 for each group) in a 1.5-ml Eppendorf tube. The samples were homogenized to precipitate the protein and extract the metabolites. After centrifugation for 10 min at 4°C at 20000×g, 100 μl supernatant was transferred to a chromatography (GC) vial and evaporated to dryness using an SPD2010-230 SpeedVac Concentrator (Thermo Savant, Holbrook, United States). Methoxyamine (30 μl) in pyridine (10 mg/μl) was added to the dried GC vial and shaken to dissolve the metabolites for 5 min. The methoxymation reaction proceeded for 16 h at room temperature. Then, 30 μl of N-methyl-N-(trimethylsilyl) trifluoroacetamide (MSTFA) with 1% TMCS was added to the trimethylsilylation reaction for 1 h. Finally, 30 μl of heptane, including methyl myristate (30 μg/ml), was added to each solution, and the solution was mixed by vortexing for 30 s. GC-MS analysis was performed using a GCMSSQP2010 (Shimadzu Corp., Tokyo, Japan) gas chromatography system, and detailed GCMS parameters are provided in the supporting information. The metabolites were identified by the mass spectra and retention index of the detected compounds with reference standards or those available libraries: the National Institute of Standards and Technology (NIST) library 2.0 (2012), Wiley 9 (Wiley–VCH Verlag GmbH & Co. KGaA, Weinheim, Germany) and our own laboratory at China Pharmaceutical University. Each peak area was normalized based on the internal standard (IS).

2.3.2 LC-MS Analysis

1000 μl methanol-ultrapure water (9:1) containing IS (^{13}C-glutamine) was added to 20 mg of liver tissue samples (n = 8–9 for each group) in a 1.5-ml Eppendorf tube. The samples were homogenized to precipitate the protein and extract the metabolites. The mixture was centrifuged for 10 min at 4°C at 20000×g. After centrifugation, 400 μl supernatant was transferred to a new Eppendorf tube. The mixture was centrifuged for 10 min at 4°C at 20000×g again. Two hundred microliters of supernatant was transferred to a new Eppendorf tube. Then, the process was repeated. Finally, 100 μl supernatant was collected and added to the chromatography (LC) vial. LC/MS analysis was performed by LC-Q-TOF/MS (AB Sciex), and detailed LC-MS parameters are provided in the supporting information.

Principal component analysis (PCA) and partial least squares discriminant analysis (PLS-DA) were applied using SIMCA-P 14.1. According to the PCA algorithm, each point of the PCA score plot represents the summarized information of all the molecules measured in a single sample. Thus, the distance between points indicates the similarity of metabolic components between samples. PLS-DA can be used to elucidate the separation between groups of variables. MetaboAnalyst3.0 (http://www.metaboanalyst.ca/MetaboAnalyst/) was used to perform KEGG enrichment analysis and generate heatmaps, and the Kyoto Encyclopedia of Genes and Genomes (KEGG) (http://www.genome.jp/kegg/ligand.html) was used to search the related metabolic pathways based on the differential metabolites identified.

2.4 Proteomics Analysis

The cold acetone method was used to extract the total proteins. The mouse liver samples (n = 5 for each group) were homogenized in SDS protein lysis buffer (8 M urea, 2% SDS, 1x Protease Inhibitor Cocktail (Roche Ltd. Basel, Switzerland)) by vortex oscillation and passage through a high-throughput tissue grinding machine thrice. The supernatant was collected after centrifugation at 12000 g at 4°C for 20 min. The concentrations of the protein extracts were determined using a BCA Protein Assay Kit. After trypsin digestion (Promega, Madison, WI), the peptide mixture was redissolved in 0.1% TFA and fractionated by high pH separation using a Pierce High pH Reversed-Phase Peptide Fractionation Kit (Product No. 84868, Thermo Fisher Scientific, MA, United States). Finally, eight fractions were collected and combined into six fractions; each fraction was dried in a vacuum concentrator for the next step. Then, nano-HPLC–MS/MS analysis was performed by online nanospray LC–MS/MS on an Orbitrap Exploris™ 480 mass spectrometer (Thermo Fisher Scientific, MA, United States) coupled to an EASY-nanoLC 1200 system (Thermo Fisher Scientific, MA, United States). Spectronaut 13 (Biognosys AG, Switzerland) was used to process and analyze the raw DIA data. Proteins were annotated using the GO, KEGG and COG/KOG databases (http://www.geneontology.org) to obtain their functions. After Student's t test, proteins with a Q value < 0.05 and absolute AVG log2 ratio > 0.58 were filtered as differentially expressed proteins.

2.5 Transcriptomics Analysis

Global mRNA was extracted with TRIzol from the mouse liver samples (n = 5 for each group) of the control, IV and IG groups. The input material for the RNA sample preparations was a total amount of 2 μg RNA per sample. Sequencing libraries were generated using the NEBNext® Ultra™ RNA Library Prep Kit for Illumina® (#E7530L, NEB, United States) according to the manufacturer's instructions, and index codes were added to attribute sequences to each sample. Briefly, the mRNA was purified from total RNA by poly-T oligo-attached magnetic beads. Fragmentation was performed using divalent cations under elevated temperature in NEBNext First Strand Synthesis Reaction Buffer (5X). First strand cDNA was synthesized using random hexamer primers and RNase H. Second strand cDNA

synthesis was subsequently performed using buffer, dNTPs, DNA polymerase I and RNase H. The library fragment was purified with QiaQuick PCR kits and eluted with EB buffer. Then, terminal repair, A-tailing and adapter addition were implemented. The target products were retrieved, and PCR was performed. Finally, the library was completed. A Qubit® RNA Assay Kit in Qubit® 3.0 was used to measure the RNA concentration of the library to preliminarily quantify and then dilute the sample to 1 ng/μl. An Agilent Bioanalyzer 2100 system (Agilent Technologies, CA, United States) was used to assess insert size, and a StepOnePlus™ Real-Time PCR System (valid library concentration>10 nM) was used to qualify accurate quantification of insert size. Clustering of the index-coded samples was performed on a cBot cluster generation system by HiSeq PE Cluster Kit v4-cBot-HS (Illumina) following the manufacturer's recommendations. After cluster generation, 150-bp paired-end reads were generated by running a double-ended sequencing program (PE) on the HiSeq sequencing platform. The ENSEMBL database (http://www.ensembl.org/index.html) was used to obtain the reference genomes and the annotation file. HiSeq was used to count each gene in each sample. Genes with a Q value < 0.05 and absolute AVG log2 ratio > 1 were identified as significantly expressed genes.

2.6 Biochemical Analysis

Serum biochemistry analyses of alanine aminotransferase (ALT), aspartate aminotransferase (AST), alkaline phosphatase (ALP), albumin (ALB), blood urea nitrogen (BUN), creatinine (CREA) and dehydrogenase (LDH) were performed by Zhongda Hospital Southeast University (Nanjing, China) (n = 8 for each group).

2.7 Quantitative RT–PCR

Total RNA was isolated from mouse liver samples (n = 8 for each group) using TRI Reagent (Sigma, Nanjing). The mRNA concentrations were quantified using a NanoDrop ND-1000 spectrophotometer (Thermo Scientific, Nanjing). The diluted mRNA (0.5 μg/μl) was reverse-transcribed according to the manufacturer's protocol (Takara Biomedicals, Nanjing), and the gene expression levels were determined by SYBR-green-based real-time-PCR (ABI ViiA 7 Real-time PCR system, Applied Biosystems, United States). β-actin and GAPDH mRNA levels were used for internal normalization. The sequences of TNF-a, IL-6 and IL-1β primers used for qRT–PCR in our study are listed in **Supplementary Table S4**.

2.8 Histological Analysis

Liver samples (n = 3) were fixed in formalin for 24 h. Then, the fixed samples were embedded in paraffin and sectioned for histopathology analyses with hematoxylin and eosin (H&E) staining.

2.9 Data Analysis and Statistical Analysis

The results are presented as the means ± standard deviation (SD). Statistical analysis was performed by GraphPad Prism 7.0 (GraphPad, San Diego, CA, United States). Unpaired Student's t-test and one-way ANOVA with Tukey's correction were used as appropriate. A p value < 0.05 was considered statistically significant for all data.

3 RESULTS

3.1 Physicochemical Properties of the Mesoporous Silica Nanoparticles

Preliminary analysis of the physicochemical properties of the mesoporous silicon nanoparticles was performed using scanning electron microscopy (SEM), transmission electron microscopy (TEM) and nitrogen adsorption-desorption analysis. As shown in the SEM image in **Supplementary Figure S1A**, the morphology of the MSNs was approximately spherical, and the MSNs exhibited good monodispersity and a uniform particle diameter at approximately 80 nm. **Supplementary Figure S1B** shows that the materials have worm-like mesostructured. The measured BET specific surface area of the MSNs was 751.193 m^2/g. The average pore size and pore volume determined by the Barrett–Joyner–Halenda method were 2.76 nm and 0.746 cc/g, respectively (**Supplementary Figures S1C,D**).

3.2 Biochemical, Histopathological and Inflammatory Factors Indicate Hepatic Injury due to Intravenous or Oral Administration of Mesoporous Silica Nanoparticles

After oral administration or intravenous injection of MSNs for 10 days, the ALT and AST levels were measured to assess hepatic injury. As shown in **Supplementary Figures S1A, S2**, compared with the control group, oral administration significantly reduced AST, BUN and LDH activities, but these activities were within the normal range. Intravenous injection significantly elevated ALT activities and decreased ALP activities beyond the normal range and downregulated BUN within the normal range. The ALB and CREA concentrations were not changed in the IG and IV groups compared with the control group. Moreover, the mRNA expression of inflammatory cytokines, including IL-1β, IL-6 and TNFα, was measured in the liver tissues of mice. All IL-1β, IL-6 and TNFα expression levels were significantly upregulated in the IV group, and IL-1β and IL-6 expression levels were increased in the IG group compared with the control group (**Figure 1B**). In addition, representative pathological micrographs of the liver tissue sections are presented (**Figure 1C**). HE staining pathological images did not show obvious inflammatory cells in the IG group, whereas spotty necrosis accompanied by inflammatory cell infiltration was observed in the IV group (red arrow). Overall, these results indicated that oral administration of MSNs induced a proinflammatory response in the liver and that intravenous injection of MSNs induced significant hepatic injury in mice.

3.3 Metabolomics Reveals Metabolic Perturbation in Mouse Liver Exposed to Mesoporous Silica Nanoparticles Administered via the Intravenous or Oral Route

The metabolomics profiles of the liver samples were analyzed based on a PCA score plot (**Figure 2A**). The control and IV groups were obviously separated in the PCA score plot, and the

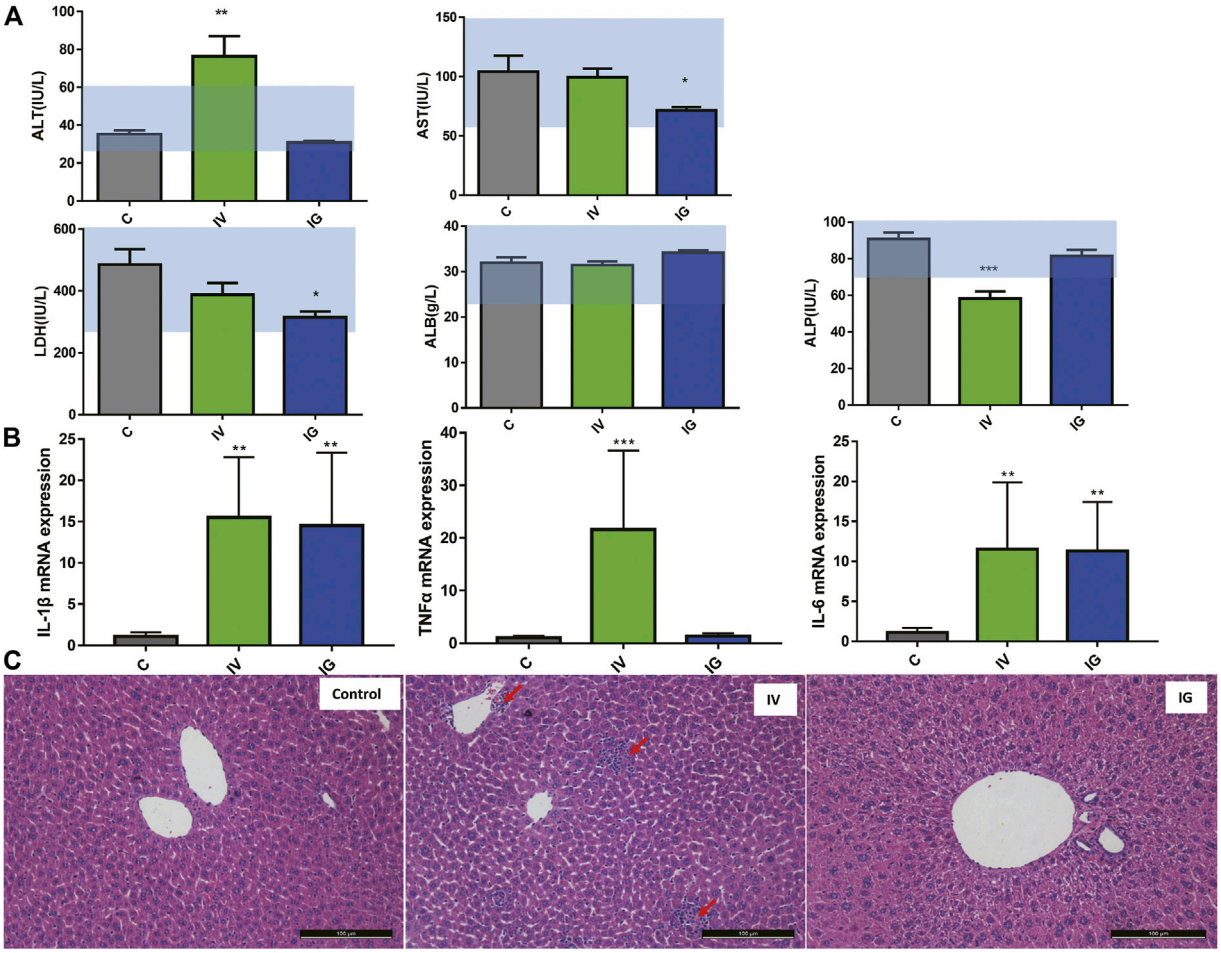

FIGURE 1 | (A) Effect of different exposure methods (IV and IG) on serum biochemistry, including ALT, AST, ALP, LDH and ALB. Light blue bars indicate the range of values obtained from healthy ICR mice. **(B)** IL-1b, TNFa and IL-6 mRNA expression in mouse liver. **(C)** Histological examination of liver from the mouse of control group, IV and IG group, red arrow: inflammation site. The data are expressed as the mean ± SD, $*p < 0.05$, $**p < 0.01$, and $***p < 0.001$ compared with the control.

control with IG groups exhibited slight separation. Additionally, a three-component PLS-DA model was constructed (**Figure 2B**). The PLS-DA score plot revealed the goodness of fit and high predictability of the model, demonstrating good separation between the IV group and the control group as well as the IG group and the control group. These PCA and PLS-DA score plot results suggested that intravenous injection with MSNs exhibited remarkable differences and dramatic metabolic disturbances compared to the control group or IG group.

In total, compared to the control group, 18 differentially metabolites was involved in carbohydrate metabolism, 21 differentially was metabolites involved in amino acid and derivative metabolism, 23 differentially metabolites was involved in purine and pyrimidine nucleotide metabolism, 4 differentially metabolites was associated with fatty acid and ketone bodies, 8 differentially metabolites was involved in vitamin and GSH metabolism, and 8 differentially metabolites of others were identified (**Supplementary Table S1**). Based on KEGG enrichment pathway analysis (**Figures 2C,D**), the main perturbed metabolic pathways we focused on included the tricarboxylic acid (TCA) cycle, glycolysis, nicotinamide and glutathione metabolism, pentose phosphate pathway (PPP), amino acid metabolism, and purine and pyrimidine nucleotide metabolism.

3.4 Correlation Analysis of Transcriptomic and Proteomic Data in Mouse Liver Upon Exposure to Mesoporous Silica Nanoparticles by Intravenous or Oral Administration

The proteomics and transcriptomics profiles from the liver samples in different groups (control, IV and IG) were evaluated using PCA and PLS-DA score plots. Proteomics and transcriptomics analyses yielded similar PCA and PLS-DA score plots. The IV group was located far from the control group, and the control group was not separated from the IG group in contrast to that observed in the PCA score plot (**Figures 3A,C**). These results indicated that intravenous injection with MSNs was significantly different from the control and IG groups. It was difficult to distinguish between the control group and IG group.

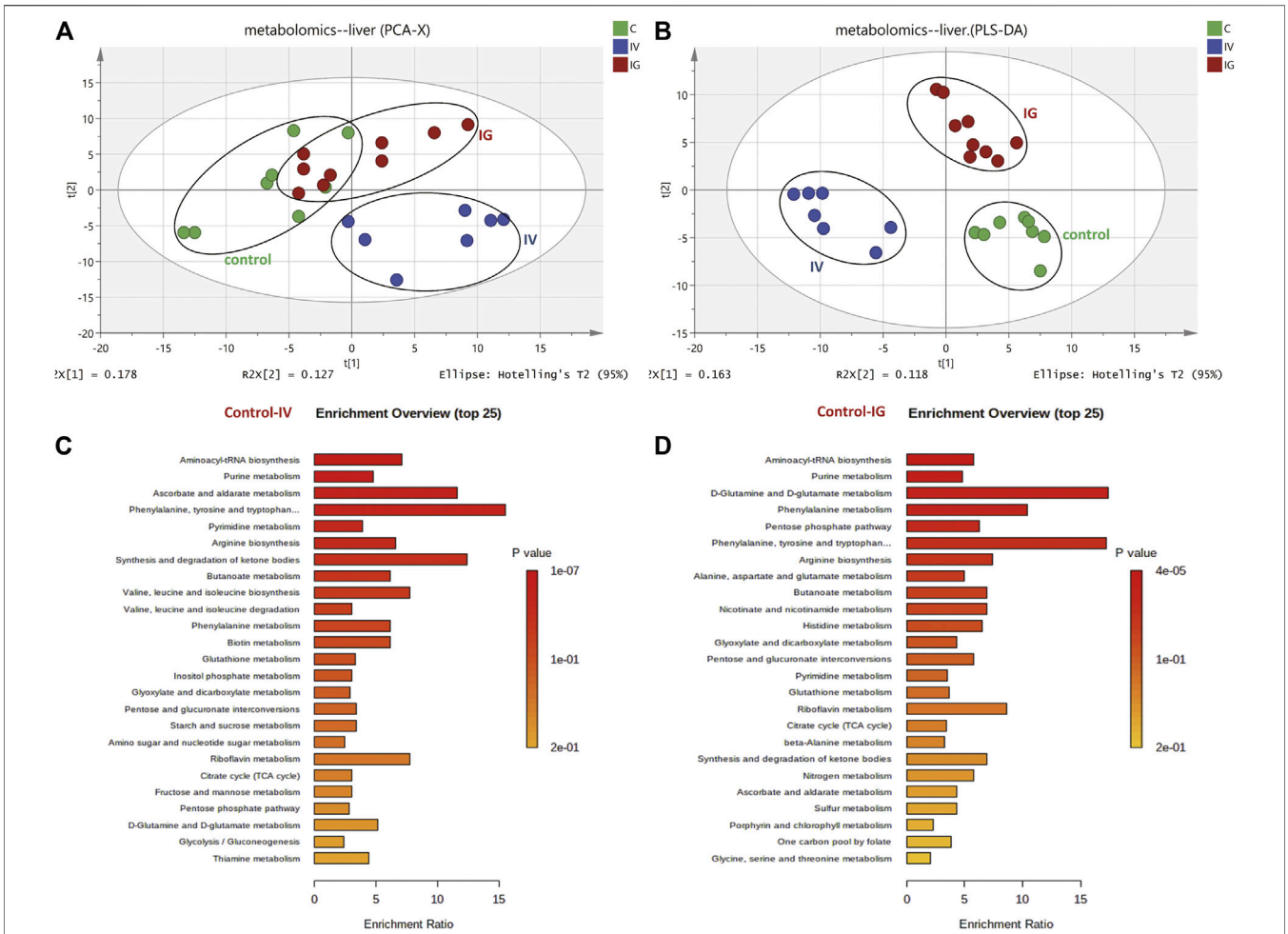

FIGURE 2 | Effect of Mesoporous Silica Nanoparticles (MSNs) on mouse liver metabolites by different exposure methods (IV and IG) using HPLC–MS and GC–MS. **(A)** Principal component analysis (PCA) scoring maps of metabolites. **(B)** Partial least squares discriminant analysis (PLS-DA) scoring maps of metabolites. **(C)** KEGG metabolic pathway of the liver samples between the control and IV groups. **(D)** KEGG metabolic pathway of the liver samples between the control and IG groups.

PLS-DA presented good separation between the IV group, IG group and control group (**Figures 3B,D**).

A total of 8,190 proteins and 27,185 expressed genes were identified (**Supplementary Figure S3**). Upon oral administration of MSNs, 2 differentially expressed proteins and 42 differentially expressed genes were identified compared to the control group. Of these, 1 protein and 8 genes were upregulated, and 1 protein and 34 genes were downregulated. No overlap was noted between the regulated proteins and genes. Under intravenous injection with MSNs, 1,509 differentially expressed proteins and 1,376 differentially expressed genes were identified compared to the control group. Of these, 1,609 proteins and 1,250 genes were upregulated, and 781 proteins and 126 genes were downregulated. In total, 175 identical upregulations and 15 downregulations were noted between proteins and genes (**Figure 3E**, **Supplementary Table S2**). The 2 differentially expressed proteins in the IG group compared with the control group were Cyp2c39 and Plin2, whereas Cyp2c39 and Plin2 genes were not differentially regulated (**Supplementary Table S3**). KEGG pathway analysis was used to analyze the significant proteins and genes noted between the IV group and control group. Based on KEGG enrichment pathway analysis, we focused on metabolic pathways and inflammation (**Figure 3F**).

3.5 Energy Metabolism and Oxidative Phosphorylation

The mitochondrion is a very important subcellular organelle given its role ROS and energy metabolism. **Figure 4** shows that the levels of proteins of respiratory chain complexes I, II, III, IV and V of mitochondrion were obviously decreased and the levels of proteins of V-type proton ATPase of lysosomes were increased in the IV group compared with the control group. However, the IG group exhibited no changes in mitochondrial proteins. The mRNA expression levels of respiratory chain complexes were not significantly altered in the IV group and IG group compared with the control group.

Lactate levels were significantly decreased in the IV group compared with the control group. In addition, the levels of 3-

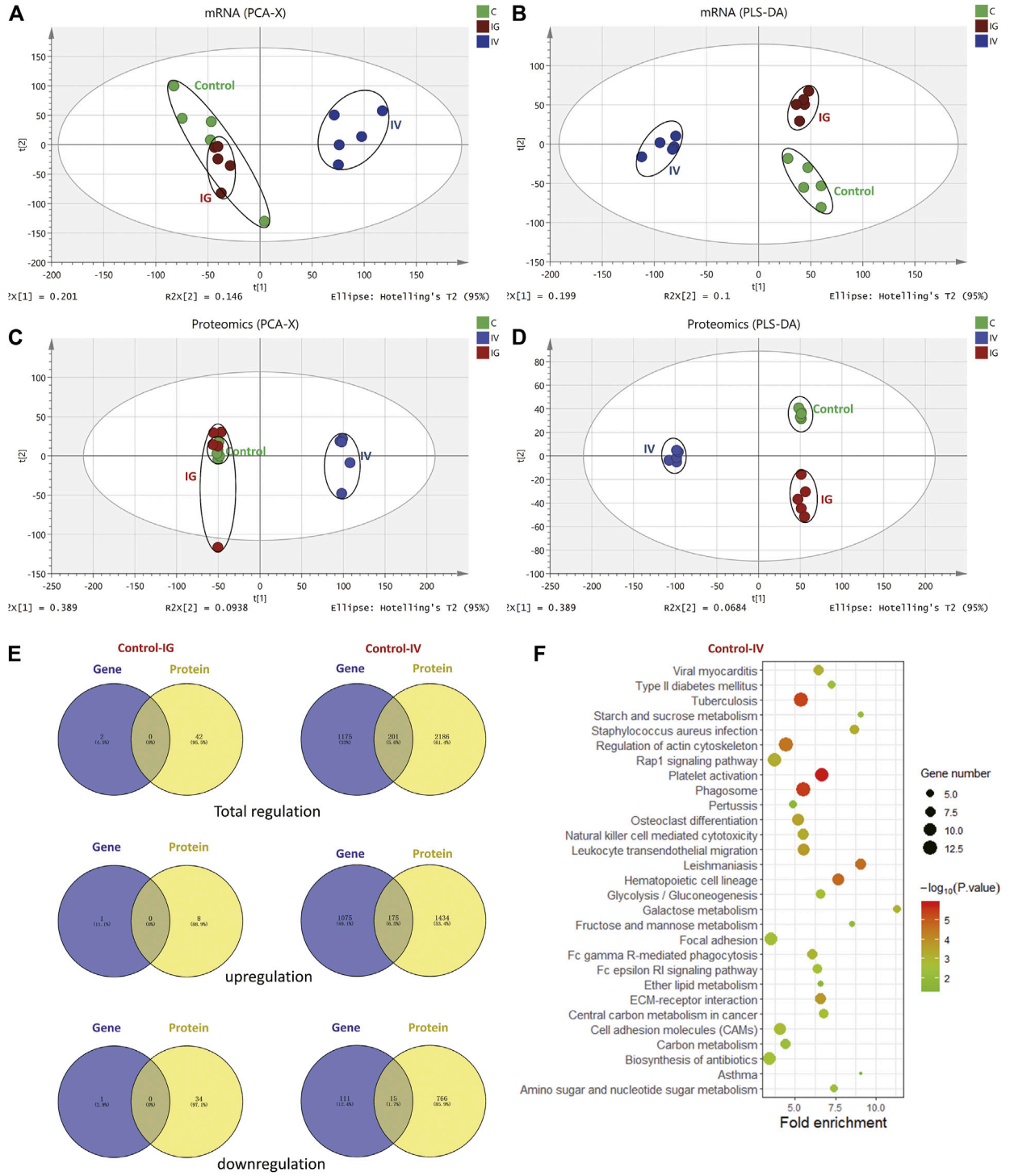

FIGURE 3 | Effect of Mesoporous Silica Nanoparticles (MSNs) administered by different routes (IV and IG) on mouse liver proteins and genes as determined by proteomics and transcriptomics. **(A)** PCA, **(B)** PLS-DA of transcriptomics, **(C)** PCA, **(D)** PLS-DA of proteomics. **(E)** Venn diagrams depict overlapping proteomics and transcriptomics data. The left panel shows the regulation of genes and proteins in the IG group compared with the control group. The right panel shows the regulation of genes and proteins in the IV group compared with the control group. **(F)** KEGG pathway analysis revealed the top 20 pathways based on the same regulation of proteins and genes between the control and IV groups.

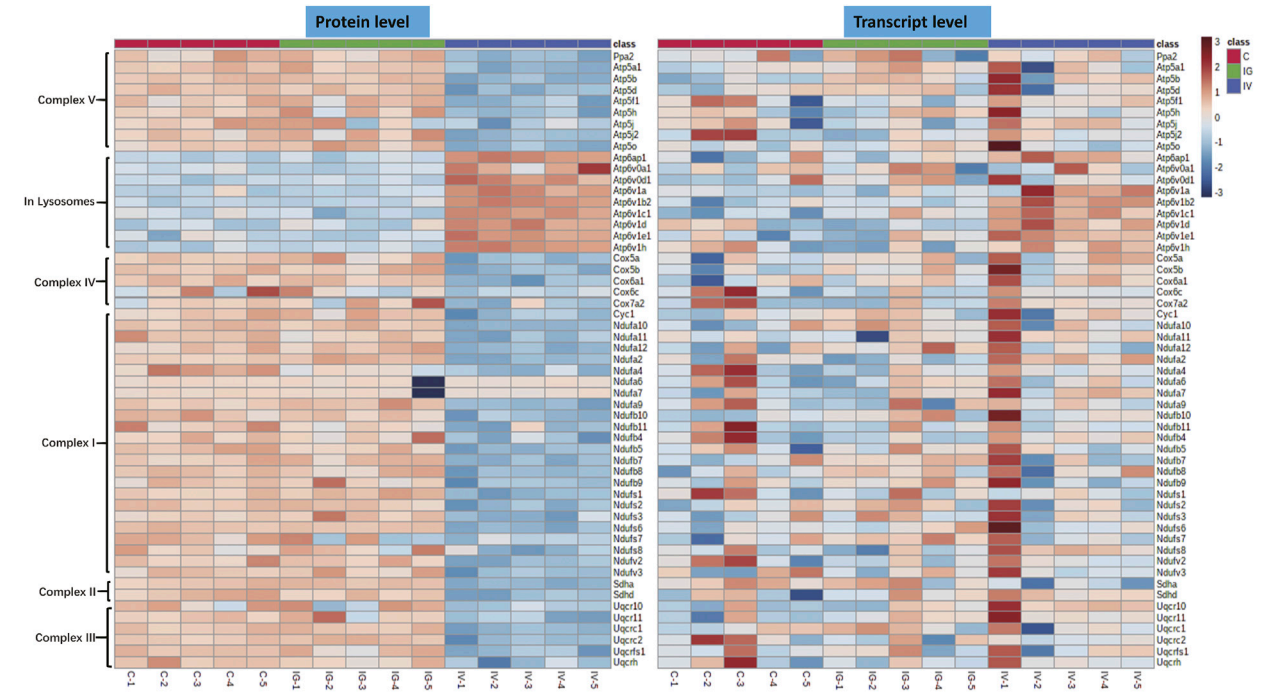

FIGURE 4 | Effect of Mesoporous Silica Nanoparticles (MSNs) administered by different routes (IV and IG) on mitochondrial oxidative phosphorylation complexes. Heatmaps of genes and proteins involved in respiratory chain complexes I, II, III, IV and V of mitochondria and V-type proton ATPase of lysosomes.

phosphoglyceric acid (3-PGA), fructose 1,6-bisphosphate (F1,6P), aconitate, alpha-ketoglutarate (a-KG), succinate, oxaloacetic acid, fumarate and malate were significantly increased in the IV group, and aconitate level was significantly increased in the IG group compared with the control group (**Figure 5A**, **Supplementary Figure S1**). The heatmaps in **Figures 5B,D** display the expression changes in the metabolite, protein and transcript levels of carbohydrates of the TCA cycle and glycolysis. These results showed significant differences between the IV group and the control group. Proteins and genes involved in energy metabolism, including hexokinase (HK), 6-phosphofructokinase 1 (PFK) and pyruvate kinase (PK), were upregulated (**Figure 5A**, **Supplementary Figure S2**). The data demonstrated that intravenous injection altered TCA cycle and glycolysis, whereas oral administration had minimal effects.

3.6 Antioxidant Pathway

The antioxidant pathway in the mouse liver was significantly affected by oral administration or intravenous injection of MSNs. The PPP, glutathione, NADPH biosynthesis pathways and SOD3 reduce ROS to maintain redox equilibrium. We found significant upregulation of serine, glycine, 6-phosphogluconate, biotin, thiamine, FAD, NAD+, NADPH, NADP+ and oxidized glutathione and downregulation of folate in the IV group compared with the control group. The levels of serine, glycine, 6-phosphogluconate, ribose 5-phosphate, dihydrofolic acid, FAD, NAD+ and oxidized glutathione were significantly increased, and NADPH and GSH/GSSG levels were downregulated in the IG group compared with the control group (**Figures 6A–D**, **Supplementary Table S1**). The heatmaps in **Figures 6E,F** display the expression changes in the metabolite, protein and transcript levels associated with PPP, glutathione and NADPH metabolism. These results revealed significant differences between the IV group and the control group. The upregulated glutathione and NADPH metabolism proteins and genes included CD38, glutathione peroxidase (GPX) and glutathione S-transferase (GST) (**Figures 6A–D**, **Supplementary Table S2**).

3.7 Purine and Pyrimidine Metabolism and Biosynthesis

A number of purine and pyrimidine nucleotides were aberrantly altered in mice treated with MSNs orally administered or intravenously injected via the tail vein. For instance, compared with the control group, the levels of GMP, IMP, ITP, UDP, ATP, ADP, dGTP, dGDP, guanine, xanthine, xanthosine, cytidine and deoxyuridine were notably increased, and the levels of dUMP, hypoxanthine, thymine, deoxyadenosine, GTP, inosine and adenosine were significantly reduced in the IV group. However, the levels of IMP, ITP, UTP, ADP, dUMP, guanosine, inosine and hypoxanthine were significantly increased in the IG group compared to the control group (**Figure 7D**, **Supplementary Table S1**). The heatmaps in **Figures 7C,E** display the expression changes in the metabolite, protein and transcript levels of nucleotides and nucleosides. These results revealed significant differences between the IV group and the control group. Numerous proteins and genes associated with purine and pyrimidine nucleotides were

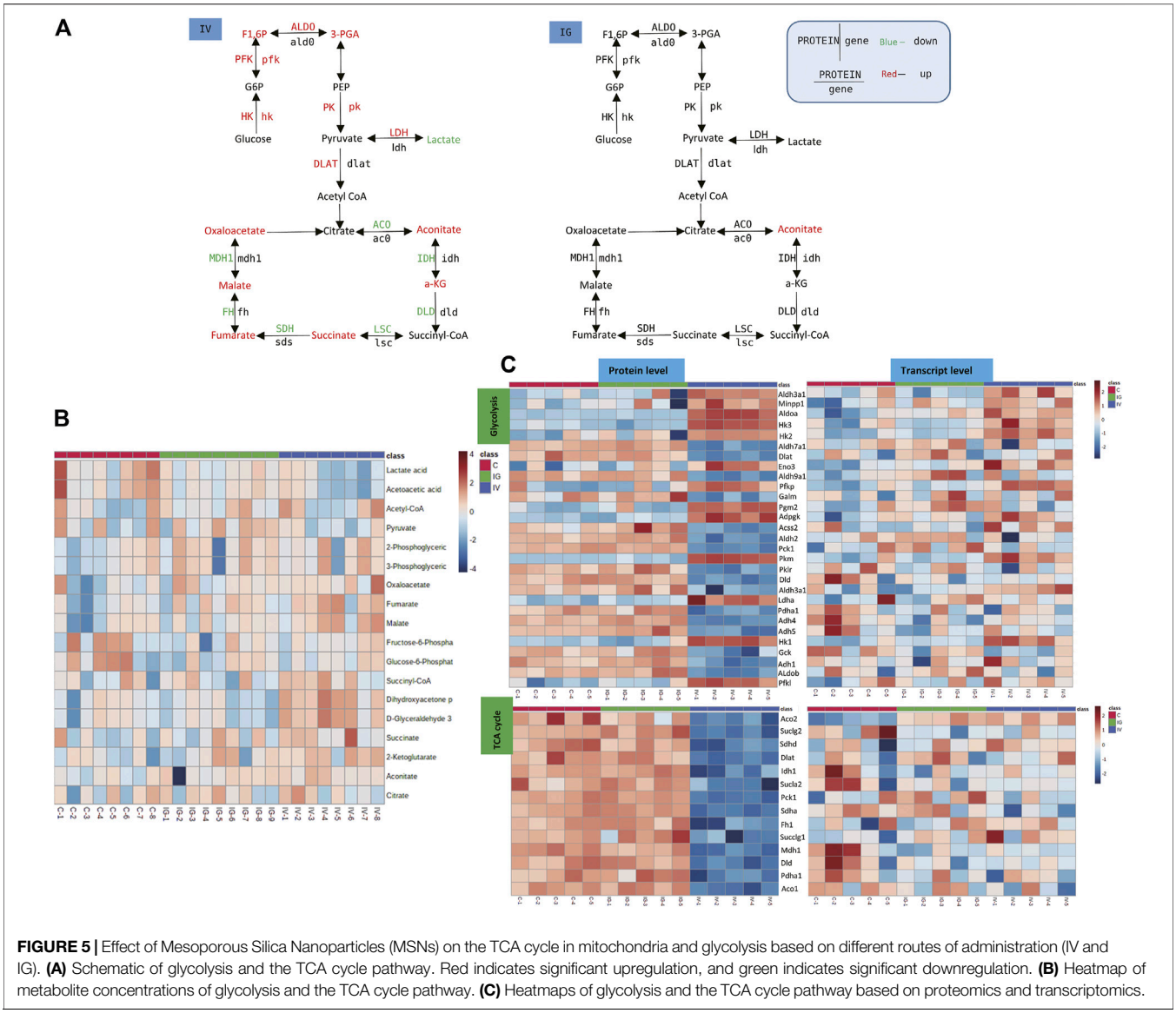

FIGURE 5 | Effect of Mesoporous Silica Nanoparticles (MSNs) on the TCA cycle in mitochondria and glycolysis based on different routes of administration (IV and IG). **(A)** Schematic of glycolysis and the TCA cycle pathway. Red indicates significant upregulation, and green indicates significant downregulation. **(B)** Heatmap of metabolite concentrations of glycolysis and the TCA cycle pathway. **(C)** Heatmaps of glycolysis and the TCA cycle pathway based on proteomics and transcriptomics.

upregulated: 3′,5′-cyclic-nucleotide phosphodiesterase (PDE), adenylate kinase (AK), ribonucleoside-diphosphate reductase subunit M2 (RRM2), adenosine triphosphatase (ENTDP2) and uridine phosphorylase (UPP) (**Figures 7A,B**).

4 DISCUSSION

Our data showed that intravenous injection of MSNs caused significant changes in parameters related to liver function, histopathological sections, and biological system results based on metabolomics, genomics, and proteomics. We observed obvious injury to the liver, upregulation of inflammatory factors of the liver and induced glycolysis, the tricarboxylic acid cycle, and oxidative phosphorylation related to mitochondrial energy metabolism, enhanced succinic acid and glutathione synthesis associated with inflammation and oxidative stress, and an abnormal PPP activity for nucleic acid synthesis. Oral administration of MSNs also increased levels of inflammatory factors and altered metabolomics, transcriptomics and proteomics profiles. However, the effect was significantly weaker than that of intravenous administration, even though the dose was much higher than that of intravenous injection. After intravenous injection, all the particles directly enter the systemic circulation and are more likely to accumulate in the liver and thus cause liver damage (Cho et al., 2009; Geraets et al., 2014; Elgrabli et al., 2015). However, after oral administration, most of the particles gather in the gut, and only a small amount of these particles enter the liver via the hepatic portal vein and then systemic circulation. We presume it is the key reason why liver function was affected by oral particles, but the effect was weaker than that of intravenous injection. In support of this hypothesis, a previous study showed that liver tissue is highly exposed to these refractory particles after

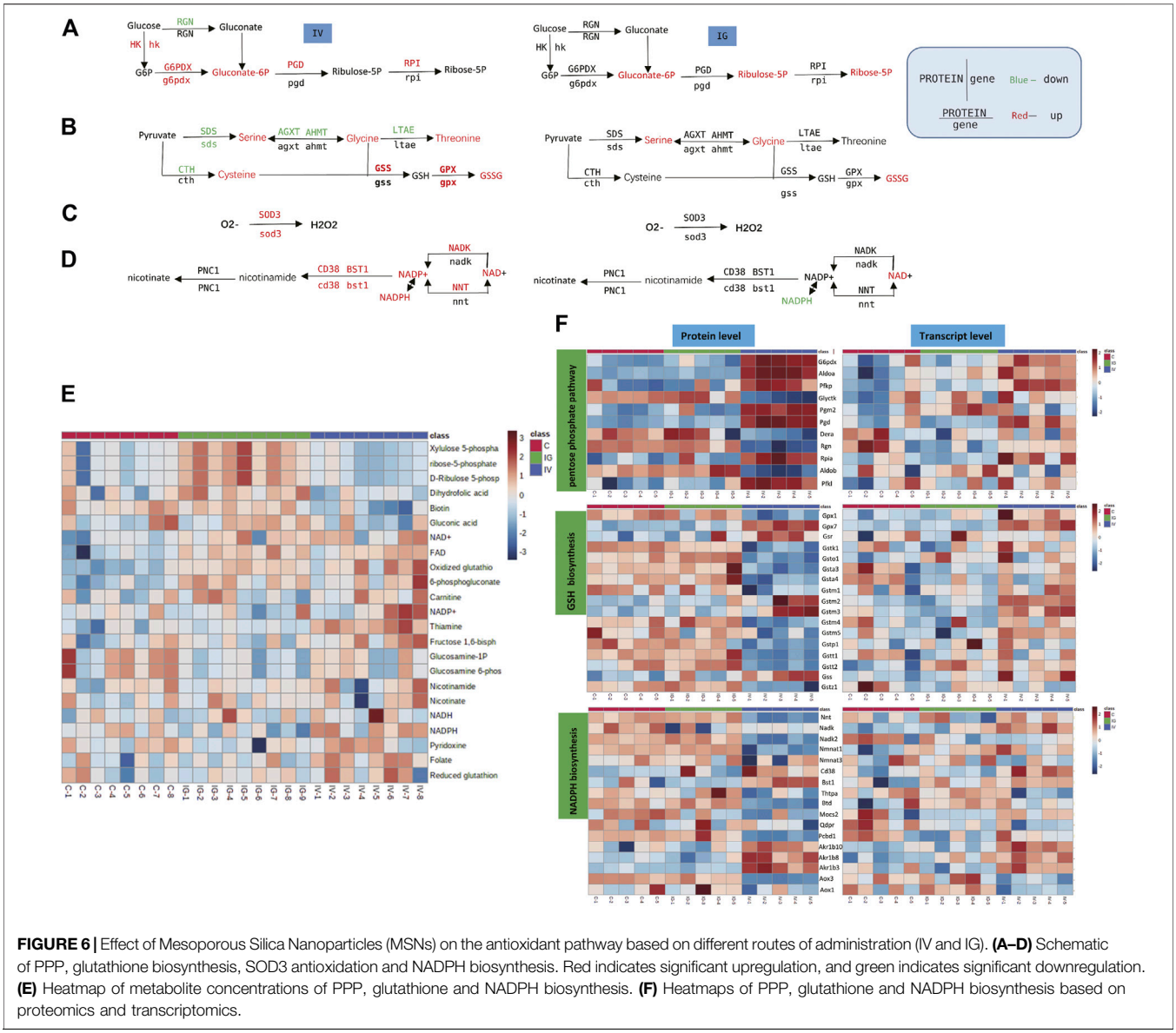

FIGURE 6 | Effect of Mesoporous Silica Nanoparticles (MSNs) on the antioxidant pathway based on different routes of administration (IV and IG). **(A–D)** Schematic of PPP, glutathione biosynthesis, SOD3 antioxidation and NADPH biosynthesis. Red indicates significant upregulation, and green indicates significant downregulation. **(E)** Heatmap of metabolite concentrations of PPP, glutathione and NADPH biosynthesis. **(F)** Heatmaps of PPP, glutathione and NADPH biosynthesis based on proteomics and transcriptomics.

injection, and liver tissue is also exposed to these particles after oral administration (Cho et al., 2009; Geraets et al., 2014; Elgrabli et al., 2015). Consistently, a number of studies (Yu et al., 2012; Dogra et al., 2018) have reported that the particle exposure level in liver tissue increased significantly after oral administration of MSNs, suggesting that oral nanoparticles can be absorbed into the liver through the intestine and ultimately affect liver tissue.

Based on systematic biological proteomics, transcriptome and metabolomics data, the effects of intravenous and gavage administration on liver tissues were evaluated. We observed that MSN administration, especially intravenous administration, significantly affects the metabolism of small molecules, proteins and genes in the liver. Transcriptomics and proteomics revealed a mutual and consistent effect of MSNs on GPX, SOD3 and G6PD genes/proteins related to oxidative stress; HK and PFK genes/proteins related to glycolysis; and UUP, AK and RRM2 genes/proteins related to nucleic acid synthesis. These results suggest that liver injury is closely related to the nucleic acid synthesis pathway, oxidative stress, glycolysis and mitochondrial energy metabolism. The metabolomics results showed significant changes in many metabolites involved in metabolism, and these results are consistent with the results of transcriptomics and proteomics studies. For example, the perturbed metabolites GSSG, NADPH, NADP+, succinic acid and hypoxanthine are closely related to oxidative stress as uncovered by transcriptomic and proteomic data. IMP, UDP, and GMP are key metabolites involved in nucleic acid synthesis. In addition, the TCA intermediates, F1,6P and 3-PGA are important in glycolysis/mitochondrial energy metabolism. The integrated analysis of proteomic, transcriptomic and metabolomics data suggested consistent effects of MSNs on key metabolic pathways, especially the

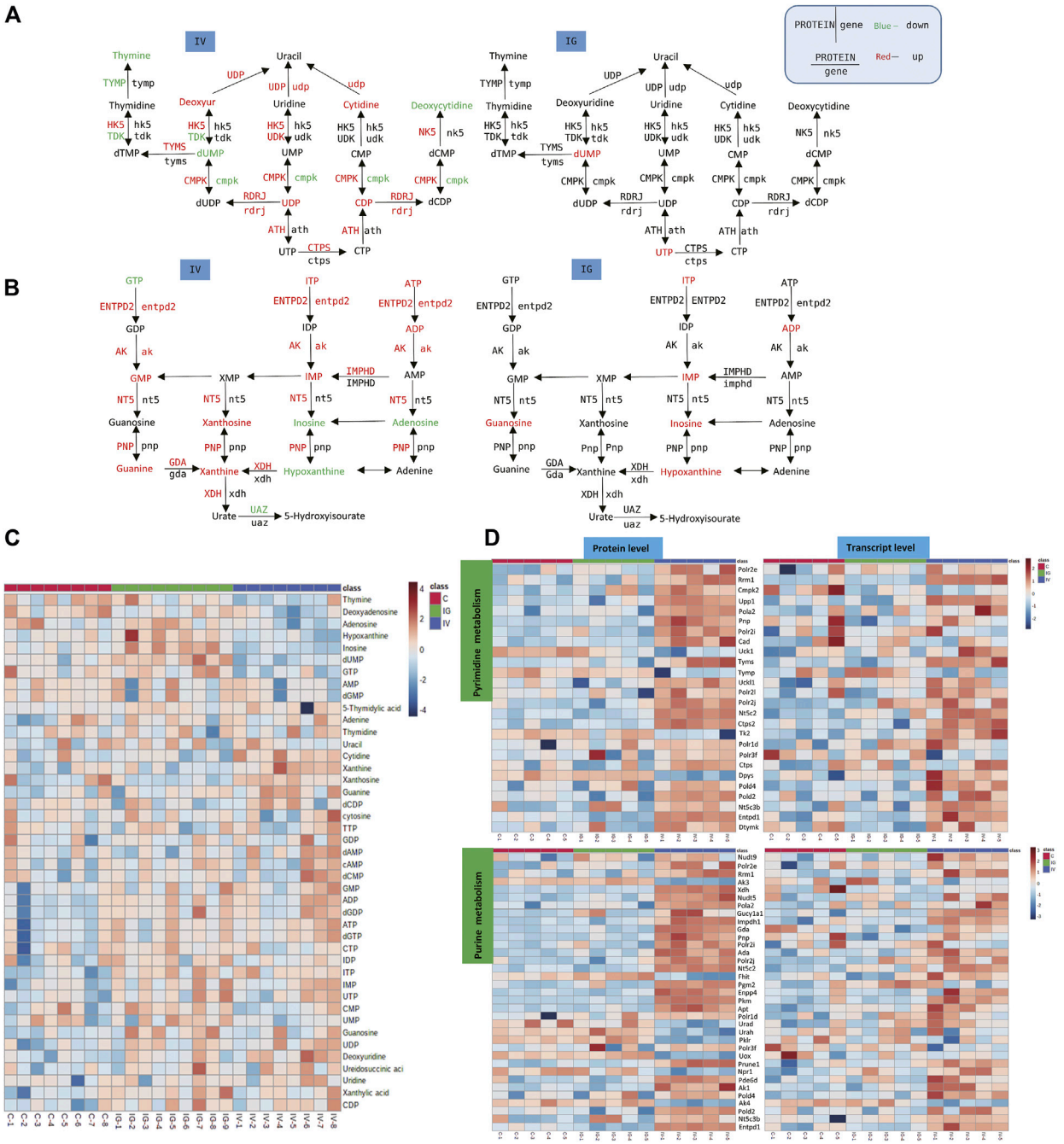

FIGURE 7 | Effect of Mesoporous Silica Nanoparticles (MSNs) on purine and pyrimidine nucleotides based on different routes of administration (IV and IG). **(A, B)** Schematic of purine and pyrimidine nucleotide metabolism; red indicates significant upregulation, and green indicates significant downregulation. **(C)** Heatmap of concentrations of metabolites of purine and pyrimidine nucleotide metabolism. **(D)** Heatmaps of purine and pyrimidine nucleotide metabolism based on proteomics and transcriptomics.

nucleic acid synthesis pathway, oxidative stress, and glycolysis/mitochondrial energy metabolism in the liver.

To our surprise, transcriptions and proteins analysis indicated inconsistent data, i.e., the expression at protein level showed regularly consistent within each group, and distinctly different from the other groups, while the expression at transcription level did not. Usually, the expression at transcription and protein levels matches well with each other, and with the activities, for examples, the mRNA and protein expression levels of isocitrate dehydrogenase, succinate dehydrogenase, malate dehydrogenase and other enzymes in the respiratory chain

complex protein and TCA cycle are consistent. However, occasionally, the correlations don't match between mRNA expression level and protein level in microorganism and mammalian (Gygi et al., 1999; Maier et al., 2009; Rossignol et al., 2009; Schwanhüusser et al., 2011; Liu et al., 2016). Although the underlying mechanism is not well understood, data suggested that ROS and/or oxidative stress was involved in their diverse effect on mRNA and protein expression levels. For an example, Song et al. (2022) reported that, due to the time lag effect in protein modification, gene transcription and translation, the expressions of SOD and GPX subtype genes did not change in accordance with those at protein levels. It was presumed that the oxidative stress or altered ROS level perturbed mRNA translation efficiency, and also affected protein degradation rates and the folding and modification efficiency of proteins, e.g., in mitochondria and nucleus (Tan et al., 2017; Latonen et al., 2018; Sun et al., 2019). In this study, we observed a significant oxidative stress in liver, indicating that the inconsistency of expression at mRNA and protein levels was involved in oxidative stress induced by MSNs.

Mitochondria are the primary site of cellular energy production, and the TCA cycle is the main pathway responsible for energy generation. The liver is not only the material transformation center of the body but also a center with intensive energy loading (Akram, 2014; Panieri and Santoro, 2016). Our data showed that after MSN injection, mitochondrial respiratory chain protein complexes I, II, III, IV and V decreased. In addition, oxidative phosphorylation was reduced, and circulating TCA intermediates generally increased. These results suggest that TCA metabolism was affected and ATP production decreased. To compensate for the loss caused by reduced energy production, cells generally tend to upregulate glycolysis. Therefore, the F1,6P and 3PGA metabolites as well as HK, PFK, PK genes and proteins in the glycolysis pathway were upregulated. On the other hand, nanoparticles typically induce oxidative stress and mitochondrial dysfunction (Li et al., 2016; Lim et al., 2019; Sun et al., 2019). To alleviate mitochondrial damage, the downregulation of the mitochondrial respiratory chain was observed and characterized by reduced mitochondrial respiratory chain protein complexes I, II, III, IV and V, including TCA metabolism. Because the production of ROS greatly contributes to oxidative stress and inflammatory factors (Hur and Gray, 2011; Nishijima et al., 2017; Snezhkina et al., 2020), the elevation of inflammatory factors indicates that MSN-induced inflammation occurs independently of ROS levels. Previous studies have shown that the accumulation of succinic acid, an intermediate substance in the TCA cycle, can stimulate inflammation and induce upregulation of inflammatory factors (Tannahill et al., 2013). Metabolomics data showed that MSNs injection led to a significant increase in succinic acid, indicating that it is related to inflammation and inflammatory factors (Lim et al., 2019; Mohamed et al., 2020). Moreover, liver injury triggers the repair and regeneration of liver cells. Therefore, metabolic pathway analysis showed an enhanced PPP pathway in the liver, which is primarily responsible for increased synthesis of nucleic acids for the construction of genetic materials. Compared with intravenous injection, intragastric administration of MSNs did not induce abnormalities in mitochondrial function; however, distinct changes in antioxidant pathways, such as glutathione synthesis and PPP, and the key metabolites of hypoxanthine and NADPH synthesis were noted. In general, the milder effects of oral administration on metabolism and metabolic pathways can be attributed to the reduced amount of particles entering the liver compared with that observed with intravenous injection.

The literature (Lu et al., 2010; Yu et al., 2012; Fu et al., 2013; Isoda et al., 2013; Hassankhani et al., 2015; Chatterjee et al., 2016; Abdelhalim et al., 2018; Li et al., 2018; Abdel-Latif et al., 2021; Sun et al., 2021) and our previous studies (Lu et al., 2010; Yu et al., 2012; Fu et al., 2013; Isoda et al., 2013; Hassankhani et al., 2015; Chatterjee et al., 2016; Abdelhalim et al., 2018; Li et al., 2018; Abdel-Latif et al., 2021; Sun et al., 2021) have shown that silica particles with particle sizes of 10–1000 nm cause significant damage to the liver, whereas particles with sizes greater than 100 nm cause significant damage to the kidney. To study the effect of particles on the liver, we selected MSNs with an average particle size of 80 nm with a normal particle size distribution. Our data showed that MSNs have a significant impact on liver tissue morphology, cell function and metabolism. This study focuses on nondegradable particles, so their effects on the function and metabolism of the liver cannot be directly extrapolated to degradable particles. Considering that undegradable and degradable particles have different dynamic fates *in vivo*, the influence of degradable particles on tissues and organs, especially liver tissue, needs to be further studied and clarified.

5 CONCLUSION

Intravenous injection of MSNs induced inflammation, and significant liver toxicity was noted. Based on metabolomics, proteomics and transcriptomics analyses, this systematic biological study suggested perturbed mitochondrial energy metabolism of the TCA, oxidative phosphorylation and glycolysis and stimulated oxidative stress involved in the synthesis of the glutathione pathway and nucleotides via the PPP. Oral administration of MSNs did not induce distinct hepatic injury but did stimulate inflammatory factors and affected metabolic pathways involved in the PPP, glutathione synthesis and oxidative stress albeit to a lesser extent than intravenous injection, even at much higher doses. The data suggested that intravenous injection of nanoparticles of pharmaceutical excipients substantially affected hepatic function and metabolism and induced oxidative stress in the liver.

DATA AVAILABILITY STATEMENT

The datasets presented in this study can be found in online repositories. The names of the repository/repositories and

accession number(s) can be found below: mass spectrometry proteomics data have been deposited to the ProteomeXchange Consortium via the PRIDE partner repository with the dataset identifier PXD030757 and transcriptomics data can be found here: National Center for Biotechnology Information (NCBI) BioProject database under accession numbers PRJNA794322.

ETHICS STATEMENT

The animal study was reviewed and approved by the Institutional Review Board of Animal Ethics Committee of China Pharmaceutical University.

AUTHOR CONTRIBUTIONS

Conceptualization, JL, HX, and GW software, JL and RS; validation, GW and HX; formal analysis, JL and RS; investigation, JL and RS; resources, GW and HX; data curation, JL; writing—original draft preparation, JL; writing—review and editing, HX; project administration, GW and HX; funding acquisition, GW and HX.

SUPPLEMENTARY MATERIAL

The Supplementary Material for this article can be found online at: https://www.frontiersin.org/articles/10.3389/fphar.2022.835359/full#supplementary-material

REFERENCES

Aa, N., Lu, Y., Yu, M., Tang, H., Lu, Z., Sun, R., et al. (2021). Plasma Metabolites Alert Patients with Chest Pain to Occurrence of Myocardial Infarction. *Front. Cardiovasc. Med.* 8, 652746. doi:10.3389/fcvm.2021.652746

Abdelhalim, M. A. K., Moussa, S. A. A., Qaid, H. A., and Al-Ayed, M. S. (2018). Potential Effects of Different Natural Antioxidants on Inflammatory Damage and Oxidative-Mediated Hepatotoxicity Induced by Gold Nanoparticles. *Int. J. Nanomed.* 13, 7931–7938. doi:10.2147/IJN.S171931

Abdel-Latif, H. M. R., Shukry, M., El Euony, O. I., Mohamed Soliman, M., Noreldin, A. E., Ghetas, H. A., et al. (2021). Hazardous Effects of Sio2 Nanoparticles on Liver and Kidney Functions, Histopathology Characteristics, and Transcriptomic Responses in Nile tilapia (*Oreochromis niloticus*) Juveniles. *Biology* 10, 183–219. doi:10.3390/biology10030183

Akram, M. (2014). Citric Acid Cycle and Role of its Intermediates in Metabolism. *Cel. Biochem. Biophys.* 68, 475–478. doi:10.1007/s12013-013-9750-1

Baeza, A., Colilla, M., and Vallet-Regí, M. (2015). Advances in Mesoporous Silica Nanoparticles for Targeted Stimuli-Responsive Drug Delivery. *Expert Opin. Drug Deliv.* 12, 319–337. doi:10.1517/17425247.2014.953051

Birault, A., Giret, S., Théron, C., Gallud, A., Da Silva, A., Durand, D., et al. (2020). Sequential Delivery of Synergistic Drugs by Silica Nanocarriers for Enhanced Tumour Treatment. *J. Mater. Chem. B* 8, 1472–1480. doi:10.1039/c9tb02225b

Chatterjee, N., Yang, J., Atluri, R., Lee, W., Hong, J., and Choi, J. (2016). Amorphous Silica Nanoparticle-Induced Perturbation of Cholesterol Homeostasis as a Function of Surface Area Highlights Safe-By-Design Implementation: an Integrated Multi-OMICS Analysis. *RSC Adv.* 6, 68606–68614. doi:10.1039/C6RA06006D

Chen, Z., Han, S., Zhou, D., Zhou, S., and Jia, G. (2019). Effects of Oral Exposure to Titanium Dioxide Nanoparticles on Gut Microbiota and Gut-Associated Metabolism *In Vivo*. *Nanoscale* 11, 22398–22412. doi:10.1039/c9nr07580a

Chen, Z., Han, S., Zheng, P., Zhou, D., Zhou, S., and Jia, G. (2020). Effect of Oral Exposure to Titanium Dioxide Nanoparticles on Lipid Metabolism in Sprague-Dawley Rats. *Nanoscale* 12, 5973–5986. doi:10.1039/c9nr10947a

Cho, M., Cho, W. S., Choi, M., Kim, S. J., Han, B. S., Kim, S. H., et al. (2009). The Impact of Size on Tissue Distribution and Elimination by Single Intravenous Injection of Silica Nanoparticles. *Toxicol. Lett.* 189, 177–183. doi:10.1016/j.toxlet.2009.04.017

Dogra, P., Adolphi, N. L., Wang, Z., Lin, Y. S., Butler, K. S., Durfee, P. N., et al. (2018). Establishing the Effects of Mesoporous Silica Nanoparticle Properties on *In Vivo* Disposition Using Imaging-Based Pharmacokinetics. *Nat. Commun.* 9, 4551–4564. doi:10.1038/s41467-018-06730-z

Elgrabli, D., Beaudouin, R., Jbilou, N., Floriani, M., Pery, A., Rogerieux, F., et al. (2015). Biodistribution and Clearance of TiO2 Nanoparticles in Rats after Intravenous Injection. *PLoS ONE* 10, e0124490–13. doi:10.1371/journal.pone.0124490

Fu, C., Liu, T., Li, L., Liu, H., Chen, D., and Tang, F. (2013). The Absorption, Distribution, Excretion and Toxicity of Mesoporous Silica Nanoparticles in Mice Following Different Exposure Routes. *Biomaterials* 34, 2565–2575. doi:10.1016/j.biomaterials.2012.12.043

Garbuzenko, O. B., Mainelis, G., Taratula, O., and Minko, T. (2014). Inhalation Treatment of Lung Cancer: the Influence of Composition, Size and Shape of Nanocarriers on Their Lung Accumulation and Retention. *Cancer Biol. Med.* 11, 44–55. doi:10.7497/j.issn.2095-3941.2014.01.004

Geraets, L., Oomen, A. G., Krystek, P., Jacobsen, N. R., Wallin, H., Laurentie, M., et al. (2014). Tissue Distribution and Elimination after Oral and Intravenous Administration of Different Titanium Dioxide Nanoparticles in Rats. *Part. Fibre Toxicol.* 11, 30–21. doi:10.1186/1743-8977-11-30

Griese, M. (1999). Pulmonary Surfactant in Health and Human Lung Diseases: State of the Art. *Eur. Respir. J.* 13, 1455–1476. doi:10.1183/09031936.99.13614779

Gygi, S. P., Rochon, Y., Franza, B. R., and Aebersold, R. (1999). Correlation between Protein and mRNA Abundance in Yeast. *Mol. Cel. Biol.* 19, 1720–1730. doi:10.1128/mcb.19.3.1720

Hassankhani, R., Esmaeillou, M., Tehrani, A. A., Nasirzadeh, K., Khadir, F., and Maadi, H. (2015). *In Vivo* toxicity of Orally Administrated Silicon Dioxide Nanoparticles in Healthy Adult Mice. *Environ. Sci. Pollut. Res. Int.* 22, 1127–1132. doi:10.1007/s11356-014-3413-7

He, Q., Zhang, Z., Gao, F., Li, Y., and Shi, J. (2011). *In Vivo* Biodistribution and Urinary Excretion of Mesoporous Silica Nanoparticles: Effects of Particle Size and PEGylation. *Small* 7, 271–280. doi:10.1002/smll.201001459

He, Y., Xu, H., Ma, S., Zhang, P., Huang, W., and Kong, M. (2014). Fabrication of Mesoporous Spherical Silica Nanoparticles and Effects of Synthesis Conditions on Particle Mesostructure. *Mater. Lett.* 131, 361–365. doi:10.1016/j.matlet.2014.06.026

He, Y., Su, Z., Xue, L., Xu, H., and Zhang, C. (2016). Co-delivery of Erlotinib and Doxorubicin by pH-Sensitive Charge Conversion Nanocarrier for Synergistic Therapy. *J. Control. Release* 229, 80–92. doi:10.1016/j.jconrel.2016.03.001

He, Y., Li, J., Long, M., Liang, S., and Xu, H. (2017). Tuning Pore Size of Mesoporous Silica Nanoparticles Simply by Varying Reaction Parameters. *J. Non-Crystalline Sol.* 457, 9–12. doi:10.1016/j.jnoncrysol.2016.11.023

Huang, X., Li, L., Liu, T., Hao, N., Liu, H., Chen, D., et al. (2011). The Shape Effect of Mesoporous Silica Nanoparticles on Biodistribution, Clearance, and Biocompatibility *In Vivo*. *ACS Nano* 5, 5390–5399. doi:10.1021/nn200365a

Hur, W., and Gray, N. S. (2011). Small Molecule Modulators of Antioxidant Response Pathway. *Curr. Opin. Chem. Biol.* 15, 162–173. doi:10.1016/j.cbpa.2010.12.009

Isoda, K., Tetsuka, E., Shimizu, Y., Saitoh, K., Ishida, I., and Tezuka, M. (2013). Liver Injury Induced by Thirty- and Fifty-Nanometer-Diameter Silica Nanoparticles. *Biol. Pharm. Bull.* 36, 370–375. doi:10.1248/bpb.b12-00738

Latonen, L., Afyounian, E., Jylhä, A., Nättinen, J., Aapola, U., Annala, M., et al. (2018). Integrative Proteomics in Prostate Cancer Uncovers Robustness against Genomic and Transcriptomic Aberrations during Disease Progression. *Nat. Commun.* 9, 1176. doi:10.1038/s41467-018-03573-6

Lee, S. B., Kim, H. L., Jeong, H. J., Lim, S. T., Sohn, M. H., and Kim, D. W. (2013). Mesoporous Silica Nanoparticle Pretargeting for PET Imaging Based on a Rapid Bioorthogonal Reaction in a Living Body. *Angew. Chem. Int. Ed. Engl.* 52, 10549–10552. doi:10.1002/anie.201304026

Li, L., Liu, T., Fu, C., Tan, L., Meng, X., and Liu, H. (2015). Biodistribution, Excretion, and Toxicity of Mesoporous Silica Nanoparticles after Oral Administration Depend on Their Shape. *Nanomedicine* 11, 1915–1924. doi:10.1016/j.nano.2015.07.004

Li, X., Zhang, C., Zhang, X., Wang, S., Meng, Q., Wu, S., et al. (2016). An Acetyl-L-Carnitine Switch on Mitochondrial Dysfunction and rescue in the Metabolomics Study on Aluminum Oxide Nanoparticles. *Part. Fibre Toxicol.* 13, 4–19. doi:10.1186/s12989-016-0115-y

Li, J., He, X., Yang, Y., Li, M., Xu, C., and Yu, R. (2018). Risk Assessment of Silica Nanoparticles on Liver Injury in Metabolic Syndrome Mice Induced by Fructose. *Sci. Total Environ.* 628-629, 366–374. doi:10.1016/j.scitotenv.2018.02.047

Lim, S. L., Ng, C. T., Zou, L., Lu, Y., Chen, J., Bay, B. H., et al. (2019). Targeted Metabolomics Reveals Differential Biological Effects of Nanoplastics and nanoZnO in Human Lung Cells. *Nanotoxicology* 13, 1117–1132. doi:10.1080/17435390.2019.1640913

Liu, T., Li, L., Fu, C., Liu, H., Chen, D., and Tang, F. (2012). Pathological Mechanisms of Liver Injury Caused by Continuous Intraperitoneal Injection of Silica Nanoparticles. *Biomaterials* 33, 2399–2407. doi:10.1016/j.biomaterials.2011.12.008

Liu, Y., Beyer, A., and Aebersold, R. (2016). On the Dependency of Cellular Protein Levels on mRNA Abundance. *Cell* 165, 535–550. doi:10.1016/j.cell.2016.03.014

Lu, X., Tian, Y., Zhao, Q., Jin, T., Xiao, S., and Fan, X. (2010). Integrated Metabonomics Analysis of the Size-Response Relationship of Silica Nanoparticles-Induced Toxicity in Mice. *Nanotechnology* 22, 055101. doi:10.1088/0957-4484/22/5/055101

Lu, X., Ji, C., Jin, T., and Fan, X. (2015). The Effects of Size and Surface Modification of Amorphous Silica Particles on Biodistribution and Liver Metabolism in Mice. *Nanotechnology* 26, 175101–175115. doi:10.1088/0957-4484/26/17/175101

Maier, T., Güell, M., and Serrano, L. (2009). Correlation of mRNA and Protein in Complex Biological Samples. *FEBS Lett.* 583, 3966–3973. doi:10.1016/j.febslet.2009.10.036

Mohamed, H. R. H., Welson, M., Yaseen, A. E., and El-Ghor, A. A. (2020). Estimation of Genomic Instability and Mutation Induction by Graphene Oxide Nanoparticles in Mice Liver and Brain Tissues. *Environ. Sci. Pollut. Res. Int.* 27, 264–278. doi:10.1007/s11356-019-06930-0

Nemmar, A., Yuvaraju, P., Beegam, S., Yasin, J., Kazzam, E. E., and Ali, B. H. (2016). Oxidative Stress, Inflammation, and DNA Damage in Multiple Organs of Mice Acutely Exposed to Amorphous Silica Nanoparticles. *Int. J. Nanomed.* 11, 919–928. doi:10.2147/IJN.S92278

Nishijima, N., Hirai, T., Misato, K., Aoyama, M., Kuroda, E., Ishii, K. J., et al. (2017). Human Scavenger Receptor A1-Mediated Inflammatory Response to Silica Particle Exposure Is Size Specific. *Front. Immunol.* 8, 379–390. doi:10.3389/fimmu.2017.00379

Panieri, E., and Santoro, M. M. (2016). Ros Homeostasis and Metabolism: A Dangerous Liason in Cancer Cells. *Cell Death Dis* 7, e2253–12. doi:10.1038/cddis.2016.105

Park, E. J., Bae, E., Yi, J., Kim, Y., Choi, K., Lee, S. H., et al. (2010). Repeated-dose Toxicity and Inflammatory Responses in Mice by Oral Administration of Silver Nanoparticles. *Environ. Toxicol. Pharmacol.* 30, 162–168. doi:10.1016/j.etap.2010.05.004

Patton, J. S., and Byron, P. R. (2007). Inhaling Medicines: Delivering Drugs to the Body through the Lungs. *Nat. Rev. Drug Discov.* 6, 67–74. doi:10.1038/nrd2153

Peeters, P. M., Perkins, T. N., Wouters, E. F., Mossman, B. T., and Reynaert, N. L. (2013). Silica Induces NLRP3 Inflammasome Activation in Human Lung Epithelial Cells. *Part. Fibre Toxicol.* 10, 3–11. doi:10.1186/1743-8977-10-3

Pietroiusti, A., Stockmann-Juvala, H., Lucaroni, F., and Savolainen, K. (2018). Nanomaterial Exposure, Toxicity, and Impact on Human Health. *Wiley Interdiscip. Rev. Nanomed Nanobiotechnol.* 10, e1513. doi:10.1002/wnan.1513

Rosário, F., Duarte, I. F., Pinto, R. J. B., Santos, C., Hoet, P. H. M., and Oliveira, H. (2021). Biodistribution and Pulmonary Metabolic Effects of Silver Nanoparticles in Mice Following Acute Intratracheal Instillations. *Environ. Sci. Pollut. Res.* 28, 2301–2314. doi:10.1007/s11356-020-10563-z

Rosenholm, J. M., Zhang, J., Linden, M., and Sahlgren, C. (2016). Mesoporous Silica Nanoparticles in Tissue Engineering-Aa Perspective. *Nanomedicine (Lond)* 11, 391–402. doi:10.2217/nnm.15.212

Rossignol, T., Kobi, D., Jacquet-Gutfreund, L., and Blondin, B. (2009). The Proteome of a Wine Yeast Strain during Fermentation, Correlation with the Transcriptome. *J. Appl. Microbiol.* 107, 47–55. doi:10.1111/j.1365-2672.2009.04156.x

Schwanhäusser, B., Busse, D., Li, N., Dittmar, G., Schuchhardt, J., Wolf, J., et al. (2011). Global Quantification of Mammalian Gene Expression Control. *Nature* 473, 337–342. doi:10.1038/nature10098

Shin, J. H., Jeon, K., Kim, J. K., Kim, Y., Jo, M. S., Lee, J. S., et al. (2017). Subacute Inhalation Toxicity Study of Synthetic Amorphous Silica Nanoparticles in Sprague-Dawley Rats. *Inhal. Toxicol.* 29, 567–576. doi:10.1080/08958378.2018.1426661

Snezhkina, A. V., Kudryavtseva, A. V., Kardymon, O. L., Savvateeva, M. V., Melnikova, N. V., Krasnov, G. S., et al. (2020). ROS Generation and Antioxidant Defense Systems in normal and Malignant Cells. *Oxidative Med. Cell Longevity* 2019, 1–17. doi:10.1155/2019/6175804

Song, Y., Li, Y., Xu, Q., and Liu, Z. (2016). Mesoporous Silica Nanoparticles for Stimuli-Responsive Controlled Drug Delivery: Advances, Challenges, and Outlook. *Int. J. Nanomedicine* 12, 87–110. doi:10.2147/IJN.S117495

Song, P., Jiang, N., Zhang, K., Li, X., Li, N., Zhang, Y., et al. (2022). Ecotoxicological Evaluation of Zebrafish Liver (*Danio rerio*) Induced by Dibutyl Phthalate. *J. Hazard. Mater.* 425, 128027. doi:10.1016/j.jhazmat.2021.128027

Sun, J., Zhou, Q., and Hu, X. (2019). Integrating Multi-Omics and Regular Analyses Identifies the Molecular Responses of Zebrafish Brains to Graphene Oxide: Perspectives in Environmental Criteria. *Ecotoxicol. Environ. Saf.* 180, 269–279. doi:10.1016/j.ecoenv.2019.05.011

Sun, M., Zhang, J., Liang, S., Du, Z., Liu, J., Sun, Z., et al. (2021). Metabolomic Characteristics of Hepatotoxicity in Rats Induced by Silica Nanoparticles. *Ecotoxicol. Environ. Saf.* 208, 111496. doi:10.1016/j.ecoenv.2020.111496

Tan, H., Yang, K., Li, Y., Shaw, T. I., Wang, Y., Blanco, D. B., et al. (2017). Integrative Proteomics and Phosphoproteomics Profiling Reveals Dynamic Signaling Networks and Bioenergetics Pathways Underlying T Cell Activation. *Immunity* 46, 488–503. doi:10.1016/j.immuni.2017.02.010

Tang, F., Li, L., and Chen, D. (2012). Mesoporous Silica Nanoparticles: Synthesis, Biocompatibility and Drug Delivery. *Adv. Mater.* 24, 1504–1534. doi:10.1002/adma.201104763

Tannahill, G. M., Curtis, A. M., Adamik, J., Palsson-Mcdermott, E. M., Mcgettrick, A. F., Goel, G., et al. (2013). Succinate Is an Inflammatory Signal that Induces IL-1β through HIF-1α. *Nature* 496, 238–242. doi:10.1038/nature11986

Trewyn, B. G., Giri, S., Slowing, I. I., and Lin, V. S. (2007). Mesoporous Silica Nanoparticle Based Controlled Release, Drug Delivery, and Biosensor Systems. *Chem. Commun. (Camb)* 31, 3236–3245. doi:10.1039/B701744H

Yu, T., Hubbard, D., Ray, A., and Ghandehari, H. (2012). *In Vivo* biodistribution and Pharmacokinetics of Silica Nanoparticles as a Function of Geometry, Porosity and Surface Characteristics. *J. Control. Release* 163, 46–54. doi:10.1016/j.jconrel.2012.05.046

Zhang, X., Luan, J., Chen, W., Fan, J., Nan, Y., Wang, Y., et al. (2018). Mesoporous Silica Nanoparticles Induced Hepatotoxicity via NLRP3 Inflammasome Activation and Caspase-1-dependent Pyroptosis. *Nanoscale* 10, 9141–9152. doi:10.1039/c8nr00554k

Zhao, D., Zhang, Y., Xu, C., Dong, C., Lin, H., Zhang, L., et al. (2012). Pharmacokinetics, Tissue Distribution, and Plasma Protein Binding Study of Platinum Originating from Dicycloplatin, a Novel Antitumor Supramolecule, in Rats and Dogs by ICP-MS. *Biol. Trace Elem. Res.* 148, 203–208. doi:10.1007/s12011-012-9364-2

Conflict of Interest: The authors declare that the research was conducted in the absence of any commercial or financial relationships that could be construed as a potential conflict of interest.

Publisher's Note: All claims expressed in this article are solely those of the authors and do not necessarily represent those of their affiliated organizations, or those of the publisher, the editors and the reviewers. Any product that may be evaluated in this article, or claim that may be made by its manufacturer, is not guaranteed or endorsed by the publisher.

frontiers in Pharmacology

MINI REVIEW
published: 21 February 2022
doi: 10.3389/fphar.2022.768556

Molecular Docking as a Therapeutic Approach for Targeting Cancer Stem Cell Metabolic Processes

Babak Arjmand[1], Shayesteh Kokabi Hamidpour[1], Sepideh Alavi-Moghadam[1], Hanieh Yavari[1], Ainaz Shahbazbadr[1], Mostafa Rezaei Tavirani[2], Kambiz Gilany[3,4,5] and Bagher Larijani[6]**

[1]Cell Therapy and Regenerative Medicine Research Center, Endocrinology and Metabolism Molecular-Cellular Sciences Institute, Tehran University of Medical Sciences, Tehran, Iran, [2]Proteomics Research Center, Shahid Beheshti University of Medical Sciences, Tehran, Iran, [3]Reproductive Immunology Research Center, Avicenna Research Institute (ARI), Tehran, Iran, [4]Department of Biomedical Sciences, Institute of Tropical Medicine Antwerp, Antwerp, Belgium, [5]Breast Cancer Research Center, Motamed Cancer Institute, Tehran, Iran, [6]Endocrinology and Metabolism Research Center, Endocrinology and Metabolism Clinical Sciences Institute, Tehran University of Medical Sciences, Tehran, Iran

OPEN ACCESS

Edited by:
Linsheng Liu,
The First Affiliated Hospital of Soochow University, China

Reviewed by:
Aneta Radziwon-Balicka,
Nordsjællands Hospital, Denmark
Ting Ye,
Southwest Medical University, China

***Correspondence:**
Babak Arjmand
barjmand@sina.tums.ac.ir
Bagher Larijani
emrc@tums.ac.ir

Specialty section:
This article was submitted to Translational Pharmacology, a section of the journal Frontiers in Pharmacology

Received: *31 August 2021*
Accepted: *13 January 2022*
Published: *21 February 2022*

Citation:
Arjmand B, Hamidpour SK, Alavi-Moghadam S, Yavari H, Shahbazbadr A, Tavirani MR, Gilany K and Larijani B (2022) Molecular Docking as a Therapeutic Approach for Targeting Cancer Stem Cell Metabolic Processes. Front. Pharmacol. 13:768556. doi: 10.3389/fphar.2022.768556

Cancer stem cells (CSCs) are subpopulation of cells which have been demonstrated in a variety of cancer models and involved in cancer initiation, progression, and development. Indeed, CSCs which seem to form a small percentage of tumor cells, display resembling characteristics to natural stem cells such as self-renewal, survival, differentiation, proliferation, and quiescence. Moreover, they have some characteristics that eventually can demonstrate the heterogeneity of cancer cells and tumor progression. On the other hand, another aspect of CSCs that has been recognized as a central concern facing cancer patients is resistance to mainstays of cancer treatment such as chemotherapy and radiation. Owing to these details and the stated stemness capabilities, these immature progenitors of cancerous cells can constantly persist after different therapies and cause tumor regrowth or metastasis. Further, in both normal development and malignancy, cellular metabolism and stemness are intricately linked and CSCs dominant metabolic phenotype changes across tumor entities, patients, and tumor subclones. Hence, CSCs can be determined as one of the factors that correlate to the failure of common therapeutic approaches in cancer treatment. In this context, researchers are searching out new alternative or complementary therapies such as targeted methods to fight against cancer. Molecular docking is one of the computational modeling methods that has a new promise in cancer cell targeting through drug designing and discovering programs. In a simple definition, molecular docking methods are used to determine the metabolic interaction between two molecules and find the best orientation of a ligand to its molecular target with minimal free energy in the formation of a stable complex. As a comprehensive approach, this computational drug design method can be thought more cost-effective and time-saving compare to other conventional methods in cancer treatment. In addition, increasing productivity and quality in pharmaceutical research can be another advantage of this molecular modeling method. Therefore, in recent years, it can be concluded that molecular docking can be considered as one of the novel strategies at the forefront of the cancer battle via targeting cancer stem cell metabolic processes.

Keywords: cancer, cancer stem cells, drug designing, metabolic processes, molecular docking

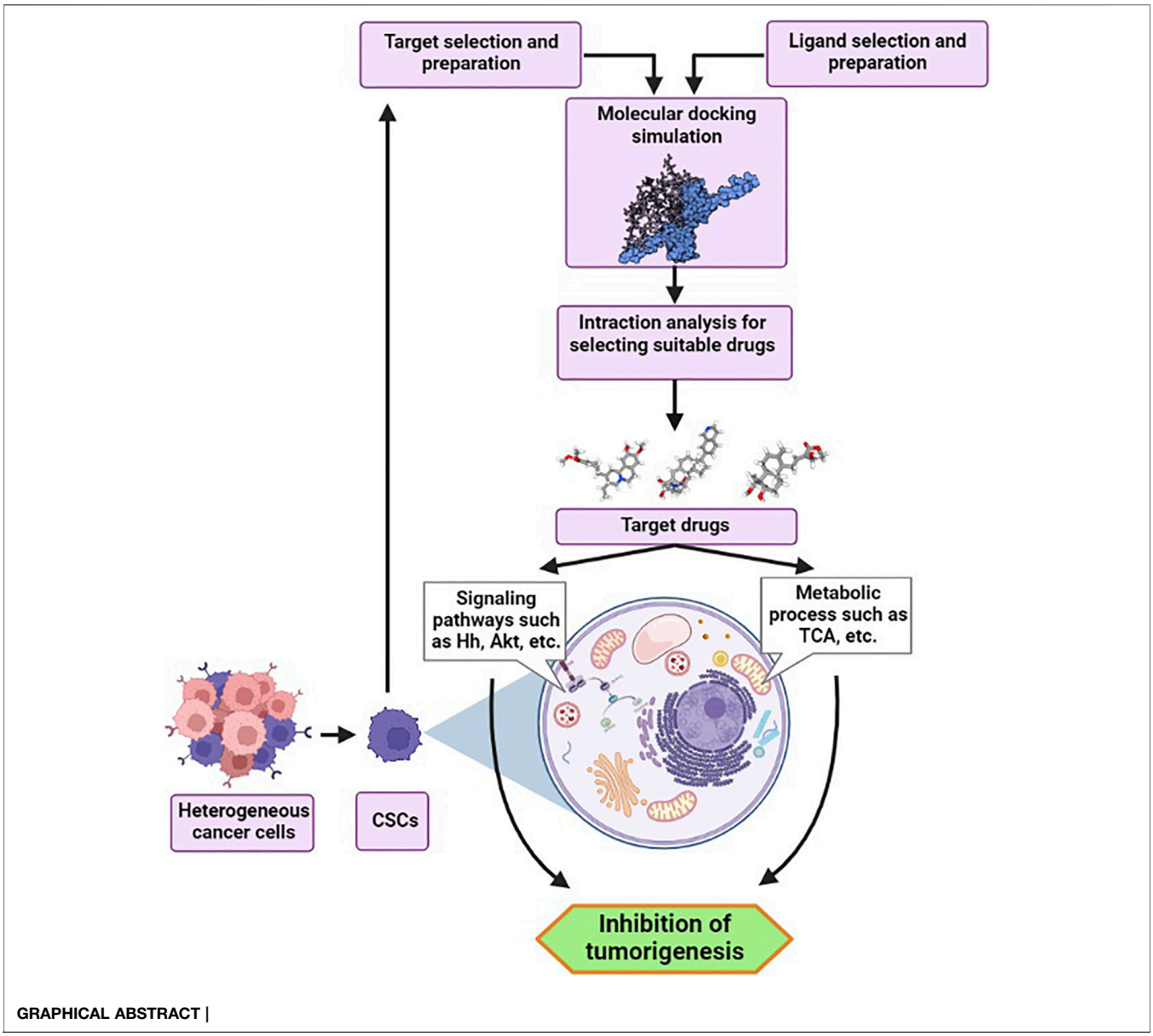

GRAPHICAL ABSTRACT |

INTRODUCTION

Cancer is considered as one of the worldwide life-threatening and the leading causes of human mortality (Vineis and Wild, 2014; Organization, 2020). According to the latest data released by the International Agency for Research on Cancer (IARC) on 14 December 2020, the annual incidence of cancer in 2020 reached 19.3 million cases and 10 million deaths. Furthermore, evidence based on the World Health Organization (WHO) suggests that there would be 29.5 million new cancer diagnoses and 16.4 million cancer deaths per year by 2040 (Shah et al., 2019; Sung et al., 2021). Accordingly, given the rapid development of oncology researches and the advancement of novel biotechnology approaches, determining different aspects of cancer progression can pave the way for improved cancer prognosis and treatment alternatives (Goyal et al., 2006; Charmsaz et al., 2018; Pucci et al., 2019). Herein, one of the challenges in the field of cancer treatment is the heterogeneity of tumor cells, which may lead to anti-cancer drug resistance or cancer treatment failure. Therefore, a full understanding of tumor heterogeneity can provide a clear picture of cancer progression and lead to the discovery of new cancer therapy options by researchers (y Cajal et al., 2020). Tumor heterogeneity is a condition in which tumor cells differ in various biological aspects such as function, differentiation, tumorigenesis, and sensitivity to anti-cancer therapies (Prager et al., 2019). In addition, depending on the type of heterogeneity, heterogeneous groups of tumor cells can have the same or distinct genomic content (Prager et al., 2019). In addition, heterogeneous populations of tumor cells can have the same or different genome content depending on the type of heterogeneity (Bedard et al., 2013). Hereupon, tumor heterogeneity can be divided into three types: 1) intertumor

TABLE 1 | Most frequently applied markers for cancer stem cells isolation.

CSCs Marker	Marker type	Expression location	Function	Cancer Type	References
CD44	Surface marker	Leukocytes, Endothelial cells, Hepatocytes, Mesenchymal cells	Activation of tyrosine kinase receptors by binding to extracellular matrix, Cell migration, Distinction, Increasing the speed of tumor cells entrance into blood vessels in metastasis	Breast, prostate, lung	Abbaszadegan et al. (2017); Bao et al., (2013)
CD133	Surface marker	Embryonic epithelial stem cell, Hematopoietic stem cells	Organizer of the plasma membrane topology, Conservation of plasma membrane`s lipid structure, Development of head and neck squamous cell carcinoma	Breast, prostate, lung, head, neck	Abbaszadegan et al. (2017); Bao et al. (2013); Yu and Cirillo, (2020)
CD117	Surface marker	Mesenchymal adult stem cells, Cardiac adult stem cell, Ovary	Stem cell factor`s receptor, Drug target molecules	Ovarian	Jin et al. (2017)
CD90	Surface marker	Between normal hematopoietic stem cells and leukemic CSCs	Identifying leukemic CSCs from hematopoietic stem cell subpopulation	Leukemia	Bao et al. (2013); Kumar et al., (2016)
CD24	Surface marker	Pancreatic carcinoma	Identifying CSCs in pancreas cancer	Pancreas	Gopalan et al., (2018); Jin et al. (2017)
ALDH1	Intracellular marker	Normal stem cells, Malignant stem cells, Progenitor cells	Regulator of stem cells propagation and distinction	Breast	Ajani et al., (2015); Abbaszadegan et al., (2017)
P63	Basal cell marker	Basal regenerative cells of many epithelial tissues, Prostate, Urothelial	Prostate progression, Diagnostic factor of prostate cancer	Prostate	Grisanzio and Signoretti, (2008); Klonisch et al. (2008)

ALDH1: Aldehyde dehydrogenase isoform 1; CSCs, Cancer stem cells.

heterogeneity which is related to the variation of tumor cells among different patients, 2) intersite heterogeneity which is referred to the variation of cells among distinct tumors within a patient such as tumors in the primary site and tumors in the metastatic site, and 3) intratumor heterogeneity which is linked with heterogeneous populations of cells in a single tumor (Piraino et al., 2019). Oncology studies were shown that the cancer stem cells (CSCs) model is one of the models responsible for the generation of heterogeneous populations of cells, especially intratumor heterogeneity type (Prasetyanti and Medema, 2017; Turnquist et al.). Moreover, it can be caused by different factors such as genetics, epigenetics, and various micro-environmental features (Wang et al., 2015). Indeed, CSCs are a subgroup of cancerous tumor cells that display stemness abilities in the same manner as normal stem cells. For instance, they can self-renew to form the same daughter cells and give rise to differentiated multiple lineages of cells which form tumors. Additionally, the quiescence state is one of the distinguishing characteristics of cancer and normal stem cells, and it can play a role in therapeutic resistance and cancer progression (Hung et al., 2019; Lee et al., 2020). Furthermore, CSCs can make the treatment process more challenging because of their resistance to therapeutic approaches such as chemo and radiation therapies. The mentioned therapeutic resistance can be due to a variety of factors and mechanisms, including tumor environment, epigenetic effects, multidrug resistance proteins (MRPs) expression, various signaling pathways, effective mechanisms in DNA damage resistance, and the epithelial-to-mesenchymal transition (EMT) process (Phi et al., 2018). On the other hand, the function of metabolic pathways and processes are crucial in the growth, proliferation and survival of CSCs. In this respect, many investigations at the cellular and molecular level were indicated that unique forms of metabolic processes such as oxidative phosphorylation (OXPHOS), carbohydrate, and lipid metabolisms are observed in CSCs (Chae and Kim, 2018; Yadav et al., 2020). Therefore, the science of metabolomics, as well as the understanding of alterations associated with metabolic processes, could be useful in recognizing CSC behaviors and developing specific therapeutic methods for various types of cancers (Gilany et al., 2018; Rahim et al., 2018; Arjmand, 2019a, 2019b; Goodarzi et al., 2019; Larijani et al., 2019; Tayanloo-Beik et al., 2020), as well as the understanding of alterations associated with metabolic processes, could be useful in recognizing CSC behaviors and developing specific therapeutic methods for various types of cancers (Cuyàs et al., 2017). Additionally, scientists have been pushed to employ targeted approaches for treating cancer due to the problems in CSCs resistance to therapeutic methods. Molecular docking is one of the targeted approaches that play an important role in drug discovery and pharmaceutical researches. This computer-assisted drug design method is based on mathematical algorithms in which the effective biological binding-conformation between the drug and the target molecule can be evaluated. Indeed, the mentioned drug designing is based on the molecular structure that makes it possible to model and predict the molecular interactions as well as evaluate the biochemical processes (Meng et al., 2011; Phillips et al., 2018). Hereupon, in the present study, the cellular and molecular characteristics, signaling pathways, metabolic processes, and drug resistance of CSCs have been reviewed. We have also focused our discussion on molecular docking as a novel therapeutic approach in CSCs targeting.

THE BIOLOGY OF CANCER STEM CELLS

CSCs are a subset of cancer cells or tumor-initiating cells (TICs) that serve as stem cells and contribute to the original tumor's phenotypic variety (Lobo et al., 2007). They are found in variable

TABLE 2 | CSCs signaling pathways characteristics.

Signaling Pathway	Examples of Ligands	Receptors/Co-receptors	Function in CSCs	Type of Cancer	References
Wnt	WNT1, WNT2	Members of the Frizzled, LRP5and LRP6	Self-renewal	Ductal breast carcinomas	Dong, Ying, and Shi, (2019);
	WNT2B, WNT3	ROR1 and ROR2	Tumorigenesis	Colorectal	Niehrs, (2012);
	WNT3A, WNT4	PTK7	Dedifferentiation	Papillary thyroid	Yang L et al. (2020)
	WNT5A, WNT5B	RYK	Apoptosis regulation	Esophageal	
	WNT6, WNT7A	MUSK	Metastasis	Colorectal	
	WNT7B, WNT8A, WNT8B, WNT9A, WNT9B, WNT10A, WNT10B, WNT11, WNT16	Proteoglycan families	—	—	
Notch	Delta-like proteins (DLL1, DLL3, DLL4)	Notch1	Proliferation	Glioblastoma	Karamboulas and Ailles, (2013); Yang L et al. (2020)
	Jagged proteins (JAG1 and JAG2)	Notch2	Cell survival	Leukemia	
	—	Notch3	Self-renewal	Ovarian	
	—	Notch4	Differentiation	Colon	
	—	—	Migration	Gastric	
	—	—	Metastasis	Breast	
	—	—	Apoptosis inhibition	Pancreatic	
	—	—	Cell fate specification	Prostate	
	—	—	Asymmetric division	Skin	
	—	—	—	Non small-cell lung	
	—	—	—	Liver	
Hh	Shh	Ptch1, and to a lesser extent, Ptch2, Cdon	Self-renewal	CML	Cochrane et al., (2015); Yang L et al. (2020)
	Ihh	Boc	Tumor growth	AML	
	Dhh	Gas1	Differentiate into transient amplifying cells	ALL	
	—	—	Metastasis	Glioma, Multiple Myeloma	
	—	—	—	Metastatic Melanoma	
	—	—	—	Breast	
	—	—	—	Gastric	
	—	—	—	Colon	
	—	—	—	Pancreatic	
	—	—	—	Prostate	
	—	—	—	Small Cell and	
	—	—	—	Non-Small Cell	
	—	—	—	Lung Cancer	
NF-κB	Lipopolysaccharide	TLRs	Inflammation	Gastrointestinal	Yang L et al. (2020)
	IL-1β	TNFR	Stress responses	Genitourinary	
	TNF-α	IL-1R	Cell survival	Gynecological	
	bacterial cell components	CD40	Proliferation	Head	
	—	BAFFR	Tumorigenesis	Neck	
	—	LTβR	Some key angiogenesis factors and adhesion molecules expression, Self-renewal	Breast	
	—	—	Metastasis	Multiple myeloma	
	—	—	Apoptosis regulation	Blood cancer	
JAK-STAT	ILE, PDGF-C, OSM, CXCL12, HGF, TGF-β, EGF, Gastrin, IGF, Mk, BDNF, NT-3, gp130	ILFR, PDGFR, OSMR, CXCR7, c-MET, TGFR, EGFR, GRPR, IGF1R, Notch-1/2, TrkB, TrkC, IL-6/IL-6Rα	Tumorigenesis, Metastasis, Chemoresistance, EMT transition, Proliferation, Inflammation, Survival	Prostate, Breast, Gastric, Lung	Jin, (2020)
PI3K/AKT/mTOR	Insulin and epithelial growth factor	ErbB-1; HER1, HER2 (c-ErbB-2), HER3 (c-ErbB-3), and HER4 (c-ErbB-4) CXCR4, IGF-1R	Cell proliferation, Angiogenesis, Metabolism, Differentiation, Survival, Self-renewal, Tumorigenesis	Ovarian, Cervical, Breast, Glioblastoma, Gastric, Pancreatic, Colorectal, Prostate, Hepatocellular	Chen et al. (2019); Miricescu et al. (2021); Xia and Xu, (2015)
TGF/SMAD	TGF-β1, 2 and 3	TGFβR1, TGFβR2	Cell proliferation, Epithelial-mesenchymal transition, Differentiation, Angiogenesis, Inflammation	Liver, Breast, Gastric, Skin, Glioblastoma, Leukemia Colorectal	Bellomo et al., (2016); Liu et al., (2018)

(Continued on following page)

TABLE 2 | (*Continued*) CSCs signaling pathways characteristics.

Signaling Pathway	Examples of Ligands	Receptors/Co-receptors	Function in CSCs	Type of Cancer	References
PPAR	Lipid-derived substrates	PPAR-α, PPAR-δ, PPAR-γ	Proliferation, Maintenance of sphere-formation ability, Expression of CSC Markers	Colorectal, Ovarian, Glioblastoma, Breast	Kuramoto et al. (2021); Tyagi et al., (2011)

ALL: acute lymphocytic leukemia; AML, acute myeloid leukemia; BAFFR, B cell-activating factor receptor; BDNF, Brain-derived neurotrophic factor; Boc, Brother of Cdon; CAM, cell adhesion molecule; CDON, CAM-related downregulated by oncogenes; CML, chronic myeloid leukaemia; c-Met, Mesenchymal-epithelial transition factor; CXCL, C-X-C motif chemokine ligand; CXCR, C-X-C chemokine receptor; Dhh, Desert hedgehog; DLL, Delta-like proteins; EGF, epidermal growth factor; EGFR, epidermal growth factor receptor; EMT, Epithelial-to-mesenchymal transition; ErbB-1, Erythroblastic leukemia viral oncogene homolog 1; GAS1, Growth Arrest Specific 1; Gp130, Glycoprotein 130; GRPR, Gastrin-releasing peptide receptor HER, human epidermal growth factor receptor; HGF, hepatocyte growth factor; IGF, Insulin-like growth factor; IGF1R, Insulin-like growth factor receptor 1; Ihh, Indian hedgehog; IL-1β, Interleukin 1 beta; IL-1R, Interleukin-1 receptor; IL-6, Interleukin 6; IL-6Rα, Interleukin 6 receptor alpha; ILFR, leukemia inhibitory factor receptor; JAG, jagged protein; JAK-STAT, Janus kinase/signal transducer and activator of transcription; LRP, Low-density lipoprotein receptor-related protein; LTβR, lymphotoxin beta receptor; MK, Heparin-binding growth factor Midkine; MUSK, muscle associated receptor tyrosine kinase; NF-κB, Nuclear factor kappa-light-chain-enhancer of activated B cells; NT-3, Neurotrophin-3; OSM, Oncostatin M; OSMR, Oncostatin M receptor; PDGF-C, Platelet-derived growth factor C; PDGF-R, Platelet-derived growth factor receptors; PI3K/AKT/mTOR, Phosphoinositide 3-kinase/AKT/mammalian target of rapamycin; PPAR, Peroxisome proliferator-activated receptor; Ptch, Patched; PTK7, Protein tyrosine kinase 7; ROR, Receptor tyrosine kinase-like orphan receptor; RYK, receptor tyr kinase; SHH, sonic hedgehog; TGF-β, transforming growth factor beta; TGFβR, transforming growth factor beta receptor; TLRs, Toll-like receptors; TNF-α, tumor necrosis factor alpha; TNFR, tumor necrosis factor receptor; TrkB, Tropomyosin receptor kinase B; TrkC, Tropomyosin receptor kinase C.

amounts in different tumors. Furthermore, evaluating cell surface markers is the main strategy for detecting CSCs. Normal stem cells and CSCs have many similar characteristics (Jin et al., 2017; Khatami et al., 2019) such as 1) Self-Renewal (Lobo et al., 2007) 2) Differentiation capacity (Mohr et al., 2015) 3) Tumorigenesis (Zhu and Fan, 2018) 4) Capacity of developing resistance to drugs/cytotoxic substances and radiation (Schöning et al., 2017). Despite their similarities, there are some distinctions between cancer and somatic stem cells. The first is the origin of these two types of stem cells: natural somatic stem cells arise during embryonic development and separate from each other. They differentiate and produce a variety of mature cells, while CSCs are differentiated from normal adult stem cells or by multiple mutations in a single cell. The second is the ability to regenerate itself: somatic stem cells regenerate more regular than CSCs, although both types of cells can regenerate themselves. Finally, the organogenesis ability of these two cells is studied: both cells have the ability to organogenesis, but CSCs produce abnormal tissue, whereas somatic stem cells' organogenesis produces normal tissue (Gjorevski et al., 2014).

Cancer Stem Cells Isolation Markers

Since, CSCs are a small part of a big heterogeneous cell population of human cancer, isolation and division of such small human cancer cells can be a significant step in a delicate study of various aspects of cancer. Herein, identifying CSCs markers is a key factor (Tang et al., 2007). Most of the CSCs markers originate from human embryonic stem cells (hESCs) or adult stem cells (Jin et al., 2017; Najafi et al., 2019). The expression of CSCs isolation markers varies depending on a number of factors, including cell lines, tumor histotypes, isolation methods, and survey CSCs markers in vivo or *in vitro* investigations (Tirino et al., 2013). On the one hand, CSCs markers have a beneficial therapeutic effect on several types of cancers by targeting CSCs in order to eliminate tumor recurrences (Jin et al., 2017; Najafi et al., 2019). Moreover, the majority of surface markers can be harmed by interactions between enzymes and tumor tissues, and this destruction could be regarded a disadvantage (Abbaszadegan et al., 2017). Some various CSCs markers with their unique characteristics were reviewed in **Table 1**.

Cancer Stem Cells Signaling Pathways

In general, signaling pathways can help to precisely regulate the biological function of both CSCs and regular stem cells. Numerous signaling pathways such as Wnt, Notch, Hh, nuclear factor-κB (NF-κB), Janus kinase/signal transducers and activators of transcription (JAK-STAT), phosphoinositide 3-kinase/AKT/mammalian target of rapamycin (PI3K/AKT/mTOR), transforming growth factor (TGF)/SMAD, and peroxisome proliferator-activated receptor (PPAR) are among the intracellular factors that make a major contribution in regulating stem cell functions. Therefore, excessive or abnormal activity and even suppression of mentioned signal transduction pathways can convert the normal stem cells into cancerous. These pathways are regulated and controlled by the function of factors such as diverse proteins, microRNAs, long noncoding RNAs, and endogenous or exogenous factors, just as they change the self-renewal, survival, proliferation, differentiation, and usually tumorigenesis of CSCs (**Table2**). Signaling pathways interact with one another in a large and complicated network known as "crosstalk," which is a crucial fact. Subsequently, crosstalk between signaling pathways can influence the regulation of several phenotypic features and drug resistance in CSCs (Matsui, 2016; Yang L et al., 2020). Hereupon, a deep understanding of the signaling processes underlying CSCs can pave the way for small molecules and pharmacological inhibitors to target them (Du et al., 2019).

Cancer Stem Cells Metabolic Processes

Metabolic reprogramming is one of critically important characteristics of CSCs compared to other cancer and non-cancer cells, which plays a pivotal role in demonstration of cell functions such as proliferation, fate determination and the cancer progression. In this process, the cellular energy metabolism used by CSCs, such as different types of hydrophobic natural compounds and organic substances

metabolisms, adenosine triphosphate (ATP) production pathways, etc., differs from that of other cells. In other words, the presence of more metabolites and high-energy compounds in CSCs suggests that they have a different metabolic profile compared to the other. Furthermore, studies demonstrate that oncogenic mutations, tumor suppressants, and, particularly tumor microenvironment features, can all have a major impact on the many components engaged in such metabolic processes. Nevertheless, mentioned metabolic processes and the components involved can be considered as therapeutic targets for cancer treatment (Mukha and Dubrovska, 2020; Peixoto and Lima, 2018; Zhu et al., 2020).

Glycolysis

CSCs such as normal cells are used glucose through glycolysis process to gain energy and survive. The methods for glucose metabolism in a CSC include OXPHOS and glycolytic phosphorylation, which are selected based on the presence of oxygen. Moreover, they play an important role in differentiation, self-renewal and homeostasis. Generally, high glucose levels increase the number of CSCs, while low glucose levels lower the quantity of CSCs (Falahzadeh et al., 2019). CSCs are adaptable cells that can cope with a wide range of situations, including low oxygen levels, insufficient blood vessel development, hyperoxidation, and hypoxia (Luo and Wicha, 2015). If the CSCs are in a state of hypoxia (lack of oxygen), the proper metabolic pathway is chosen. Herein, they enter the glycolytic pathway, which eventually leads to the formation of lactate (Yi et al., 2018). According to Warburg, CSCs require more energy than other normal cells due to their high growth and proliferation. Although the glycolytic process provides less energy, CSCs prefer it since it is shorter (Dando et al., 2015). Lactate produced by the glycolytic pathway has the ability to influence CSC function and is involved in processes including metastasis, angiogenesis, and differentiation (Tamada et al., 2012). If the cell is in a state of hyperoxia (low oxygen), it enters the oxidative pathway, where pyruvate created from glucose enters the mitochondria. Then proceeds via the Krebs cycle and OXPHOS pathway to make energy. According to researches, the first alteration in CSC metabolism is a shift from aerobic to anaerobic sugar metabolism, in which oncogenes such as Akt 1 and C-Myc can regulate the glycolytic pathway by acting on the Warburg effect (Dando et al., 2015).

Metabolisms Related to Mitochondria

Almost every cell activity relies on the hydrolysis of energy-rich compounds such as ATP. Hereupon, the continuous production and replenishment of such energetic compounds are prioritized by the cells (Dunn and Grider, 2020). Mitochondria are one of the major organelles of cells in which contributes significantly in energy transduction by producing energy-carrying molecules. The mitochondria play a key role by activating the OXPHOS, tricarboxylic acid cycle (TCA), and fatty acid oxidation (FAO) in the cell. Additionally, biosynthetic precursors production, innate immune activation, modulation of the reactive oxygen species (ROS), control of calcium homeostasis, and trigger to apoptotic process are also some of the major activities of mitochondria within a cell (Zong et al., 2016). Owing to the mitochondria biosynthetic and bioenergetics activities, compelling evidence suggests that it also have a crucial impact on CSCs function (De Francesco et al., 2018). The difference in the amount of energy required for cancer stem cells compare to other cells can lead to differences in the quantity of mitochondrial function in them. Studies show that mitochondrial function can be affected by the type of tumor heterogeneity. Evidence also points that epigenetic and micro environmental features are among the factors that can result in altered mitochondrial function in CSCs (García-Heredia and Carnero, 2020). Investigations at the cellular and molecular level imply that changes leading to the production of cancer stem cells can increase the mitochondrial mass (Shin and Cheong, 2019) and membrane potential which are a reflection of electrical and biochemical alterations in CSCs mitochondria (Zhang et al., 2015). Furthermore, changes in mitochondrial DNA (mtDNA) can also affect the expression of some nuclear genes during the retrograde signaling that ultimately lead to inducing EMT process and producing CSCs (Guha et al., 2014). Reciprocally, many mitochondrial proteins are encoded by nuclear DNA (nDNA). Accordingly, mutations or changes in nDNA may eventually lead to altered mitochondrial activity in CSCs (Guerra et al., 2017). In addition to the interaction between mitochondria and the nucleus, disruption of some signaling pathways can affect the role of mitochondria in tumorigenesis. For instance, one of the major functions of PI3K/AKT/mTOR pathway is the regulation of pre-apoptotic proteins such as B-cell lymphoma 2 Associated X, Apoptosis Regulator (BAX) in relation to mitochondria which ultimately leads to apoptosis through this organelle. However, overexpression of apoptosis inhibitor genes in CSCs causes abnormal activation of the mentioned signaling pathway, which can lead to cancer cell proliferation, survival, and drug resistance of cancer cells (Frasson et al., 2015; Liu et al., 2020). Whereas the study of mitochondrial role in relation to other parts of cell on a large scale can be challenging, it should be narrow down the study to the major functions of mitochondria. Therefore, to promote research in the assessment of CSCs, such part particularly focuses on tricarboxylic acid cycle (TCA) and electron transport-linked phosphorylation process, synthesis and degradation of lipids, reactive oxygen species (ROS) generation system, and alternative metabolic pathways such as amino acid metabolism in CSCs.

Tricarboxylic Acid Cycle (TCA) and Electron Transport-Linked Phosphorylation Process

Unlike normal cells, CSCs require metabolic adaptation in order to supply fuel and materials for tumorigenesis purposes. Both TCA and OXPHOS which occur alternately following aerobic glycolysis, play an important role in the development of CSCs features. For instance, a reduction in the amount of TCA enzymes can be seen in some CSCs. Additionally, the TCA cycle is associated with different processes such as FAO, glutamine metabolism, and so on. Hence, the TCA cycle can play a key role in the development of stemness capabilities in CSCs under the influence of other metabolites (Yadav et al., 2020). Along with

TCA, OXPHOS has an important role in tumorigenesis. As already mentioned, glycolysis is the preferred energy production process compared to the OXPHOS in many CSCs. Although mitochondrial-related bioenergetics processes can produce higher rates of energy-rich compounds, the glycolysis pathway can provide the factors needed for the growth and proliferation of CSCs more timely and rapidly. However, CSCs in some types of cancers such as leukemia, ovarian, glioblastoma, breast, lung, and pancreatic ductal adenocarcinoma (PDAC) do not comply with this rule and prefer the OXPHOS pathway rather than glycolysis (Peixoto and Lima, 2018; Snyder et al., 2018). OXPHOS-dependent CSCs can acquire their needed energy from the uptake and chemical changes on some metabolites such as pyruvate, lactate, ketone bodies, and some amino acids. However, extracellular uptake is not the only way to get the nutrients needed by OXPHOS-dependent CSCs functions (Gentric et al., 2017; Jagust et al., 2019a). They can also supply the required nutrients through metabolic symbiosis with glycolysis to perform their bioenergetics and biosynthetic processes. Interestingly, the restriction of nutrient levels in the surrounding microenvironment of OXPHOS-dependent CSCs has not a huge impact on cell functions. Because in specific tumor microenvironments, they can counteract this limitation with their selective advantages. Therefore, this strategy can make a significant contribution to CSCs survival (Krstic et al., 2017; Zhu et al., 2020). Since mitochondrial-related processes have important effects on the energy and materials supplying of CSCs to grow and develop tumors, targeting different components of these processes can be an efficient approach in the treatment of various types of cancers (Jagust et al., 2019b).

Synthesis and Degradation of Lipids

Lipid, as one of the cell membrane`s basic constitutive elements, is necessary for different cell activities, such as signaling conduction, energy production, etc. Sterols, monoglycerides, diacylglycerides, triglycerides, phospholipids, and glycolipids are different components of lipid structure. additionally, most of the lipids originated from fatty acids (Snaebjornsson et al., 2020; Visweswaran et al., 2020). Furthermore, lipid droplets (LDs) act as a lipid storage and in comparison with normal cells, cancer cells have more LDs. Regarding the metabolism of lipid, CSCs have been affected by this kind of metabolism through different strategies such as CSCs maintaining, complying energy desire of CSCs (Visweswaran et al., 2020), increasing CSCs numbers (Mancini et al., 2018), and protecting CSCs from chemotherapeutic agents-induced peroxidation (Begicevic et al., 2019). Moreover, NANOG, sterol regulatory element-binding transcription factor 1(SREBP1), MYC, stearoyl-CoA desaturase (SCD), fatty acid synthase (FASN), ACVL3, CD36, carnitine palmitoyltransferase 1 (CPT1A), and carnitine palmitoyltransferase 1B (CPT1B) are some main modulators for this metabolism. In this respect, there are some alterations in lipid metabolism which lead to different outcomes, such as the effectiveness on the capability of self-renewal, invasion, metastasis, and drug resistance (Giacomini et al., 2020). On the other hand, CSC biomass production, stimulation of the Wnt/-catenin, and Hippo/YAP signaling pathways are some of the other effects that have been linked to CSC activity and cancer progression (Chae and Kim, 2018; Yi et al., 2018; Jagust et al., 2019b). In this context, the altered lipid metabolism can also have some therapeutic effects in the field of CSCs by the CSCs blockage and lessen CSCs chemoresistance ultimately, lipid metabolism contains different signaling pathways that conserve undifferentiating status and the survival of CSCs. Some of these signaling pathways are Notch signaling, Hippo cascades, Hedgehog (Hh) signaling, and Wnt signaling (Giacomini et al., 2020).

Reactive Oxygen Species Generation System

In addition to energy production processes, other pathways can play vital roles in multiple aspects of the generation and maintenance of the CSCs function. ROS production is one of these pathways which contribute to cancer recurrence, CSCs metastasis, and resistance to conventional therapies. Generation of ROS can be a consequence of electron transferring through mitochondrial membrane. In addition, enzymes in some other organelles and even immune reactions can play a role in the production of these oxygen species. Studies have also shown that chemotherapy and radiotherapy can eventually lead to increased ROS within cells (Liou and Storz, 2010; Zhou et al., 2014). In general, the antioxidant system acts as a defense barrier against increasing ROS. Maintaining a balance between the amount of antioxidants and ROS can play an important role in cell stability and homeostasis. If this balance is upset and the ROS level increases, cellular stress and eventually cell death occurs (Poljsak et al., 2013; Kurutas, 2016). In contrast, in the case of CSCs, the expression of antioxidants is much higher than in ROS production and keeps the ROS levels low (Shi et al., 2012). Hence, it can promote self-renewal, survival, and resistance to anti-cancer treatments. According to the stated argumentation, ROS can be an appropriate objective for discovering targeted therapies to fight against cancer. For instance, using approaches to increase ROS levels or disruption of antioxidant systems within CSCs can lead to cell aging and apoptosis. Therefore, an effective step can be taken to treat various types of cancer by extensively and accurately examining of ROS modulation in CSCs (Zhou et al., 2014; Ding et al., 2015).

Amino Acid Metabolism as an Alternative Metabolic Pathway

CSCs are flexible cells that rely on alternative fuels such as the amino acid glutamine to maximize their growth and proliferation under different environmental conditions (De Francesco et al., 2018). In glucose deficiency, the growth and survival of CSCs are highly dependent on glutamine, which enters the cell through its specific vectors during the path of glutaminolysis and is converted to glutamate by the enzyme mitochondrial glutaminase, thus entering the Krebs cycle (Deshmukh et al., 2016). Glutamine, as a source of nitrogen, plays an important role in mediating metabolites, which eventually synthesize various substances, including protein, lipids, and nucleotide acids (Deshmukh et al., 2016). CSCs of various tumors, including the pancreas, pancreas, ovaries, and lungs, are glutamine-dependent

(Deshmukh et al., 2016). The pentose phosphate (PPP) pathway is also used as an alternative pathway for fuel generation in CSCs. PPP is performed in two forms: reversible (non-oxidative) and irreversible (oxidative) (Giacomini et al., 2020), which is an alternative pathway for glucose metabolism during the irreversible pathway of PPP. In this pathway, glucose 6-phosphate (G6P) is converted to ribose 5-phosphate in several steps with the production of nicotinamide adenine dinucleotide phosphate (NADPH), and finally essential nucleotides are synthesized by forming ribose groups (Riganti et al., 2012; Polat et al., 2021). However, in reversible PPP, ribose 5-phosphate is converted to glyceride aldehyde 3 phosphate in a series of reversible reactions and is eventually used for glycolysis (Polat et al., 2021). Ketone bodies (acetone, acetate, 3-hydroxybutyrate) are among the high-energy fuels used by CSCs to grow and propagate metastases (Jagust et al., 2019b). When there is not enough glucose in CSCs, ketone bodies are released into the blood and converted directly to Acetyl-CoA by the two enzymes OXCT1 and ACAT1. Then acetyl-CoA enters the citric acid (CAC) cycle and produces more ATP in the cell (Ozsvari et al., 2017). In addition to glutamine, lysine is another amino acid that CSCs use to make fuel, as well as TICs, which contain many enzymes; They perform the process of lysine catabolism (Jagust et al., 2019b). As a result of the lysine pathway, glutamate is synthesized and cysteine uptake is increased in CSCs (Peixoto and Lima, 2018).

The Chemoresistance of Cancer Stem Cells

Chemoresistance is defined as a pivotal factor of defeated chemotherapy treatment in various cancers. This factor relapses affected agents of chemotherapy such as cell death and tumor bulk`s size decrement. In this respect, CSCs considerably execute the role of referred relapsing and also it has the capability of showing resistance against chemotherapeutics by its insensitivity (Abdullah and Chow, 2013; Zhao, 2016). Chemoresistance of CSCs leads to a high risk of metastases, less survival speed (Nunes et al., 2018), and the permanence of CSCs (Chuthapisith et al., 2010). Furthermore, a comparison between normal cancer cells and CSCs revealed that, CSCs intrinsically have a higher amount of chemotherapy resistance than normal cancer cells (Thomas et al., 2014). Many factors are involved in CSCs resistance occurrence, which some of them are as detailed below:

- *Tumor microenvironment (TME):* One of the factors involved in the regulation of stemness characteristics and chemoresistance of CSCs, is the autocrine and paracrine interactions of CSCs with the components of their surrounding environment, which is referred to as the TME. In recent years, the key role of TME and its components including extracellular matrix, immune cells, endothelial cells, cancer-associated adipocytes (CAAs), and cancer-associated fibroblasts (CAFs) in the onset, metastasis, recurrence, and drug resistance of cancer have been investigated. The results of these studies show that targeting the TME can be an effective approach in the treatment of cancer (Gaggianesi et al., 2021).
- *Epigenetics*: Another major factor in the chemoresistance of CSCs is the role of mechanisms followed epigenetic alterations. Studies reveal that epigenetic processes such as DNA methylation, nucleosome remodeling, histone modification, and non-coding RNAs changes are generally associated with the development of normal stem cell characteristics. However, disruption in the normal function of epigenetic factors lead to the development of tumorigenic properties in CSCs (Toh et al., 2017).
- *Epithelial Mesenchymal Transition (EMT)*: EMT is a biological phenomenon during processes such as embryonic development, wound healing, and tissue regeneration. However, in the case of cancer, EMT can suppress epithelial features and convert the cell into the mesenchymal state through signaling pathways such as Wnt, Notch, and Hedgehog, which can lead to the development of tumor features (Singh and Settleman, 2010).
- *Multidrug resistance (MDR)*: High levels of MDR is another main factor involved in the chemoresistance of CSCs that occurs after applying long-term or high-dose treatment for cancer patients. Generally, two mechanisms can be considered for the effect of MDR on CSCs: 1) Preventing the drug from reaching an effective concentration: studies imply that the function of efflux pumps such as P-glycoprotein (P-gp) encoded by ABCB1, transporters, and enzymes such as cytochrome P450 and glutathione S-transferase play significant roles in mediating drug resistance. 2) Drug detoxification: based on studies, it has been realized that avoiding apoptosis and activating DNA repair mechanisms are of fundamental importance to induce continuous growth and proliferation of CSCs. (Cho and Kim, 2020).
- *The quiescent state*: Quiescence or dormancy is a survival strategy for CSCs. In the quiescent state, cell division stops for a while, and cells live with minimal metabolic activity, but still retain the ability to reactivate the cell cycle (Chen et al., 2021). In this state, both intrinsic (e.g., p53 signaling, reactive oxygen species, hypoxia inducible factor-1a, nuclear factor of activated T cells c1, and negative regulators of mTOR) and non-intrinsic factors (e.g., Tie2/angiopoietin-1, TGF-b and bone morphogenic proteins, thrombopoietin, N-cadherin and integrins, osteopontin, and Wnt/b-catenin signaling) are involved (Li and Bhatia, 2011). According to studies, TME and epigenetic mechanisms have a major contribution to the maintenance of the quiescentstate of CSCs as well as evade immune surveillance and destruction, and tumor relapse. Therefore, the presence and persistence of the quiescence or dormancy state in CSCs can lead to the survival of CSCs and cell resistance to treatments such as chemotherapy (Chen et al., 2021).
- *Self-renewal*: Self-renewal is one of the noted hallmarks of CSCs that results from a malfunction of self-renewal pathways (SRPs). Studies indicate that Hh, Wnt, Notch, and B-cell-specific Moloney murine leukemia virus integration site 1 (BMI1) pathways have a crucial role in inducing the self-renewal in CSCs. In recent years, the

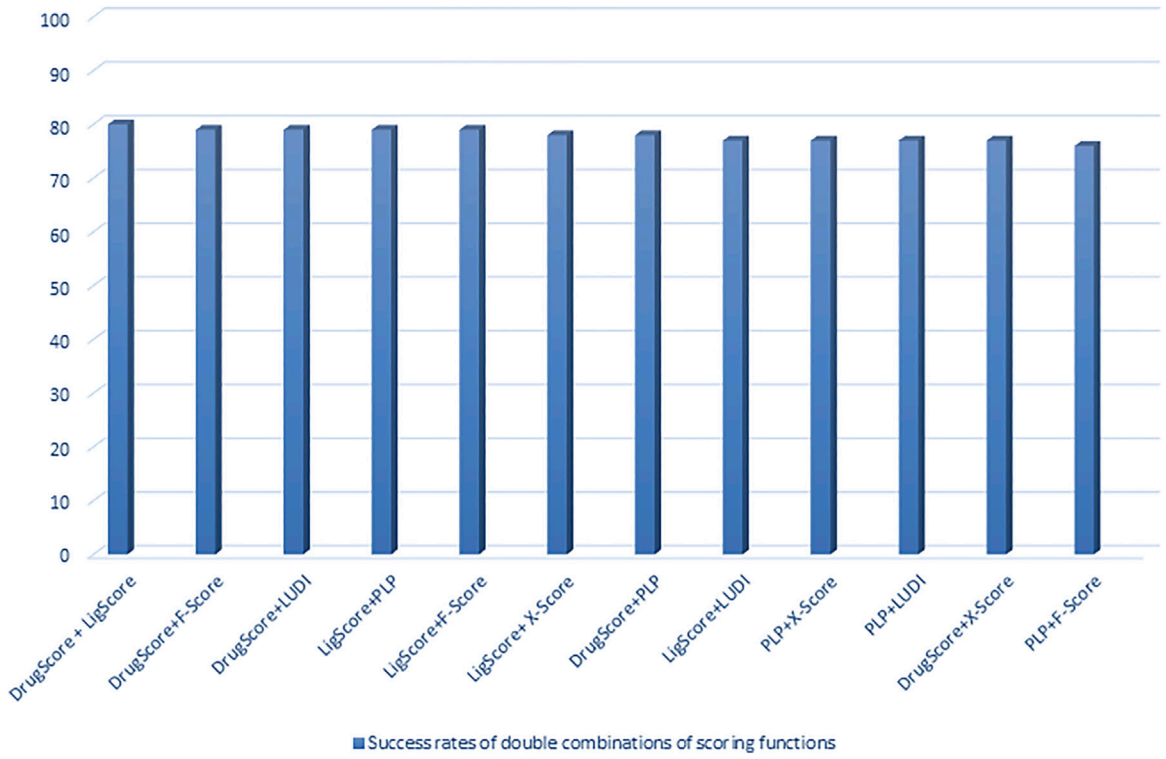

FIGURE 1 | Success rates of double combinations of the six relatively successful scoring functions in consensus scoring. All numbers are in percent (Wang et al., 2003).

targeting of SRPs has attracted attention as an efficient therapeutic approach in cancer treatment to reduce cancer recurrence and chemotherapy resistance possibility (Borah et al., 2015).

It should also be noted that according to metabolic studies, cancer cells that have undergone chemoresistance are metabolically altered and adapted. For example, processes such as fatty acid oxidation, glutaminolysis activation, glycolysis activation, lactate production, adaptive mitochondrial reprogramming, ornithine decarboxylase, and polyamine production, and PPP and NADPH production can be observed in chemoresistance cancer cells (Chen et al., 2020).

MOLECULAR DOCKING STUDY; A THERAPEUTIC APPROACH FOR ANTI-CANCER DRUG DESIGNING

Drug Discovery is considered as a multi-process platform in which a specific chemical compound with desired biological activity on the drug target can be selected and eventually enter the drug development as a candidate drug. In this platform, both chemical compounds and biological targets are evaluated from different aspects by using various approaches. Since both drug discovery and development are time-consuming and cost-intensive programs, they pose many challenges for researchers in drug designing and discovering for various diseases such as different types of cancer. Therefore, the use of new technologies can pave the way discovering new drugs with high therapeutic potential and take a big step towards disease treatment. Compound screening assays are one of mentioned methods that can help with hit identification, validation, lead generation, and optimization processes, as well as evaluating the compounds' effects on the therapeutic target. With the advancement of technology and the integration of computational science with biological and pharmaceutical studies, approaches such as virtual screening are widely applied in drug designing and discovering programs (Reddy et al., 2007; Hughes et al., 2011; Mohs and Greig, 2017; Cui et al., 2020). In this context, virtual screening aims to evaluate and filter a limited number of suitable chemical compounds from large libraries of small molecules by using mathematical calculations. Structure-based virtual screening (SBVS) is one of the virtual screening methods which attempts to model and analyze the efficient biological binding-conformation between a ligand and a target molecule by using the molecular docking technique (Liao et al., 2013). Molecular docking is one of the cutting-edge computational drug designing technologies in which the most effective and stable state form of the ligand-receptor

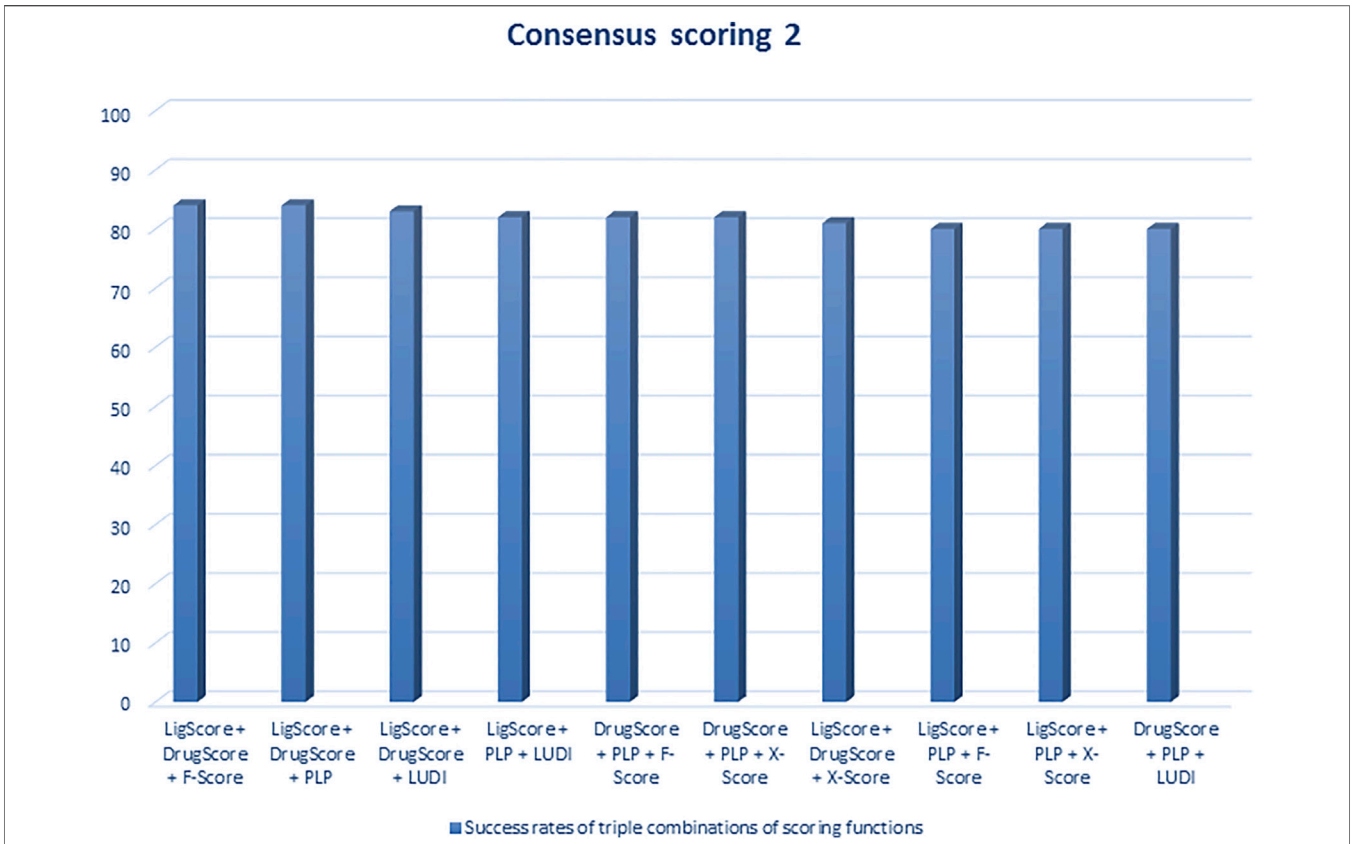

FIGURE 2 | Success rates of triple combinations of the six relatively successful scoring functions in consensus scoring. All numbers are in percent (R. Wang et al., 2003).

complex can be predicted (Morris and Lim-Wilby, 2008). The determination of the three-dimensional structure of the target and ligand molecules is at the top of the entire process priority list. Therefore, some techniques such as x-ray crystallography, nuclear magnetic resonance (NMR) spectroscopy, cryo-electron microscopy (cryo-EM), and homology modeling are not only useful in determining molecular structure, but also as complementary tools in drug development (Allen and Stokes, 2013; Kershaw et al., 2013; Sturlese et al., 2015; Lohning et al., 2017). Molecular docking includes searching algorithms and scoring function as two fundamental aspects of docking programs. Searching algorithms can be defined as a process that can lead to exploring the predominant and effective matching docking modes of ligand to the molecular target among the myriad configurations. Because a large number of binding modes are actually found between a ligand and a biological target molecule, searching algorithms not only can consider the optimum possible orientations of the ligand with the target but also can be an economical and time-saving solution in the docking process (Meng et al., 2011; Salmaso and Moro, 2018). Molecular dynamics, distance geometry methods, point complementary methods, fragment-based methods, Mote Carlo methods, genetic algorithms, systematic searches, and incremental construction, are some of the examples of search algorithms that can be used in modeling and evaluating the binding form of a ligand molecule to the objective receptor.

After the algorithm searching, it is time for the scoring function to step into the docking arena to find the good pose between the ligand and the target molecule. Scoring function refers to a process in which putative docking modes are ranked by evaluating their binding affinity and lowest binding energy to achieve top-ranked poses between a ligand and a target molecule. Force field function, Empirical scoring functions, knowledge based scoring functions, knowledge-based potentials, machine learning based scoring functions, comparative assessment of scoring functions, physics-based methods, and descriptor-based scoring functions are some of the examples of scoring function classifications in molecular docking (Madhavilatha and Babu, 2019; Sethi et al., 2019).

Regarding scoring function, the study of Wang et al. (2003) is one of the best examples of meticulous studies of popular scoring functions in molecular docking. In this study, the authors compared 11 popular scoring functions, including four scoring functions of the LigFit module in Cerius2 (LigScore, PLP, PMF, and LUDI), four scoring functions of the CScore module in SYBYL (FScore, G-Score, D-Score, and ChemScore), the scoring function of the AutoDock program, and two stand-alone scoring functions (DrugScore and X-Score) by performing them on 100 protein–ligand complexes to scrutinize their performance and sift the most effective and efficient methods among them. In this regard,

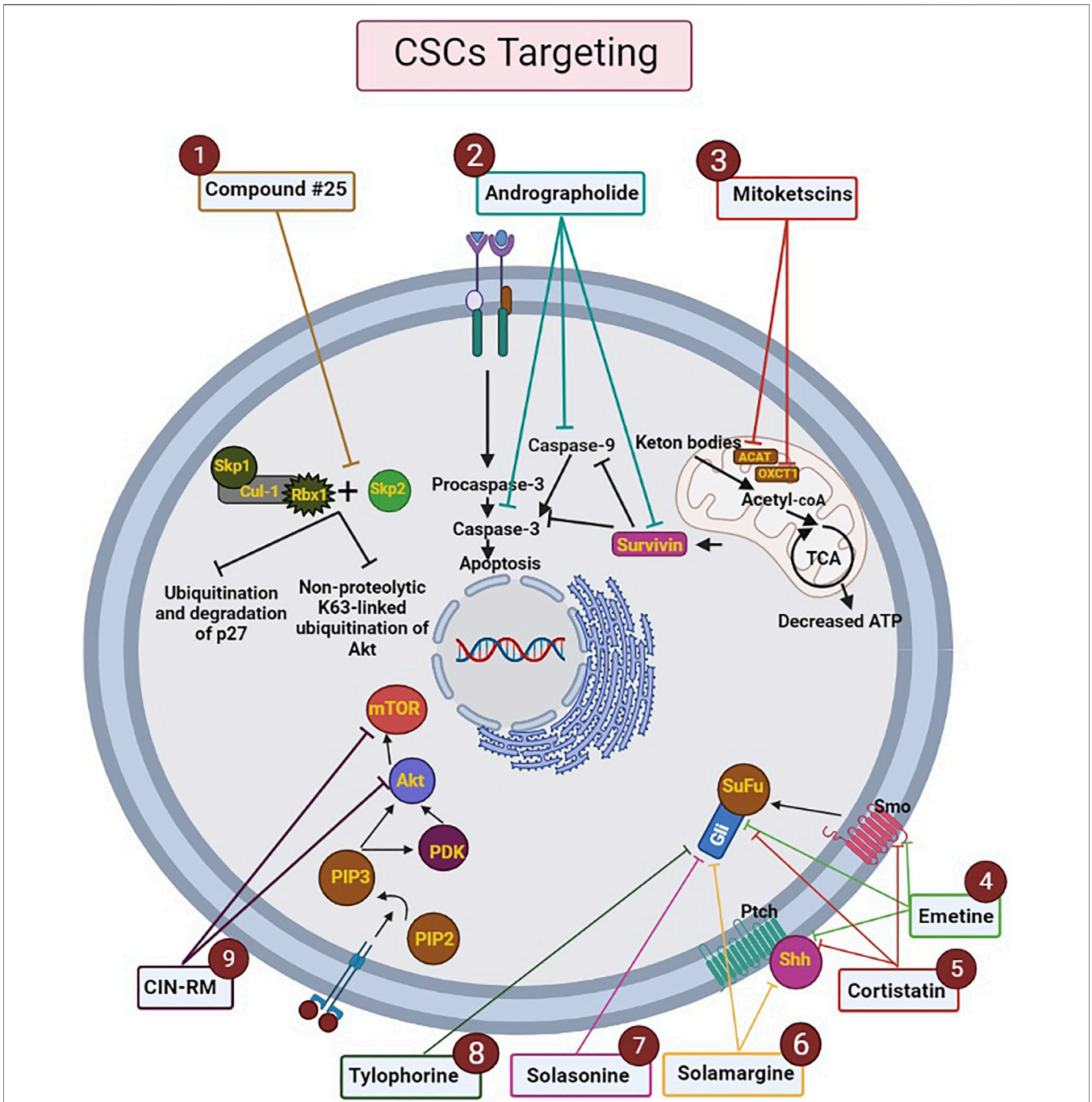

FIGURE 3 | Mechanism of action of drugs analyzed by molecular docking on the metabolic processes of CSCs. The ligands and targets have been investigated by molecular docking. Nine effective drugs, including compound #25, andrographolide, mitoketoscins, emetine, cortistatin, solamargine, solasonine, tylophorine, and CIN-RM are known to affect the biological processes and signaling pathways of CSCs. 1) Compound #25 prevents the assembly of the Skp2-SCF complex by binding to Skp2. Hence, it inhibits two pathways including non-proteolytic K63-linked ubiquitination of Akt and ubiquitination and degradation of p27, which ultimately inhibit the development of tumor features. 2) Andrographolide increases intrinsic apoptosis in CSCs (especially in breast cancer) by inhibiting survivin, caspase-9, and caspase-3.3) Mitoketoscins stop the recycling of ketone bodies into Acetyl-CoA by inhibiting two proteins, including OXCT1 and ACAT1. Hence ATP production is stopped and oxidative mitochondrial metabolism in CSCs is inhibited. 4) Emetine and 5) Cortistatin, can target CSCs by binding to sonic Hh, Smo and, gli protein. 6) Solamargine can affect sonic hedgehog and gli proteins by its pharmacophores. 7) Solasonine and 8) Tylophorine modulate the Hh pathway by affecting gli proteins. 9) CIN-RM can lead to upstream inhibition of the Akt pathway and reduction of CSCs markers, which decrease the expression level of transcription factors involved in self-renewal, such as c-Myc, Nanog, Oct4, and Sox2. CIN-RM can inhibit mTOR pathway. Abbreviations: ATP, Adenosine triphosphate; CIN-RM, Hydroquinone 5-O-cinnamoyl ester of renieramycin M; CSCs, Cancer stem cells; Hh, Hedgehog; mTOR, Mammalian target of rapamycin; Smo, smoothened (Chan et al., 2013; Hongwiangchan et al., 2021; Jaitak, 2016; Liu et al., 2014; Madhunapantula et al., 2011; Ozsvari et al., 2017; Wanandi et al., 2020).

after generating a set of docked conformations for each ligand by Autodac software, each 11 scoring function was tested and implemented on the maintained set and significant results were obtained. In this study, the authors used root-mean-square deviation ≤2.0 Å as a criterion for examining those scoring functions. Based on the analysis of the mentioned criterion, it was concluded that six scoring functions, including PLP, F-Score, LigScore, DrugScore, LUDI, and X-Score achieved high success rates (about 66–76%). In addition, the study implied that the combination of some of those scoring functions and generating the consensus scoring scheme can also increase the success rate (about 80%) (**Figures 1**, **2**). In addition to success rates, the authors examined the correlation between 100 complexes' binding scores and experimentally determined protein-ligand binding affinities. As a result of this experiment, X-Score, PLP, DrugScore, and G-Score could represent correlation coefficients of more than 0.50, which demonstrate superiority over other scoring functions. Since the best scoring function should perform excellently in both docking and scoring, the three scoring functions, including X-Score, DrugScore, and PLP, can be considered the top scoring functions in molecular docking, according to the study by Wang et al. (Wang et al., 2003).

TARGETING CANCER STEM CELLS METABOLIC PROCESS BY MOLECULAR DOCKING

Molecular docking is a substantial method for estimating the interaction between macromolecules such as protein and small molecules such as ligand. On the other hand, molecular docking is also capable of analyzing the molecular kinds of behavioral variability for those molecules which are located at the binding site of a targeted protein. Also, molecular docking is a computational approach and some docking programs are required to carry out its many functions. Some of the most considerable docking programs are Gold, Fred, and Flex. Moreover, they are useful in the prevision of protein and ligand`s binding conjunction (Kumar et al., 2013; Pagadala et al., 2017). In this respect, molecular docking is applied in different CSCs-related pathways including metabolic pathways and signaling pathways. Shedding light on metabolic pathways, the activity modification which can be applied by cancer cells, result in the production of metabolic precursors which leads to cancer cells anabolic and energetic requirement fulfilling. Furthermore, different metabolic pathways take a part in tumor progression and malignant tumor alterations. Accordingly, metabolic reprogramming is considered as one of the cancer insignias (Jagust et al., 2019b).

Herein, there will be a few examples in the context of some molecular docking usages in metabolic pathways such as 1) mitoketoscins application in targeting metabolic tumor promoters (OXCT1 and ACAT1) in both ketone re-utilization and mitochondrial function (Ozsvari et al., 2017). 2) Survivin protein interaction with andrographolide, which can lead to having an influence on human breast CSCs apoptosis (Wanandi et al., 2020). 3) S-phase kinase-associated protein-2 (Skp2) inhibition process by compound #25 which can result in CSCs survival suppression (Chan et al., 2013).

The other molecular docking-affected pathway in CSCs is the signaling pathway. This pathway is useful for targeted CSCs therapies expansion (Koury et al., 2017), embryonic evolvement, maintaining CSCs, etc. (Karamboulas and Ailles, 2013). Some molecular inhibitor agents of Wnt, Notch, Hh, and some other signaling pathways are implying as one of the important effects of molecular docking process on signaling pathways (Yang Y et al., 2020).

Modulating some target proteins is a striking aspect of molecular docking which has done by natural products. Natural products are able to be considered on the ground of multi-targeting drugs. As such, alkaloids are one of the natural products that have the strength to act as an anticancer lead molecule in the molecular docking process of CSCs. In this regard, Jaitak et al. provided an in-depth analysis of multitargeting drugs as an effective strategy to fight against CSCs and prevent disease recurrence. In this study, the authors examined the effect of some alkaloids that have anticancer potentiality by focusing on the Hh pathway in cancer stem cells. After selection and preparation of target ligands and proteins, Grid parameter selection and validation, implementation of glide docking module of Schrö6; dinger Maestro 9.6 suite, and determination of ADME profile for the studied alkanoid ligands, significant results were discovered. For instance, according to the findings of this study, emetine, and cortistatin, were able to target CSCs maintenance feature by binding to sonic Hh, smoothened (Smo) and, gli protein. Therefore, these two drugs can be applied as multi-targeting drugs in a combination with cancer chemotherapy compounds. Moreover, solamargine alkaloid could also have a good effect on gli protein and sonic hedgehog due to its pharmacophores. Furthermore, both solasonine and tylophorine modulated the Hh pathway and exert anticancer effects on CSCs by affecting only gli proteins. However, unlike other drugs, solamargine and solasonine need to improve the properties of ADME features (Jaitak, 2016).

In addition to alkaloids, the targeting of overexpressed CD44 surface marker in triple-negative breast cancer (TNBC) tissues can have an anticancer effect on CSCs. Regarding targeting CD44 surface markers, Yang et al. determined the positive role of drug carriers including Gambogic acid (GA)-loaded, zirconium-89 (89Zr)-labeled, chitosan (CS)-decorated multifunctional liposomes (MLPs) on TNBC CSCs by designing two *in vitro* and *in vivo* experiments. In this study, researchers examined 3D mammospheres and TNBC tissues of 32 women who were diagnosed with TNBC and found that the CD44 surface marker was overexpressed in the disease. Therefore, in this study, 89Zr@CS-MLPs were constructed and predicted how the drug carriers interact with CD44 surface markers in TNBC by applying molecular docking and dynamics simulations methods. The results obtained from the *in vitro* (examination on tumor cell lines) and *in vivo* (examination on mice) experiments were implied that 89Zr@CS-MLPs has a great potentiality for TNBC-targeted therapy as a drug carrier. Additionally, since Zr has a long half-life, it can also be used as an ideal radiolabel for positron emission tomography (PET) imaging of cancer. Moreover, 89Zr@CS-GA-MLPs have a high ability to target CSCs *in vivo* (Yang R et al., 2020).

In 2021, Hongwiangchan et al. demonstrated that hydroquinone 5-O-cinnamoyl ester of renieramycin M (CIN-RM) can be recognized as a fundamental approach in targeting lung CSCs

which has been confirmed by molecular docking computational analysis. The effect of CIN-RM is based on the reduction of CSCs markers and upstream inhibition of the AKT pathway. As a result of inhibition of Akt, the expression level of transcription factors involved in self-renewal, such as c-Myc, Nanog, Oct4, and Sox2, are decreased. It is, therefore, CSCs are suppressed and tumor growth can be inhibited. To a lesser extent, CIN-RM also induces its inhibitory effect on the mTOR pathway, but the inhibitory effect of CIN-RM on the protein kinase C (PKC) signal pathway was not significant. Another important result obtained in this study is that CIN-RM even has an effect on inactivating the AKT pathway related to c-Myc regulation of lung non-stem cancer cells, which can be a promising therapeutic approach in cancer treatment (**Figure 3**) (Hongwiangchan et al., 2021).

CONCLUSION AND FUTURE PERSPECTIVE

A comprehensive analyzing of CSCs, including signaling pathways and metabolic activities, as well as recognizing their distinctions with normal cells, is an essential technique in cancer targeted treatment (Bjerkvig et al., 2005; Shyh-Chang and Ng, 2017). Major obstacles to molecular binding as a targeted therapeutic technique include receptor flexibility, ligand flexibility, and drug resistance, all of which have contributed to cancer therapy failure (Meng et al., 2011). Computational methods or computer tools, which are a form of artificial intelligence (AI), have recently proven to be a useful approach in a variety of domains, including structure prediction, molecular bond modeling, and junction prediction (Menke et al., 2021). The mentioned methods are divided into two groups: classical and machine learning (ML), of which ML is widely used in molecular binding. Computational methods play a key role in molecular binding for drug design and discovery, and results can be analyzed cheaper and often faster than other conventional methods (Torres et al., 2019). Eventually, with the advancement of science and the identification of various computational methods, computing software and hardware are still being updated, and researchers are looking for the most accurate way to target CSCs for cancer treatment (Phillips et al., 2018).

AUTHOR CONTRIBUTIONS

All authors contributed to the study conception and design. SK Hamidpour, HY, and AS wrote the first draft. MT and KG helped to study and gather information. SA-M extensively edited the manuscript. BL participated in a critical review. BA helped supervise the project and gave final approval of the version to be published.

REFERENCES

Abbaszadegan, M. R., Bagheri, V., Razavi, M. S., Momtazi, A. A., Sahebkar, A., and Gholamin, M. (2017). Isolation, Identification, and Characterization of Cancer Stem Cells: A Review. *J. Cel Physiol* 232 (8), 2008–2018. doi:10.1002/jcp.25759

Abdullah, L. N., and Chow, E. K. (2013). Mechanisms of Chemoresistance in Cancer Stem Cells. *Clin. Transl Med.* 2 (1), 3–9. doi:10.1186/2001-1326-2-3

Ajani, J. A., Song, S., Hochster, H. S., and Steinberg, I. B. (2015). *Cancer Stem Cells: The Promise and the Potential. Paper Presented at the Seminars in Oncology*.

Allen, G. S., and Stokes, D. L. (2013). "Modeling, Docking, and Fitting of Atomic Structures to 3D Maps from Cryo-Electron Microscopy," in *Electron Crystallography of Soluble and Membrane Proteins* (Berlin, Germany: Springer), 229–241. doi:10.1007/978-1-62703-176-9_13

Arjmand, B. (2019a). *Genomics, Proteomics, and Metabolomics*.

Arjmand, B. (2019b). *Genomics, Proteomics, and Metabolomics: Stem Cells Monitoring in Regenerative Medicine*. Berlin, Germany: Springer Nature.

Bao, B., Ahmad, A., Azmi, A. S., Ali, S., and Sarkar, F. H. (2013). Overview of Cancer Stem Cells (CSCs) and Mechanisms of Their Regulation: Implications for Cancer Therapy. *Curr. Protoc. Pharmacol.* 14 (1), 14.25. doi:10.1002/0471141755.ph1425s61

Bedard, P. L., Hansen, A. R., Ratain, M. J., and Siu, L. L. (2013). Tumour Heterogeneity in the Clinic. *Nature* 501 (7467), 355–364. doi:10.1038/nature12627

Begicevic, R. R., Arfuso, F., and Falasca, M. (2019). Bioactive Lipids in Cancer Stem Cells. *World J. Stem Cell* 11 (9), 693–704. doi:10.4252/wjsc.v11.i9.693

Bellomo, C., Caja, L., and Moustakas, A. (2016). Transforming Growth Factor β as Regulator of Cancer Stemness and Metastasis. *Br. J. Cancer* 115 (7), 761–769. doi:10.1038/bjc.2016.255

Bjerkvig, R., Tysnes, B. B., Aboody, K. S., Najbauer, J., and Terzis, A. J. (2005). Opinion: the Origin of the Cancer Stem Cell: Current Controversies and New Insights. *Nat. Rev. Cancer* 5 (11), 899–904. doi:10.1038/nrc1740

Borah, A., Raveendran, S., Rochani, A., Maekawa, T., and Kumar, D. S. (2015). Targeting Self-Renewal Pathways in Cancer Stem Cells: Clinical Implications for Cancer Therapy. *Oncogenesis* 4 (11), e177. doi:10.1038/oncsis.2015.35

Chae, Y. C., and Kim, J. H. (2018). Cancer Stem Cell Metabolism: Target for Cancer Therapy. *BMB Rep.* 51 (7), 319–326. doi:10.5483/bmbrep.2018.51.7.112

Chan, C. H., Morrow, J. K., Li, C. F., Gao, Y., Jin, G., Moten, A., et al. (2013). Pharmacological Inactivation of Skp2 SCF Ubiquitin Ligase Restricts Cancer Stem Cell Traits and Cancer Progression. *Cell* 154 (3), 556–568. doi:10.1016/j.cell.2013.06.048

Charmsaz, S., Prencipe, M., Kiely, M., Pidgeon, G. P., and Collins, D. M. (2018). Innovative Technologies Changing Cancer Treatment. *Cancers (Basel)* 10 (6), 208. doi:10.3390/cancers10060208

Chen, K., Zhang, C., Ling, S., Wei, R., Wang, J., and Xu, X. (2021). The Metabolic Flexibility of Quiescent CSC: Implications for Chemotherapy Resistance. *Cel Death Dis.* 12 (9), 1–12. doi:10.1038/s41419-021-04116-6

Chen, M., Sharma, A., Lin, Y., Wu, Y., He, Q., Gu, Y., et al. (2019). Insluin and Epithelial Growth Factor (EGF) Promote Programmed Death Ligand 1(PD-L1) Production and Transport in colon Cancer Stem Cells. *BMC cancer* 19 (1), 153. doi:10.1186/s12885-019-5364-3

Chen, X., Chen, S., and Yu, D. (2020). Metabolic Reprogramming of Chemoresistant Cancer Cells and the Potential Significance of Metabolic Regulation in the Reversal of Cancer Chemoresistance. *Metabolites* 10 (7), 289. doi:10.3390/metabo10070289

Cho, Y., and Kim, Y. K. (2020). Cancer Stem Cells as a Potential Target to Overcome Multidrug Resistance. *Front. Oncol.* 10, 764. doi:10.3389/fonc.2020.00764

Chuthapisith, S., Eremin, J., El-Sheemey, M., and Eremin, O. (2010). Breast Cancer Chemoresistance: Emerging Importance of Cancer Stem Cells. *Surg. Oncol.* 19 (1), 27–32. doi:10.1016/j.suronc.2009.01.004

Cochrane, C. R., Szczepny, A., Watkins, D. N., and Cain, J. E. (2015). Hedgehog Signaling in the Maintenance of Cancer Stem Cells. *Cancers (Basel)* 7 (3), 1554–1585. doi:10.3390/cancers7030851

Cui, W., Aouidate, A., Wang, S., Yu, Q., Li, Y., and Yuan, S. (2020). Discovering Anti-cancer Drugs via Computational Methods. *Front. Pharmacol.* 11, 733. doi:10.3389/fphar.2020.00733

Cuyàs, E., Verdura, S., Fernández-Arroyo, S., Bosch-Barrera, J., Martin-Castillo, B., Joven, J., et al. (2017). Metabolomic Mapping of Cancer Stem Cells for Reducing and Exploiting Tumor Heterogeneity. *Oncotarget* 8 (59), 99223–99236. doi:10.18632/oncotarget.21834

Dando, I., Dalla Pozza, E., Biondani, G., Cordani, M., Palmieri, M., and Donadelli, M. (2015). The Metabolic Landscape of Cancer Stem Cells. *IUBMB life* 67 (9), 687–693. doi:10.1002/iub.1426

De Francesco, E. M., Sotgia, F., and Lisanti, M. P. (2018). Cancer Stem Cells (CSCs): Metabolic Strategies for Their Identification and Eradication. *Biochem. J.* 475 (9), 1611–1634. doi:10.1042/BCJ20170164

Deshmukh, A., Deshpande, K., Arfuso, F., Newsholme, P., and Dharmarajan, A. (2016). Cancer Stem Cell Metabolism: a Potential Target for Cancer Therapy. *Mol. Cancer* 15 (1), 69–10. doi:10.1186/s12943-016-0555-x

Ding, S., Li, C., Cheng, N., Cui, X., Xu, X., and Zhou, G. (2015). Redox Regulation in Cancer Stem Cells. *Oxid Med. Cel Longev* 2015, 750798. doi:10.1155/2015/750798

Dong, J. J., Ying, L., and Shi, K. Q. (2019). Expression of the Wnt Ligands Gene Family and its Relationship to Prognosis in Hepatocellular Carcinoma. *Cancer Cel Int* 19 (1), 34–11. doi:10.1186/s12935-019-0743-z

Du, F. Y., Zhou, Q. F., Sun, W. J., and Chen, G. L. (2019). Targeting Cancer Stem Cells in Drug Discovery: Current State and Future Perspectives. *World J. Stem Cell* 11 (7), 398–420. doi:10.4252/wjsc.v11.i7.398

Dunn, J., and Grider, M. H. (2020). *Physiology, Adenosine Triphosphate (ATP).*

Falahzadeh, K., Jalalvand, M., Alavi-Moghadam, S., Bana, N., and Negahdari, B. (2019). "Trying to Reveal the Mysteries of Stem Cells Using "Omics" Strategies," in *Genomics, Proteomics, and Metabolomics* (Berlin, Germany: Springer), 1–50. doi:10.1007/978-3-030-27727-7_1

Frasson, C., Rampazzo, E., Accordi, B., Beggio, G., Pistollato, F., Basso, G., et al. (2015). Inhibition of PI3K Signalling Selectively Affects Medulloblastoma Cancer Stem Cells. *Biomed. Research International* 2015, 973912. doi:10.1155/2015/973912

Gaggianesi, M., Di Franco, S., Pantina, V. D., Porcelli, G., D'Accardo, C., Verona, F., et al. (2021). Messing up the Cancer Stem Cell Chemoresistance Mechanisms Supported by Tumor Microenvironment. *Front. Oncol.* 2021, 2847. doi:10.3389/fonc.2021.702642

García-Heredia, J. M., and Carnero, A. (2020). Role of Mitochondria in Cancer Stem Cell Resistance. *Cells* 9 (7), 1693.

Gentric, G., Mieulet, V., and Mechta-Grigoriou, F. (2017). Heterogeneity in Cancer Metabolism: New Concepts in an Old Field. *Antioxid. Redox Signal.* 26 (9), 462–485. doi:10.1089/ars.2016.6750

Giacomini, I., Ragazzi, E., Pasut, G., and Montopoli, M. (2020). The Pentose Phosphate Pathway and its Involvement in Cisplatin Resistance. *Int. J. Mol. Sci.* 21 (3), 937. doi:10.3390/ijms21030937

Gilany, K., Jafarzadeh, N., Mani-Varnosfaderani, A., Minai-Tehrani, A., Sadeghi, M. R., Darbandi, M., et al. (2018). Metabolic Fingerprinting of Seminal Plasma from Non-obstructive Azoospermia Patients: Positive versus Negative Sperm Retrieval. *J. Reprod. Infertil* 19 (2), 109–114.

Gjorevski, N., Ranga, A., and Lutolf, M. P. (2014). Bioengineering Approaches to Guide Stem Cell-Based Organogenesis. *Development* 141 (9), 1794–1804. doi:10.1242/dev.101048

Goodarzi, P., Alavi-Moghadam, S., Payab, M., Larijani, B., Rahim, F., Gilany, K., et al. (2019). Metabolomics Analysis of Mesenchymal Stem Cells. *Int. J. Mol. Cel Med* 8 (Suppl. 1), 30–40. doi:10.22088/IJMCM.BUMS.8.2.30

Gopalan, V., Islam, F., and Lam, A. K.-y. (2018). "Surface Markers for the Identification of Cancer Stem Cells," in *Cancer Stem Cells* (Berlin, Germany: Springer), 17–29. doi:10.1007/978-1-4939-7401-6_2

Goyal, L., Hingmire, S., and Parikh, P. M. (2006). Newer Diagnostic Methods in Oncology. *Med. J. Armed Forces India* 62 (2), 162–168. doi:10.1016/S0377-1237(06)80062-6

Grisanzio, C., and Signoretti, S. (2008). p63 in Prostate Biology and Pathology. *J. Cel Biochem* 103 (5), 1354–1368. doi:10.1002/jcb.21555

Guerra, F., Arbini, A. A., and Moro, L. (2017). Mitochondria and Cancer Chemoresistance. *Biochim. Biophys. Acta Bioenerg.* 1858 (8), 686–699. doi:10.1016/j.bbabio.2017.01.012

Guha, M., Srinivasan, S., Ruthel, G., Kashina, A. K., Carstens, R. P., Mendoza, A., et al. (2014). Mitochondrial Retrograde Signaling Induces Epithelial-Mesenchymal Transition and Generates Breast Cancer Stem Cells. *Oncogene* 33 (45), 5238–5250. doi:10.1038/onc.2013.467

Hongwiangchan, N., Sriratanasak, N., Wichadakul, D., Aksorn, N., Chamni, S., and Chanvorachote, P. (2021). Hydroquinone 5-O-Cinnamoyl Ester of Renieramycin M Suppresses Lung Cancer Stem Cells by Targeting Akt and Destabilizes C-Myc. *Pharmaceuticals (Basel)* 14 (11), 1112. doi:10.3390/ph14111112

Hughes, J. P., Rees, S., Kalindjian, S. B., and Philpott, K. L. (2011). Principles of Early Drug Discovery. *Br. J. Pharmacol.* 162 (6), 1239–1249. doi:10.1111/j.1476-5381.2010.01127.x

Hung, K. F., Yang, T., and Kao, S. Y. (2019). Cancer Stem Cell Theory: Are We Moving Past the Mist? *J. Chin. Med. Assoc.* 82 (11), 814–818. doi:10.1097/JCMA.0000000000000186

Jagust, P., de Luxán-Delgado, B., Parejo-Alonso, B., and Sancho, P. (2019b). Metabolism-based Therapeutic Strategies Targeting Cancer Stem Cells. *Front. Pharmacol.* 10, 203. doi:10.3389/fphar.2019.00203

Jagust, P., de Luxán-Delgado, B., Parejo-Alonso, B., and Sancho, P. (2019). Metabolism-Based Therapeutic Strategies Targeting Cancer Stem Cells. *Front. Pharmacol.* 10, 203. doi:10.3389/fphar.2019.00203

Jaitak, V. (2016). Molecular Docking Study of Natural Alkaloids as Multi-Targeted Hedgehog Pathway Inhibitors in Cancer Stem Cell Therapy. *Comput. Biol. Chem.* 62, 145–154.

Jin, W. (2020). Role of JAK/STAT3 Signaling in the Regulation of Metastasis, the Transition of Cancer Stem Cells, and Chemoresistance of Cancer by Epithelial-Mesenchymal Transition. *Cells* 9 (1), 217. doi:10.3390/cells9010217

Jin, X., Jin, X., and Kim, H. (2017). Cancer Stem Cells and Differentiation Therapy. *Tumour Biol.* 39 (10), 1010428317729933. doi:10.1177/1010428317729933

Karamboulas, C., and Ailles, L. (2013). Developmental Signaling Pathways in Cancer Stem Cells of Solid Tumors. *Biochim. Biophys. Acta* 1830 (2), 2481–2495. doi:10.1016/j.bbagen.2012.11.008

Kershaw, N. M., Wright, G. S., Sharma, R., Antonyuk, S. V., Strange, R. W., Berry, N. G., et al. (2013). X-ray Crystallography and Computational Docking for the Detection and Development of Protein-Ligand Interactions. *Curr. Med. Chem.* 20 (4), 569–575. doi:10.2174/0929867311320040008

Khatami, F., Tavangar, S. M., and Pour, N. K. (2019). "Genomics, Proteomics, and Metabolomics of Cancer Stem Cells (CSCs)," in *Genomics, Proteomics, and Metabolomics* (Berlin, Germany: Springer), 159–179. doi:10.1007/978-3-030-27727-7_9

Klonisch, T., Wiechec, E., Hombach-Klonisch, S., Ande, S. R., Wesselborg, S., Schulze-Osthoff, K., et al. (2008). Cancer Stem Cell Markers in Common Cancers - Therapeutic Implications. *Trends Mol. Med.* 14 (10), 450–460. doi:10.1016/j.molmed.2008.08.003

Koury, J., Zhong, L., and Hao, J. (2017). Targeting Signaling Pathways in Cancer Stem Cells for Cancer Treatment. *Stem Cell Int.* 2017, 2925869. doi:10.1155/2017/2925869

Krstic, J., Trivanovic, D., Jaukovic, A., Santibanez, J. F., and Bugarski, D. (2017). Metabolic Plasticity of Stem Cells and Macrophages in Cancer. *Front. Immunol.* 8, 939. doi:10.3389/fimmu.2017.00939

Kumar, A., Bhanja, A., Bhattacharyya, J., and Jaganathan, B. G. (2016). Multiple Roles of CD90 in Cancer. *Tumour Biol.* 37 (9), 11611–11622. doi:10.1007/s13277-016-5112-0

Kumar, D., Shankar, S., and Srivastava, R. K. (2013). Rottlerin-induced Autophagy Leads to the Apoptosis in Breast Cancer Stem Cells: Molecular Mechanisms. *Mol. Cancer* 12 (1), 171. doi:10.1186/1476-4598-12-171

Kuramoto, K., Yamamoto, M., Suzuki, S., Togashi, K., Sanomachi, T., Kitanaka, C., et al. (2021). Inhibition of the Lipid Droplet-Peroxisome Proliferator-Activated Receptor α Axis Suppresses Cancer Stem Cell Properties. *Genes (Basel)* 12 (1), 99. doi:10.3390/genes12010099

Kurutas, E. B. (2016). The Importance of Antioxidants Which Play the Role in Cellular Response against Oxidative/nitrosative Stress: Current State. *Nutr. J.* 15 (1), 71. doi:10.1186/s12937-016-0186-5

Larijani, B., Goodarzi, P., Payab, M., Alavi-Moghadam, S., Rahim, F., Bana, N., et al. (2019). Metabolomics and Cell Therapy in Diabetes Mellitus. *Int. J. Mol. Cel Med* 8 (Suppl. 1), 41–48. doi:10.22088/IJMCM.BUMS.8.2.41

Lee, S. H., Reed-Newman, T., Anant, S., and Ramasamy, T. S. (2020). Regulatory Role of Quiescence in the Biological Function of Cancer Stem Cells. *Stem Cel Rev Rep* 16 (6), 1185–1207. doi:10.1007/s12015-020-10031-8

Li, L., and Bhatia, R. (2011). Stem Cell Quiescence. *Clin. Cancer Res.* 17 (15), 4936–4941. doi:10.1158/1078-0432.CCR-10-1499

Liao, C., Peach, M. L., Yao, R., and Nicklaus, M. C. (2013). "Molecular Docking and Structure-Based Virtual Screening," in *Future Medicine*. doi:10.4155/ebo.13.181

Liou, G. Y., and Storz, P. (2010). Reactive Oxygen Species in Cancer. *Free Radic. Res.* 44 (5), 479–496. doi:10.3109/10715761003667554

Liu, R., Chen, Y., Liu, G., Li, C., Song, Y., Cao, Z., et al. (2020). PI3K/AKT Pathway as a Key Link Modulates the Multidrug Resistance of Cancers. *Cell Death Dis* 11 (9), 797. doi:10.1038/s41419-020-02998-6

Liu, S., Chen, S., and Zeng, J. (2018). TGF-β S-ignaling: A C-omplex R-ole in T-umorigenesis (Review). *Mol. Med. Rep.* 17 (1), 699–704. doi:10.3892/mmr.2017.7970

Liu, Y., Liu, X., Chen, L.-C., Du, W.-Z., Cui, Y.-Q., Piao, X.-Y., et al. (2014). Targeting Glioma Stem Cells via the Hedgehog Signaling Pathway. *Neuroimmunology and Neuroinflammation* 1, 51–59.

Lobo, N. A., Shimono, Y., Qian, D., and Clarke, M. F. (2007). The Biology of Cancer Stem Cells. *Annu. Rev. Cel Dev. Biol.* 23, 675–699. doi:10.1146/annurev.cellbio.22.010305.104154

Lohning, A. E., Levonis, S. M., Williams-Noonan, B., and Schweiker, S. S. (2017). A Practical Guide to Molecular Docking and Homology Modelling for Medicinal Chemists. *Curr. Top. Med. Chem.* 17 (18), 2023–2040. doi:10.2174/1568026617666170130110827

Luo, M., and Wicha, M. S. (2015). Metabolic Plasticity of Cancer Stem Cells. *Oncotarget* 6 (34), 35141–35142. doi:10.18632/oncotarget.6177

Madhavilatha, K. N., and Babu, G. R. M. (2019). Systematic Approach for Enrichment of Docking Outcome Using Consensus Scoring Functions. *J. Phys. Conf. Ser.* 1228, 012019. doi:10.1088/1742-6596/1228/1/012019

Madhunapantula, S. V., Mosca, P. J., and Robertson, G. P. (2011). The Akt Signaling Pathway: an Emerging Therapeutic Target in Malignant Melanoma. *Cancer Biol. Ther.* 12 (12), 1032–1049. doi:10.4161/cbt.12.12.18442

Mancini, R., Noto, A., Pisanu, M. E., De Vitis, C., Maugeri-Saccà, M., and Ciliberto, G. (2018). Metabolic Features of Cancer Stem Cells: the Emerging Role of Lipid Metabolism. *Oncogene* 37 (18), 2367–2378. doi:10.1038/s41388-018-0141-3

Matsui, W. H. (2016). Cancer Stem Cell Signaling Pathways. *Medicine (Baltimore)* 95 (Suppl. 1), S8. doi:10.1097/MD.0000000000004765

Meng, X. Y., Zhang, H. X., Mezei, M., and Cui, M. (2011). Molecular Docking: a Powerful Approach for Structure-Based Drug Discovery. *Curr. Comput. Aided Drug Des.* 7 (2), 146–157. doi:10.2174/157340911795677602

Menke, J., Maskri, S., and Koch, O. (2021). Computational Ion Channel Research: from the Application of Artificial Intelligence to Molecular Dynamics Simulations. *Cell Physiol. Biochem. Int. J. Exp. Cell. Physiol. Biochem. Pharmacol.* 55 (S3), 14–45.

Miricescu, D., Totan, A., Stanescu-Spinu, I.-I., Badoiu, S. C., Stefani, C., and Greabu, M. (2021). PI3K/AKT/mTOR Signaling Pathway in Breast Cancer: From Molecular Landscape to Clinical Aspects. *Int. J. Mol. Sci.* 22 (1), 173. doi:10.3390/ijms22179512

Mohr, M., Zänker, K. S., and Dittmar, T. (2015). Cancer (Stem) Cell Differentiation: An Inherent or Acquired Property? *Med. Hypotheses* 85 (6), 1012–1018. doi:10.1016/j.mehy.2015.08.017

Mohs, R. C., and Greig, N. H. (2017). Drug Discovery and Development: Role of Basic Biological Research. *Alzheimers Dement (N Y)* 3 (4), 651–657. doi:10.1016/j.trci.2017.10.005

Morris, G. M., and Lim-Wilby, M. (2008). "Molecular Docking," in *Molecular Modeling of Proteins* (Berlin, Germany: Springer), 365–382. doi:10.1007/978-1-59745-177-2_19

Mukha, A., and Dubrovska, A. (2020). Metabolic Targeting of Cancer Stem Cells. *Front. Oncol.* 10, 537930. doi:10.3389/fonc.2020.537930

Najafi, M., Farhood, B., and Mortezaee, K. (2019). Cancer Stem Cells (CSCs) in Cancer Progression and Therapy. *J. Cel Physiol* 234 (6), 8381–8395. doi:10.1002/jcp.27740

Niehrs, C. (2012). The Complex World of WNT Receptor Signalling. *Nat. Rev. Mol. Cel Biol* 13 (12), 767–779. doi:10.1038/nrm3470

Nunes, T., Hamdan, D., Leboeuf, C., El Bouchtaoui, M., Gapihan, G., Nguyen, T. T., et al. (2018). Targeting Cancer Stem Cells to Overcome Chemoresistance. *Int. J. Mol. Sci.* 19 (12), 4036. doi:10.3390/ijms19124036

Organization, W. H. (2020). *WHO Report on Cancer: Setting Priorities, Investing Wisely and Providing Care for All*. Geneve, Switzerland: WHO.

Ozsvari, B., Sotgia, F., Simmons, K., Trowbridge, R., Foster, R., and Lisanti, M. P. (2017). Mitoketoscins: Novel Mitochondrial Inhibitors for Targeting Ketone Metabolism in Cancer Stem Cells (CSCs). *Oncotarget* 8 (45), 78340–78350. doi:10.18632/oncotarget.21259

Pagadala, N. S., Syed, K., and Tuszynski, J. (2017). Software for Molecular Docking: a Review. *Biophys. Rev.* 9 (2), 91–102. doi:10.1007/s12551-016-0247-1

Peixoto, J., and Lima, J. (2018). Metabolic Traits of Cancer Stem Cells. *Dis. Model. Mech.* 11 (8), 33464. doi:10.1242/dmm.033464

Phi, L. T. H., Sari, I. N., Yang, Y.-G., Lee, S.-H., Jun, N., Kim, K. S., et al. (2018). Cancer Stem Cells (CSCs) in Drug Resistance and Their Therapeutic Implications in Cancer Treatment. *Stem Cell Int.* 2018, 5416923. doi:10.1155/2018/5416923

Phillips, M. A., Stewart, M. A., Woodling, D. L., and Xie, Z.-R. (2018). *Has Molecular Docking Ever Brought us a Medicine. Molecular Docking*. London, UK: IntechOpen, 141–178.

Piraino, S. W., Thomas, V., O'Donovan, P., and Furney, S. J. (2019). *Mutations: Driver versus Passenger*.

Polat, I. H., Tarrado-Castellarnau, M., Bharat, R., Perarnau, J., Benito, A., Cortés, R., et al. (2021). Oxidative Pentose Phosphate Pathway Enzyme 6-Phosphogluconate Dehydrogenase Plays a Key Role in Breast Cancer Metabolism. *Biology (Basel)* 10 (2), 85. doi:10.3390/biology10020085

Poljsak, B., Šuput, D., and Milisav, I. (2013). Achieving the Balance between ROS and Antioxidants: when to Use the Synthetic Antioxidants. *Oxid Med. Cel Longev* 2013, 956792. doi:10.1155/2013/956792

Prager, B. C., Xie, Q., Bao, S., and Rich, J. N. (2019). Cancer Stem Cells: the Architects of the Tumor Ecosystem. *Cell Stem Cell* 24 (1), 41–53. doi:10.1016/j.stem.2018.12.009

Prasetyanti, P. R., and Medema, J. P. (2017). Intra-tumor Heterogeneity from a Cancer Stem Cell Perspective. *Mol. Cancer* 16 (1), 41–49. doi:10.1186/s12943-017-0600-4

Pucci, C., Martinelli, C., and Ciofani, G. (2019). Innovative Approaches for Cancer Treatment: Current Perspectives and New Challenges. *Ecancermedicalscience* 13, 961. doi:10.3332/ecancer.2019.961

Rahim, F., Arjmand, B., Shirbandi, K., Payab, M., and Larijani, B. (2018). Stem Cell Therapy for Patients with Diabetes: a Systematic Review and Meta-Analysis of Metabolomics-Based Risks and Benefits. *Stem Cel Investig* 5, 40. doi:10.21037/sci.2018.11.01

Ramón Y Cajal, S., Sesé, M., Capdevila, C., Aasen, T., De Mattos-Arruda, L., Diaz-Cano, S. J., et al. (2020). Clinical Implications of Intratumor Heterogeneity: Challenges and Opportunities. *J. Mol. Med. (Berl)* 98 (2), 161–177. doi:10.1007/s00109-020-01874-2

Reddy, A. S., Pati, S. P., Kumar, P. P., Pradeep, H. N., and Sastry, G. N. (2007). Virtual Screening in Drug Discovery -- a Computational Perspective. *Curr. Protein Pept. Sci.* 8 (4), 329–351. doi:10.2174/138920307781369427

Riganti, C., Gazzano, E., Polimeni, M., Aldieri, E., and Ghigo, D. (2012). The Pentose Phosphate Pathway: an Antioxidant Defense and a Crossroad in Tumor Cell Fate. *Free Radic. Biol. Med.* 53 (3), 421–436. doi:10.1016/j.freeradbiomed.2012.05.006

Salmaso, V., and Moro, S. (2018). Bridging Molecular Docking to Molecular Dynamics in Exploring Ligand-Protein Recognition Process: An Overview. *Front. Pharmacol.* 9 (923), 923. doi:10.3389/fphar.2018.00923

Schöning, J. P., Monteiro, M., and Gu, W. (2017). Drug Resistance and Cancer Stem Cells: the Shared but Distinct Roles of Hypoxia-inducible Factors HIF 1α and HIF 2α. *Clin. Exp. Pharmacol. Physiol.* 44 (2), 153–161.

Sethi, A., Joshi, K., Sasikala, K., and Alvala, M. (2019). Molecular Docking in Modern Drug Discovery: Principles and Recent Applications. *Drug Discov. Develop. New Adv* 2019, 27–39.

Shah, S. C., Kayamba, V., Peek, R. M., Jr, and Heimburger, D. (2019). Cancer Control in Low- and Middle-Income Countries: Is it Time to Consider Screening? *J. Glob. Oncol.* 5, 1–8. doi:10.1200/JGO.18.00200

Shi, X., Zhang, Y., Zheng, J., and Pan, J. (2012). Reactive Oxygen Species in Cancer Stem Cells. *Antioxid. Redox Signal.* 16 (11), 1215–1228. doi:10.1089/ars.2012.4529

Shin, M. K., and Cheong, J. H. (2019). Mitochondria-centric Bioenergetic Characteristics in Cancer Stem-like Cells. *Arch. Pharm. Res.* 42 (2), 113–127. doi:10.1007/s12272-019-01127-y

Shyh-Chang, N., and Ng, H. H. (2017). The Metabolic Programming of Stem Cells. *Genes Dev.* 31 (4), 336–346. doi:10.1101/gad.293167.116

Singh, A., and Settleman, J. (2010). EMT, Cancer Stem Cells and Drug Resistance: an Emerging axis of Evil in the War on Cancer. *Oncogene* 29 (34), 4741–4751. doi:10.1038/onc.2010.215

Snaebjornsson, M. T., Janaki-Raman, S., and Schulze, A. (2020). Greasing the Wheels of the Cancer Machine: the Role of Lipid Metabolism in Cancer. *Cell Metab* 31 (1), 62–76. doi:10.1016/j.cmet.2019.11.010

Snyder, V., Reed-Newman, T. C., Arnold, L., Thomas, S. M., and Anant, S. (2018). Cancer Stem Cell Metabolism and Potential Therapeutic Targets. *Front. Oncol.* 8, 203. doi:10.3389/fonc.2018.00203

Sturlese, M., Bellanda, M., and Moro, S. (2015). NMR-assisted Molecular Docking Methodologies. *Mol. Inform.* 34 (8), 513–525. doi:10.1002/minf.201500012

Sung, H., Ferlay, J., Siegel, R. L., Laversanne, M., Soerjomataram, I., Jemal, A., et al. (2021). Global Cancer Statistics 2020: GLOBOCAN Estimates of Incidence and

Mortality Worldwide for 36 Cancers in 185 Countries. *CA A. Cancer J. Clin.* 71 (3), 209–249. doi:10.3322/caac.21660

Tamada, M., Nagano, O., Tateyama, S., Ohmura, M., Yae, T., Ishimoto, T., et al. (2012). Modulation of Glucose Metabolism by CD44 Contributes to Antioxidant Status and Drug Resistance in Cancer Cells. *Cancer Res.* 72 (6), 1438–1448. doi:10.1158/0008-5472.CAN-11-3024

Tang, C., Ang, B. T., and Pervaiz, S. (2007). Cancer Stem Cell: Target for Anti-cancer Therapy. *FASEB J.* 21 (14), 3777–3785. doi:10.1096/fj.07-8560rev

Tayanloo-Beik, A., Sarvari, M., Payab, M., Gilany, K., Alavi-Moghadam, S., Gholami, M., et al. (2020). OMICS Insights into Cancer Histology; Metabolomics and Proteomics Approach. *Clin. Biochem.* 84, 13–20. doi:10.1016/j.clinbiochem.2020.06.008

Thomas, M., Coyle, K., Sultan, M., Vaghar-Kashani, A., and Marcato, P. (2014). Chemoresistance in Cancer Stem Cells and Strategies to Overcome Resistance. *Chemotherapy* 3 (125), 2.

Tirino, V., Desiderio, V., Paino, F., De Rosa, A., Papaccio, F., La Noce, M., et al. (2013). Cancer Stem Cells in Solid Tumors: an Overview and New Approaches for Their Isolation and Characterization. *FASEB J.* 27 (1), 13–24. doi:10.1096/fj.12-218222

Toh, T. B., Lim, J. J., and Chow, E. K. (2017). Epigenetics in Cancer Stem Cells. *Mol. Cancer* 16 (1), 29–20. doi:10.1186/s12943-017-0596-9

Torres, P. H. M., Sodero, A. C. R., Jofily, P., and Silva-Jr, F. P., Jr (2019). Key Topics in Molecular Docking for Drug Design. *Int. J. Mol. Sci.* 20 (18), 4574. doi:10.3390/ijms20184574

Turnquist, C., Watson, R. A., Protheroe, A., Verrill, C., and Sivakumar, S. (2019). Tumor Heterogeneity: Does it Matter? *Expert Rev. Anticancer Ther.* 19 (10), 857–867. doi:10.1080/14737140.2019.1667236

Tyagi, S., Gupta, P., Saini, A. S., Kaushal, C., and Sharma, S. (2011). The Peroxisome Proliferator-Activated Receptor: A Family of Nuclear Receptors Role in Various Diseases. *J. Adv. Pharm. Technol. Res.* 2 (4), 236–240. doi:10.4103/2231-4040.90879

Vineis, P., and Wild, C. P. (2014). Global Cancer Patterns: Causes and Prevention. *Lancet* 383 (9916), 549–557. doi:10.1016/S0140-6736(13)62224-2

Visweswaran, M., Arfuso, F., Warrier, S., and Dharmarajan, A. (2020). Aberrant Lipid Metabolism as an Emerging Therapeutic Strategy to Target Cancer Stem Cells. *Stem cells* 38 (1), 6–14. doi:10.1002/stem.3101

Wanandi, S. I., Limanto, A., Yunita, E., Syahrani, R. A., Louisa, M., Wibowo, A. E., et al. (2020). In Silico and *In Vitro* Studies on the Anti-cancer Activity of Andrographolide Targeting Survivin in Human Breast Cancer Stem Cells. *PloS one* 15 (11), e0240020. doi:10.1371/journal.pone.0240020

Wang, A., Chen, L., Li, C., and Zhu, Y. (2015). Heterogeneity in Cancer Stem Cells. *Cancer Lett.* 357 (1), 63–68. doi:10.1016/j.canlet.2014.11.040

Wang, R., Lu, Y., and Wang, S. (2003). Comparative Evaluation of 11 Scoring Functions for Molecular Docking. *J. Med. Chem.* 46 (12), 2287–2303. doi:10.1021/jm0203783

Xia, P., and Xu, X. Y. (2015). PI3K/Akt/mTOR Signaling Pathway in Cancer Stem Cells: from Basic Research to Clinical Application. *Am. J. Cancer Res.* 5 (5), 1602–1609.

Yadav, U. P., Singh, T., Kumar, P., Sharma, P., Kaur, H., Sharma, S., et al. (2020). Metabolic Adaptations in Cancer Stem Cells. *Front. Oncol.* 10, 1010. doi:10.3389/fonc.2020.01010

Yang, L., Shi, P., Zhao, G., Xu, J., Peng, W., Zhang, J., et al. (2020). Targeting Cancer Stem Cell Pathways for Cancer Therapy. *Signal. Transduct Target. Ther.* 5 (1), 8–35. doi:10.1038/s41392-020-0110-5

Yang, R., Lu, M., Ming, L., Chen, Y., Cheng, K., Zhou, J., et al. (2020). 89Zr-Labeled Multifunctional Liposomes Conjugate Chitosan for PET-Trackable Triple-Negative Breast Cancer Stem Cell Targeted Therapy. *Int. J. Nanomedicine* 15, 9061–9074. doi:10.2147/IJN.S262786

Yang, Y., Li, X., Wang, T., Guo, Q., Xi, T., and Zheng, L. (2020). Emerging Agents that Target Signaling Pathways in Cancer Stem Cells. *J. Hematol. Oncol.* 13, 60–18. doi:10.1186/s13045-020-00901-6

Yi, M., Li, J., Chen, S., Cai, J., Ban, Y., Peng, Q., et al. (2018). Emerging Role of Lipid Metabolism Alterations in Cancer Stem Cells. *J. Exp. Clin. Cancer Res.* 37 (1), 1–18. doi:10.1186/s13046-018-0784-5

Yu, S. S., and Cirillo, N. (2020). The Molecular Markers of Cancer Stem Cells in Head and Neck Tumors. *J. Cel Physiol* 235 (1), 65–73. doi:10.1002/jcp.28963

Zhang, B. B., Wang, D. G., Guo, F. F., and Xuan, C. (2015). Mitochondrial Membrane Potential and Reactive Oxygen Species in Cancer Stem Cells. *Fam. Cancer* 14 (1), 19–23. doi:10.1007/s10689-014-9757-9

Zhao, J. (2016). Cancer Stem Cells and Chemoresistance: The Smartest Survives the Raid. *Pharmacol. Ther.* 160, 145–158. doi:10.1016/j.pharmthera.2016.02.008

Zhou, D., Shao, L., and Spitz, D. R. (2014). Reactive Oxygen Species in normal and Tumor Stem Cells. *Adv. Cancer Res.* 122, 1–67. doi:10.1016/B978-0-12-420117-0.00001-3

Zhu, P., and Fan, Z. (2018). Cancer Stem Cells and Tumorigenesis. *Biophys. Rep.* 4 (4), 178–188. doi:10.1007/s41048-018-0062-2

Zhu, X., Chen, H. H., Gao, C. Y., Zhang, X. X., Jiang, J. X., Zhang, Y., et al. (2020). Energy Metabolism in Cancer Stem Cells. *World J. Stem Cell* 12 (6), 448–461. doi:10.4252/wjsc.v12.i6.448

Zong, W. X., Rabinowitz, J. D., and White, E. (2016). Mitochondria and Cancer. *Mol. Cel* 61 (5), 667–676. doi:10.1016/j.molcel.2016.02.011

Conflict of Interest: The authors declare that the research was conducted in the absence of any commercial or financial relationships that could be construed as a potential conflict of interest.

Publisher's Note: All claims expressed in this article are solely those of the authors and do not necessarily represent those of their affiliated organizations, or those of the publisher, the editors, and the reviewers. Any product that may be evaluated in this article, or claim that may be made by its manufacturer, is not guaranteed or endorsed by the publisher.

GLOSSARY

IARC: international agency for research on cancer

WHO: world health organization

CSCs: cancer stem cells

MRPs: multidrug resistance proteins

EMT: epithelial-to-mesenchymal transition

OXPHOS: oxidative phosphorylation

hESCs: human embryonic stem cells

NF-κB: nuclear factor-κB

JAK-STAT: janus kinase/signal transducers and activators of transcription

PI3K/AKT/mTOR: phosphoinositide 3-kinase/AKT/mammalian target of rapamycin

TGF: transforming growth factor

PPAR: peroxisome proliferator-activated receptor

ATP: adenosine triphosphate

TCA: tricarboxylic acid cycle

FAO: fatty acid oxidation

ROS: reactive oxygen species

Skp2: S-phase kinase-associated protein-2

mtDNA: mitochondrial DNA

nDNA: nuclear DNA

BAX: B-cell lymphoma 2 associated X, apoptosis regulator

PDAC: pancreatic ductal adenocarcinoma

LDs: lipid droplets

SREBP1: sterol regulatory element-binding transcription factor 1

SCD: stearoyl-CoA desaturase

FASN: fatty acid synthase

CPT: carnitine palmitoyltransferase

Hh: hedgehog

PPP: pentose phosphate pathway

G6P: glucose 6-phosphate

NADPH: nicotinamide adenine dinucleotide phosphate

CAC: citric acid cycle

NMR: nuclear magnetic resonance

Cryo-EM: cryo-electron microscopy

TICs: tumor-initiating cells

SBVS: structure-based virtual screening

EM: electron microscopy

TNBC: triple-negative breast cancer

Smo: smoothened

GA: gambogic acid

CS: chitosan

MLPs: multifunctional liposomes

CIN-RM: hydroquinone 5-O-cinnamoyl ester of renieramycin M

PET: positron emission tomography

PKC: protein kinase C

AI: artificial intelligence

frontiers in Pharmacology

ORIGINAL RESEARCH
published: 07 March 2022
doi: 10.3389/fphar.2022.837543

Gut Microbiota-Mediated Elevated Production of Secondary Bile Acids in Chronic Unpredictable Mild Stress

Yuchen Qu[1†], Cunjin Su[1†], Qinhong Zhao[1], Aiming Shi[1], Fenglun Zhao[1], Liuxing Tang[1], Delai Xu[1], Zheng Xiang[1], Yang Wang[2], Yueyuan Wang[1], Jie Pan[1] and Yunli Yu[1]**

[1]Department of Pharmacy, The Second Affiliated Hospital of Soochow University, Suzhou, China, [2]College of Pharmaceutical Science, Soochow University, Suzhou, China

A growing body of evidence suggests that gut microbiota could participate in the progression of depression *via* the microbiota–gut–brain axis. However, the detailed microbial metabolic profile changes in the progression of depression is still not fully elucidated. In this study, a liquid chromatography coupled to mass spectrometry-based untargeted serum high-throughput metabolomics method was first performed to screen for potential biomarkers in a depressive-like state in a chronic unpredictable mild stress (CUMS)-induced mouse model. Our results identified that the bile acid and energy metabolism pathways were significantly affected in CUMS progression. The detailed bile acid profiles were subsequently quantified in the serum, liver, and feces. The results showed that CUMS significantly promoted the deconjugation of conjugated bile acid and secondary bile acid biosynthesis. Furthermore, 16S rRNA gene sequencing revealed that the increased secondary bile acid levels in the feces positively correlated with *Ruminococcaceae_UCG-010*, *Ruminococcus*, and *Clostridia_UCG-014* abundance. Taken together, our study suggested that changes in family *Ruminococcaceae* abundance following chronic stress increased biosynthesis of deoxycholic acid (DCA), a unconjugated secondary bile acid in the intestine. Aberrant activation of secondary bile acid biosynthesis pathway thereby increased the hydrophobicity of the bile acid pool, which might, in turn, promoted metabolic disturbances and disease progression in CUMS mice.

Keywords: CUMS, bile acid, gut microbiota, depression, *Ruminococcaceae*

OPEN ACCESS

Edited by:
Linsheng Liu,
The First Affiliated Hospital of Soochow University, China

Reviewed by:
Xiaoliang Li,
Heilongjiang University of Chinese Medicine, China
Di Zhao,
China Pharmaceutical University, China

****Correspondence:***
Yunli Yu
haoyyl0902@163.com
Jie Pan
panzy1122@163.com

[†]These authors have contributed equally to this work and share first authorship

Specialty section:
This article was submitted to Translational Pharmacology, a section of the journal Frontiers in Pharmacology

Received: *16 December 2021*
Accepted: *25 January 2022*
Published: *07 March 2022*

Citation:
Qu Y, Su C, Zhao Q, Shi A, Zhao F, Tang L, Xu D, Xiang Z, Wang Y, Wang Y, Pan J and Yu Y (2022) Gut Microbiota-Mediated Elevated Production of Secondary Bile Acids in Chronic Unpredictable Mild Stress. Front. Pharmacol. 13:837543. doi: 10.3389/fphar.2022.837543

INTRODUCTION

According to the World Health Organization, an estimated 3.8% of the global population has been affected by depression and the number is still increasing worldwide (World Health Organization, 2021). Modern psychology- and biology-related concepts revealed that depression is not only a common psychological disorder, but also a physical disease complex involving the imbalance of neurotransmitters, injury of neurogenesis, decline of neuroplasticity, and abnormality of neuronal circuitry (Chaudhury et al., 2015; Liu et al., 2017). Recently, with the development of gut microbiota research, a growing body of evidence indicates that the microbiota–gut–brain axis plays an essential role in regulating human behavior and brain function (Foster and McVey Neufeld, 2013; Liang et al., 2018).

An important function of the gut microbiota is participating in bile acid metabolism. Bile acids are the major constituents of the human bile synthesized from cholesterol by perivenous hepatocytes,

playing an important role in dietary fat digestion and absorption (Hofmann., 1999). Most bile acids undergo enterohepatic circulation and microbial biotransformation in the intestinal tract (Chiang and Ferrell, 2018). Cholic and chenodeoxycholic acid are the two primary bile acids synthesized in the liver by a series of enzymatic reactions (Russell., 2003), conjugated with either glycine or taurine, and stored in the gallbladder (He et al., 2003). Bile acids are then secreted into the gastrointestinal tract, where they are subsequently deconjugated, dehydroxylated, and oxidized in the intestinal lumen by gut microbes to generate hydrophobic secondary bile acids: deoxycholic and lithocholic acid (Ridlon et al., 2014).

Recent studies revealed that bile acids might serve as intermediate messengers between the gut and the brain (Monteiro-Cardoso et al., 2021), while the relationship between bile acids and depression have rarely been investigated. In this study, we constructed a chronic unpredictable mild stress (CUMS) model to mimic depression-like symptoms in mice. We sought to explore potential gut microbiota-associated metabolites and the relationship between bile acid metabolic profiles and gut microbiota altered in CUMS progression.

MATERIALS AND METHODS

Chemicals and Reagents

Cholic acid (CA), chenodeoxycholic acid (CDCA), ursodeoxycholic acid (UDCA), deoxycholic acid (DCA), lithocholic acid (LCA), taurocholic acid (TCA), taurochenodeoxycholic acid (TCDCA), tauroursodeoxycholic acid (TUDCA), taurodeoxycholic acid (TDCA), taurolithocholic acid (TLCA), glycocholic acid (GCA), glycochenodeoxycholic acid (GCDCA), glycoursodeoxycholic acid (GUDCA), glycodeoxycholic acid (GDCA), and lithocholic acid-2,2,3,4,4-d5 (internal standard) were all purchased from Sigma-Aldrich (St. Louis, MO, USA). Glycolithocholic acid (GLCA) was purchased from J&K Scientific Ltd. (Shanghai, China). HPLC-grade ammonium formate (≥99%), ammonium acetate, methanol, and acetonitrile were purchased from Merck KGaA (Darmstadt, Germany). HPLC-grade formic acid (99%) was purchased from Anaqua Chemicals Supply (Wilmington, USA).

Animals and CUMS Experiment

Seven-week-old male ICR mice were purchased from SLAC Laboratory Animal Co., Ltd. (Shanghai, China). After their arrival, mice were single-caged and divided into the normal control group and the CUMS model group of 12 animals each randomly based on their body weight and sucrose preference test results. Mice were acclimated for 7 days in a temperature-(23–26°C) and humidity-controlled (40–60%) room under a 12-h light/dark cycle (lights on 07:00–19:00) with free access to food and water. During the modeling period, mice were weighed biweekly.

CUMS progression contained a total of 8 different stimulations including: 1) food deprivation for 24 h, 2) water deprivation for 24 h, 3) damp sawdust for 24 h, 4) tail pinching for 2 min, 5) restraint for 1 h, 6) cage tilting at 45° for 24 h, 7) cold swimming for 10 min, and 8) day and night reversal for 24 h. Two or three types of stimulations were delivered daily and randomly to the mice in the model groups for 56 days.

Behavioral Tests and Sample Collection

Depression-related behavioral tests including the sucrose preference test (SPT), forced swim test (FST), and tail suspension test (TST) were performed during the experimental period.

For the SPT, all mice were habituated to 1% sucrose solution during the adaptation cycles. After the adaptation progression, mice were deprived of water and food for 12 h and were provided with free access to two tubes containing 20 ml of sucrose solution (1% w/v) and water respectively for 5 h. The sucrose preference rate was calculated subsequently using the following formula: sucrose preference = volume of sucrose consumed/total volume (water and sucrose) consumed × 100%. We performed the SPT on day 57 to evaluate the modeling effect.

We conducted the forced swim and tail suspension tests on days 58 and 59, respectively. During the forced swim test, the mice were individually placed into glass cylinders (height of 40 cm, diameter of 18 cm) containing 25°C water at a depth of 15 cm for 10 min. Immobility time was measured of last 4 min was recorded to estimate the symptom of depression. During the tail suspension test, mice were individually suspended by their tails for 6 min using a small piece of tape on the shelf, placed at the height of 60 cm above the floor. The duration of immobility during the final 4 min was recorded to measure depressive status.

On day 60, serum and feces were collected after 12 h of fasting. Livers and intestinal contents were removed immediately after the mice had been sacrificed. All samples were stored in a freezer at −80°C for further processing.

Untargeted Metabolomic Analysis

Serum samples were thawed on ice and 400 μl of methanol was subsequently added into 100 μl of serum sample in an EP tube. The mixture was vortexed for 1 min and centrifuged at 15,000 g for 10 min at 4°C. The supernatant was then transferred into another EP tube and evaporated to dry with an Eppendorf Vacufuge Concentrator 5305. The residue was resuspended in 150 ul of 80% methanol and filtered through a 0.22-μm nylon syringe filter. For all samples, equal volumes of solutions were mixed into quality controlled samples to evaluate instrument analysis stability and repeatability.

The separation of the target compounds was performed on a Waters ACQUITY UPLC HSS T3 (2.1 mm × 150 mm, 1.8 μm) liquid chromatography column at 40°C with a ACQUITY UPLC CSH C18 VanGuard Pre-column (2.1 mm × 5 mm, 1.7 μm) using a Dionex Ultimate 3000 UPLC system. The mobile phase contained 0.1% aqueous formic acid and 0.1% formic acid in acetonitrile in positive ion mode and 5 mM ammonium formate aqueous buffer and acetonitrile in negative ion mode. The mobile phase flow rate was 0.25 ml/min and the injection volume was 5 μL both in the positive and negative ion modes. **Supplementary Table S1** presents the detailed gradient elution conditions. The Q

Exactive Orbitrap mass spectrometer (Thermo Fisher Scientific, USA) equipped with an ESI interface was applied for mass spectrometry analysis. The optimal parameters were as follows: sheath gas flow rate, 30 arb; aux gas flow rate, 10 arb; capillary temperature, 325°C; scan range: 81–1000 Da; stepped normalized collision energy, 30 in NCE mode; spray voltage, 3.5 kV (positive)/−2.5 kV (negative). All MS spectra were acquired and analyzed using the Xcalibur 4.0 software (Thermo Fisher Scientific).

Data Processing and Metabolite Identification

Metabolomics analysis was carried out by BioNovoGene (Suzhou, China). After the raw data files were converted into an mzXML format by the ProteoWizard software (v3.0.8789), the freely available XCMS software was used to perform peak identification, filtration, alignment, and integration. The three-dimensional data matrix, including retention time, mass to charge ratio, and intensity, was converted into a table for further process analysis. In order to compare the data of different magnitudes, the peak area of the data was batch-normalized before multivariate statistical analysis. The data were then uploaded into SIMCA-P 13.0 to perform principal component analysis (PCA) and orthogonal partial least squares discriminant analysis (OPLS-DA). Autoscaling was used in all the models to achieve more scientific, reliable, and intuitive results. The variable importance in the project values (VIP) obtained from the OPLS-DA model and *p*-value from Student's t-test were used to select the potential metabolites in the study. Metabolites with VIP >1 and *p*-value < 0.05 were considered statistically significant. These potential metabolites were subsequently subjected to pathway analysis performed through MetaboAnalyst 5.0 (https://www.metaboanalyst.ca/).

Bile Acid Quantification in the Serum, Feces, and Liver

The bile acid profiles in the serum, feces, and liver were quantified using our previously validated UPLC-Q/Orbitrap-HRMS methods. Briefly, the bile acids in the feces and liver were extracted with 5 vol of deionized water by Qiagen TissueLyserII. For the feces samples, 200 uL of acetonitrile and 10 uL of 14% ammonia solution were added into 100 uL of fecal suspensions spiked with internal standard. For the serum and liver homogenates, 400 uL of acetonitrile was added into 100 uL of sample spiked with internal standard. The mixture was vortexed for 1 min and centrifuged at 20,000 g for 10 min at 4°C. The supernatant was then transferred into another EP tube and evaporated to dry with a vacuum centrifugal concentrator. The residue was resuspended in 100 uL of 80% methanol and filtered through a 0.22-μm nylon syringe filter. All blank matrix used for the calibration standard configurations and quality control samples were prepared using the activated carbon adsorption method.

The separation of the target compounds was performed on the same instrument and column as described above. The mobile phase flow rate and injection volume were 0.2 ml/min and 5 μL, respectively, with 10 mM ammonium formate aqueous buffer (A) and acetonitrile (B). The optimized gradient elution (0–7 min, 35–60% B; 7–8.5 min, 60–95% B; 8.5–12 min, 95% B; 12–12.3 min, 95%–35% B; 12.3–16 min, 35% B) was performed to separate the different bile acid components. Acquisition was performed in negative selective ion monitoring mode. All MS spectra were acquired and analyzed using the Xcalibur 4.0 software.

16S rRNA Sequencing Analysis

Total genomic DNA from the intestinal contents (5 samples from each of the control and model group) was extracted using the HiPure Stool DNA Kit (Megan, Guangzhou, China) according to the manufacturer's protocols. The DNA concentration was measured using the Equalbit dsDNA HS Assay Kit (Novizan, Nanjing China). The NGS library preparation and Illumina sequencing was performed by GENEWIZ, Inc. (Suzhou, China). Approximately 20–30 ng of DNA was used to generate amplicons. The V3 and V4 hypervariable microbial 16S rDNA regions were amplified by PCR using a panel of proprietary primers designed by GENEWIZ. A linker with an index was then added to the end of the PCR product of 16S rDNA by PCR for NGS sequencing. The obtained sequencing library was subsequently purified with magnetic beads, followed by library quality control checks using a microplate reader and agarose gel electrophoresis. The library was then quantified to 10 nM and PE250/FE300 paired-end sequencing was performed using an Illumina MiSeq instrument (Illumina, San Diego, CA, USA).

Next, the forward and reverse reads were joined in pairs, followed by filtering the sequences containing N in the splicing results and retaining the sequences with a length beyond 200 bp. The obtained longer sequences were used to perform sequence clustering using VSEARCH (1.9.6) (sequence similarity was set to 97%) against the Silva_138 16SrRNA database (http://www.arb-silva.de/). The Ribosomal Database Program classifier was used to assign taxonomic categories to predict the community composition at the genus levels. Sequence data associated with this project have been deposited in the NCBI database (Accession Number: PRJNA796629).

Statistical Analysis

All statistical analyses were performed using the GraphPad Prism 9.0 software. A two-tailed t-test was performed to compare between the groups and statistically significant differences were labeled with one, two, three, or four asterisks corresponding to $p < 0.05$, $p < 0.01$, or $p < 0.001$, respectively. Correlations between the gut microbiotic abundance and bile acid profiles were estimated using Pearson's correlation analysis.

RESULTS

Body Weight Changes and Depression-Like Behavior Validation

The body weight of the animals was measured before and during the treatment period. The mice in the model group gained less

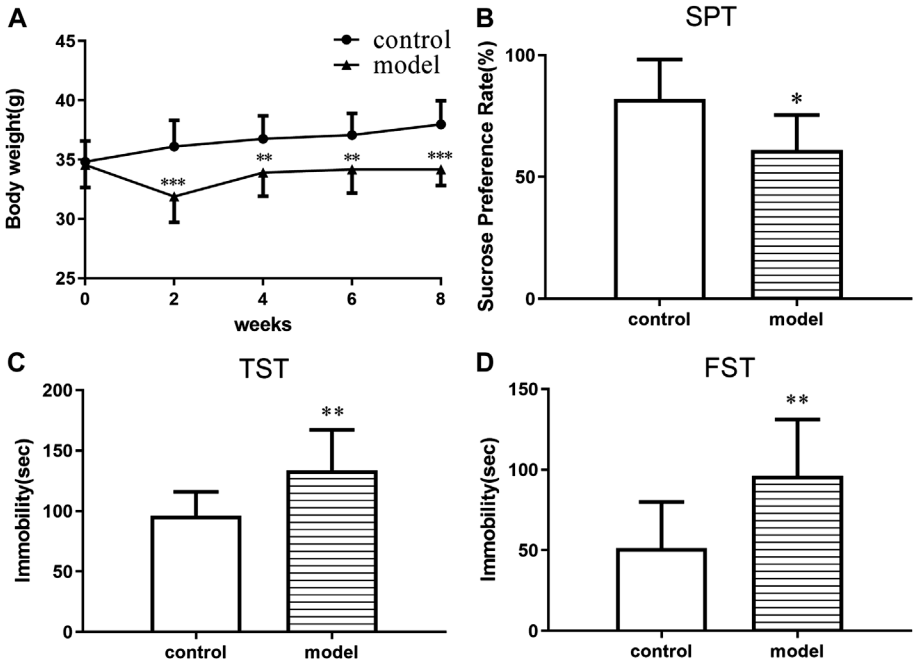

FIGURE 1 | CUMS effects on body weight and depressive-like behaviors in ICR mice. **(A)** Body weight change. **(B)** Sucrose preference in the sucrose preference test. **(C)** Immobility time in the forced swimming test. **(D)** Immobility time in the tail suspension test. *p < 0.05. **p < 0.01. ***p < 0.001. Error bar, SD.

weight than control group at the end of the CUMS progression (**Figures 1A–D**). In addition, significant CUMS effects were present in the case of the sucrose consumption in SPT, immobility time in both FST and TST compared with the control group. The results demonstrated that a CUMS mouse model was successfully created.

Differential Metabolite Screening in Untargeted Metabolomic Analysis

To investigate the impact of chronic stress upon the metabolomic profiling, untargeted metabolomic analysis was performed to analyze the metabolite composition in the serum of mice. The obvious separation trend from the PCA (**Supplementary Figure S1**) and the OPLS-DA (**Figures 2A,B**) score plot indicated metabolic differences between the groups. Our OPLS-DA permutation test showed that the model we established was not over-fitting (**Figures 2C,D**).

In order to screen out potential metabolites, we used the VIP value of the OPLS-DA model beyond 1.0 and the p-value of the two-tailed unpaired Student's t-test results less than 0.05 as a threshold to distinguish the metabolites from the model and control groups. A total of 74 metabolites were significantly changed during the CUMS progression. **Table 1** shows the detailed information of these metabolites. The affected pathways mainly involved amino acid, sugar, nucleotide metabolism, unsaturated fatty acid biosynthesis and metabolism, vitamin synthesis and absorption, and bile acid metabolism. **Supplementary Figure S2A** and **Supplementary Table S2** show the bubble chart of the KEGG pathway analysis and the detailed information of the pathway analysis, respectively. We found that the two main primary bile acid (chenodeoxycholic acid and taurocholic acid) levels were significantly altered in the model group, indicating abnormalities in bile acid synthesis or metabolism.

Effect of CUMS on Bile Acid Composition in the Serum

To further examine the bile acid metabolism disrupted by CUMS progression, we quantified the detailed bile acid profiles in the serum using our previously established method (**Supplementary Figure S3** shows the chromatographic separation of the different components). CUMS significantly increased the level of three free bile acids, UDCA (345%↑, p = 0.0314), CDCA (220%↑, p = 0.0152), and DCA (197%↑, p = 0.0009), whereas it significantly reduced the level of taurine-conjugated primary bile acid TCA (56%↓, p = 0.0452) (**Figure 3A**). The taurine-conjugated-to-free bile acid ratios in the model group were significantly lower than those in the control group (**Figure 4A**). In addition, the hydrophobicity index (HI) of the circulating bile acid pool was calculated as described previously (Heuman, 1989). We observed that the HI in the model group was significantly higher than that in the control group (**Figure 4B**).

Effect of CUMS on Bile Acid Composition in the Liver and Feces

Next, we quantified the bile acid profiles in the liver and feces to evaluate the effect of CUMS on bile acid biosynthesis and

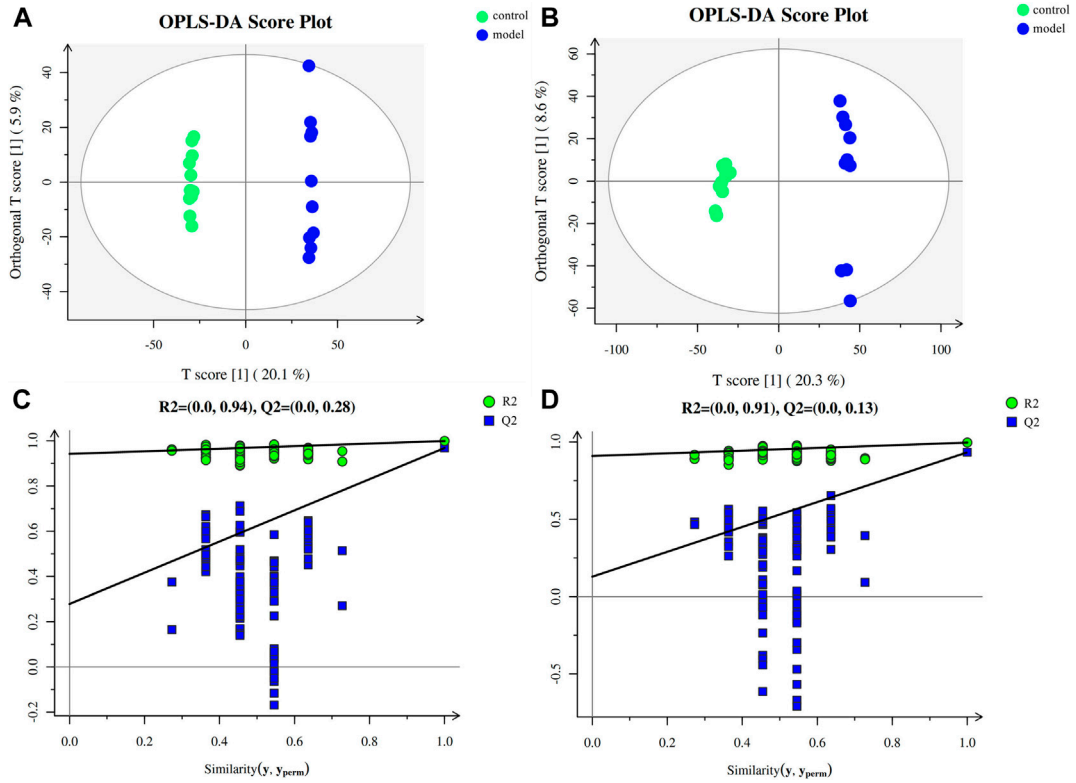

FIGURE 2 | Multivariate data analysis and permutation test. **(A)** OPLS-DA score map for positive ion mode data. **(B)** OPLS-DA score map for negative ion mode data. **(C)** OPLS-DA permutation test for the positive ion mode data. **(D)** OPLS-DA permutation test for the negative ion mode data.

metabolism. CUMS significantly increased the secondary bile acid levels in the feces and liver (**Figures 3B,C**). In particular, the model group liver samples showed increased DCA (148%↑, p = 0.0198), TDCA (166%↑, p = 0.0222), and TLCA (137%↑, p = 0.0028) levels and the model group feces samples showed increased DCA (117%↑, p = 0.0343), TDCA (304%↑, p = 0.0034), and GDCA (306%↑, p = 0.0061) levels.

Since DCA is the microbial metabolic product of TCA, we calculated the relative TCA-to-DCA ratios in the control and model groups to indirectly address the effects of the gut microbiota. The TCA/DCA ratio significantly decreased in the serum and liver of model group (**Figure 5**). Our results indicated that CUMS markedly promoted intestinal secondary bile acid formation.

Association Between the Gut Microbiotic Abundance and Bile Acid Profiles

We identified a total of 65 bacteria in the intestinal tract from the intestinal content samples at the genus level and summarized the heatmap of the relative abundance in the top 30 genera (**Figure 6A**). Pearson's correlation analysis (**Figure 6B**) indicated that increased secondary bile acid levels in the feces significantly and positively correlated with three members of the phylum *Firmicutes*: *Ruminococcaceae_UCG-010*, *Ruminococcus*, and *Clostridia_UCG-014*. This result suggested that changes in the secondary bile acid formation might be associated with altered gut microbiota composition in the intestine.

DISCUSSION

In this study, we constructed a CUMS model to mimic depressive behavior in ICR mice with adverse stress in order to explore how depression could affect metabolism. These mice were weighed every 2 weeks and significant body weight gain reduction could be observed in model groups compared to the control. The SPT results showed that 8 weeks of CUMS significantly reduced sucrose solution consumption. The tail suspension and the forced swim tests are the most direct and effective methods to evaluate depressive behaviors in animals (Can et al., 2012; Slattery and Cryan, 2012). The immobility time of the model group during both the TST and FST significantly increased compared with that of the control. These behavioral results consistently supported that we successfully developed a CUMS model in ICR mice.

Metabolomics is an important component of systems biology, which can directly reflect the state of organisms (Fiehn, 2002). Our PCA and OPLS-DA score plots showed significant separation of the different groups, indicating that obvious metabolic differences occurred during CUMS progression. However, the pathway enrichment map revealed that the most

TABLE 1 | Identification of different metabolites.

Metabolites	KEGG ID	Model/control	Metabolites	KEGG ID	Model/control
S-Adenosylhomocysteine	C00021	↓	N-Acetylserotonin	C00978	↑
Pyruvic acid	C00022	↓	N-Acetyl-L-aspartic acid	C01042	↑
L-Glutamic acid	C00025	↑	4-Hydroxyphenylpyruvic acid	C01179	↓
Oxoglutaric acid	C00026	↑	Anserine	C01262	↑
L-Aspartic acid	C00049	↑	Linoleic acid	C01595	↑
L-Arginine	C00062	↑	Kynurenic acid	C01717	↑
L-Serine	C00065	↑	Pyroglutamic acid	C01879	↑
D-Fructose	C00095	↑	5-Methylcytosine	C02376	↑
2-Ketobutyric acid	C00109	↓	Xanthurenic acid	C02470	↑
Fumaric acid	C00122	↓	Chenodeoxycholic acid	C02528	↑
Adenine	C00147	↓	Ureidopropionic acid	C02642	↑
L-Proline	C00148	↑	N-Formyl-L-methionine	C03145	↓
5-Methylthioadenosine	C00170	↓	3-Hydroxykynurenine	C03227	↑
L-Lactic acid	C00186	↑	2-Oxoarginine	C03771	↓
3-Phosphoglyceric acid	C00197	↑	2-Dehydro-3-deoxy-L-rhamnonate	C03979	↑
Thymidine	C00214	↓	D-Octopine	C04137	↑
Butyric acid	C00246	↑	13-L-Hydroperoxylinoleic acid	C04717	↑
L-Sorbose	C00247	↓	Taurocholic acid	C05122	↓
Nicotinic acid	C00253	↓	Phenylethylamine	C05332	↑
Riboflavin	C00255	↑	beta-D-Fructose 6-phosphate	C05345	↑
Gluconic acid	C00257	↑	5(S)-HpETE	C05356	↓
Uridine	C00299	↓	Ergothioneine	C05570	↓
Retinal	C00376	↓	3,4-Dihydroxymandelic acid	C05580	↑
Carnosine	C00386	↑	Metanephrine	C05588	↑
cis-Aconitic acid	C00417	↑	5-Hydroxyindoleacetic acid	C05635	↑
Prostaglandin H2	C00427	↓	Prostaglandin G2	C05956	↓
Saccharopine	C00449	↓	Prostaglandin J2	C05957	↓
Nicotinamide ribotide	C00455	↓	6-Keto-prostaglandin F1a	C05961	↑
Retinol	C00473	↓	Salidroside	C06046	↓
Cytidine	C00475	↑	Skatole	C08313	↑
Glutaric acid	C00489	↓	13S-hydroxyoctadecadienoic acid	C14762	↑
L-Fucose	C00507	↓	12-KETE	C14807	↑
L-Arabinonate	C00545	↑	9(S)-HPODE	C14827	↑
5-Dehydro-4-deoxy-D-glucarate	C00679	↓	12,13-DHOME	C14829	↑
Betaine	C00719	↑	Stearidonic acid	C16300	↓
Glucaric acid	C00818	↓	Traumatic Acid	C16308	↑
Indole-3-acetic acid	C00954	↑	(2E,4Z,7Z,8E)-Colnelenic acid	C16320	↑

Different metabolites were identified from the OPLS-DA, model based on VIP > 1 and $p < 0.05$, *↑ indicates upregulated metabolites. ↓indicates downregulated metabolites.*

impacted pathways mainly involved the energy metabolism, extensively studied in the field of depression. Upon further analysis of these metabolites, two primary bile acids were significantly altered in the model group, indicating that CUMS progression might cause bile acid metabolism disorder. In order to clarify how CUMS could affect bile acid metabolism, we quantified the detailed bile acid profiles in the serum, liver, and feces by UPLC-Q/Orbitrap-HRMS.

Bile acids are a group of amphipathic steroid molecules generated by hepatic and bacterial enzymes, playing an important role in regulating metabolism and immune response (Hofmann, 1999; Jia et al., 2018). Recent evidence suggests that bile acids might also play a role in mediating microbiota–gut–brain axis functions by interacting with their receptors in the brain (Monteiro-Cardoso et al., 2021). Specifically, altered bile acid profiles were associated with cognitive impairment in Alzheimer's and Parkinson's disease (MahmoudianDehkordi et al., 2019; Baloni et al., 2020; Li et al., 2021). Bile acid administration, particularly that of TUDCA and UDCA, contributed to neurologic symptom improvements in animal models of Alzheimer's, Parkinson's, and Huntington disease (Keene et al., 2002; Lo et al., 2013; Cuevas et al., 2020). However, bile acid metabolism in depression has rarely been described. There is an urgent need to elucidate how chronic stress affects bile acid profiles.

It is well-known that a variety of bile acid subtypes are present within the circulating bile acid pool (Yang et al., 2017). It has been difficult to appreciate the exact contribution of each bile acid to the whole body since each bile acid has the ability to bind and modulate the activity of transmembrane and nuclear receptors (Kundu et al., 2015). Different bile acid subtypes exhibit varying degrees of hydrophobicity, determined by factors such as state of ionization and hydroxyl group number, position, and orientation (Heuman, 1989). Circulating bile acid profile HIs quantitatively define the composite hydrophilic-hydrophobic balance of a mixture of bile acids (Heuman, 1989). Since multiple biological, physical, and chemical properties are related to the ability of compounds to bind to or dissolve in hydrophobic domains such as membrane, micelles, or certain receptor sites, HI can be used to evaluate how bile acid profile alterations impact

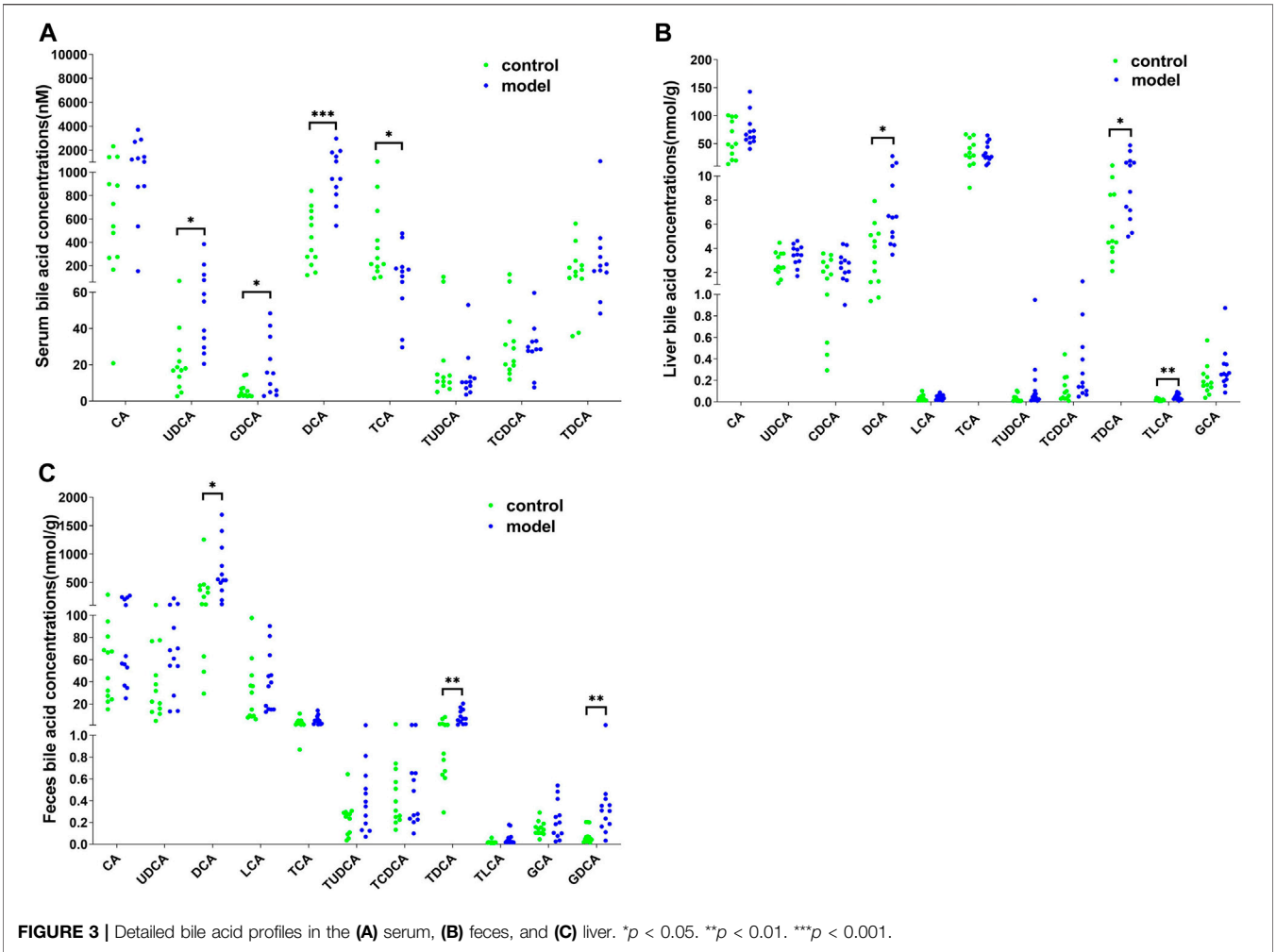

FIGURE 3 | Detailed bile acid profiles in the **(A)** serum, **(B)** feces, and **(C)** liver. *$p < 0.05$. **$p < 0.01$. ***$p < 0.001$.

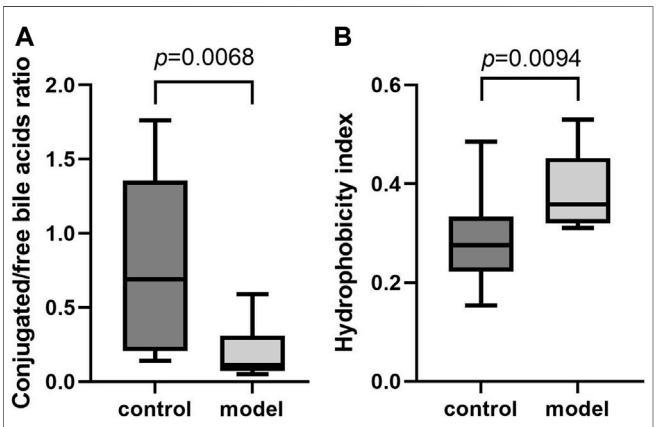

FIGURE 4 | Comparisons of bile acid composition in the serum. **(A)** Boxplot for conjugated bile acid-to-free bile acid concentration ratio. **(B)** Boxplot for bile acid hydrophobicity index.

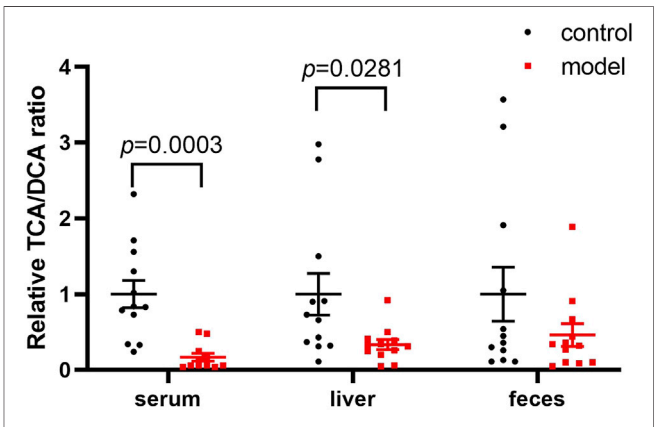

FIGURE 5 | Comparisons of the relative TCA-to-DCA concentration ratio. Data represent ratio values normalized to percentage of model group and are shown as mean ± SEM.

body function (Haeusler et al., 2013). Therefore, we calculated the circulating bile acid pool HI in the serum and observed remarkably raised bile acid pool HI in the model group.

Apart from HI, the conjugated/free and primary/secondary form ratios are additional characteristics of host bile acid homeostasis. We observed that the conjugated-to-free form

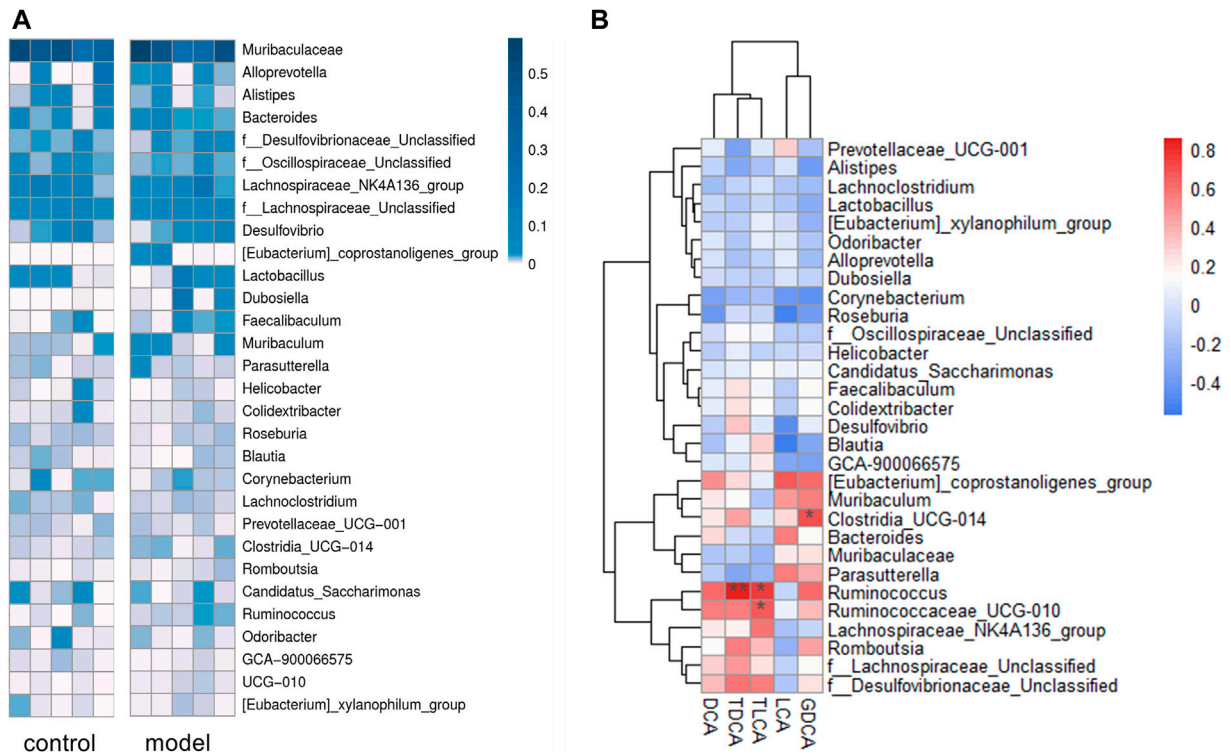

FIGURE 6 | Sequencing data analysis at the generic level. **(A)** Heat map of the top 30 genera relative abundances. **(B)** Relationship between fecal secondary bile acid levels and the top 30 genera microbial relative abundances. The legends show the relative abundances and correlation values respectively. *$p < 0.05$. **$p < 0.01$.

ratios in the serum significantly reduced in the model group. In addition, secondary bile acid levels, especially that of DCA, markedly increased in the model group. Since DCA is the metabolic product of TCA, we further compared the TCA/DCA ratio in control and model groups. Consequently, the TCA/DCA ratios in the serum and liver significantly decreased in the model group. These results indicated that the secondary bile acid biosynthesis pathway had been activated during CUMS progression, potentially explaining the increased HI in the serum.

Mitochondrial dysfunction and oxidative stress are supposed to be involved in the pathophysiology of depression (Bansal and Kuhad, 2016; Bhatt et al., 2020). Indeed, hydrophobic bile acid species show cytotoxicity due to their detergent action and oxidation effects (Perez and Briz, 2009), whereas hydrophilic bile acids, such as TUDCA mentioned above, exert strong cytoprotective effects by mitochondrial membrane stabilization (Castro et al., 2004). Previous studies demonstrated that multiple bile acids could penetrate the blood-brain barrier, although the involved mechanisms have not yet been fully understood (Mertens et al., 2017). Notably, free bile acids could diffuse across phospholipid bilayers and their brain concentrations correlate with their serum concentrations (Kamp et al., 1993; Higashi et al., 2017). Since chronic stress can disrupt brain homeostasis and increase the blood-brain barrier permeability (Lee et al., 2018), free bile acids might penetrate more easily the blood-brain barrier in the depressive state. In particular, increased DCA level can induce apoptosis and DNA damage (Washo-Stultz et al., 2002; Fu et al., 2019), potentially exacerbating neuroinflammation and oxidative stress contributing to the progression of depression pathology. In our analyses, with CUMS progression, the increased free bile acid levels in serum might have contributed to bile acid composition changes in the brain. This is of particular concern given that the increased DCA level might affect brain physiology.

In addition to direct effects on the central nervous system function, bile acids might also be involved in the metabolic disorders during CUMS progression by regulating receptor such as FXR (farnesoid X receptor) and TGR5 (Takeda G protein-coupled receptor 5). FXR mainly functions as a bile acid sensor in the bile acid regulation feedback and its most potent ligand is CDCA (Liu et al., 2020). Furthermore, current evidence suggests FXR also participates in bile acid-mediated energy metabolism. FXR deficient mice exhibited impaired glucose tolerance and reduced insulin sensitivity (Ma et al., 2006). FXR activation in the intestine promotes the release of fibroblast growth factor (FGF) 15/19, proved to serve as important regulators to improve glucose metabolism in the gut–brain axis by binding FGF receptors in the hypothalamus (Liu et al., 2018). TGR5 is a G protein-coupled bile acid receptor that mediates glucose homeostasis by producing glucagon-like peptide 1. TGR5 is mainly activated by secondary bile acids, including LCA, DCA, and TLCA *in vivo* (Liu et al., 2020). Our serum untargeted metabolomics results revealed multiple

carbohydrate metabolism pathways were significantly enriched, which might be associated with the bile acid metabolism disorders in CUMS progression. Beyond that, the latest research indicated that bile acid receptors in the brain were also directly involved in the pathogenesis of depression. The protein and mRNA expressions of FXR in hippocampus were significantly increased in CUMS induced depressive rats (Chen et al., 2018), and FXR overexpression aggravated depression-like behaviors by inhibiting brain-derived neurotrophic factor signaling in the hippocampus (Hu et al., 2020). Multiple types of chronic stressors significantly reduced TGR5 expression in hippocampal CA3 pyramidal neurons of C57BL/6J mice, whereas genetic overexpression of TGR5 or intra-CA3 infusion of the TGR5 agonist was able to reverse depressive-like behaviors by CA3 pyramidal neurons activation (Wang et al., 2021). In our present study, hepatic FXR and TGR5 expressions were not significantly altered in CUMS progression (data not shown), indicating that CUMS might exert different effects on bile acid reporters in different tissues. Bile acid profile and FXR and TGR5 expression in the brain will be the focus of our further investigation to elucidate the regulation of the pathogenesis of depression.

It is known that gut microbiota plays an essential role in the development of depression (Sanada et al., 2020), recognized as a possible reason for depression causing bile acid metabolism disorder. The deconjugation of conjugated bile acids *in vivo* is mainly catalyzed by bile salt hydrolase, widely expressed by multiple common commensal genera, especially *Bacteroides*, *Lactobacillus,* and *Clostridium* (Song et al., 2019; Adhikari et al., 2020). Another microbial bile salt transformation *in vivo* is to form secondary bile acids from primary bile acids by 7α-dehydroxylation. Currently known bacteria expressing 7α-dehydroxylase are all of the *Ruminococcaceae* and *Lachnospiraceae* families (Stellwag and Hylemon, 1978; Takamine and Imamura, 1995). As shown in **Supplementary Figure S4**, two genera of family *Ruminococcaceae*, *Ruminococcaceae_UCG-010* and *Ruminococcus*, were significantly positively correlated with the secondary bile acid levels in feces, which might partly explain the increased secondary bile acids in model group.

Accumulating number of studies demonstrated that *Ruminococcaceae* might affect brain function and behavior. Tran et al. found that the abundance of *Ruminococcaceae* were correlated with the apolipoprotein E genotype in healthy participants (Tran et al., 2019). Depletion of *Ruminococcaceae* was proved to be closely associated with reduced cognitive functions Alzheimer's disease (Vogt et al., 2017; D'Amato et al., 2020). At the genus level, the genus *Ruminococcus* is well known as butyric acid-producing bacteria which plays an important role in intestinal inflammation (Louis and Flint, 2017; Henke et al., 2019) (elevated butyric acid level was also observed in model group from the serum untargeted metabolomics data). Recent research revealed the importance of decreasing *Ruminococcus* for duloxetine to reduce depressive behavior (Lukić et al., 2019), indirectly indicating that *Ruminococcus* involved in the occurrence and progression of depression. Our current results further complement these previous study findings demonstrating the critical role of *Ruminococcaceae* by regulating bile acid metabolism in microbiota–gut–brain axis.

CONCLUSION

Our findings provide a novel perspective to elucidate the microbiota–gut–brain crosstalk in depression. Chronic stress-induced gut microbiota modifications, especially changes in relative abundance of family *Ruminococcaceae*, contributed to increased biosynthesis of secondary bile acid DCA in the intestine. This gut microbiota-mediated bile acid metabolic imbalance subsequently increased the hydrophobicity of the bile acid pool, which might in turn promote the energy metabolism disorder and pathophysiological changes in CUMS progression.

DATA AVAILABILITY STATEMENT

The datasets presented in this study can be found in online repositories. The names of the repository/repositories and accession number(s) can be found below: NCBI database (BioProject: PRJNA796629, BioSample:SAMN24905304).

ETHICS STATEMENT

The animal study was reviewed and approved by Ethics Committee of Soochow University.

AUTHOR CONTRIBUTIONS

YQ and CS: designed the study and wrote the manuscript. YQ, QZ, FZ, LT, DX, ZX, and YW: performed the experiments. YQ, AS, and YW analyzed metabolomic data. JP and YY supervised the project and revised the manuscript.

FUNDING

This work was supported by Natural Science Foundation of China (82173879), Jiangsu Pharmaceutical Association (Q202019, H202122), Lift Project for Discipline Construction of The Second Affiliated Hospital of Soochow University (XKTJ-XK202010), the Second Affiliate Hospital of Soochow University Talent Promotion Project (XKTJ-RC202013, XKTJ-RC202014), Suzhou Science Foundation (SYS2019058) Suzhou Health Talent Project (GSW2020025), Suzhou Science and Technology Development Plan (SS2019042).

SUPPLEMENTARY MATERIAL

The Supplementary Material for this article can be found online at: https://www.frontiersin.org/articles/10.3389/fphar.2022.837543/full#supplementary-material

REFERENCES

Adhikari, A. A., Seegar, T. C. M., Ficarro, S. B., McCurry, M. D., Ramachandran, D., Yao, L., et al. (2020). Development of a Covalent Inhibitor of Gut Bacterial Bile Salt Hydrolases. *Nat. Chem. Biol.* 16 (3), 318–326. doi:10.1038/s41589-020-0467-3

Baloni, P., Funk, C. C., Yan, J., Yurkovich, J. T., Kueider-Paisley, A., Nho, K., et al. (2020). Metabolic Network Analysis Reveals Altered Bile Acid Synthesis and Metabolism in Alzheimer's Disease. *Cell. Rep. Med.* 1 (8), 100138. doi:10.1016/j.xcrm.2020.100138

Bansal, Y., and Kuhad, A. (2016). Mitochondrial Dysfunction in Depression. *Curr. Neuropharmacol.* 14 (6), 610–618. doi:10.2174/1570159x14666160229114755

Bhatt, S., Nagappa, A. N., and Patil, C. R. (2020). Role of Oxidative Stress in Depression. *Drug Discov. Today* 25 (7), 1270–1276. doi:10.1016/j.drudis.2020.05.001

Can, A., Dao, D. T., Terrillion, C. E., Piantadosi, S. C., Bhat, S., and Gould, T. D. (2012). The Tail Suspension Test. *J. Vis. Exp.* (59), e3769. doi:10.3791/3769

Castro, R. E., Solá, S., Ramalho, R. M., Steer, C. J., and Rodrigues, C. M. (2004). The Bile Acid Tauroursodeoxycholic Acid Modulates Phosphorylation and Translocation of Bad via Phosphatidylinositol 3-kinase in Glutamate-Induced Apoptosis of Rat Cortical Neurons. *J. Pharmacol. Exp. Ther.* 311 (2), 845–852. doi:10.1124/jpet.104.070532

Chaudhury, D., Liu, H., and Han, M. H. (2015). Neuronal Correlates of Depression. *Cell. Mol. Life Sci.* 72, 4825–4848. doi:10.1007/s00018-015-2044-6

Chen, W. G., Zheng, J. X., Xu, X., Hu, Y. M., and Ma, Y. M. (2018). Hippocampal FXR Plays a Role in the Pathogenesis of Depression: A Preliminary Study Based on Lentiviral Gene Modulation. *Psychiatry Res.* 264, 374–379. doi:10.1016/j.psychres.2018.04.025

Chiang, J. Y. L., and Ferrell, J. M. (2018). Bile Acid Metabolism in Liver Pathobiology. *Gene Expr.* 18 (2), 71–87. doi:10.3727/105221618X15156018385515

Cuevas, E., Burks, S., Raymick, J., Robinson, B., Gómez-Crisóstomo, N. P., Escudero-Lourdes, C., et al. (2020). Tauroursodeoxycholic Acid (TUDCA) Is Neuroprotective in a Chronic Mouse Model of Parkinson's Disease. *Nutr. Neurosci.* 1, 1–18. doi:10.1080/1028415X.2020.1859729

D'Amato, A., Di Cesare Mannelli, L., Lucarini, E., Man, A. L., Le Gall, G., Branca, J. J. V., et al. (2020). Faecal Microbiota Transplant from Aged Donor Mice Affects Spatial Learning and Memory via Modulating Hippocampal Synaptic Plasticity- and Neurotransmission-Related Proteins in Young Recipients. *Microbiome* 8 (1), 140. doi:10.1186/s40168-020-00914-w

Fiehn, O. (2002). Metabolomics--the Link between Genotypes and Phenotypes. *Plant Mol. Biol.* 48 (1-2), 155–171. doi:10.1007/978-94-010-0448-0_11

Foster, J. A., and McVey Neufeld, K. A. (2013). Gut-brain axis: How the Microbiome Influences Anxiety and Depression. *Trends. Neurosci.* 36 (5), 305–312. doi:10.1016/j.tins.2013.01.005

Fu, T., Coulter, S., Yoshihara, E., Oh, T. G., Fang, S., Cayabyab, F., et al. (2019). FXR Regulates Intestinal Cancer Stem Cell Proliferation. *Cell* 176 (5), 1098–1112e18. doi:10.1016/j.cell.2019.01.036

Haeusler, R. A., Astiarraga, B., Camastra, S., Accili, D., and Ferrannini, E. (2013). Human Insulin Resistance Is Associated with Increased Plasma Levels of 12α-Hydroxylated Bile Acids. *Diabetes* 62 (12), 4184–4191. doi:10.2337/db13-0639

He, D., Barnes, S., and Falany, C. N. (2003). Rat Liver Bile Acid CoA:amino Acid N-Acyltransferase: Expression, Characterization, and Peroxisomal Localization. *J. Lipid. Res.* 44 (12), 2242–2249. doi:10.1194/jlr.M300128-JLR200

Henke, M. T., Kenny, D. J., Cassilly, C. D., Vlamakis, H., Xavier, R. J., and Clardy, J. (2019). Ruminococcus Gnavus, a Member of the Human Gut Microbiome Associated with Crohn's Disease, Produces an Inflammatory Polysaccharide. *Proc. Natl. Acad. Sci. U. S. A.* 116 (26), 12672–12677. doi:10.1073/pnas.1904099116

Heuman, D. M. (1989). Quantitative Estimation of the Hydrophilic-Hydrophobic Balance of Mixed Bile Salt Solutions. *J. Lipid. Res.* 30 (5), 719–730. doi:10.1016/s0022-2275(20)38331-0

Higashi, T., Watanabe, S., Tomaru, K., Yamazaki, W., Yoshizawa, K., Ogawa, S., et al. (2017). Unconjugated Bile Acids in Rat Brain: Analytical Method Based on LC/ESI-MS/MS with Chemical Derivatization and Estimation of Their Origin by Comparison to Serum Levels. *Steroids* 125, 107–113. doi:10.1016/j.steroids.2017.07.001

Hofmann, A. F. (1999). The Continuing Importance of Bile Acids in Liver and Intestinal Disease. *Arch. Intern. Med.* 159 (22), 2647–2658. doi:10.1001/archinte.159.22.2647

Hu, W., Wu, J., Ye, T., Chen, Z., Tao, J., Tong, L., et al. (2020). Farnesoid X Receptor-Mediated Cytoplasmic Translocation of CRTC2 Disrupts CREB-BDNF Signaling in Hippocampal CA1 and Leads to the Development of Depression-like Behaviors in Mice. *Int. J. Neuropsychopharmacol.* 23 (10), 673–686. doi:10.1093/ijnp/pyaa039

Jia, W., Xie, G., and Jia, W. (2018). Bile Acid-Microbiota Crosstalk in Gastrointestinal Inflammation and Carcinogenesis. *Nat. Rev. Gastroenterol. Hepatol.* 15 (2), 111–128. doi:10.1038/nrgastro.2017.119

Kamp, F., Hamilton, J. A., Kamp, F., Westerhoff, H. V., and Hamilton, J. A. (1993). Movement of Fatty Acids, Fatty Acid Analogues, and Bile Acids across Phospholipid Bilayers. *Biochemistry* 32 (41), 11074–11086. doi:10.1021/bi00092a017

Keene, C. D., Rodrigues, C. M., Eich, T., Chhabra, M. S., Steer, C. J., and Low, W. C. (2002). Tauroursodeoxycholic Acid, a Bile Acid, Is Neuroprotective in a Transgenic Animal Model of Huntington's Disease. *Proc. Natl. Acad. Sci. U. S. A.* 99 (16), 10671–10676. doi:10.1073/pnas.162362299

Kundu, S., Kumar, S., and Bajaj, A. (2015). Cross-talk between Bile Acids and Gastrointestinal Tract for Progression and Development of Cancer and its Therapeutic Implications. *IUBMB. Life* 67 (7), 514–523. doi:10.1002/iub.1399

Lee, S., Kang, B. M., Kim, J. H., Min, J., Kim, H. S., Ryu, H., et al. (2018). Real-time *In Vivo* Two-Photon Imaging Study Reveals Decreased Cerebro-Vascular Volume and Increased Blood-Brain Barrier Permeability in Chronically Stressed Mice. *Sci. Rep.* 8 (1), 13064. doi:10.1038/s41598-018-30875-y

Li, P., Killinger, B. A., Ensink, E., Beddows, I., Yilmaz, A., Lubben, N., et al. (2021). Gut Microbiota Dysbiosis Is Associated with Elevated Bile Acids in Parkinson's Disease. *Metabolites* 11 (1), 29. doi:10.3390/metabo11010029

Liang, S., Wu, X., Hu, X., Wang, T., and Jin, F. (2018). Recognizing Depression from the Microbiota¯Gut¯Brain Axis. *Int. J. Mol. Sci.* 19 (6), 1592. doi:10.3390/ijms19061592

Liu, B., Liu, J., Wang, M., Zhang, Y., and Li, L. (2017). From Serotonin to Neuroplasticity: Evolvement of Theories for Major Depressive Disorder. *Front. Cel. Neurosci.* 11, 305. doi:10.3389/fncel.2017.00305

Liu, L., Liu, Z., Li, H., Cao, Z., Li, W., Song, Z., et al. (2020). Naturally Occurring TPE-CA Maintains Gut Microbiota and Bile Acids Homeostasis via FXR Signaling Modulation of the Liver-Gut Axis. *Front. Pharmacol.* 11, 12. doi:10.3389/fphar.2020.00012

Liu, S., Marcelin, G., Blouet, C., Jeong, J. H., Jo, Y. H., Schwartz, G. J., et al. (2018). A Gut-Brain axis Regulating Glucose Metabolism Mediated by Bile Acids and Competitive Fibroblast Growth Factor Actions at the Hypothalamus. *Mol. Metab.* 8, 37–50. doi:10.1016/j.molmet.2017.12.003

Lo, A. C., Callaerts-Vegh, Z., Nunes, A. F., Rodrigues, C. M., and D'Hooge, R. (2013). Tauroursodeoxycholic Acid (TUDCA) Supplementation Prevents Cognitive Impairment and Amyloid Deposition in APP/PS1 Mice. *Neurobiol. Dis.* 50, 21–29. doi:10.1016/j.nbd.2012.09.003

Louis, P., and Flint, H. J. (2017). Formation of Propionate and Butyrate by the Human Colonic Microbiota. *Environ. Microbiol.* 19 (1), 29–41. doi:10.1111/1462-2920.13589

Lukić, I., Getselter, D., Ziv, O., Oron, O., Reuveni, E., Koren, O., et al. (2019). Antidepressants Affect Gut Microbiota and Ruminococcus Flavefaciens Is Able to Abolish Their Effects on Depressive-like Behavior. *Transl. Psychiatry* 9 (1), 133. doi:10.1038/s41398-019-0466-x

Ma, K., Saha, P. K., Chan, L., and Moore, D. D. (2006). Farnesoid X Receptor Is Essential for normal Glucose Homeostasis. *J. Clin. Invest.* 116 (4), 1102–1109. doi:10.1172/JCI25604

MahmoudianDehkordi, S., Arnold, M., Nho, K., Ahmad, S., Jia, W., Xie, G., et al. (2019). Altered Bile Acid Profile Associates with Cognitive Impairment in Alzheimer's Disease-An Emerging Role for Gut Microbiome. *Alzheimers. Dement.* 15 (1), 76–92. doi:10.1016/j.jalz.2018.07.217

Mertens, K. L., Kalsbeek, A., Soeters, M. R., and Eggink, H. M. (2017). Bile Acid Signaling Pathways from the Enterohepatic Circulation to the Central Nervous System. *Front. Neurosci.* 11, 617. doi:10.3389/fnins.2017.00617

Monteiro-Cardoso, V. F., Corlianò, M., and Singaraja, R. R. (2021). Bile Acids: A Communication Channel in the Gut-Brain Axis. *Neuromolecular. Med.* 23 (1), 99–117. doi:10.1007/s12017-020-08625-z

Perez, M. J., and Briz, O. (2009). Bile-acid-induced Cell Injury and protection. *World J. Gastroenterol.* 15 (14), 1677–1689. doi:10.3748/wjg.15.1677

Ridlon, J. M., Kang, D. J., Hylemon, P. B., and Bajaj, J. S. (2014). Bile Acids and the Gut Microbiome. *Curr. Opin. Gastroenterol.* 30 (3), 332–338. doi:10.1097/MOG.0000000000000057

Russell, D. W. (2003). The Enzymes, Regulation, and Genetics of Bile Acid Synthesis. *Annu. Rev. Biochem.* 72, 137–174. doi:10.1146/annurev.biochem.72.121801.161712

Sanada, K., Nakajima, S., Kurokawa, S., Barceló-Soler, A., Ikuse, D., Hirata, A., et al. (2020). Gut Microbiota and Major Depressive Disorder: A Systematic Review and Meta-Analysis. *J. Affect. Disord.* 266, 1–13. doi:10.1016/j.jad.2020.01.102

Slattery, D. A., and Cryan, J. F. (2012). Using the Rat Forced Swim Test to Assess Antidepressant-like Activity in Rodents. *Nat. Protoc.* 7 (6), 1009–1014. doi:10.1038/nprot.2012.044

Song, Z., Cai, Y., Lao, X., Wang, X., Lin, X., Cui, Y., et al. (2019). Taxonomic Profiling and Populational Patterns of Bacterial Bile Salt Hydrolase (BSH) Genes Based on Worldwide Human Gut Microbiome. *Microbiome* 7 (1), 9. doi:10.1186/s40168-019-0628-3

Stellwag, E. J., and Hylemon, P. B. (1978). Characterization of 7-Alpha-Dehydroxylase in Clostridium Leptum. *Am. J. Clin. Nutr.* 31 (10 Suppl. l), S243–S247. doi:10.1093/ajcn/31.10.S243

Takamine, F., and Imamura, T. (1995). Isolation and Characterization of Bile Acid 7-dehydroxylating Bacteria from Human Feces. *Microbiol. Immunol.* 39 (1), 11–18. doi:10.1111/j.1348-0421.1995.tb02162.x

Tran, T. T. T., Corsini, S., Kellingray, L., Hegarty, C., Le Gall, G., Narbad, A., et al. (2019). APOE Genotype Influences the Gut Microbiome Structure and Function in Humans and Mice: Relevance for Alzheimer's Disease Pathophysiology. *FASEB j.* 33, 8221–8231. doi:10.1096/fj.201900071R

Vogt, N. M., Kerby, R. L., Dill-McFarland, K. A., Harding, S. J., Merluzzi, A. P., Johnson, S. C., et al. (2017). Gut Microbiome Alterations in Alzheimer's Disease. *Sci. Rep.* 7 (1), 13537. doi:10.1038/s41598-017-13601-y

Wang, H., Tan, Y. Z., Mu, R. H., Tang, S. S., Liu, X., Xing, S. Y., et al. (2021). Takeda G Protein-Coupled Receptor 5 Modulates Depression-like Behaviors via Hippocampal CA3 Pyramidal Neurons Afferent to Dorsolateral Septum. *Biol. Psychiatry* 89 (11), 1084–1095. doi:10.1016/j.biopsych.2020.11.018

Washo-Stultz, D., Crowley-Weber, C. L., Dvorakova, K., Bernstein, C., Bernstein, H., Kunke, K., et al. (2002). Role of Mitochondrial Complexes I and II, Reactive Oxygen Species and Arachidonic Acid Metabolism in Deoxycholate-Induced Apoptosis. *Cancer Lett.* 177 (2), 129–144. doi:10.1016/s0304-3835(01)00786-8

World Health Organization (WHO) (2021). Depression. Available online at: https://www.who.int/en/news-room/fact-sheets/detail/depression.

Yang, T., Shu, T., Liu, G., Mei, H., Zhu, X., Huang, X., et al. (2017). Quantitative Profiling of 19 Bile Acids in Rat Plasma, Liver, Bile and Different Intestinal Section Contents to Investigate Bile Acid Homeostasis and the Application of Temporal Variation of Endogenous Bile Acids. *J. Steroid Biochem. Mol. Biol.* 172, 69–78. doi:10.1016/j.jsbmb.2017.05.015

Conflict of Interest: The authors declare that the research was conducted in the absence of any commercial or financial relationships that could be construed as a potential conflict of interest.

The handling editor LL declared a shared parent affiliation with the authors at the time of the review.

Publisher's Note: All claims expressed in this article are solely those of the authors and do not necessarily represent those of their affiliated organizations, or those of the publisher, the editors and the reviewers. Any product that may be evaluated in this article, orclaim that may be made by its manufacturer, is not guaranteed or endorsed by the publisher.

frontiers in Pharmacology

REVIEW
published: 21 March 2022
doi: 10.3389/fphar.2022.805782

Fluxomics - New Metabolomics Approaches to Monitor Metabolic Pathways

Abdul-Hamid Emwas[1], Kacper Szczepski[2], Inas Al-Younis[3], Joanna Izabela Lachowicz[4] and Mariusz Jaremko[2]*

[1]King Abdullah University of Science and Technology, Core Labs, Thuwal, Saudi Arabia, [2]Smart-Health Initiative (SHI) and Red Sea Research Center (RSRC), Biological and Environmental Sciences & Engineering Division (BESE), King Abdullah University of Science and Technology (KAUST), Thuwal, Saudi Arabia, [3]King Abdullah University of Science and Technology (KAUST), Biological and Environmental Sciences & Engineering Division (BESE), Thuwal, Saudi Arabia, [4]Department of Medical Sciences and Public Health, University of Cagliari, Cittadella Universitaria, Monserrato, Italy

Fluxomics is an innovative -omics research field that measures the rates of all intracellular fluxes in the central metabolism of biological systems. Fluxomics gathers data from multiple different -omics fields, portraying the whole picture of molecular interactions. Recently, fluxomics has become one of the most relevant approaches to investigate metabolic phenotypes. Metabolic flux using ^{13}C-labeled molecules is increasingly used to monitor metabolic pathways, to probe the corresponding gene-RNA and protein-metabolite interaction networks in actual time. Thus, fluxomics reveals the functioning of multi-molecular metabolic pathways and is increasingly applied in biotechnology and pharmacology. Here, we describe the main fluxomics approaches and experimental platforms. Moreover, we summarize recent fluxomic results in different biological systems.

Keywords: fluxomics, metabolomics, nuclear magnetic resonance (NMR), mass spectrometry (MS), flux, pharmacometabolomics

OPEN ACCESS

Edited by:
Giuseppe Lucarelli, University of Bari Aldo Moro, Italy

Reviewed by:
Xinwen Wang, Northeast Ohio Medical University, United States
Junzeng Zhang, National Research Council Canada (NRC-CNRC), Canada

****Correspondence:***
Abdul-Hamid Emwas
abdelhamid.emwas@kaust.edu.sa

Specialty section:
This article was submitted to Translational Pharmacology, a section of the journal Frontiers in Pharmacology

Received: *30 October 2021*
Accepted: *24 January 2022*
Published: *21 March 2022*

Citation:
Emwas A-H, Szczepski K, Al-Younis I, Lachowicz JI and Jaremko M (2022) Fluxomics - New Metabolomics Approaches to Monitor Metabolic Pathways. Front. Pharmacol. 13:805782. doi: 10.3389/fphar.2022.805782

INTRODUCTION

Throughout recent decades discoveries explaining the complex nature of the cell have provided the scientific community with an immense amount of data. As more information has been revealed, the need for classification and quantification of this data has resulted in the creation of various–omics fields. This approach recognizes whole systems, rather than groups of separated processes (Vailati-Riboni et al., 2017). Many types of–omics have been created, the most prominent being genomics, transcriptomics, proteomics and metabolomics. All of these fields are part of systems biology - a strategy used to examine the interactions, relationships and behavior between all system constituents (Ideker et al., 2001). However, even though the fundamental–omics approaches focus only on their system of interest (e.g. the genome for genomics, or the proteome for proteomics), their constituents are connected. For example, the field of proteomics exists as the directional effect of transcriptomics that is further influenced by genomics.

Given these factors, a new discipline called fluxomics emerged that connects genomics, transcriptomics, proteomics and metabolomics. Although a new addition to the–omics family, fluxomics studies have been steadily increasing over the past 2 decades (**Figure 1**). Recent examples of fluxomics studies are shown in **Supplementary Table S1**. The emerging importance of fluxomics is reflected not only by the amount of research articles published every year but also through its potential applications in industrial biotechnology and

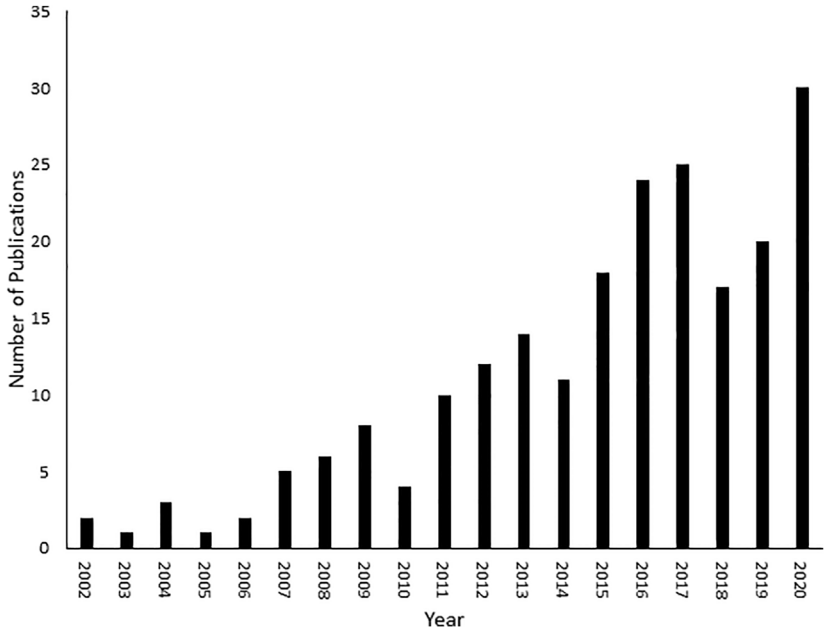

FIGURE 1 | Number of fluxomic publications. A literature review was conducted on SciFinder (https://scifinder.cas.org/scifinder/view/scifinder/scifinderExplore.jsf) using the keyword fluxomics.

pharmacology (Feng et al., 2010; Wojtowicz and Mlynarz, 2016; Hansen et al., 2017; Emwas, 2021). Several recent studies used fluxomics as an alternative approach in the field of drug discovery, by targeting bacterial metabolic pathways distinct from human metabolic routes. Viral and bacterial infection depends on the ability of pathogens to convert nutrients into energy (e.g., ATP) (Eisenreich, 2021). Importantly, bacteria have partially distinct metabolic pathways compared to their human host cells (Rohmer et al., 2011). Selective inhibition of differential mechanisms is unlikely to have major side effects in humans. Innovative drug therapies that reprogram the core carbon metabolism of human infections make bacteria more susceptible to antibiotics (Liu et al., 2019a; Stokes et al., 2019). A recent study examined the metabolomic profile of *Vibrio alginolyticus*, which is resistant to cephalosporin antibiotics, and the role of bacterial metabolism in drug and multidrug resistance. This was achieved by detecting the metabolic differences of acetyl-CoA fluxes into and through the P-cycle and fatty acid biosynthesis (Liu et al., 2019b). These findings shed light on ceftazidime (CAZ) and other antibiotic resistance pathways, as well as multidrug resistance of *Vibrio* and other pathogens. A combined metabolomics and fluxomics approach was used in studies of *Leishmania infantum promastigotes*. The origin of the detected alterations was analyzed with untargeted analysis of metabolic snapshots (of treated and untreated parasites), both resistant and responders, and by using a ^{13}C traceability experiment (Rojo et al., 2015). This showed a significant shift in amino acid metabolism, and multi-target metabolic change as a result of treatment, particularly affecting the cell redox system, which is critical for detoxification and biosynthetic activities (Rojo et al., 2015). Although there are costs and current challenges associated with fluxomics approaches, there have been studies supporting its use in models such as *Escherichia coli*, *Bacillus subtilis*, *Saccharomyces cerevisiae* or *Pichia pastoris* (Feng et al., 2010; Zahrl et al., 2017). These studies provided information such as optimal fermentation conditions, improved ethanol and riboflavin production and better yield in protein expression (Feng et al., 2010; Zahrl et al., 2017; Choi et al., 2018). The constant development and improvement of analytical tools and methodologies in fluxomics will only increase its future prevalence (Wiechert et al., 2001; Beyß, 2019; Foguet et al., 2019; Giraudeau, 2020).

ADVANTAGES AND DISADVANTAGES OF CHROMATOGRAPHY AND NUCLEAR MAGNETIC RESONANCE TOOLS IN FLUXOMICS

Similar to other -omics fields, fluxomics is a technology driven field where recent advances in instrumentation, software and databases have significantly contributed to development. Different analytical tools and approaches in fluxomics have been reviewed recently (Wiechert et al., 2007; Niittylae et al., 2009; Klein and Heinzle, 2012; Winter and Krömer, 2013; Niedenführ et al., 2015). Even if different analytical tools are utilized in fluxomics/metabolomics research, nuclear magnetic resonance (NMR) spectroscopy (Giraudeau, 2020) and mass spectrometry (MS) (Wiechert et al., 2007; Choi and

Antoniewicz, 2019; Babele and Young, 2020) are the most commonly used tools in metabolomic studies.

Each applied analytical platform, either NMR or MS, has its strength, advantages and limitations. For example, gas chromatography-mass spectrometry (GC-MS) is commonly used in fluxomics analyses but is only applicable for volatile metabolites or ones that can be treated to become volatile compounds through derivatization processes. Liquid chromatography-mass spectrometry (LC-MS) provides potent approaches that offer combined sensitivity and selectivity. MS approaches such as different ionization modes (positive or negative) or mass analyzer technology can be used to increase the number of detected metabolites. Nevertheless, chromatographic experiments require specific sample pre-treatment, have limited experimental time scales, and do not depict the 3D structure or interactions of the molecule.

Beside its exceptionally high sensitivity, mass spectrometry is usually combined with other powerful analytical platforms, mainly gas chromatography (GC) or liquid chromatography (LC), bringing powerful advantages that can overcome both peak overlaps and the low sensitivities of NMR approaches (Kvitvang et al., 2014; Kvitvang and Bruheim, 2015; Lien et al., 2015; Sá et al., 2017).

NMR is a non-destructive, non-selective and fast method that has been widely used for molecular identification and structural elucidation used with minimal sample preparation requirements (Atiqullah et al., 2015; Alahmari et al., 2019; Dhahri et al., 2020). While the sample is placed in a static magnetic field, it can be recovered for future analysis using other techniques and it is possible to obtain spectral results regarding how molecules move, flex, react, appear/disappear, or bind with other molecules over several time scales, providing an optimum approach for fluxomics (Blindauer et al., 1997; Wolak et al., 2012; Nargund et al., 2013; Davaasuren et al., 2017).

Thanks to the unique features briefly mentioned above, NMR is one of the main analytical techniques in metabolomics, and as such it is crucial to accurately highlight its advantages and limitations for different metabolomics applications (Emwas

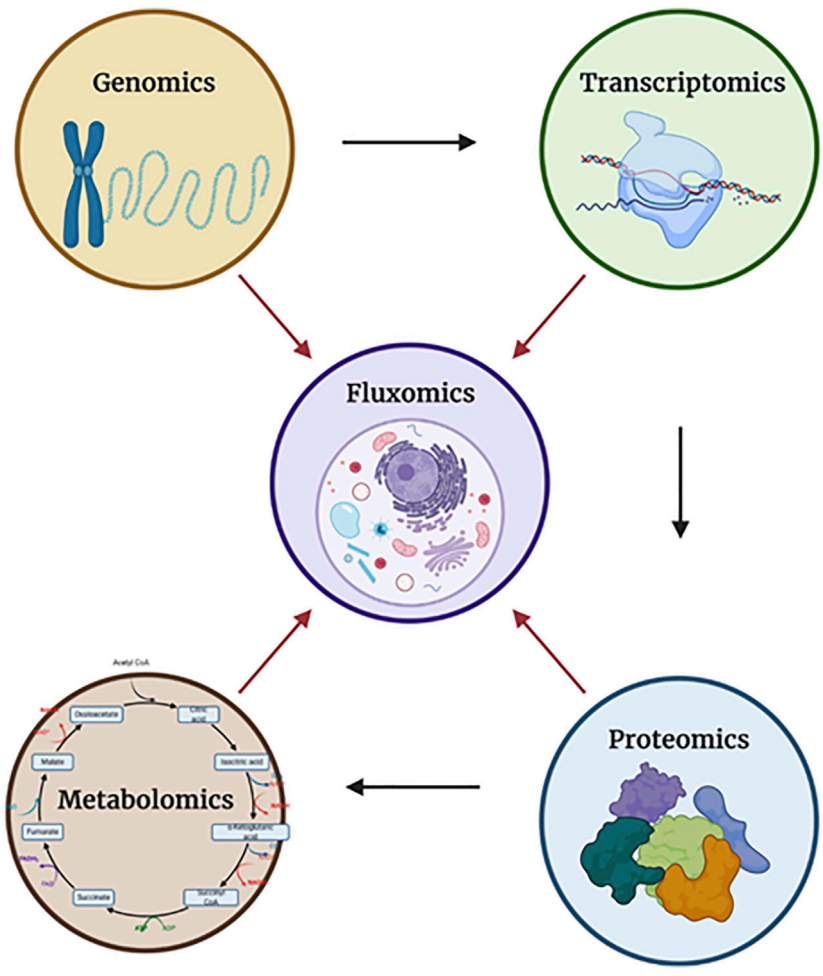

FIGURE 2 | The relationships between each of the "-omics". Each of the arrows shows the direction in which a particular "-omic" influences another. In the case of fluxomics, it combines all approaches, granting better understanding. Dauner describes observed flux/activity as a two component - capacity-based and kinetics-based - regulation (**Figure 3**). Created with Biorender.com.

et al., 2019). NMR spectroscopy, particularly hydrogen detection NMR (commonly referred to as proton or ^{1}H-NMR spectroscopy) can be inherently quantitative, providing a potent analytical tool for metabolomics studies (Dona et al., 2016; Markley et al., 2017). In comparison to other analytical platforms such as GC-MS and LC-MS (Ciborowski et al., 2012; Guo et al., 2013; Raji et al., 2013; Liu et al., 2014), NMR does not require extra steps for sample preparation or metabolite isolation prior to measurement, such as chromatographic separation and/or chemical derivatization. On the other hand, spectral overlap and low signal sensitivity are still the main limitations of NMR approaches, and detection of metabolites at very low concentrations is still beyond the capability of even the most sensitive NMR technologies (Emwas and Bjerrum, 2015).

Even if NMR spectroscopy offers indisputable advantages, low sensitivity is still its main limitation in fluxomic research (Emwas et al., 2013; Clendinen et al., 2014; Emwas et al., 2016; Giraudeau, 2020). Overlapping of peaks is also a major challenge in peak assignment, limiting the number of metabolites that can be identified by NMR spectroscopy (Emwas et al., 2018; O'Rourke et al., 2018; Giraudeau, 2020). The sensitivity of NMR spectroscopy has been improved significantly by dynamic-nuclear polarization (DNP) (Ardenkjær-Larsen et al., 2003; Emwas et al., 2008; Ludwig et al., 2010), cryo-probes, ultra-high magnetic fields (Deborde et al., 2017; Emwas et al., 2019), and the development of new faster methods. However, sensitivity remains a main limitation in the field (Emwas et al., 2019; Robertson et al., 2020; Chandra et al., 2021). For instance, secondary metabolites (usually existing at very low concentrations) are beyond the detection limit of NMR spectroscopy, while for volatile molecules can be detected by GC-MS combined with the mass spectrum and retention time (Emwas et al., 2015; Kohlstedt and Wittmann, 2019). Thus, integrating NMR spectroscopy with MS methods is important to give more comprehensive analysis (Fan et al., 2014; Elbaz et al., 2015; Emwas and Bjerrum, 2015; Sá et al., 2017; Bergès et al., 2021).

FLUXOMICS

Fluxomics is a new metabolomics application, which is focused on actual rates within metabolic networks. Since the reaction rates (fluxes) of metabolic pathways cannot be measured directly due to the intrinsic properties of metabolism such as dynamics, the fluxes can be measured indirectly by the shifts in metabolite levels (Cascante and Marin, 2008; Winter and Krömer, 2013). What distinguishes fluxomics from other–omics is the fact that the fluxome (total set of fluxes in metabolic network of a cell) occur as a resultant of all other "–omes" combined (mainly the proteome and the metabolome). While the genome, transcriptome, proteome and metabolome focus only on their own elements–for example the interactions between proteins in the proteome–the fluxome captures the real and dynamic picture of phenotypes by observing the interactions between all of the "-omes", therefore granting a unique synergistic insight (Cascante and Marin, 2008; Aon and Cortassa, 2015) (**Figure 2**).

Capacity-based regulation is a function related strictly to gene regulatory processes of the cell. Those processes such as enzyme production and stability within the cell (E_i) will differ, depending on the cell and its function in a multicellular organism. As for kinetic regulation, it is a function of kinetic parameters of

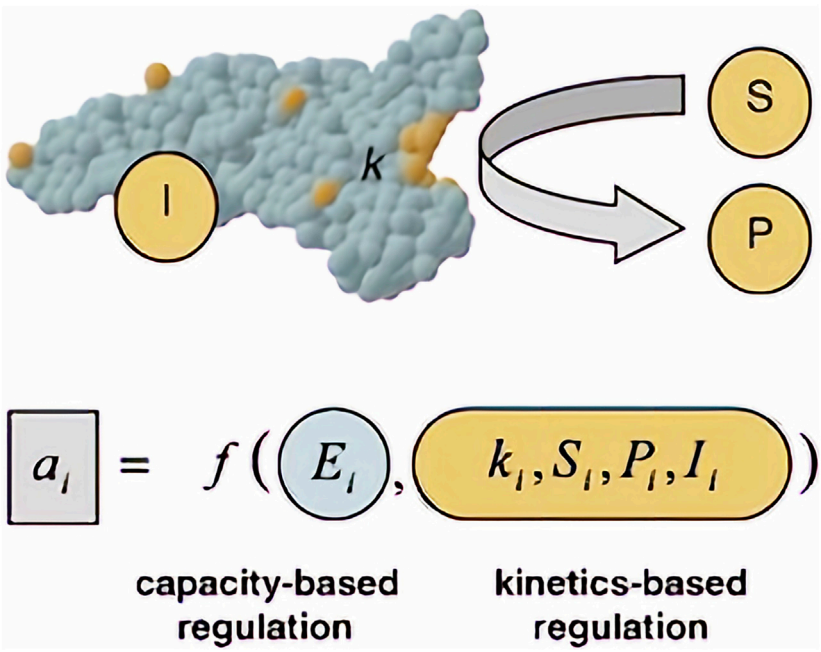

FIGURE 3 | Observed flux/activity *a* of a reaction step I. Adapted with permission from (Dauner, 2010).

enzymes catalyzing the reaction (k) (accounting also for enzyme modifications such as phosphorylation), concentration of substrate (S) and product (P) and effector/signaling molecules (I). (Dauner, 2010). Those variables can be measured by using e.g. quantitative proteomics to calculate enzyme concentration (E_i) (Ong et al., 2003; Mann, 2006; Winter and Krömer, 2013) and quantitative metabolomics for substrate, product and effector concentrations (Winter and Krömer, 2013).

The type of approach used to describe the metabolic network will depend on its nature. For example, metabolic flux analysis (MFA) identifies the whole set of fluxes in a part of the metabolic network of a microorganism *in vivo* (Wiechert et al., 2005). Information about fluxes is obtained by assuming an intracellular pseudo-steady state (a state, where intracellular metabolites do not accumulate in the cell and the balance between the consumption and production fluxes of a metabolite is in equilibrium) and reaction stoichiometry (a fixed configuration of the metabolic network that does not account for cell adaptation to the environmental changes), to estimate the balances around intracellular metabolites, by calculating the uptake rates of substrates and secretion rates of metabolites (Stephanopoulos et al., 1998; Provost and Bastin, 2006; Antoniewicz, 2015). Those rates are measured by monitoring external rate changes such as substrate consumption (glucose uptake rate), biomass synthesis (growth rate), energy consumption and production (CO_2 evolution rate), and metabolite production. The final result is a metabolic flux map with an estimate of the flux of each reaction (**Figure 4**).

For mathematical explanation of the flux calculation, the reader is referred to (Stephanopoulos et al., 1998; Provost and Bastin, 2006; Shimizu and Shimizu, 2013). A variant of MFA called dynamic metabolic flux analysis (DMFA) focuses on describing metabolic fluxes in a metabolic non-steady state, in which a time-series of extracellular concentration and rate measurements are used. In this approach the experiment is divided into a set of time intervals from which the external rates are calculated for each time interval. Then the results are averaged and combined to obtain a time profile of related fluxes (Antoniewicz, 2013; Antoniewicz, 2015).

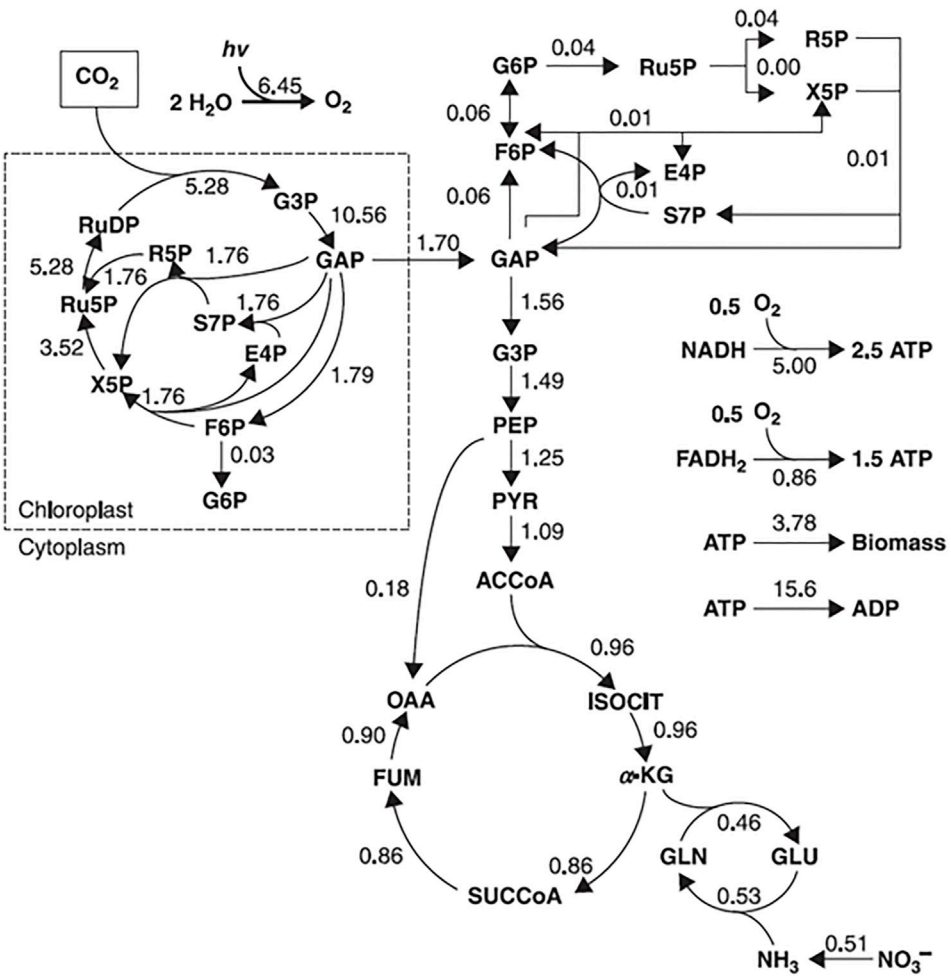

FIGURE 4 | Example of a flux map, representing a metabolic flux distribution of Chlorella cells in autotrophic cultures. The flux values are expressed in mmol/g/h. Adapted with permission from (Shimizu and Shimizu, 2013).

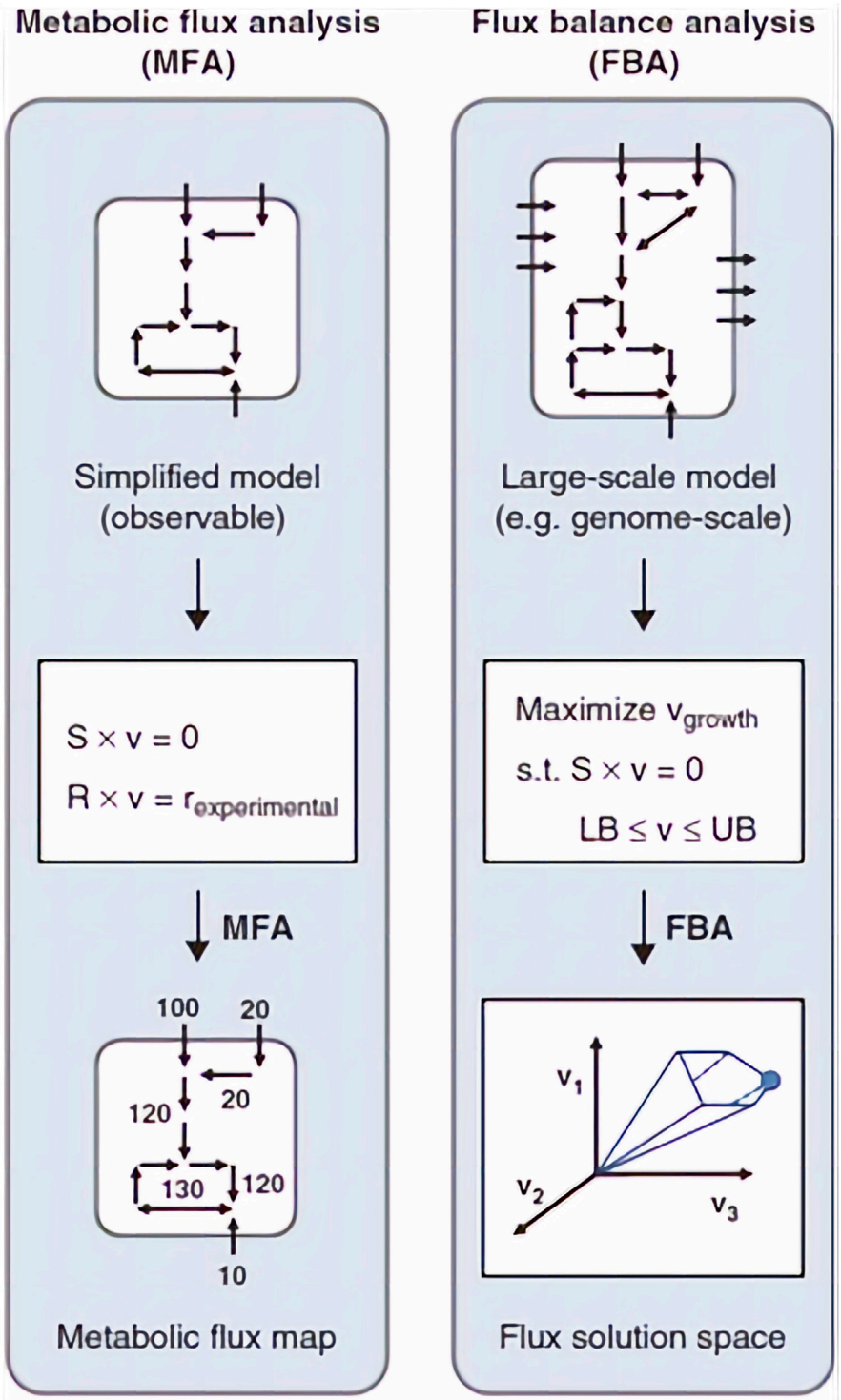

FIGURE 5 | The basics of MFA and FBA approaches. *S* is the stoichiometric matrix, *v* is the flux vector, r is the external metabolic rates. In MFA, fluxes are calculated by fitting extracellular rates measured experimentally. In FBA, a flux solution space is determined by assuming a biological objective, for example, maximization of growth rate, and solving a linear optimization problem. Adapted with permission from (Antoniewicz, 2015).

Another approach to describe a metabolic network is called flux balance analysis (FBA). When compared to MFA, FBA works on a broader scale, and it enables reconstruction of a metabolic network on the genome-scale level. These reconstructions utilize all information about metabolic reactions in an organism and the genes that encode each enzyme. However, this approach does not

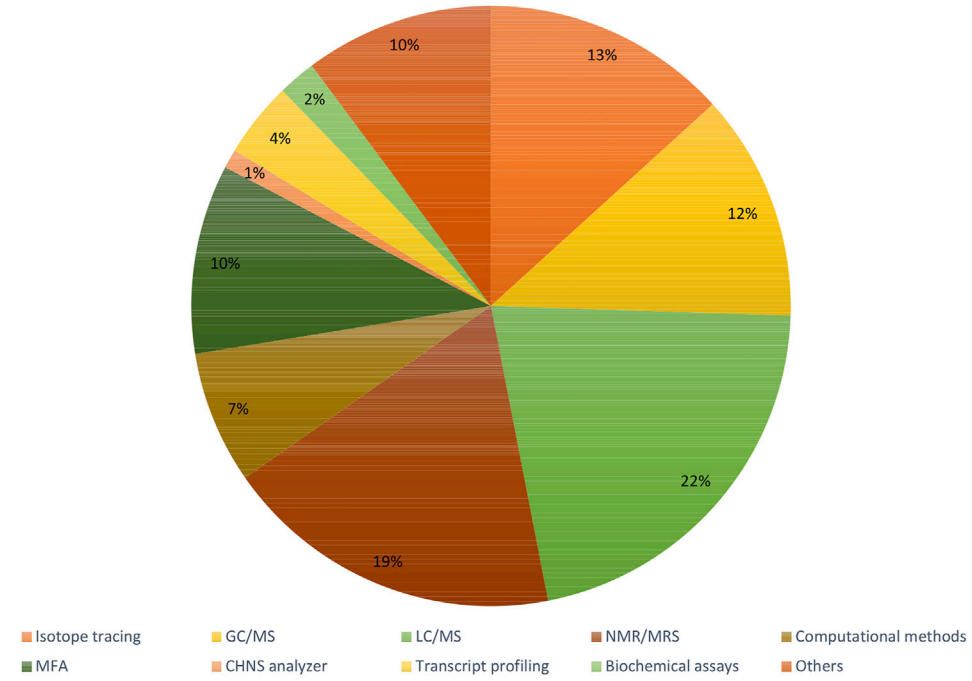

FIGURE 6 | Summary of the most used techniques within fluxomic studies.

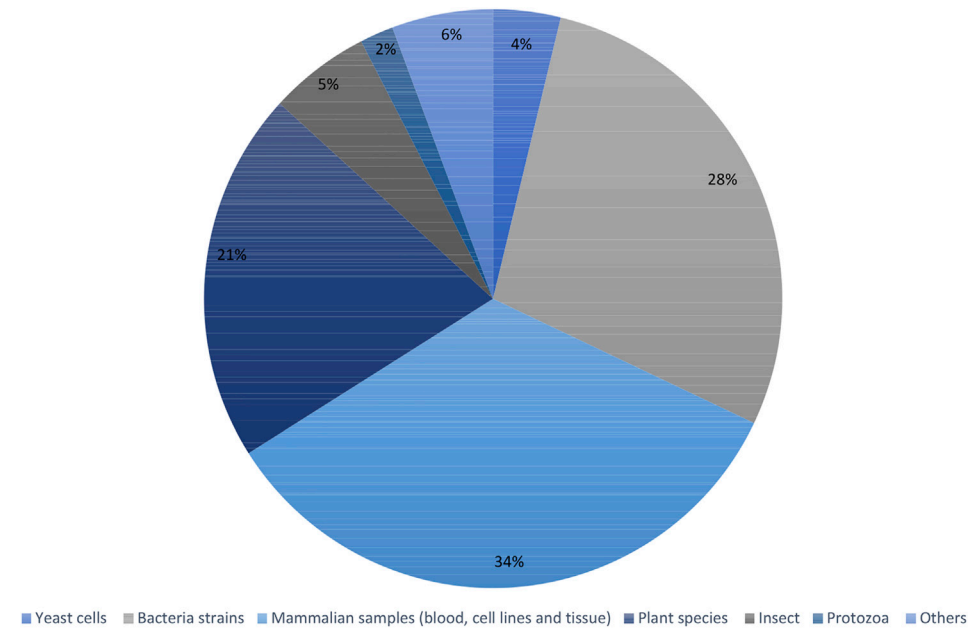

FIGURE 7 | Summary of the most used organisms within fluxomic studies.

count for regulatory interactions and detailed kinetics, giving only partial biological information of the situation of systems at steady state. To obtain fluxes from FBA, first a reconstructed metabolic network must be converted to a mathematical matrix. Within this matrix, a set of constraints is imposed by mass balance equations and reaction bounds. Then, based on the biological objective (e.g., biomass production), linear programming is used to determine the sought fluxes by either maximizing or minimizing objective

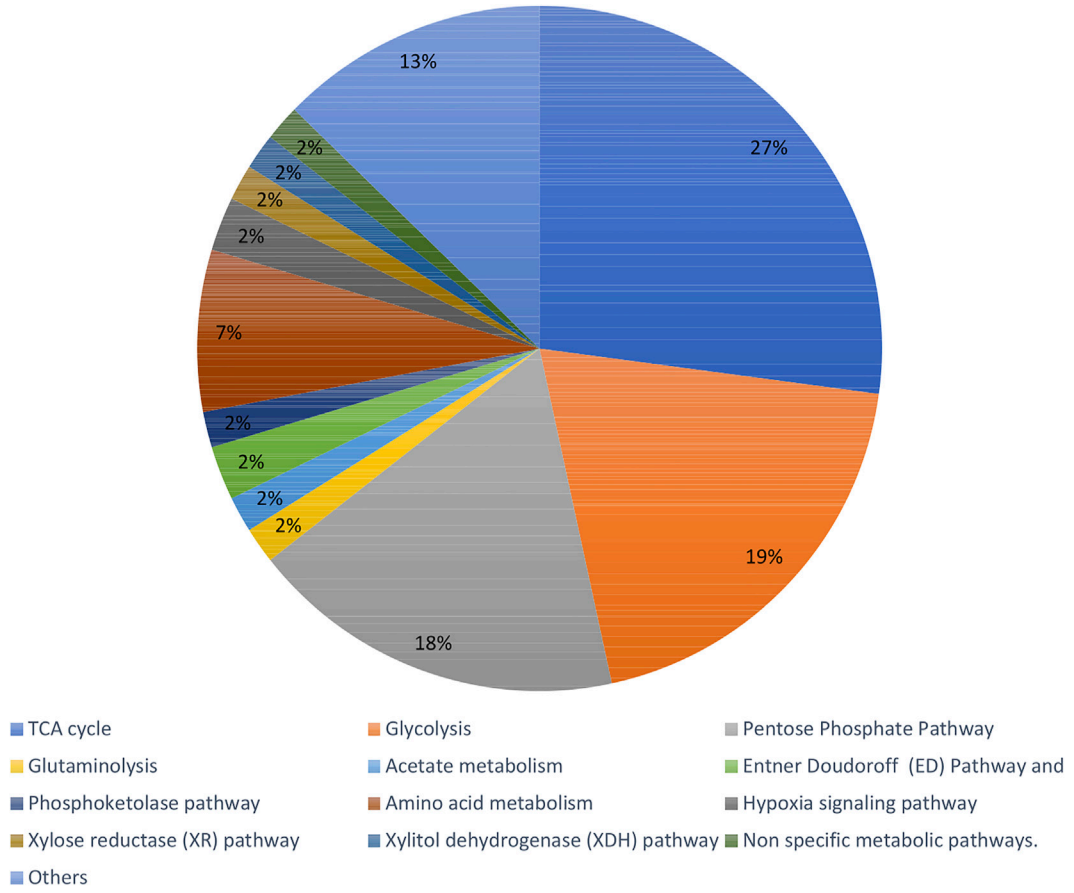

FIGURE 8 | Summary of the commonly described pathways within fluxomic studies.

function while considering given constrains (Orth et al., 2010; Antoniewicz, 2015; Aon and Cortassa, 2015). The differences between the MFA and FBA approaches are shown in **Figure 5**.

Extracellular fluxes between different cells and their environment can also be determined by using ^{13}C-isotope substrate followed by NMR monitoring of ^{13}C-labeled metabolite propagation through the metabolic intermediates in certain metabolic pathways. ^{13}C-labeled fluxomics is an extension of FBA in which all the precursors (substrates) used by the cells are ^{13}C-enriched. Consumed substrates are later incorporated into the metabolic pathways connected to the used substrate. The level of incorporation will depend on intracellular fluxes that could be measured using NMR and/or MS. The information obtained from those experiments can be utilized to discriminate metabolic variants (isotopic profiling), measure specific fluxes (targeted flux analysis–TFA) and investigate the whole fluxome (global fluxomics) (Wiechert et al., 2001; Krömer et al., 2008; Heux et al., 2017). For example, GC-MS and NMR were employed to monitor metabolic flux in neural stem cells (NSCs) using labeled carbon -^{13}C glucose. By following ^{13}C labeling pattern and monitoring an isotopic non-stationary metabolic flux analysis, it was demonstrated that pyruvate entered the tricarboxylic acid (TCA) cycle mostly through pyruvate carboxylase (81%) (Sá et al., 2017). Another practical example of isotope labelling is to identify isotopomers (one of the different labeling states in which a particular metabolite can be encountered). The isotopomer redistribution of a metabolite is calculated based on the percentage value of each isotopomer within the metabolite pool. The information obtained from such an approach describes how the various isotopomers react with each other (Wiechert et al., 2001). Isotopic labelling is not limited only to ^{13}C. Other elements such as ^{15}N, ^{18}O or ^{31}P can also be used to study, e.g. nitrogen metabolism and muscle energetics (Klein and Heinzle, 2012; Nemutlu, 2015).

Isotope labelling was recently used to determine whether pyruvate or glutamine are anaplerotic sources requiring pyruvate carboxylase (PC) and glutaminase 1 (GLS1) activity. Sellers et al. (Sellers et al., 2015) utilized NMR-based metabolomics approaches to monitor the Krebs cycle of patients with early-stage non–small-cell lung cancer (NSCLC) infused with uniformly ^{13}C-labeled glucose followed by tissue resection. NMR analysis of patient cancerous tissues showed enhancement of pyruvate carboxylase (PC) activity. Furthermore, results from patient cancer tissues cultured in $^{13}C_6$-glucose or $^{13}C_5$,$^{15}N_2$-glutamine tracers provided clear evidence of selective activation of PC over glutaminase (GLS) in NSCLC (Sellers et al., 2015).

Another prominent example of isotope labelling used for fluxomics is work by Cocuron *et. al.* (Cocuron et al., 2019), comparing the metabolism of two different maize lines - Alex and LH59. The goal of this work was to test if a change in carbon metabolism may increase oil content in maize kernels to help sustain the demand for vegetable oil. Cocuron et al. labeled Alex embryos with ^{13}C labeled glucose and utilized NMR, GC-MS and LC-MS/MS to measure carbon flow through the metabolic network (^{13}C-MFA). Alex line embryos (which accumulate more oil when compared to LH59) increased the amount of Glucose 6-phosphate (G6P) entering into the plastid, the aldolase in the plastid, the export of TPs (Glyceraldehyde 3-phosphate) to the cytosol, the glycolytic flux in the cytosol, Phosphoenolpyruvate carboxylase (PEPC), and plastidic malic enzyme. It was concluded that increasing the levels of plastidic malic enzyme should enhance the fatty acid content of seeds (Cocuron et al., 2019).

In the recent studies, *Bergès et al.* utilized both NMR and MS approaches to obtain high resolution fluxotypes for huge numbers of a strains in a library. They define fluxotype as "*the particular distribution of metabolic fluxes measured for a given strain under given physiological conditions*" (Bergès et al., 2021). The authors studied the fluxotype of 180 different *E. coli* strains with deleted y-genes. Bacteria were grown in ^{13}C labeled glucose as a single source of carbon while monitoring metabolic fluxes. Deletion of two y-genes led to a significant modification of metabolic fluxes indicating the role of the studied genes in metabolic regulation (Bergès et al., 2021).

Both NMR and MS have been frequently used to investigate the impact of fluxomics in drug delivery and pharmacology. For instance, the production of artemisinic acid in an engineered *E. coli* strain that encodes *S. cerevisiae* enzymes allows the cell to enter the mevalonate pathway and supplement endogenous isopentenyl pyrophosphate (IPP) biosynthesis. This then enhances the production of the antimalarial drug artemisinin. This shift in pathways relies on the flux rate and metabolites concentration (Ro et al., 2006).

In addition, the emergence of multi-drug resistant strains of *tuberculosis* provides a need to develop additional medications for disease treatment. The application of fluxomics to target metabolic enzymes and genome-scale models can be used for analysis, discovery, and as hypothesis-generating tools, which will hopefully assist the rational drug development process. These models need to be able to assimilate data from large datasets and analyze them. A study in 2007 reconstructed the metabolic network of *Mycobacterium tuberculosis* H37Rv (Jamshidi and Palsson, 2007). This strain can produce many of the complex compound's characteristic to *tuberculosis*, such as mycolic acids and mycocerosates. Researchers in this study grew this bacterium *in silico* on various media, analyzed the model in the context of multiple high-throughput data sets, and finally they analyzed the network in an 'unbiased' manner by calculating Hard Coupled Reaction (HCR) sets and FBA. The results showed growth rates comparable to experimental observations in different media, and by considering HCR sets in the context of known drug targets for *tuberculosis* treatment they proposed new alternative, but equivalent drug targets (Jamshidi and Palsson, 2007).

Recent articles proving the constant increase in popularity of the fluxomic field have been collected in **Supplementary Table S1**. The summary of most popular techniques, organisms and pathways described within the studies are shown in **Figures 6–8**.

TABLE 1 | Examples of databases useful for fluxomic-related studies.

Database	Link	Brief description	Ref
Central Carbon Metabolic Flux database (CeCaFDB)	www.cecafdb.org	Contains 581 cases of quantitative flux results among 36 organisms. CeCaFDB can be used for comparison and alignment of different fluxes and to understand how they are changed by other factors	Zhang et al. (2015)
Datanator	www.datanator.info	Multisource database containing information about metabolites, RNA, proteins and reactions. Datanor will include information about fluxes in near future, in which case it could be used for comparative analyses of relationships between variable systems and their constituents	Roth, (2021)
BiGG Models	www.bigg.ucsd.edu	Contains more than 100 genome-scale metabolic network reconstructions that provide information about biochemical reactions, metabolites and genes related to metabolism for a specific organism	King, (2015)
The Human Metabolome database (HMDB)	www.hmdb.ca	Contains 220,945 metabolite entries (both water-soluble and lipid soluble) with 8,610 protein sequences (enzymes/transporters) linked to them including pathways and reactions related to the metabolite. Provides users with data obtained by MS and NMR analyses performed on urine, blood, and cerebrospinal fluid samples	(Wishart et al., 2007; Wishart et al., 2018)
SABIO-RK	www.sabio.h-its.org	Contains information about biochemical reactions and their kinetics. Provides the user with information about the involvement of reaction in various pathways, modifiers of reaction enzymes involved in reactions and measured kinetic data (including kinetic rate equations)	Wittig, (2011)
Braunschweig Enzyme database (BRENDA)	www.brenda-enzymes.org	The largest depository of all classified enzymes, including biochemical and molecular information. The database includes information such as enzyme class, reaction in which the enzyme is involved, specificity of reaction, functional parameters of the reaction, localization of enzyme, the application of enzymes, and ligand-related data	Chang et al. (2009)

FLUXOMICS DATABASES

Rising interest in–omics fields (i.e., proteomics, genomics, and metabolomics) has resulted in an increased number of recent studies. The massive amount of data produced from these studies must be properly managed to increase its accessibility. This has given rise to various -omics databases such as PeptideAtlas (http://www.peptideatlas.org/) (Deutsch et al., 2008), PRIDE (https://www.ebi.ac.uk/pride/) (Martens et al., 2005) (proteomics related databases), Human Metabolome database (HMDB) (www.hmdb.ca) (Wishart et al., 2007) and METLIN (https://metlin.scripps.edu/) (Smith et al., 2005) (metabolomics related databases).

Fluxomics still has not reached its true potential, partly due to a lack of uniform data standards in the reconstruction of metabolic networks (Crown and Antoniewicz, 2013) (Thiele and Palsson, 2010). Therefore, there is an emerging need to construct new and user-friendly databases, which not only store, but also match flux results and create metabolic network models. Recently, novel solutions to reach these ambitious goals have been developed and are briefly described here.

The Central Carbon Metabolic Flux database (CeCaFDB, available at http://www.cecafdb.org) is a novel database published in 2014 that focus on central carbon metabolic systems of microbes and animal cells. The database contains 581 cases of quantitative flux results among 36 organisms including: *Homo sapiens*, *Escherichia coli*, *Saccharomyces cerevisiae* and *Pichia pastoris*. Based on user input it can utilize four modules (vector-based similarity, a stoichiometry-based comparison, a topology-based similarity, and enzyme-topology based similarity) for comparison and alignment of different flux distributions. Additionally, this database provides the opportunity to perform similarity calculations by utilizing deposited data and altering genetic and environmental factors (Zhang et al., 2015).

Datanator (https://datanator.info) is an integrated multisource database that contains quantitative molecular data of several types including metabolite concentrations, RNA modifications and half-lives, protein abundances and modifications, and reaction rate parameters. Developed in 2020, Datanator includes various data for 1,030 organisms integrated from over 8,000 articles. Although it does not contain flux related data yet, the authors are planning to include it in the near future, as well as information on RNA/protein localizations and protein half-lives. In such case, Datanator would be a valuable source for comparative analyses of relationships between variable networks and systems (Roth, 2021).

BiGG Models (http://bigg.ucsd.edu) is a large-scale database containing genome-scale metabolic network reconstructions. It contains more than 100 genome-scale metabolic models. Those models contain information about biochemical reactions, metabolites and genes related to the metabolism of specific organisms. The information provided in BIGG Models is standardized across different models, which allows users to browse, share and visualize the networks in a structured manner (King, 2015).

Besides those three databases, various other databases used in different–omics fields can be used to obtain partial information that can be useful for studying the fluxes. Some of them are listed in **Table 1**.

CONCLUSION

Matching genomic, transcriptomic, proteomic, and metabolomic data is essential for global understanding of biological systems. Fluxomics provides insight into actual rates within metabolic networks, both because of both cellular activity and environmental changes. Such knowledge can be obtained using different approaches including metabolic flux analysis (MFA), dynamic metabolic flux analysis (DMFA), flux balance analysis (FBA) or ^{13}C-labeled metabolite monitoring. In addition to this wide variety of approaches in fluxomics, the significant advances in instrumentation methods such as NMR and MS, along with new databases and software, increase the prevalence of fluxomics studies. Nowadays, fluxomics gives rewarding data of complexed multi-molecular interactions in biological systems, which has never been observed before.

AUTHOR CONTRIBUTIONS

A-HE was responsible for section "Advantages and disadvantages of chromatography and nuclear magnetic resonance tools in fluxomics", conceptualization, review, and editing of the manuscript. KS wrote sections: "Introduction", "Fluxomics", "Fluxomics Databases" and "Conclusion". IA-Y provided information on fluxomics studies for the section: "Introduction" and **Supplementary Table S1**. JL contributed to the section "Advantages and disadvantages of chromatography and nuclear magnetic resonance tools in fluxomics". MJ was responsible for the conceptualization, review, and editing of the manuscript.

FUNDING

We would like to thank King Abdullah University of Science and Technology for financial support.

ACKNOWLEDGMENTS

We would like to thank King Abdullah University of Science and Technology for financial support. We would like to acknowledge Life Science Editors for editorial services. Special thanks to Kristin Strandenes, EddaTxT, Norway for her suggestions and feedback.

SUPPLEMENTARY MATERIAL

The Supplementary Material for this article can be found online at: https://www.frontiersin.org/articles/10.3389/fphar.2022.805782/full#supplementary-material

REFERENCES

Alahmari, F., Dey, S., Emwas, A.-H., Davaasuren, B., and Rothenberger, A. (2019). Layered Copper Thioaluminate K2Cu3AlS4: Synthesis, crystal Structure, Characterization and Solid-State 27Al and 39K NMR Studies. *J. Alloys Comp.* 776, 1041–1047. doi:10.1016/j.jallcom.2018.10.239

Antoniewicz, M. R. (2013). Dynamic Metabolic Flux Analysis-Ttools for Probing Transient States of Metabolic Networks. *Curr. Opin. Biotechnol.* 24 (6), 973–978. doi:10.1016/j.copbio.2013.03.018

Antoniewicz, M. R. (2015). Methods and Advances in Metabolic Flux Analysis: a Mini-Review. *J. Ind. Microbiol. Biotechnol.* 42 (3), 317–325. doi:10.1007/s10295-015-1585-x

Aon, M., and Cortassa, S. (2015). Systems Biology of the Fluxome. *Processes* 3 (3), 607–618. doi:10.3390/pr3030607

Ardenkjær-Larsen, J. H., Millard, P., and Enjalbert, B. (2003). Increase in Signal-To-Noise Ratio of > 10,000 Times in Liquid-State NMR. *Proceedings of the National Academy of Science*. 100(18): p. 10158–10163. doi:10.1073/pnas.1733835100

Atiqullah, M., al-Harthi, M. A., Anantawaraskul, S., and Emwas, A.-H. M. (2015). Ethylene Homo- and Copolymerization Chain-Transfers: A Perspective from Supported (N BuCp) 2 ZrCl 2 Catalyst Active centre Distribution. *J. Chem. Sci.* 127 (4), 717–728. doi:10.1007/s12039-015-0828-8

Babele, P. K., and Young, J. D. (2020). Applications of Stable Isotope-Based Metabolomics and Fluxomics toward Synthetic Biology of Cyanobacteria. *Wiley Interdiscip. Rev. Syst. Biol. Med.* 12, e1472. doi:10.1002/wsbm.1472

Bergès, C., Cahoreau, E., Millard, P., Enjalbert, B., Dinclaux, M., Heuillet, M., et al. (2021). Exploring the Glucose Fluxotype of the *E. coli* Y-Ome Using High-Resolution Fluxomics. *Metabolites* 11 (5), 271. doi:10.3390/metabo11050271

Beyß, M., (2019). The Design of FluxML: A Universal Modeling Language for 13C Metabolic Flux Analysis. *Front. Microbiol.* 10, 10. doi:10.3389/fmicb.2019.0102

Blindauer, C. A., Emwas, A. H., Holý, A., Dvořáková, H., Sletten, E., and Sigel, H. (1997). Complex Formation of the Antiviral 9-[2-(Phosphonomethoxy)Ethyl] Adenine (PMEA) and of its N 1, N 3, and N 7 Deaza Derivatives with Copper(II) in Aqueous Solution. *Chem. Eur. J.* 3 (9), 1526–1536. doi:10.1002/chem.19970030922

Cascante, M., and Marin, S. (2008). Metabolomics and Fluxomics Approaches. *Essays Biochem.* 45, 67–81. doi:10.1042/bse0450067

Chandra, K., Al-Harthi, S., Sukumaran, S., Almulhim, F., Emwas, A.-H., Atreya, H. S., et al. (2021). NMR-based Metabolomics with Enhanced Sensitivity. *RSC Adv.* 11 (15), 8694–8700. doi:10.1039/D1RA01103K

Chang, A., Scheer, M., Grote, A., Schomburg, I., and Schomburg, D. (2009). BRENDA, AMENDA and FRENDA the Enzyme Information System: New Content and Tools in 2009. *Nucleic Acids Res.* 37, D588–D592. doi:10.1093/nar/gkn820

Choi, J., and Antoniewicz, M. R. (2019). Tandem Mass Spectrometry for 13C Metabolic Flux Analysis: Methods and Algorithms Based on EMU Framework. *Front. Microbiol.* 10, 31. doi:10.3389/fmicb.2019.00031

Choi, K. R., Kim, W. J., and Lee, S. Y. (2018). Metabolomics for Industrial Fermentation. *Bioproc. Biosyst Eng* 41 (7), 1073–1077. doi:10.1007/s00449-018-1967-3

Ciborowski, M., Lipska, A., Godzien, J., Ferrarini, A., Korsak, J., Radziwon, P., et al. (2012). Combination of LC-MS- and GC-MS-based Metabolomics to Study the Effect of Ozonated Autohemotherapy on Human Blood. *J. Proteome Res.* 11 (12), 6231–6241. doi:10.1021/pr3008946

Clendinen, C. S., Lee-McMullen, B., Williams, C. M., Stupp, G. S., Vandenborne, K., Hahn, D. A., et al. (2014). 13C NMR Metabolomics: Applications at Natural Abundance. *Anal. Chem.* 86 (18), 9242–9250. doi:10.1021/ac502346h

Cocuron, J. C., Koubaa, M., Kimmelfield, R., Ross, Z., and Alonso, A. P. (2019). A Combined Metabolomics and Fluxomics Analysis Identifies Steps Limiting Oil Synthesis in Maize Embryos. *Plant Physiol.* 181 (3), 961–975. doi:10.1104/pp.19.00920

Crown, S. B., and Antoniewicz, M. R. (2013). Publishing 13C Metabolic Flux Analysis Studies: a Review and Future Perspectives. *Metab. Eng.* 20, 42–48. doi:10.1016/j.ymben.2013.08.005

Dauner, M. (2010). From Fluxes and Isotope Labeling Patterns towards In Silico Cells. *Curr. Opin. Biotechnol.* 21 (1), 55–62. doi:10.1016/j.copbio.2010.01.014

Davaasuren, B., Emwas, A. H., and Rothenberger, A. (2017). MAu2GeS4-Chalcogel (M = Co, Ni): Heterogeneous Intra- and Intermolecular Hydroamination Catalysts. *Inorg. Chem.* 56 (16), 9609–9616. doi:10.1021/acs.inorgchem.7b01099

Deborde, C., Moing, A., Roch, L., Jacob, D., Rolin, D., and Giraudeau, P. (2017). Plant Metabolism as Studied by NMR Spectroscopy. *Prog. Nucl. Magn. Reson. Spectrosc.* 102-103, 61–97. doi:10.1016/j.pnmrs.2017.05.001

Deutsch, E. W., Lam, H., and Aebersold, R. (2008). PeptideAtlas: a Resource for Target Selection for Emerging Targeted Proteomics Workflows. *EMBO Rep.* 9 (5), 429–434. doi:10.1038/embor.2008.56

Dhahri, M., Sioud, S., Dridi, R., Hassine, M., Boughattas, N. A., Almulhim, F., et al. (2020). Extraction, Characterization, and Anticoagulant Activity of a Sulfated Polysaccharide from Bursatella Leachii Viscera. *ACS Omega* 5 (24), 14786–14795. doi:10.1021/acsomega.0c01724

Dona, A. C., Kyriakides, M., Scott, F., Shephard, E. A., Varshavi, D., Veselkov, K., et al. (2016). A Guide to the Identification of Metabolites in NMR-Based Metabonomics/metabolomics Experiments. *Comput. Struct. Biotechnol. J.* 14, 135–153. doi:10.1016/j.csbj.2016.02.005

Eisenreich, W., (2021). Persistence of Intracellular Bacterial Pathogens—With a Focus on the Metabolic Perspective. *Frontiers in Cellular and Infection Microbiology*, 2021. 10, doi:10.3389/fcimb.2020.615450

Elbaz, A. M., Gani, A., Hourani, N., Emwas, A.-H., Sarathy, S. M., and Roberts, W. L. (2015). TG/DTG, FT-ICR Mass Spectrometry, and NMR Spectroscopy Study of Heavy Fuel Oil. *Energy Fuels* 29 (12), 7825–7835. doi:10.1021/acs.energyfuels.5b01739

Emwas, A.-H. M., Al-Talla, Z. A., and Kharbatia, N. M. (2015). "*Sample Collection and Preparation of Biofluids and Extracts for Gas Chromatography-Mass Spectrometry*,". Editor J. T. Bjerrum (New York, NY: Springer New York), 75–90. doi:10.1007/978-1-4939-2377-9

Emwas, A.-H. M., Salek, R. M., Griffin, J. L., and Merzaban, J. (2013). NMR-based Metabolomics in Human Disease Diagnosis: Applications, Limitations, and Recommendations. *Metabolomics* 9 (5), 1048–1072. doi:10.1007/s11306-013-0524-y

Emwas, A.-H. M. (2015). "The Strengths and Weaknesses of NMR Spectroscopy and Mass Spectrometry with Particular Focus on Metabolomics Research,". Editor J. T. Bjerrum (New York, NY: Springer New York), 161–193. doi:10.1007/978-1-4939-2377-910.1007/978-1-4939-2377-9_13

Emwas, A.-H. M., Alghrably, M., Al–Harthi, S., Poulson, B. G., Szczepski, K., Chandra, K., et al. (2019). "New Advances in Fast Methods of 2D NMR Experiments," in *Nuclear Magnetic Resonance*. Editors N. Khaneja (London, United Kingdom: IntechOpen). Available at: https://www.intechopen.com/chapters/70360

Emwas, A. H., Roy, R., McKay, R. T., Ryan, D., Brennan, L., Tenori, L., et al. (2016). Recommendations and Standardization of Biomarker Quantification Using NMR-Based Metabolomics with Particular Focus on Urinary Analysis. *J. Proteome Res.* 15 (2), 360–373. doi:10.1021/acs.jproteome.5b00885

Emwas, A. H., Roy, R., McKay, R. T., Tenori, L., Saccenti, E., Gowda, G. A. N., et al. (2019). NMR Spectroscopy for Metabolomics Research. *Metabolites* 9, 9. doi:10.3390/metabo9070123

Emwas, A. H., Saccenti, E., Gao, X., McKay, R. T., Dos Santos, V. A. P. M., Roy, R., et al. (2018). Recommended Strategies for Spectral Processing and post-processing of 1D 1H-NMR Data of Biofluids with a Particular Focus on Urine. *Metabolomics* 14 (3), 31. doi:10.1007/s11306-018-1321-4

Emwas, A. H., Marin, S., and Selivanov, V. A. (2008). Determinants for Optimal Enhancement in *Ex Situ* DNP Experiments. *Appl. Magn. Reson.* 34 (3-4), 483–494. doi:10.1007/s00723-008-0120-x

Emwas, A., Szczepski, K., McKay, R. T., Asfour, H., Chang, C., Lachowicz, J., et al. (2021). "Pharmacometabolomics: A New Horizon in Personalized Medicine," in Metabolomics — Methodology and Applications in Medical Sciences and Life Sciences, (London, United Kingdom: IntechOpen). doi:10.5772/intechopen.98911

Fan, J., Ye, J., Kamphorst, J. J., Shlomi, T., Thompson, C. B., and Rabinowitz, J. D. (2014). Quantitative Flux Analysis Reveals Folate-dependent NADPH Production. *Nature* 510 (7504), 298–302. doi:10.1038/nature13236

Feng, X., Page, L., Rubens, J., Chircus, L., Colletti, P., Pakrasi, H. B., et al. (2010). Bridging the gap between Fluxomics and Industrial Biotechnology. *J. Biomed. Biotechnol.* 2010, 460717. doi:10.1155/2010/460717

Foguet, C., Jayaraman, A., Marin, S., Selivanov, V. A., Moreno, P., Messeguer, R., et al. (2019). p13CMFA: Parsimonious 13C Metabolic Flux Analysis. *Plos Comput. Biol.* 15, e1007310. doi:10.1371/journal.pcbi.1007310

Giraudeau, P. (2020). NMR-based Metabolomics and Fluxomics: Developments and Future Prospects. *Analyst* 145 (7), 2457–2472. doi:10.1039/D0AN00142B

Guo, J., Zhang, M., Elmore, C. S., and Vishwanathan, K. (2013). An Integrated Strategy for *In Vivo* Metabolite Profiling Using High-Resolution Mass Spectrometry Based Data Processing Techniques. *Anal. Chim. Acta* 780, 55–64. doi:10.1016/j.aca.2013.04.012

Hansen, A. S. L., Lennen, R. M., Sonnenschein, N., and Herrgård, M. J. (2017). Systems Biology Solutions for Biochemical Production Challenges. *Curr. Opin. Biotechnol.* 45, 85–91. doi:10.1016/j.copbio.2016.11.018

Heux, S., Bergès, C., Millard, P., Portais, J. C., and Létisse, F. (2017). Recent Advances in High-Throughput 13C-Fluxomics. *Curr. Opin. Biotechnol.* 43, 104–109. doi:10.1016/j.copbio.2016.10.010

Ideker, T., Galitski, T., and Hood, L. (2001). A New Approach to Decoding Life: Systems Biology. *Annu. Rev. Genomics Hum. Genet.* 2 (1), 343–372. doi:10.1146/annurev.genom.2.1.343

Jamshidi, N., and Palsson, B. Ø. (2007). Investigating the Metabolic Capabilities of *Mycobacterium tuberculosis* H37Rv Using the In Silico Strain iNJ661 and Proposing Alternative Drug Targets. *BMC Syst. Biol.* 1 (1), 26. doi:10.1186/1752-0509-1-26

King, Z. A., (2015). *BiGG Models: A Platform for Integrating, Standardizing and Sharing Genome-Scale Models*. *Nucleic Acids Res.* 44, 44. doi:10.1093/nar/gkv1049

Klein, S., and Heinzle, E. (2012). Isotope Labeling Experiments in Metabolomics and Fluxomics. *Wiley Interdiscip. Rev. Syst. Biol. Med.* 4 (3), 261–272. doi:10.1002/wsbm.1167

Kohlstedt, M., and Wittmann, C. (2019). GC-MS-based 13C Metabolic Flux Analysis Resolves the Parallel and Cyclic Glucose Metabolism of Pseudomonas Putida KT2440 and *Pseudomonas aeruginosa* PAO1. *Metab. Eng.* 54, 35–53. doi:10.1016/j.ymben.2019.01.008

Krömer, J., Quek, L.-E., and Nielsen, L. (2008). *13C-fluxomics: A Tool for Measuring Metabolic Phenotypes*. *Aust Biochem*, 2008. 40

Kvitvang, H. F., and Bruheim, P. (2015). Fast Filtration Sampling Protocol for Mammalian Suspension Cells Tailored for Phosphometabolome Profiling by Capillary Ion Chromatography - Tandem Mass Spectrometry. *J. Chromatogr. B Analyt Technol. Biomed. Life Sci.* 998-999, 45–49. doi:10.1016/j.jchromb.2015.06.018

Kvitvang, H. F., Kristiansen, K. A., and Bruheim, P. (2014). Assessment of Capillary Anion Exchange Ion Chromatography Tandem Mass Spectrometry for the Quantitative Profiling of the Phosphometabolome and Organic Acids in Biological Extracts. *J. Chromatogr. A.* 1370, 70–79. doi:10.1016/j.chroma.2014.10.029

Lien, S. K., Niedenführ, S., Sletta, H., Nöh, K., and Bruheim, P. (2015). Fluxome Study of Pseudomonas Fluorescens Reveals Major Reorganisation of Carbon Flux through central Metabolic Pathways in Response to Inactivation of the Anti-sigma Factor MucA. *BMC Syst. Biol.* 9 (1), 6. doi:10.1186/s12918-015-0148-0

Liu, M. L., Zheng, P., Liu, Z., Xu, Y., Mu, J., Guo, J., et al. (2014). GC-MS Based Metabolomics Identification of Possible Novel Biomarkers for Schizophrenia in Peripheral Blood Mononuclear Cells. *Mol. Biosyst.* 10 (9), 2398–2406. doi:10.1039/C4MB00157E

Liu, S. R., Peng, X. X., and Li, H. (2019). Metabolic Mechanism of Ceftazidime Resistance in Vibrio Alginolyticus. *Infect. Drug Resist.* 12, 417–429. doi:10.2147/IDR.S179639

Liu, Y., Li, R., Xiao, X., and Wang, Z. (2019). Bacterial Metabolism-Inspired Molecules to Modulate Antibiotic Efficacy. *J. Antimicrob. Chemother.* 74 (12), 3409–3417. doi:10.1093/jac/dkz230

Ludwig, C., Marin-Montesinos, I., Saunders, M. G., Emwas, A. H., Pikramenou, Z., Hammond, S. P., et al. (2010). Application of *Ex Situ* Dynamic Nuclear Polarization in Studying Small Molecules. *Phys. Chem. Chem. Phys.* 12 (22), 5868–5871. doi:10.1039/C002700F

Mann, M. (2006). Functional and Quantitative Proteomics Using SILAC. *Nat. Rev. Mol. Cel Biol* 7 (12), 952–958. doi:10.1038/nrm2067

Markley, J. L., Brüschweiler, R., Edison, A. S., Eghbalnia, H. R., Powers, R., Raftery, D., et al. (2017). The Future of NMR-Based Metabolomics. *Curr. Opin. Biotechnol.* 43, 34–40. doi:10.1016/j.copbio.2016.08.001

Martens, L., Hermjakob, H., Jones, P., Adamski, M., Taylor, C., States, D., et al. (2005). PRIDE: the Proteomics Identifications Database. *Proteomics* 5 (13), 3537–3545. doi:10.1002/pmic.200401303

Nargund, S., Joffe, M. E., Tran, D., Tugarinov, V., and Sriram, G. (2013). "Nuclear Magnetic Resonance Methods for Metabolic Fluxomics," in *Systems Metabolic Engineering*. Editor H. S. Alper (Totowa, NJ: Humana Press), 335–351. doi:10.1007/978-1-62703-299-510.1007/978-1-62703-299-5_16

Nemutlu, E. (2015). *CHAPTER 9 18O-Assisted 31P NMR and Mass Spectrometry For Phosphometabolomic Fingerprinting And Metabolic Monitoring*, in Metabolic Profiling: Disease and Xenobiotics. *The Royal Society of Chemistry* 2015. p. 255–286. doi:10.1039/9781849735162-00255

Niedenführ, S., Wiechert, W., and Nöh, K. (2015). How to Measure Metabolic Fluxes: a Taxonomic Guide for (13)C Fluxomics. *Curr. Opin. Biotechnol.* 34, 82–90. doi:10.1016/j.copbio.2014.12.003

Niittylae, T., Chaudhuri, B., Sauer, U., and Frommer, W. B. (2009). Comparison of Quantitative Metabolite Imaging Tools and Carbon-13 Techniques for Fluxomics. *Methods Mol. Biol.*, 553, 355–372. doi:10.1007/978-1-60327-563-7

Ong, S. E., Foster, L. J., and Mann, M. (2003). Mass Spectrometric-Based Approaches in Quantitative Proteomics. *Methods* 29 (2), 124–130. doi:10.1016/S1046-2023(02)00303-1

O'Rourke, A., Fisher, K. J., and Newman, K. L. (2018). Identification of a 3-Alkylpyridinium Compound from the Red Sea Sponge Amphimedon Chloros with *In Vitro* Inhibitory Activity against the West Nile Virus NS3 Protease. *Molecules* 23 (6), 1472. doi:10.3390/molecules23061472

Orth, J. D., Thiele, I., and Palsson, B. Ø. (2010). What Is Flux Balance Analysis? *Nat. Biotechnol.* 28 (3), 245–248. doi:10.1038/nbt.1614

Provost, A., and Bastin, G. (2006). *Metabolic Flux Analysis: An Approach for Solving Non-stationary Underdetermined Systems*.

Raji, M., Amad, M., and Emwas, A. H. (2013). Dehydrodimerization of Pterostilbene during Electrospray Ionization Mass Spectrometry. *Rapid Commun. Mass. Spectrom.* 27 (11), 1260–1266. doi:10.1002/rcm.6571

Ro, D. K., Paradise, E. M., Ouellet, M., Fisher, K. J., Newman, K. L., Ndungu, J. M., et al. (2006). Production of the Antimalarial Drug Precursor Artemisinic Acid in Engineered Yeast. *Nature* 440 (7086), 940–943. doi:10.1038/nature04640

Robertson, C., Lucas, R. A., and Le Gresley, A. (2020). Scope and Limitations of Nuclear Magnetic Resonance Techniques for Characterisation and Quantitation of Vitamin D in Complex Mixtures. *Skin Res. Technol.* 26 (1), 112–120. doi:10.1111/srt.12773

Rohmer, L., Hocquet, D., and Miller, S. I. (2011). Are Pathogenic Bacteria Just Looking for Food? Metabolism and Microbial Pathogenesis. *Trends Microbiol.* 19 (7), 341–348. doi:10.1016/j.tim.2011.04.003

Rojo, D., Canuto, G. A., Castilho-Martins, E. A., Tavares, M. F., Barbas, C., López-Gonzálvez, Á., et al. (2015). A Multiplatform Metabolomic Approach to the Basis of Antimonial Action and Resistance in Leishmania Infantum. *PLoS One* 10, e0130675. doi:10.1371/journal.pone.0130675

Roth, Y. D. (2021). *Datanator: an Integrated Database of Molecular Data for Quantitatively Modeling Cellular Behavior*. *Nucleic Acids Res.* 49, 49. doi:10.1093/nar/gkaa1008

Sá, J. V., Kleiderman, S., Brito, C., Sonnewald, U., Leist, M., Teixeira, A. P., et al. (2017). Quantification of Metabolic Rearrangements during Neural Stem Cells Differentiation into Astrocytes by Metabolic Flux Analysis. *Neurochem. Res.* 42 (1), 244–253. doi:10.1007/s11064-016-1907-z

Sellers, K., Fox, M. P., Bousamra, M., Slone, S. P., Higashi, R. M., Miller, D. M., et al. (2015). Pyruvate Carboxylase Is Critical for Non-small-cell Lung Cancer Proliferation. *J. Clin. Invest.* 125 (2), 687–698. doi:10.1172/JCI72873

Shimizu, K. (2013). "Conventional Flux Balance Analysis and its Applications," in *Bacterial Cellular Metabolic Systems*. Editor K. Shimizu (Oxford, United Kingdom: Woodhead Publishing), 215–262. doi:10.1533/9781908818201.215

Smith, C. A., O'Maille, G., Want, E. J., Qin, C., Trauger, S. A., Brandon, T. R., et al. (2005). METLIN: a Metabolite Mass Spectral Database. *Ther. Drug Monit.* 27 (6), 747–751. doi:10.1097/01.ftd.0000179845.53213.39

Stephanopoulos, G., Nielsen, J. B., and Aristodou, A. (1998). *Metabolic Engineering: Principles and Methodologies*. Academic Press.

Stokes, J. M., Lopatkin, A. J., Lobritz, M. A., and Collins, J. J. (2019). Bacterial Metabolism and Antibiotic Efficacy. *Cell Metab* 30 (2), 251–259. doi:10.1016/j.cmet.2019.06.009

Thiele, I., and Palsson, B. Ø. (2010). A Protocol for Generating a High-Quality Genome-Scale Metabolic Reconstruction. *Nat. Protoc.* 5 (1), 93–121. doi:10.1038/nprot.2009.203

Vailati-Riboni, M., Palombo, V., and Loor, J. J. (2017). *What Are Omics Sciences?* Editor B. N. Ametaj (Springer International Publishing: Cham), 1–7. doi:10.1007/978-3-319-43033-1_1

Wiechert, W., Möllney, M., Petersen, S., and de Graaf, A. A. (2001). A Universal Framework for 13C Metabolic Flux Analysis. *Metab. Eng.* 3 (3), 265–283. doi:10.1006/mben.2001.018710.1006/mben.2001.0188

Wiechert, W., Schweissgut, O., Takanaga, H., and Frommer, W. B. (2007). Fluxomics: Mass Spectrometry versus Quantitative Imaging. *Curr. Opin. Plant Biol.* 10 (3), 323–330. doi:10.1016/j.pbi.2007.04.015

Wiechert, W., and Nöh, K. (2005). "From Stationary to Instationary Metabolic Flux Analysis," in *From Lab to Industry to Production*. Editor U. Kragl (Berlin, Heidelberg: Springer Berlin Heidelberg), 145–172. doi:10.1007/b98921

Winter, G., and Krömer, J. O. (2013). Fluxomics - Connecting 'omics Analysis and Phenotypes. *Environ. Microbiol.* 15 (7), 1901–1916. doi:10.1111/1462-2920.12064

Wishart, D. S., Feunang, Y. D., Marcu, A., Guo, A. C., Liang, K., Vázquez-Fresno, R., et al. (2018). HMDB 4.0: the Human Metabolome Database for 2018. *Nucleic Acids Res.* 46, D608. doi:10.1093/nar/gkx1089

Wishart, D. S., Tzur, D., Knox, C., Eisner, R., Guo, A. C., Young, N., et al. (2007). HMDB: the Human Metabolome Database. *Nucleic Acids Res.* 35, D521–D526. doi:10.1093/nar/gkl923

Wittig, U. (2011). *SABIO-RK—database for Biochemical Reaction kinetics*. *Nucleic Acids Research*, 2011. 40. doi:10.1093/nar/gkr1046

Wojtowicz, W., and Mlynarz, P. (2016). Metabolomics and Fluxomics in Biotechnology: Current Trends. BioTechnologia. *J. Biotechnol. Comput. Biol. Bionanotechnology* 97, 97. doi:10.5114/bta.2016.60783

Wolak, J., Rahimi-Keshari, K., Jeffries, R. E., Joy, M. P., Todd, A., Pediatitakis, P., et al. (2012). "Noninvasive Fluxomics in Mammals by Nuclear Magnetic Resonance Spectroscopy," in *The Handbook of Metabolomics*. Editors T. W.-M. Fan, A. N. Lane, and R M. Higashi (Totowa, NJ: Humana Press), 321–392. doi:10.1007/978-1-61779-618-0

Zahrl, R. J., Peña, D. A., Mattanovich, D., and Gasser, B. (2017). Systems Biotechnology for Protein Production in Pichia pastoris. *FEMS Yeast Res.* 17, 17. doi:10.1093/femsyr/fox068

Zhang, Z., Shen, T., Rui, B., Zhou, W., Zhou, X., Shang, C., et al. (2015). CeCaFDB: a Curated Database for the Documentation, Visualization and Comparative Analysis of central Carbon Metabolic Flux Distributions Explored by 13C-Fluxomics. *Nucleic Acids Res.* 43, D549–D557. doi:10.1093/nar/gku1137

Conflict of Interest: The authors declare that the research was conducted in the absence of any commercial or financial relationships that could be construed as a potential conflict of interest.

Publisher's Note: All claims expressed in this article are solely those of the authors and do not necessarily represent those of their affiliated organizations, or those of the publisher, the editors and the reviewers. Any product that may be evaluated in this article, or claim that may be made by its manufacturer, is not guaranteed or endorsed by the publisher.

Advantages of publishing in Frontiers

OPEN ACCESS
Articles are free to read for greatest visibility and readership

FAST PUBLICATION
Around 90 days from submission to decision

HIGH QUALITY PEER-REVIEW
Rigorous, collaborative, and constructive peer-review

TRANSPARENT PEER-REVIEW
Editors and reviewers acknowledged by name on published articles

Frontiers
Avenue du Tribunal-Fédéral 34
1005 Lausanne | Switzerland

Visit us: www.frontiersin.org
Contact us: frontiersin.org/about/contact

REPRODUCIBILITY OF RESEARCH
Support open data and methods to enhance research reproducibility

DIGITAL PUBLISHING
Articles designed for optimal readership across devices

FOLLOW US
@frontiersin

IMPACT METRICS
Advanced article metrics track visibility across digital media

EXTENSIVE PROMOTION
Marketing and promotion of impactful research

LOOP RESEARCH NETWORK
Our network increases your article's readership